

**SEAFLOOR HAZARDS AND RELATED SURFICIAL GEOLOGY,  
NAVARIN BASIN PROVINCE, NORTHERN BERING SEA**

**by**

**Herman A. Karl and Paul R. Carlson**

**U.S. Geological Survey**

**Final Report  
Outer Continental Shelf Environmental Assessment Program  
Research Unit 588**

**January 1983**

## TABLE OF CONTENTS

List of Figures .....	391
List of Tables .....	397
OVERVIEW .....	399
I. Summary of Objectives, Conclusions and Implications with Respect to OCS Oil and Gas Development .....	399
II. Introduction .....	399
A. General Nature and Scope of Study .....	399
B. Specific Objectives .....	400
c. Relevance to Problems of Petroleum Development .....	400
III . Current State of Knowledge .....	400
IV. Study Area .....	401
v. Sources, Methods and Rationale of Data Collection .....	401
<b>VI.- VIII.</b> Results, Discussion, and Conclusions . . . . . (See Chapters 1-12 below)	410
IX. Needs for Further Study .....	410
References .....	411
CHAPTER 1:     REPORTS PERTAINING TO <b>NAVARIN</b> BASIN PROVINCE PUBLISHED AS OF JANUARY 1983 .....	415
CHAPTER 2:     GEOLOGIC HAZARDS H. A. Karl and P. R. Carlson .....	417
CHAPTER 3:     TEXTURAL VARIATION OF <b>SURFICIAL</b> BOTTOM SEDIMENT H. A. Karl and P. R. Carlson .....	421
CHAPTER 4:     RATES OF SEDIMENT ACCUMULATION P. R. Carlson and H. A. Karl .....	427
CHAPTER 5: <b>PRE-QUATERNARY</b> ROCKS AND SEMI-CONSOLIDATED SEDIMENT FROM THE NAVARIN CONTINENTAL MARGIN P. R. Carlson, J. G. Baldauf, and C. Larkin .....	435
CHAPTER 6: <b>ISOPACH</b> MAP OF UNIT A, YOUNGEST SEDIMENTARY SEQUENCE IN NAVARIN BASIN P. R. Carlson, J. M. Fischer, H. A. Karl, and C. Larkin .....	439
CHAPTER 7:     SUMMARY OF <b>GEOTECHNICAL</b> CHARACTERISTICS B. D. Edwards and H. J. Lee .....	445

CHAPTER 8:	HYDROCARBON GASES IN SEDIMENTS -- RESULTS FROM 1981 FIELD SEASON M. Golan-Bat and K. A. <b>Kvenvolden</b> .....	481
CHAPTER 9:	<b>BENTHIC FORAMINIFERS</b> P. <b>Quinterno</b> .....	501
CHAPTER 10:	DIATOM ANALYSIS OF SURFACE SAMPLES RECOVERED FROM <b>PERVENETS</b> CANYON J. G. <b>Baldauf</b> .....	527
CHAPTER 11:	<b>ASPARTIC</b> ACID GEOCHRONOLOGY OF MOLLUSKS D. J. Blunt and K. A. Kvenvolden .....	539
CHAPTER 12:	APPENDED REPORTS .....	545
Appendix A:	High-Resolution Seismic Reflection Profiles: Navarin Basin Province, Northern Bering Sea, 1980 P. R. <b>Carlson</b> and H. A. Karl .....	547
Appendix B:	High-Resolution Seismic Reflection Profiles: <b>Navarin</b> Basin Province, Northern Bering Sea, 1981 P. R. <b>Carlson</b> and H. A. Karl .....	551
Appendix C:	Location and Description of Sediment <b>Samples</b> : Navarin Basin Province, Bering <i>Sea</i> , 1980-81 H. A. Karl and P. R. <b>Carlson</b> .....	555
Appendix D:	Bathymetric Map of Navarin Basin Province, Northern Bering Sea J. M. Fischer, P. R. Carlson, and H. A. Karl .....	561
Appendix E:	Two Newly Discovered Submarine Canyons on Alaskan Continental Margin of Bering Sea P. R. <b>Carlson</b> , J. M. Fischer, and H. A. Karl .....	569
Appendix F:	Geologic Hazards in <b>Navarin</b> Basin Province, Northern Bering Sea P. R. <b>Carlson</b> , H. A. Karl, J. M. Fischer, and B. D. Edwards .....	597
Appendix G:	Puzzling Features in the Head of the Navarinsky Canyon, Bering Sea P. R. <b>Carlson</b> , H. A. Karl, and B. D. Edwards .....	613
Appendix H:	Large Sand Waves in Submarine Canyon Heads, Bering Sea: Preliminary Hypothesis of Their <b>Depositional</b> History H. A. Karl and P. R. <b>Carlson</b> .....	625

## LIST OF FIGURES

- Figure 1. Location map of Navarin Basin province.
- Figure 2. Bathymetric map of Navarin Basin province.
- Figure 3. Track lines of high-resolution seismic reflection profiles collected during cruise DC2/3-80-BS/NB, summer 1980.
- Figure 4. Track lines of high-resolution seismic reflection profiles collected during cruise **DC4/5-81-BS/NB**, summer 1981.
- Figure 5. Locations of sediment samples.
- Figure 6. Map of seafloor geologic hazards in Navarin Basin province.
- Figure 7. Location of sediment samples selected as **typical** examples of textural environments characterizing Navarin Basin province. (The solid triangle identifies Van Veen samples).
- Figure 8. Plot of mean diameter vs. standard deviation.
- Figure 9. Histograms of selected samples. Modes identified by **hachuring**; dominant mode is hatchured in **biomodal** samples.
- Figure 10. Location map of cores subsampled for C-14 dating.
- Figure 11. Map of dated cores showing calculated preliminary accumulation rates of sediment.
- Figure 12. Locations of dredge hauls and gravity cores, Navarin margin.
- Figure 13. **Isopach** map of unit A superimposed on selected isopachs of strata above acoustic basement. Navarin Basin isopach above basement after **Marlow** and others (1979).
- Figure 14. Isopach map of unit A, youngest stratigraphic sequence in Navarin Basin.
- Figure 15. Minisparker profile (1000 J) showings **seismic** reflector (marked by arrow) that marks the base of isopached unit A. Vertical exaggeration '8.5x.
- Figure 16. Major physiographic features of Navarin Basin province (after Fischer et al., 1982), and core locations for 1980 and 1981 R/V DISCOVERER cruises.
- Figure 17. Location map of replicate cores collected for advanced geotechnical testing of Navarin Basin province sediment, 1980 R/V DISCOVERER cruise.

- Figure 18. Comparison of  $S_v$  values as determined by calibrated spring and torque cell measurements. Anisotropic effects on  $S_v$  as shown by split and unsplit cores are small. GC indicates sample removed for **geochemical** analysis. Core G36, 1980 R/V DISCOVERER cruise.
- Figure 19. **Areal** distribution of peak undrained vane shear strength  $S_v$  at a **subbottom** depth of 1 m. Contour interval 5 kPa.
- Figure 20. Areal distribution of peak undrained vane shear strength  $S_v$  at a **subbottom** depth of 2 m. Contour interval 5 kPa.
- Figure 21. Areal distribution of peak undrained vane shear strength  $S_v$  at a **subbottom** depth of 3 m. Contour interval 5 kPa.
- Figure 22. **Areal** distribution of peak undrained vane shear strength  $S_v$  at a **subbottom** depth of 4 m. Contour interval 10 kPa.
- Figure 23. **Areal** distribution of peak undrained vane shear strength  $S_v$  at a **subbottom** depth of 5 m. Data values (in kPa) written beside appropriate core location.
- Figure 24. **Areal** distribution of salt-corrected water content ( $W_c$ ) at a **subbottom** depth of 1 m. Contour interval 50% by dry weight.
- Figure 25. **Areal** distribution of salt-corrected water content ( $W_c$ ) at a **subbottom** depth of 2m. Contour interval 50% by dry weight.
- Figure 26. **Areal** distribution of salt-corrected water content ( $W_c$ ) at a **subbottom** depth of 3m. Contour interval 50% by dry weight.
- Figure 27. Areal distribution of salt-corrected water content ( $W_c$ ) at a **subbottom** depth of 4m. Contour interval 50% by dry weight.
- Figure 28. **Areal** distribution of salt-corrected water content ( $W_c$ ) at a **subbottom** depth of 5m. Data values in % written beside appropriate core locations.
- Figure 29. Linear regression best fit lines of the increase of in place effective overburden pressure ( $\sigma'_v$ ) with **subbottom** depth for replicate cores. Data from 1980 DISCOVERER cruise.
- Figure 30. Plasticity chart for Navarin Basin province replicate cores. Data from 1980 R/V DISCOVERER cruise.
- Figure 31. Plot of excess past effective stress  $\sigma'_e$  vs. depth for Navarin Basin province replicate cores. Data from 1980 R/V DISCOVERERER cruise.
- Figure 32. Location of tests for Navarin Basin province **geotechnical** testing program on replicate cores. Refer to Table 5 for summary of **triaxial** test specifications.

- Figure 33. Plot of the normalized strength parameter  $\Lambda_0$  as defined by a log-log plot of  $S_u / \sigma'_{vc} (\text{overconsolidated}) / S_{nc}$  vs. OCR for replicate cores collected on the 1980 R/V DISCOVERER cruise. See text for explanation.
- Figure 34. Example of multiple estimates of undrained shear strength ( $S_u$ ) for paired cores G31 and G32, 1980 R/V DISCOVERER cruise.
- Figure 35. Example of multiple estimates of undrained shear strength ( $S_u$ ) for paired cores G97 and G98, 1980 R/V DISCOVERER cruise. Disparity between G97 and G98 strength estimates is due to the removal of approximately 15 m of sediment. See text for explanation.
- Figure 36. Location of hydrocarbon gas sampling sites in the Navarin Basin province. Sites are designated with core numbers.
- Figure 37. Distribution of maximum concentrations of methane in  $\mu\text{l/l}$  of wet sediment.
- Figure 38. Distribution of maximum concentrations of ethane plus propane in  $\text{nl/l}$  of wet sediment.
- Figure 39. Distribution of maximum concentrations of butane in  $\text{nl/l}$  of wet sediment.
- Figure 40. Graph of concentrations of  $C_1$  in  $\mu\text{l/l}$  and  $\text{ml/l}$  wet sediment vs. depth in centimeters for sediment samples from the eleven sites in the Navarin Basin Province where  $C_2 + C_3$  concentrations reach or exceed  $1 \mu\text{l/l}$  wet sediment at some depth interval.
- Figure 41. Graph of concentrations of  $C_2 + C_3$  in  $\text{nl/l}$  and  $\mu\text{l/l}$  wet sediment vs. depth in centimeters for sediment samples from the eleven sites in the Navarin Basin Province where  $C_2 + C_3$  concentrations reach or exceed  $1 \mu\text{l/l}$  wet sediment at some depth interval.
- Figure 42. Tally of anomalous parameters for cores in the regions indicated.
- Figure 43. Sample locations.
- Figure 44. Relative frequency percentages of the most abundant species in surface samples plotted against increasing water depth.
- Figure 45. Relative frequency percentages of the most abundant benthic foraminiferal species plotted against depth in core 81-12.
- Figure 46. Index map of the Navarin Basin province, Bering Sea.
- Figure 47. Location of surface samples collected from Pervenets Canyon (0 = 1980; 1 = 81; 2 = 82).

- Figure 48. Seismic reflection profile across **Pervenets** Canyon showing surface exposures of **stratigraphically** older reflectors. Line 33, **DC4-81-BS/NB**. See Fig. 47, transect 2 for profile location.
- Figure 49. Distribution of Denticulopsis seminae in the surface sediments (values are **in** percent).
- Figure 50. Distribution of Nitzschia grunowii in the surface sediment (values are in percent).
- Figure 51. Location of gravity cores in the northern Navarin Basin province where fossil mollusks were studied. Bathymetry is in meters.

Appendix Figures:

- Figure A1. Track line chart for 1980 DISCOVERER Cruise DC 4/5-80 **BS/NB**.
- Figure **B1**. Track line chart for 1981 DISCOVERER Cruise DC 2/3-81 **BS/NB**.
- Figure C1. Station location map.
- Figure **C2**. Map of sediment types.
- Figure **D1**. Bathymetric map of Navarin Basin province and inset showing **tracklines**.
- Figure E1. **Thalweg** profiles of main branches of St. Matthew and Middle Canyons.
- Figure E2. Transverse profiles of west (a) and east (b) branches of St. Matthew Canyon (see Fig. E3 for traverse locations).
- Figure E3. Map of St. Matthew and Middle Canyon systems, showing **thalwegs** of main branches and tributaries and locations of transverse profiles illustrated in Figures E2 and E4.
- Figure E4. Transverse profiles of west (a) and east (b) branches of Middle Canyon (see Fig. E3 for transverse profiles).
- Figure E5. Map showing locations of core and dredge samples and seismic profiles, including illustrated line drawings.
- Figure E6. Interpretive line drawing of air-gun profile across west branch of St. Matthew Canyon (see Fig. E5 for location); Vertical exaggeration (**V.E.**) 'x7.
- Figure E7. Interpretive line drawing of air-gun profile across west branch of St. Matthew Canyon (see Fig. **E5** for location) (**V.E.** -'x7 ).

- Figure E8. Interpretive line drawing of air-gun profile across west branch of St. Matthew Canyon (see Fig. E5 for location) (V.E. --x7 ).
- Figure E9. Interpretive line drawing of air-gun profile across west branch of St. Matthew Canyon (see Fig. E5 for location) (V.E. --x7 ).
- Figure E10. Interpretive line drawing of air-gun profile across west branch of St. Matthew Canyon (see Fig. E5 for location) (V.E. ~x7 ).
- Figure En. Interpretive line drawing of air-gun profile across west branch of St. Matthew Canyon (see Fig. E5 for location) (V.E. -x7 ). (BSR = Bottom simulating reflector).
- Figure F1. Location of Navarin Basin province (outlined) and lines of average monthly ice-front positions (after Webster, 1979); ice positions for the 15th of month.
- Figure F2. Preliminary map of sea-floor geologic hazards in Navarin Basin province.
- Figure F3. Air-gun profile showing slides in Navarinsky Canyon. Note buried channel (arrow) and associated cut-and-fill structures (V.E. ~x10 ).
- Figure F4. Minisparker profile showing sediment waves at head of Navarinsky Canyon (V.E. 'x7.5).
- Figure F5. Minisparker profile showing sediment waves covered by about 20 m of parallel-bedded sediment at head of Pervenets Canyon (V.E. ~x 8.5).
- Figure F6. Minisparker profile from northern part of Navarin Basin province showing acoustic anomalies interpreted to be caused by gas-charged sediment (V.E. 'x7.5).
- Figure F7. Area 1 distribution of peak undrained vane shear strength ( $S_v$ ) at 1-m **subbottom** depth.
- Figure F8. Area 1 distribution of salt-corrected water content at a 1-m subbottom depth.
- Figure F9. Interpretive line drawing of air-gun profile across graben in Navarin Basin province (see Fig. F2) (V.E. ~x8.5).

- Figure G1. Sketch map of study area in northern Bering Sea, showing locations of high-resolution seismic-reflection lines, sample stations, and areas of seafloor features.
- Figure G2. Seafloor morphologic features in head of Navarinsky Canyon, showing locations of illustrated profiles. Bathymetry after Fischer and others, 1982. Contour interval, 200 m.
- Figure G3. Seismic-reflection profiles in head of Navarinsky Canyon. (a) Line drawing of seismic-reflection profiles (20-40-in<sup>3</sup> airguns), showing relative positions of profiles in Figures G3b, G3c, and G4a. (b) Minisparker profile (1,000 J), showing sand waves. (c) Minisparker profile (1,000 J), showing pull-aparts (arrows). Vertical exaggeration (V.E.) '7.5x. See Figure G2 for locations.
- Figure G4. High-resolution profiles, showing slide zone in Navarinsky Canyon. (a) 3.5 kHz profile; V.E. '10X. (b) Uniboom profile (1200 J); V.E. ~7.5x. See Figure G2 for locations.
- Figure H1. Map of study area showing seismic survey **tracklines** and distribution of sand waves (stippled areas). Dashed lines are 1980 tracklines and solid lines are 1981 **tracklines**; 1981 data were collected during preparation of this manuscript; for clarity tracklines have not been shown within sand wave fields. The deeper sand wave area in Pervenets Canyon was defined almost entirely by buried bed forms.
- Figure H2. Example of Navarinsky Canyon field sand waves; **A**: Mini-sparker record. **B**: Interpretive drawing; solid lines define sets of sand waves; dashed lines define angle of climb; heavy vertical dashed line is a recorder time mark.
- Figure H3. **Paleogeographic** reconstruction of the depositional setting of the sand waves (stippled areas). Heavy solid line follows the present shelf edge and indicates the position of the Pleistocene shoreline assuming an arbitrary amount of tectonic and isostatic influence that caused local sea level to be 150 m below present sea level. Dashed line follows the present 130 m isobath. The area between these lines is that part of the shelf that would be submerged under 20 m of water assuming no local complications and only that sea level was lower ecstatically by 130 m. Presence of steams is speculative.

## LIST OF TABLES

- Table 1. Results of grain-size analysis on selected samples.
- Table 2. C-14 dates of Navarin samples.
- Table 3. c-14 dates and rates of sediment accumulation listed by water depth.
- Table 4. Summary of Consolidation test results.
- Table 5. **Triaxial** test specifications for Routine (R) and Special (S) cores.
- Table 6. Summary of **triaxial** test results - NSP estimate of undrained shearing strength.
- Table 7. **Hydrocarbon gas (C<sub>1</sub>-nC<sub>4</sub>)** concentrations and ratios from sediment samples from the Navarin Basin province (1981).
- Table 8. Hydrocarbon gas (**C<sub>1</sub>-nC<sub>4</sub>**) concentration and **ratio** ranges from sediment samples from the Navarin Basin province (1981). Methane (**C<sub>1</sub>**) concentrations are in pi/l; the other hydrocarbon concentrations are in nl/l.
- Table 9. Relative frequency percentages of benthic foraminifers in surface samples.
- Table 10. List of benthic **foraminiferal** species.
- Table 11. Relative frequency percentages of **benthic** foraminiferal species in core 81-12.
- Table 12. Abundance (in percent) of species encountered during the examination of surface sediments from the Pervenets Canyon region.
- Table 13." Summary of aspartic acid D/L values in mollusks from the Navarin Basin province.

### Appendix Tables:

- Table **A1.** **Tracklines** along which seismic systems were operational.
- Table **B1.** **Tracklines** along which seismic systems were operational.
- Table **E1.** Principal canyons and fan channels of the St. Matthew and Middle Systems.

- Table E2. (a) **West** Branch, St. Matthew Canyon wall gradients  
(b) East Branch, St. Matthew Canyon wall gradients
- Table E3. (a) Tributaries of the west branch of St. Matthews Canyon system  
(b) Tributaries of the east branch of St. Matthews Canyon system
- Table E4. (a) Wall gradients of the west branch of Middle Canyon  
(b) Wall gradients of the east branch of Middle Canyon
- Table** ES. (a) Tributaries of the west branch of Middle Canyon.  
(b) Tributaries of the east branch of Middle Canyon.
- Table E6. Comparison of canyons of the Beringian continental margin with **canyons** of the **east** and west coasts of the U.S. (Data for east and west coast canyons from Shepard and Dill, 1966).
- Table F1. Summary consolidation data of near-surface sediment.

## OVERVIEW

### I. Summary of Objectives, Conclusions and Implications with Respect to OCS Oil and Gas Development.

The principal objective of this study is to provide interpretive maps and reports of seafloor hazards in the Navarin **Basin** province preparatory for **OCS** lease sale 83 presently scheduled for December, 1984. Several geologic processes that are active in Navarin Basin province are potentially hazardous to commercial development. Preliminary conclusions and implications pertaining to OCS development follow:

1. Navarin **Basin** province appears to be an area of low seismicity and no faults mapped to date rupture the seafloor. However, several faults indicate movement in the last 12,000 years and, thus, are potentially active.

2. Submarine landslides are common in the heads of submarine canyons and on the upper continental slope and must be considered in the design of any seafloor structures.

3. Fields of large sediment waves have been discovered near the heads of the three large canyons. These sediment waves if active could be hazardous to seafloor structures.

4. Gas-charged sediment, present throughout a large part of the province, has reduced strength and bearing capacity as compared to strength of gas-free sediment.

5. Intense storms produce exceptionally large waves which are not only capable of eroding bottom sediment, but are also dangerous to surface structures and vessels.

6. Sea-ice commonly covers much of the Navarin Basin province for several months of the year and could pose a problem to exploration, development, or production of oil and gas during years of heavy concentrations.

### 11. Introduction

#### A. General Nature and Scope of Study

Navarin Basin province is an OCS (Outer Continental Shelf) lease sale area that is scheduled for leasing in 1984. This basin potentially contains vast accumulations of oil and gas and with the escalating energy problems will be the subject of extensive exploration activity. Preliminary to the sale, an environmental impact statement must be released by **BLM**. Our study in Navarin Basin will provide information about the seafloor geologic hazards that need to be considered during the exploration for and development of petroleum on the outer continental shelf. No previous geohazards investigations had been conducted in the Navarin **Basin** province. Thus, we began in the summer of 1980, to collect reconnaissance geophysical and geological data. This report includes preliminary findings from the 1980 and 1981 field seasons.

## B. Specific Objectives

The specific objectives of this final report are to synthesize the results of the 1980 and 1981 field seasons and to update the maps and interpretations presented in the 1980 **annual** report. These objectives are accomplished by including chapters on various specific topics newly written for this report by experts and by appending reports and papers written and published in the interval of time that occurred after the release of the 1980 annual report and before preparation of this final report.

### c. Relevance to Problems of Petroleum Development

The Navarin **Basin** province encompasses an area of 45,000 km<sup>2</sup> and contains three sedimentary basins filled with thick sequences of Cenozoic strata. Interpretation of the stratigraphy and structure of these basins suggests areas which could trap accumulations of economically exploitable hydrocarbon deposits. The province, which includes the outer continental shelf and upper slope, is deeply dissected by large submarine canyons. The steep gradients within the canyons and along the upper continental slope result in potential instability problems in a large part of the province. **Zones** of gas-charged sediment that also may cause problems of seafloor instability are present over much of the outer continental shelf in the Navarin province. All areas of unstable seafloor must be carefully considered during the design and the installation of exploration and development platforms. Preliminary data from this potential petroleum province have revealed the existence of large **bedforms** near the heads of the large submarine canyons. The potential impact of these **bedforms** as well as the occurrences of gas-charged sediment and sediment slides must be considered during development phases when planning pipelines and holding tanks.

## III. Current State of Knowledge

Prior to the summer of 1980, no geohazards data had been collected in the Navarin Basin province. Several marine geology and geophysics cruises to the Bering Sea had, however, collected data adjacent to and even within part of the province. The thick sedimentary sequence that makes up Navarin Basin was first discovered on a 1970 cruise of the R/V BARTLETT (Scholl and others, 1975, 1976). Marlow and others (1976) named this 10-15 **km** thick sedimentary sequence of Mesozoic and Cenozoic age deposits. However, detailed mapping of the "acoustic basement" was not completed until seismic-reflection surveys of 1976, 1977, and 1980 provided multi-channel coverage necessary to allow delineation of the northwest-trending basins (**Marlow** and others, 1981).

The Russians published the first generalized maps of sediment distribution in the study area (Lisitsyn, 1966). Without access to the original data, we only have been able to extract a few data points along the northern border of the Navarin province which we are using to supplement our sediment distribution maps. **Of** much greater use are data from the University of Washington cores and grab samples, some of which were collected in the eastern part of the Navarin Basin (**Knebel**, 1972). Other studies that will provide comparative **sedimentologic** data have been conducted in adjacent parts of the Bering Sea (**Anadyr** Basin: **Kummer** and **Creager**, 1971; Bristol Bay:

Sharma and others, 1977; Kvenvolden and others, 1979; Drake and others, 1980; St. George Basin, Gardner and others, 1980; Vallier and others, 1980).

Although oceanographic data have been gathered from the Bering Sea for at least 100 years (Dan, N. H., 1881 to Cacchione and others, 1982) and by scientists from numerous countries (e.g. USSR-Natarov, 1963; Japan-Takenouti and Ohtani, 1974; U.S.A.-Hughes and others, 1974), very little is known about the details of circulation and other oceanographic parameters within the Navarin Basin province. These other studies have involved water mass characteristics (Sayles and others, 1979) or large scale circulation (Hughes and others, 1974) of the entire Bering Sea or the deep Aleutian Basin or have concentrated on movement and characteristics of the water in and through the major outlets, the Bering Strait (Coachman and others, 1975) or the passes in the Aleutian Chain (Favorite, 1974).

Sea-ice is often present throughout most of the Navarin Basin province for about five months of the year, January through May. Whereas the average monthly limit of sea-ice in the Bering Sea has been determined (Webster, 1979), little is known about the movement and deformation of the sea-ice field (Tabata, 1974). The increasing availability of satellite imagery (Muench, 1974; Ahlnas and Wendler, 1980) together with winter field work (Drake and others, 1979; Paquette and Bourke, 1980) will provide needed detailed information helping to delineate the sea-ice fields in the Navarin Basin province.

#### IV. Study Area

The Navarin Basin province is located on the outer continental shelf and upper slope in the northwestern Bering Sea (Fig. 1). This promising petroleum region, scheduled for lease sale in 1984, is bounded on the northwest by the U.S.-USSR Convention Line of 1867, on the southwest by the base of the continental slope and extends to within 100 km of St. Matthew Island to the northeast and St. Paul Island to the southeast, an area of about 45,000 km<sup>2</sup>. This province consists of a very flat continental shelf (average gradient 0.02°) and a rugged continental slope (gradient ranges from 3° to 8°) that has been deeply dissected by five large submarine canyons. Bathymetric maps of the Bering Sea constructed by Pratt and Walton (1974) and Schumacher (1976), include very limited bathymetric data from the Navarin area. We have made a more detailed bathymetric map (Fig. 2) of the study area by combining the bathymetric data obtained on the DISCOVERER cruises of 1980 and 1981 and the R/V S.P. LEE cruise of 1982 with data from several U.S. Geological Survey cruises during the past decade (Scholl, Buffington, and Marlow, 1976; Marlow and Cooper, 1979). The map and a discussion of the morphology of the, Navarin continental margin are included in the appended results section (Fischer and others, 1982).

#### v. Sources, Methods and Rationale of Data Collection

The principal sources of data for this study have been the seismic reflection profiles and sediment samples collected on the 1980 and 1981 R/V DISCOVERER cruises (Carlson and Karl, 1981, 1982; Karl and Carlson, 1982). Some additional data were collected in 1980 from the USCG POLAR STAR and in

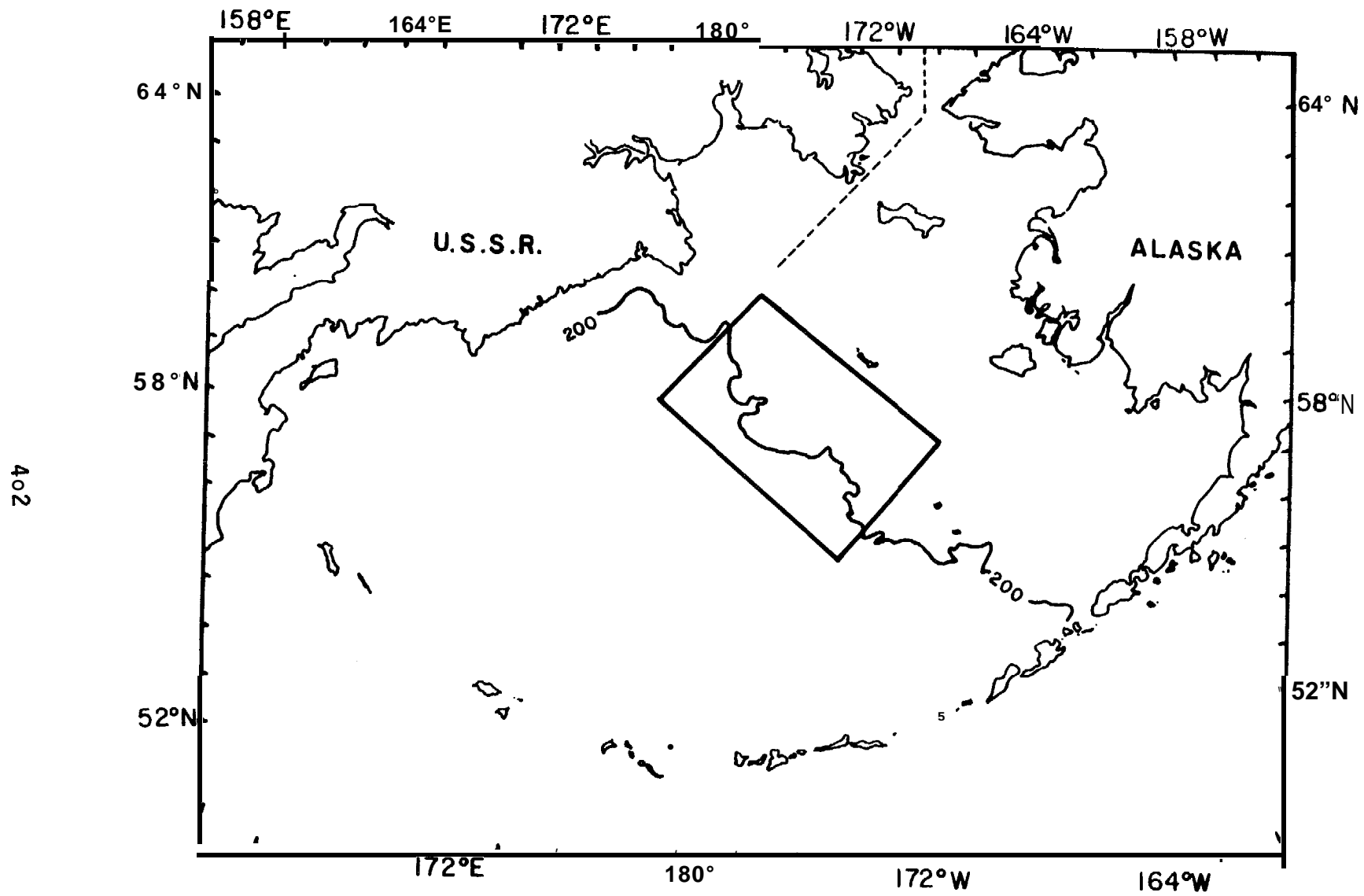


Figure 1. Location map of Navarin Basin province.

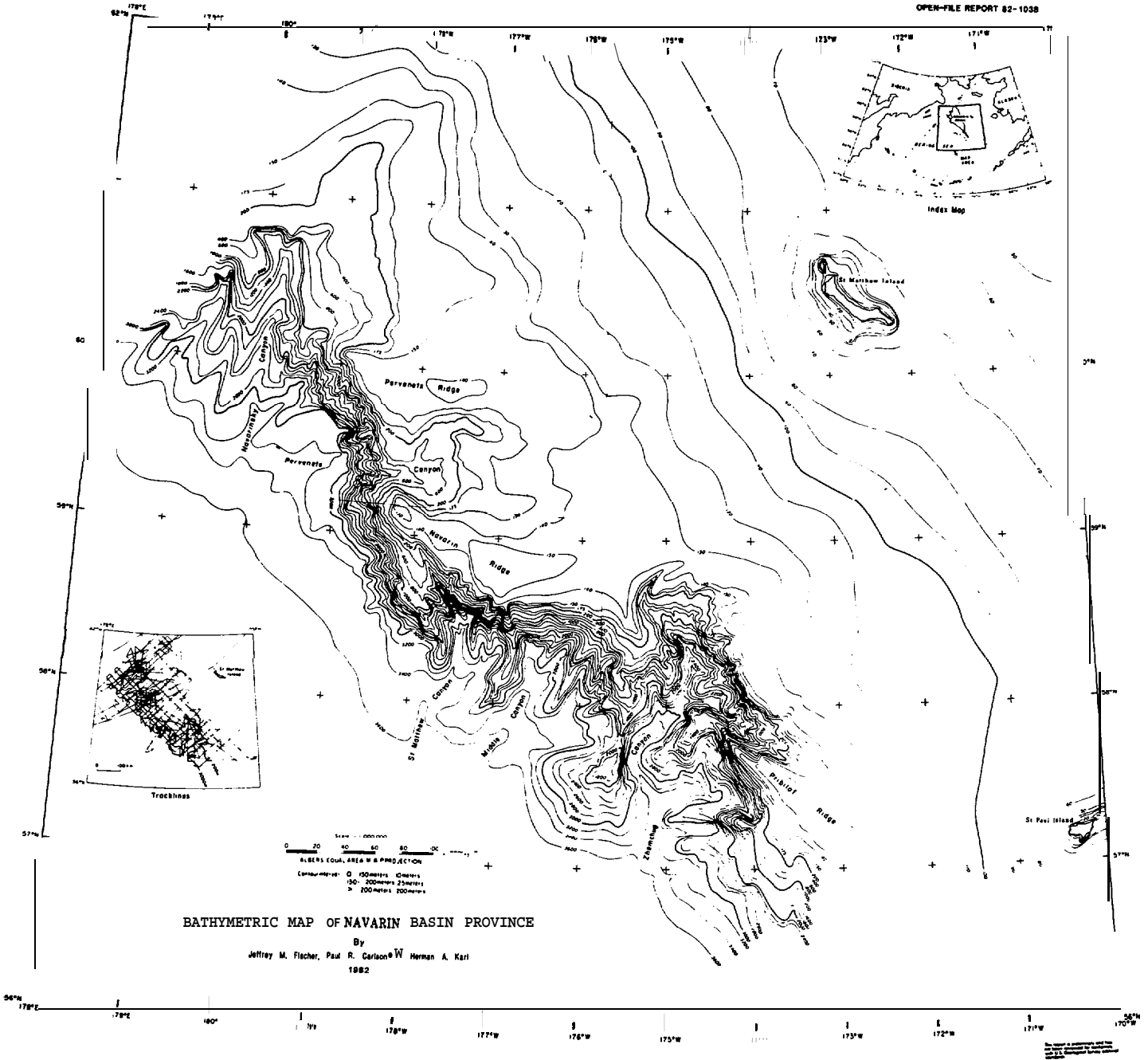


Figure 2. Bathymetric map of Navarin Basin province.

1980 and 1982 from the R/V **S.P. LEE**. We are also incorporating into our data base seismic reflection records that were collected over the past fifteen years by the **U.S.G.S.** for resource evaluation (Marlow and others, 1981). Other sources of data include studies by the University of Washington and the University of Alaska, Russian and Japanese scientists (e.g., Knebel, 1972; Sharma, 1979; Lisitsyn, 1966; Takenouti and Ohtani, 1974).

We acknowledge the assistance provided by the officers and crew of the NOAA ship DISCOVERER during the two cruises which comprise the principal source of data for this report. During DISCOVERER cruises DC **4/5-80-BS/NB** (July 2 - August 17, 1980) the scientific party collected 6700 line km of seismic reflection profiles, 104 gravity cores, 10 grab samples, and 1 dredge sample (Figs. 3, 5); 8050 line km of seismic reflection profiles, 88 gravity cores, 10 grab samples, 6 box cores, and 5 vibracores were collected during DISCOVERER cruise DC **2/3-81-BS/NB** (Figs. 4, 5). NOAA officers and survey technicians provided navigational control using LORAN C and satellite fixes.

Following is a list of the **U.S.G.S.** scientific party on each cruise.

**DC 4/5-80-BS/NB:**

Paul Carlson	Co-Chief scientist
Herman Karl	Co-Chief scientist
Brian Edwards	Engineering Geologist
Jeff Fischer	Physical Science Technician
George Ford	" " "
Sarah Griscom	" " "
Ken Johnson	" " "
Beth Lamb	Data coordinator
Grant Lichtman	Physical Science Technician
Paula Quintero	<b>Micropaleontologist</b>
Jeff Rupert	Mechanical Technician
John Saladin	Electronics Technician
Rick Vail	Electronics Technician
Tim Vogel	Geochemist
Pat Wiberg	Physical Science Technician
Bob Wilson	Mechanical Technician
Mark Yeats	Physical Science Technician

**DC 2/3-81-BS/NB:**

Paul Carlson	Chief Scientist, DC 2
Herman Karl	Chief Scientist, DC 3
Jack Baldauf	<b>Micropaleontologist</b>
Neal Barnes	Geologist
Mike Bennett	Engineering Geologist
Dave Blunt	Geochemist
Drew Comer	Geologist (MMS)
Merid Dates	Physical Science Technician
John Eriksen	Mechanical Technician
Jeff Fischer	Physical Science Technician
Dan Hurlburt	Mechanical Technician
Ken Johnson	Physical Science Technician
Jim Joyce	Physical Science Technician

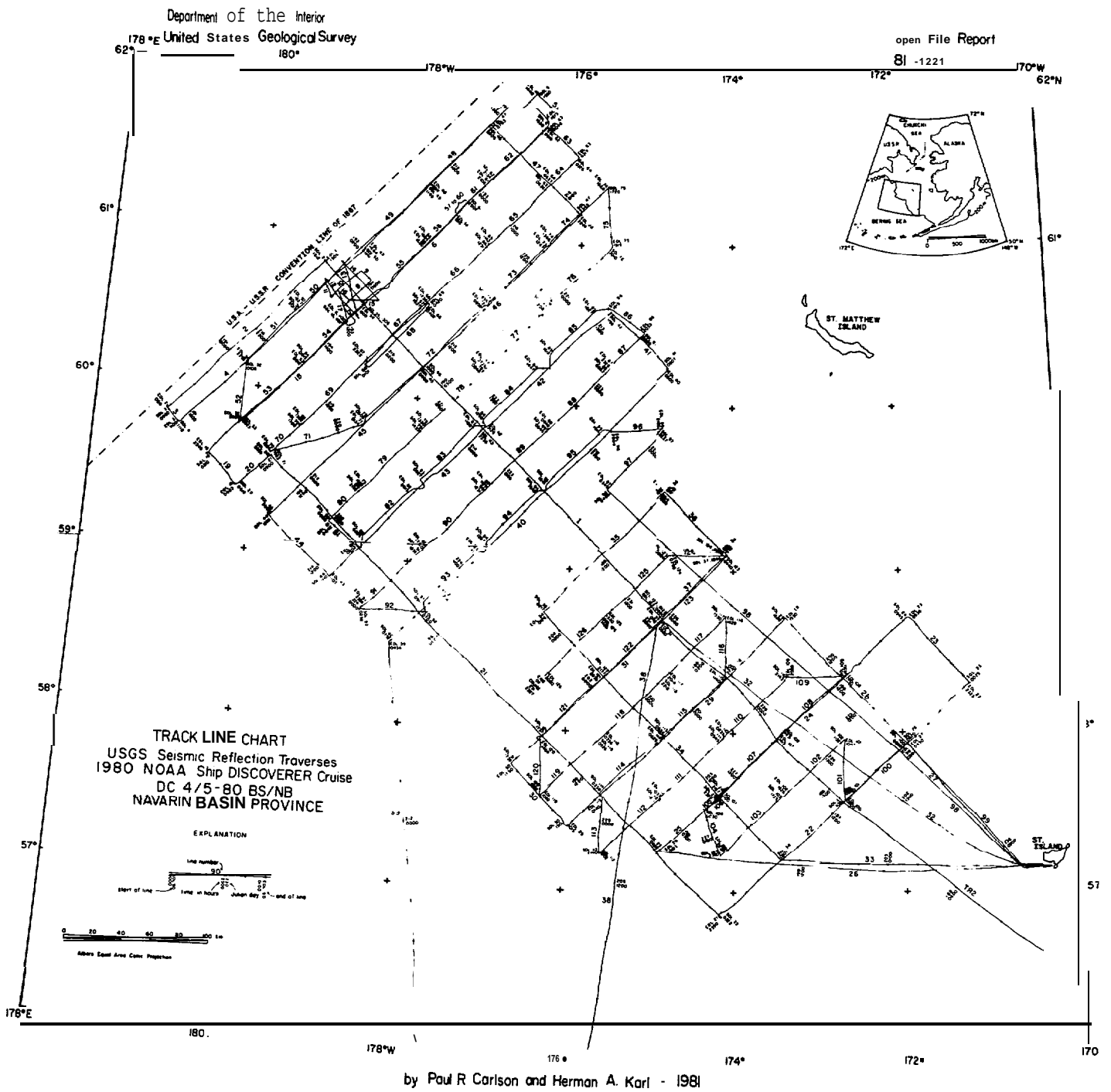


Figure 3. Track lines of high-resolution seismic reflection profiles collected during cruise DC2/3-80-BS/NB, summer 1980.

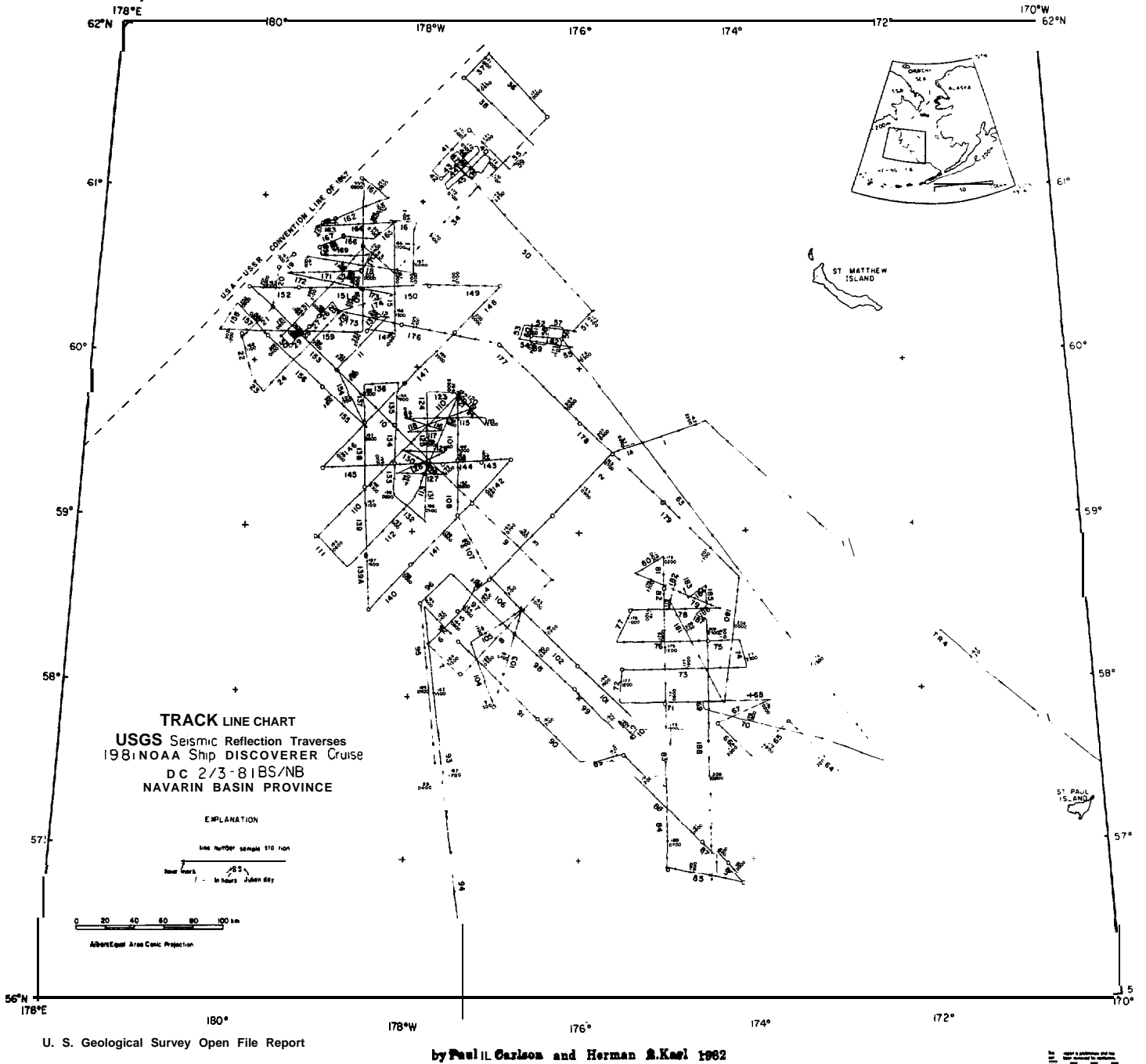


Figure 4. Track lines of high-resolution seismic reflection profiles collected during cruise DC4/5-81-BS/NB, summer, 1981.

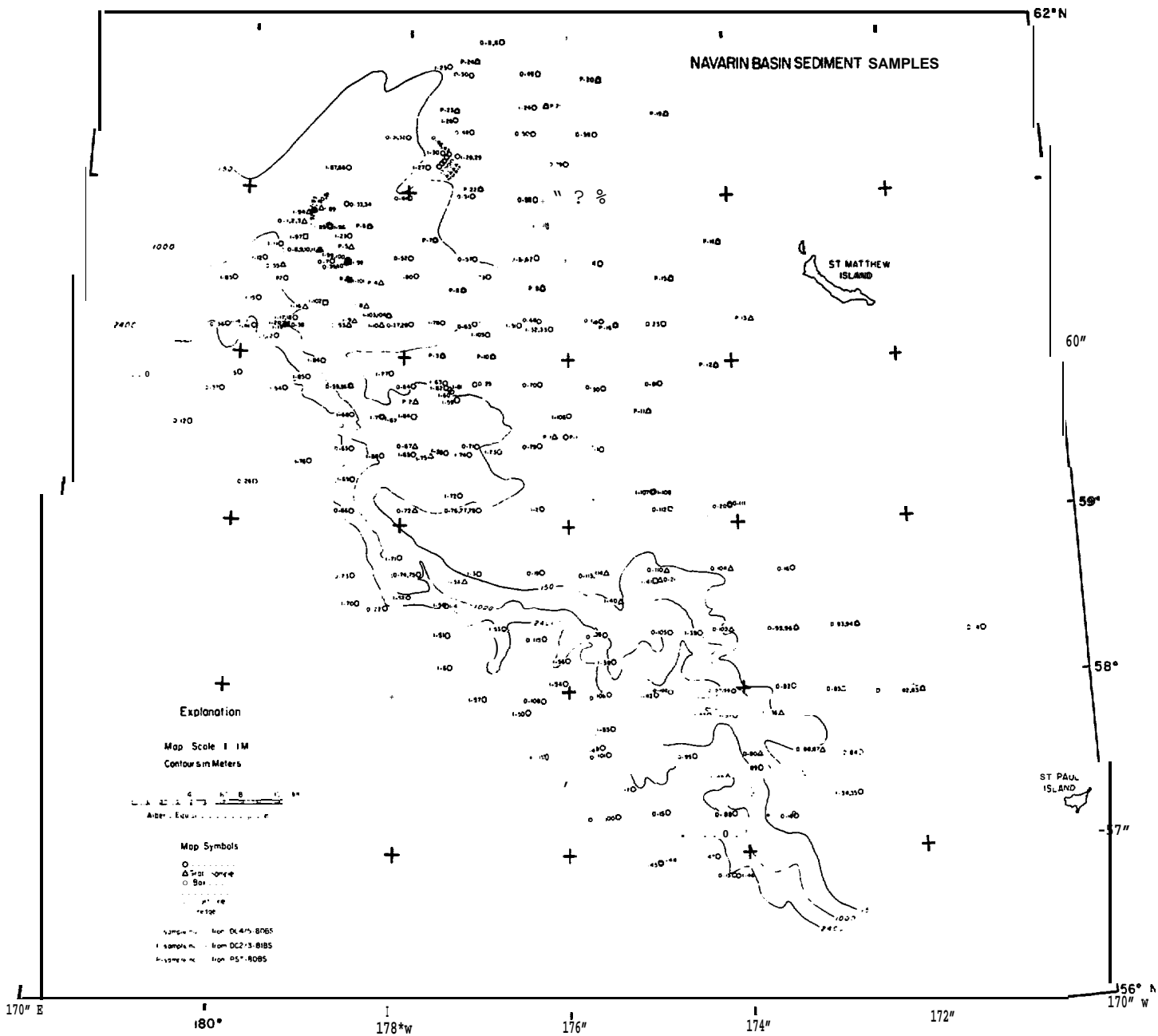


Figure 5. Locations of sediment samples.

Larry Kooker  
 Beth Lamb  
 Larry Lawver  
 Sue **McGeary**  
 Jim Nicholson  
 Robert Patrick  
 Paula Quintero  
 Robin Ross  
 John Saladin  
 Dennis Thurston  
 Tim Vogel  
 Hal Williams  
 Mark Yeats

Electronics Technician  
 Physical Science Technician  
 Geophysicist (**LDGO**)  
 Geophysicist  
 Electronic Technician  
 Electronic Technician  
**Micropaleontologist**  
 Physical Science Technician  
 Electronics Technician  
 Geologist (MMS)  
 Geochemist  
 Mechanical Technician  
 Physical Science Technician

We acknowledge also the assistance of the officers and crew of the USCG POLAR STAR and USGS R/V **S.P. LEE** and the scientific personnel on these supplemental cruises: Brian Edwards, Jeff Fischer, Richard **Garlow**, Marge Golan-Bat, Rick Herrera, Gordie Hess, Dan **Hurlburt**, Larry Kooker, Chris Larkin, Carol Madison, Bob **Mallonee**, Kevin O'Toole, Paula **Quintero**, Jim Vaughn .

#### Sampling **Methods:**

State of the art high-resolution geophysical equipment (air gun, mini-sparker, 3.5 kHz), bottom samplers (gravity corer, grab, dredge) near-bottom suspended sediment samplers, and navigation (Satellite and Loran **C**) were used to collect data on the two cruises. Spacing between track lines was approximately **30 km.**, with more closely spaced lines in selected areas. Geologic samples were collected at the intersections of **tracklines** and at locations deemed to be geologically important by the chief scientists.

The geophysical systems used on the Navarin Basin cruises were as follows:

<u>System</u>	<u>Resolution</u>
1. Air gun (up to 80 in <sup>3</sup> )	5 - 10 m
2. Minisparker (800 J)	1 - 3 m
3* 3.5 kHz	<b>1 m</b>

The bottom samplers used were: gravity corer, box corer, vibracorer, dredge, and grab samplers.

#### Analytical Methods:

The geophysical records are analyzed by standard methods, whereby slumps and shallow faults are identified by discontinuity of reflectors and by characteristic geometry, and seismic stratigraphic units are correlated by their continuity and seismic-reflection signature. The sediment cores are being studied **megascopically** and microscopically in order to classify sedimentary units and to gather data for deciphering dispersal patterns. Cores have been x-radiographed for study of internal structures that provide inferences as to depositional mechanics and **post-depositional** disturbance.

Grain size and mineralogy will be used to determine provenance and sediment pathways.

The types of analytical systems used in the **Sedimentological** Laboratory are described below:

A. General

- (1) PDP-11/34 **computer** serving as controller for several analytical devices. Used to store analyzed data and interface with the main USGS **computer**.
- (2) X-radiography unit for analyzing sedimentary structures in core samples.
- (3) Suspended sediment concentrations are determined by gravimetric analysis of material collected on filters.

B. Particle Size Analysis

- (1) Rapid sediment analyzer (height: 2.3 m; diameter: 20 cm) to measure grain-size distribution in the range of 2000 to 64 microns; fall velocities measured by a semi-conductor strain-gauge element.
- (2) **Coulter** Counter for analysis of fine-grained sediments in the size range 2 to 64 microns.
- (3) **Hydrophotometer** for analysis of fine-grained sediments in the size range 2 to 64 microns by measuring changes in light transmission.
- (4) Pipette analysis of fine-grained sediments in the size range 2 to 64 microns by measuring rate of particle setting.

C. Mineral and Chemical Analysis

- (1) **LECO** Carbon Analyzer - automatic analysis of total and organic carbon concentrations in sediments.
- (2) Carbonate Determiner attached **to** LECO unit for measuring the amount of calcium carbonate in marine sediments.
- (3) Scanning Electron Microscope (a Mini-SEM) having a capability for magnifications up to 40,000 X for viewing, identifying and photographing particulate matter.

In addition to routine geologic analysis, core samples will be subject to several routine laboratory tests to determine **geotechnical** index properties. Most routine tests will be conducted on **subsamples** from the core surface and at intervals **downcore**. Laboratory procedures will follow American Society for Testing and Materials (ASTM) standards where available.

<u>Test</u>	<u>ASTM</u>
Water content	<b>D2216</b>
Specific gravity of solids	D 854
Bulk unit weight	--
Atterberg limits	D423, 424
Vane shear strength	--

specialized tests, such as one-dimensional consolidation (ASTM D 2435) and **triaxial** compression are being conducted on replicate cores taken at a few selected stations in an endeavor **to** characterize different sedimentary facies. Core sections taken for these and other laboratory tests were sealed in wax, refrigerated and stored in an upright position until analyzed.

## **VI. - VIII. Results, Discussion, and Conclusions**

**We** have chosen to incorporate these three parts as a series of chapters to this final report. Each chapter, written by different authors, is **an** independent report on a specific topic complete within itself. **Owing** to time constraints on report submittal it was necessary for the authors to reduce and interpret great amounts of data relatively quickly, therefore we must stress the preliminary nature of these reports. The reports are organized into the following chapters:

1. Reports pertaining to Navarin Basin province published as of January 1983
2. Geologic hazards
3. Textural variations of **surficial** bottom sediment
- 4\* Rates of sediment accumulation
5. Rocks and semi-consolidated sediment from the Navarin continental margin
6. **Isopach** map of Unit A, youngest sedimentary sequence in Navarin Basin
7. Summary of **geotechnical** characteristics
8. Hydrocarbon gases in sediments - results from 1981 **field** season
9. Benthic foraminifers
10. Diatom analysis of surface samples recovered from Pervenets Canyon
11. Aspartic acid **geochronology** of mollusks
12. Appended reports and large format maps

## **IX. Needs for Further Study**

**We** have had approximately 3 months total shiptime in Navarin basin province in 1980 and 1981. During that time we have completed what is essentially a **reconnaissance** grid of seismic track lines and bottom sample stations over the 45,000 km<sup>2</sup> study area. In 1981, we not only increased systematic reconnaissance coverage but **also**, in anticipation of no further cruises, concentrated track lines and samples in those areas that contained potential geologic hazards as determined from 1980 results.

Further investigations will require that closely spaced seismic profile lines and bottom samples be located in specific sites chosen for exploratory drilling. Additionally, more closely spaced track lines are needed on a regional basis in order to map out the trace of near-surface faults and to decipher possible relationships between fault trends and zones of gas-charged sediment.

Another area of fruitful research involves the deployment of current measuring instruments to determine whether bottom currents of sufficient strength exist which may be potential hazards to pipelines and platforms. Investigations of this type also are necessary to understand the origin of the sand waves which are found in the heads of the large submarine canyons.

At least 2-3 years of additional data gathering are needed to refine our interpretations of the geology of Navarin basin province, although we feel that sufficient data has been collected for an adequate preliminary assessment of the potential geologic hazards in lease sale area **83**.

#### References

- Ahlnas, K. and Wendler, G., 1980, Meteorological parameters affecting the location of the ice edge in the Bering Sea: Transactions Am. Geophys. Union, EOS, v. 61, p. 1006.
- Cacchione, D. A., Drake, D. E., and Wiberg, P., 1982, Velocity and bottom-stress measurements in the bottom boundary layer, outer Norton Sound, Alaska: in Nelson, C. H. and Nio, S. D., eds., The northeastern Bering shelf: new perspectives of epicontinental shelf processes and depositional products: *Geologie en Mijnbouw*, v. 61, p. 71-78.
- Carlson, P. R. and Karl, H. A., 1981, High-resolution seismic reflection profiles: Navarin Basin province, northern Bering Sea, 1980: U.S. Geological Survey Open-File Report 82-1221, 4 p., 1 map, scale **1:1,000,000**.
- Carlson, P. R. and Karl, H. A., 1982, High-resolution seismic reflection profiles: Navarin Basin province, northern Bering Sea, 1981: U.S. Geological Survey Open-File Report 82-786, 5 p., 1 map, scale **1:1,000,000**.
- Coachman, L. K., Aagaard, K., and Tripp, R. B., 1975, Bering Strait, The regional physical oceanography: Seattle, Univ. of Washington Press, 186 p.
- Dan, N. H., 1881, Hydrologic des **Bering-Meer**es und der benachbarten Gewasser: *Pet. Geog. Mitt.*, v. 27, p. 361-380.
- Drake, D. E., Cacchione, D. A., Muench, R. D., and Nelson, C. H., 1980, Sediment transport in Norton Sound, Alaska: *Marine Geology*, v. 36, p. 97-126.
- Drake, D. E., Totman, C. E., and Wiberg, P. L., 1979, Sediment transport during the winter on the **Yukon prodelta** Norton Sound, Alaska: *Journal of Sedimentology Petrology*, v. 49, p. 1171-1180.
- Favorite, F., 1974, Flow into the Bering Sea through Aleutian island passes: in Hood, D. W., and Kelley, E. J., cd., *Oceanography of the Bering Sea*. Inst. Mar. *Sci.*, Univ. Alaska *Occas. Publ.* 2, p. 3-37.
- Fischer, J. M., Carlson, P. R., and Karl, H. A., 1982, Bathymetric map of Navarin Easin province, northern Bering Sea: U.S. Geological Survey Open-File Report 82-1038, 11 p., 1 map, scale **1:1,000,000**.
- Gardner, J. V., Dean, W. E., and Vallier, T. L., 1980, *Sedimentology* and geochemistry of the surface sediments, outer continental shelf, southern Bering Sea: *Marine Geology*, v. 35, p. 299-329.
- Hughes, F. W., Coachman, L. K., and Aagaard, K., 1974, Circulation, transport and water exchange in the western Bering Sea: in Hood, D. W. and Kelley, E. J., cd., *Oceanography of the Bering Sea*. Univ. Alaska Inst. Marine Science, *Occas. Publ.* 2, p. 59-98.
- Karl, H. A. and Carlson, P. R., 1982, Location and description of sediment samples: Navarin Basin province, Bering Sea, 1980-81: U.S. Geological Survey Open-File Report 82-958, 5p., 2 maps, scale **1:1,000,000**.
- Knebel, H. J., 1972, Holocene sedimentary framework of the east-central Bering Sea continental shelf: Ph.D. thesis, Univ. Washington, Seattle, 186 p.
- Kummer, J. T., and Creager, J. S., 1971, *Marine* geology and Cenozoic history of the Gulf of Anadyr: *Marine Geology*, v. 10, p. 257-280.

- Kvenvolden, K. A., Nelson, C. H., Thor, D. R., Larsen, M. C., Redden, G. D., **Rapp**, J. V., and Des **Marias**, D. J., 1979, Biogenic and thermogenic gas in gas-charged sediment of Norton Sound, Alaska: Offshore Technology Conference, Houston, Texas, Proceedings, v. 1, p. 479-486.
- Lisitsyn, A. P., 1966, Protessy **Sovremennogo Osodko'** obrazovaniya v Beringovom **More**: Akad. Nauk SSR Inst. **Okeal.**, **Moskva**, 574 p. (Recent sedimentation in the Bering Sea: Israel Program for Sci. Translations, 1969, Jerusalem; U.S. Dept. of Commerce, Clearinghouse for Federal Sci. Tech. Info., Springfield, VA, 614 p.).
- Marlow**, M. S., and Cooper, A. K., 1979, Multichannel seismic reflection profiles collected in 1977 in the northern Bering Sea: U.S. Geological Survey open-file report 79-1147.
- Marlow**, M. S., **Carlson**, P. R., Cooper, A. K., Karl, H. **A.**, McLean, H., **McMullin**, R., and Lynch, M. **B.**, 1981, Resource report for proposed OCS sale number 83 Navarin Basin, Alaska: U.S. Geological Survey open-file report 81-252, 82 p.
- Marlow**, M. S., Scholl, D. W., Cooper, **A. K.**, and Buffington, E. C., 1976, Structure and Evolution of Bering Sea shelf south of St. Lawrence Island, Bulletin of the American Association of Petroleum Geologists, v. 60, no. 1, p. 161-183.
- McManus**, D. A., **Kolla**, Venkatarathnam, Hopkins, D. M., and Nelson, C. H., 1977, Distribution of bottom sediments on the continental shelf, northern Bering Sea: U.S. Geological Survey Prof. Paper 759-C, 31 p.
- Muench, R. D., 1974, Satellite observations of Bering Sea ice: in Hood, D. w., and Takenouti, Y., **eds.**, Bering Sea oceanography: an update: Univ. Alaska, Inst. Marine Science, Report No. 75-2, p. 191-192.
- Nelson, C. H., Hopkins, D. M., and Scholl, D. W., 1974, Tectonic setting and Cenozoic sedimentary history of the Bering Sea, in Herman, **Yvonne**, cd., Marine geology and oceanography of the Arctic seas: New York, **Springer-Verlag**, p. 119-140.
- Paquette**, R. G., and **Bourke**, R. H., 1980, Winter conditions in the Bering Sea: Transactions Am. **Geophys.** Union, EOS, v. 61, p. 1006.
- Pratt, R. and Walton, F., 1974, Bathymetric map of the **Bering Shelf**: Geological Society of America, Boulder, Colorado.
- Sayles**, M. A., **Aagaard**, K., and Coachman, L. K., 1979, Oceanographic atlas of the Bering Sea **Basin**: Seattle, Univ. of Washington Press, 155 p.
- Scholl, D. W., Buffington, E. C., and **Marlow**, M. S., 1975, Plate tectonics and the structural evolution of the Aleutian Bering Sea region, in Forbes, R. B., cd., Contributions to the geology of the Bering Sea Basin and adjacent regions: **Geol. Sot. of America Spec.** Paper 151, p. 1-32.
- Scholl, D. W., Buffington, E. C., Marlow, M. S., 1976, Aleutian-Bering Sea region seismic reflection profiles: U.S. **Geol.** Survey Open-File Rept. 76-748.
- Schumacher, G. M., 1976, Bathymetric map of the Aleutian Trench and Bering Sea, U.S. Geological Survey open-file map 76-821, scale **1:2,500,000**.
- Sharma, G. D., 1979, The Alaska shelf, hydrographic, sedimentary, and **geochemical** environment: Springer-Verlag, New York, 498 p.
- Sharma**, G. D., **Naidu**, A. S., and Hood, D. W., 1972, Bristol **Bay**: model contemporary graded shelf: Am. Assoc. Petroleum Geologists, v. 56, p. **2000-20120**

- Tabata, T.**, 1974, **Movement** and deformation of drift ice as observed with sea ice radar: in Hood, **D. W.** and **Kelley, E. J.**, **eds.**, Oceanography of the Bering Sea, Univ. Alaska, Inst. Marine Science, **Occas. Publ. 2**, p. 373-382.
- Takenouti, A. Y.** and **Ohtani, K.** , 1974, Currents and water masses in the Bering Sea: a review of Japanese work: in Hood, **D. W.** and **Kelley, E. J.**, **eds.**, Oceanography of the Bering Sea, Univ. Alaska, Inst. Marine Science, **Occas. Publ. 2**, p. 39-57.
- Vallier, T. L.**, Underwood, M. B., Gardner, J. V., and Barron, J. A., 1980, Neogene sedimentation on the outer continental margin, southern Bering Sea: Marine Geology, v. 36, p. 269-287.
- Webster, B. D., 1979, Ice edge probabilities for the eastern Bering Sea: NOAA Technical Memorandum NWS AR-26, 20 p.

CHAPTER 1: REPORTS PERTAINING TO NAVARIN BASIN PROVINCE  
PUBLISHED AS OF JANUARY 1983

- Baldauf**, J. G., 1982, Identification of the Holocene-Pleistocene boundary in the Bering Sea by diatoms: *Boreas*, v. 11, p. 113-118.
- Carlson**, P. R. and Karl, H. A., 1981, Geologic hazards in Navarin Basin province, northwestern Bering Sea: U.S. Geological Survey Open-File Report 81-1217, 149 p.
- Carlson, P. R., and Karl, H. A., 1981, High-resolution seismic reflection profiles: Navarin Basin province, northern Bering Sea, 1980: U.S. Geological Survey Open-File Report 81-1221, 4 p., 1 map, scale **1:1,000,000**.
- Carlson**, P. R., and Karl, H. A., 1982, High-resolution seismic reflection profiles: Navarin Basin province, northern Bering Sea, 1981: **U.S.** Geological Survey Open-File Report 82-786, 5 p., 1 map, scale **1:1,000,000**.
- Carlson**, P. R., Fischer, J. M., and Karl, H. A., 1983, Two newly discovered submarine canyons on Alaskan continental margin of Bering Sea: U.S. Geological **Survey Open-File** Report 83-24, 36 p., 1 map, scale **1:250,000**.
- Carlson**, P. R., Karl, H. A., Fischer, J. M., and Edwards, B. D., 1982, Geologic hazards in Navarin Basin province, northern Bering Sea: 14th Offshore Technology Conference, Houston, **Tex.**, Proceedings, v. 1, p. 73-87.
- Carlson**, P. R., Karl, H. A., Johnson, K. A., and Fischer, J. M., 1981, **Morphology, sedimentology**, and genesis of three large **submarine** canyons adjacent to Navarin Basin, Bering Sea: American Assoc. Petroleum **Geol. Bull.**, V. 65, p. 909.
- Carlson, P. R., Karl, H. A., Johnson, K. A., and Fischer, J. M., 1982, Submarine canyons flanking Navarin Basin, *Bering Sea*: U.S. Geological Survey Circular (Accomplishments in Alaska), 844, p. 139-141.
- Carlson, P. R., Karl, H. A., and Quintero, Paula, 1982, Sedimentologic processes in world's largest submarine canyons, Bering Sea, Alaska: *Geol. Soc. of America*, Abstracts with Programs, v. 14, no. 7, p. 459-460.
- Fischer, J. M., **Carlson**, P. R., and Karl, H. A., 1982, Bathymetric map of Navarin **Basin** province, northern Bering Sea: U.S. Geological Survey Open-File Report 82-1038, 11 p., 1 map, scale **1:1,000,000**.
- Karl, H. A., **Cacchione**, D. A., and **Carlson**, P. R., 1982, Large sand waves in canyon heads, Bering Sea: products of internal waves or density currents: 11th International **Sedimentologic** Congress, Hamilton, Ontario, Canada, **p.** 73.
- Karl, H. A., and **Carlson**, P. R., 1981, Large sediment waves at the shelf edge, northern Bering Sea: Geological Society of America, Abstracts with Programs, v. 13, p. 483.
- Karl, H. A., and **Carlson**, P. R., 1982, Location and description of **sediment** samples: Navarin Basin province, Bering Sea, 1980-81: U.S. Geological Survey **Open-File** Report 82-958, 5 p., 2 maps, scale **1:1,000,000**.
- Karl, H. A., and **Carlson**, P. R., in press, Large sand waves in submarine canyon heads, Bering Sea: preliminary hypothesis of their depositional history: *Geo Marine Letters*, 17 **ms.p.**
- Karl, H. A., **Carlson**, P. R., and **Cacchione**, D. A., 1981, Factors influencing sediment transport at the shelf break: Am. Assoc. Petroleum **Geol. Bull.**, V. 65, p. 943.

- Karl, H. A., Carlson, P. R., and **Cacchione**, D. A., 1983, Factors that influence sediment transport at the shelf break: In: Stanley, D. J., and **Moore**, G., (editors). Shelf-slope boundary: **Critical** interface on continental margins: Society Economic Paleontologists and Mineralogists Special Publication No. 33, p. 219-231.
- Karl, H. A., Carlson, P. R., and Lamb, B., 1982, **Sediment** waves in the head of Navarinsky, Pervenets, and **Zhemchug** submarine canyons, northwestern Bering Sea: U.S. Geological Survey Circular (Accomplishments in Alaska) 844, p. **141-143**.
- Marlow**, M. S., **Carlson**, P., Cooper, A. K., Karl, H., McLean, H., **McMullin**, R., and Lynch, M. B., 1981, Hydrocarbon resource report for proposed OCS lease sale 83, Navarin Basin, Alaska: U.S. Geological Survey Open-File Report 81-252, 75 p.
- Quinterno, Paula, Blueford, J. R., and **Baldauf**, J. G., 1981, **Micropaleontologic** analysis of Navarin Basin, Bering Sea, Alaska: American Assoc. Petroleum **Geol. Bull.**, v. 65, p. 975.
- Vogel**, T. M., **Kvenvolden**, K. A., **Carlson**, P. R., and **Karl**, H. A., 1981, **Geochemical** prospecting for hydrocarbons in the Navarin Basin province: American Assoc. Petroleum **Geol. Bull.**, v. 65, p. 1004.

## CHAPTER 2: GEOLOGIC HAZARDS

by

ii. A. Karl and P. R. **Carlson**

Based on data collected during the 1980 and 1981 DISCOVERER cruises (**Carlson** and Karl, 1981; 1982; Karl and **Carlson**, 1982) and the results of an Environmental Hazards Workshop that was part of the **Navarin** Synthesis meeting convened by NOAA/OCSEAP and held in Anchorage on 25-27 October, 1982, **we** have identified 10 elements and processes that are potential hazards to commercial development of the Navarin basin province. These are:

- Sea ice
- Superstructure icing
- Waves
- Fog
- Sediment mass movement
- **Seismicity**
- Faulting
- Gas-charged sediment
- Large **bedforms**
- Unstable sediment

Sea ice, superstructure icing, **waves**, and fog obviously are not seafloor geologic hazards, and, therefore, **we** do not discuss these at length. These **enviromental** hazards are considered by other OCSEAP **investigators-**oceanographers and **meteorologists-** and specific treatments **of** these hazards are found in their reports. In this report we only mention briefly the effects of these four hazards on commercial development. Superstructure icing and fog are operational hazards and must be dealt with on a day-to-day basis. The wave climate in the Navarin area can be severe; however, industry is currently operating in areas that have a more severe wave climate, for example, the North Sea. Sea ice is a problem for part of the year in **Navarin**, however, it is less of a problem than in the Beaufort Sea which is presently being developed for oil and gas. Water depth and distance from land, **however**, are factors **which** may complicate development of Navarin basin. Consequently, structures that are now successful in the North Sea and the Beaufort Sea may require additional engineering before use in **Navarin** basin.

The six elements and processes that are seafloor geologic hazards have been described in depth in several reports and papers written and published since the 1980 annual report, Geologic Hazards in Navarin basin, **was** issued; these articles are reproduced as appendices to this report. Figure 6 shows the distribution of geohazards mapped during the 1980 and 1981 field seasons; maps of **geotechnical** indices are presented in Chapter 7 of this report.

Mass movement of sediment is ubiquitous on the slope in **water** depths greater than about 200 m and in the heads of the submarine canyons (Fig. 6; appendices F and G). Sediment mass movement is the process most likely to pose a hazard to the siting of drilling structures, production platforms, and pipelines. We are not able to assess the **recency** or the frequency of mass



failures in **Navarin** basin province. Industry has built structures in areas prone to the mass failure of sediment deposits, the Mississippi delta, for example; however, the scale of the slump and slide blocks and the water depth in **Navarin** basin province may pose additional engineering problems.

Only six earthquakes, each less than magnitude 6, have been reported from Navarin Basin Province (Meyers, 1979). This data base spans less than the last 100 years. Even though earthquakes have occurred infrequently during the historic past in Navarin basin province, the numerous examples of sediment mass movement, for want of a better triggering mechanism, suggest that frequent earthquakes of significant magnitude have occurred in the geologic past (see appendix G). **Seismicity**, must be considered in design criteria. However, as a potential hazard it is certainly less likely a problem than in an area like southern California - a region **which** has undergone extensive petroleum development.

None of the faults mapped to date show any offset of **the** Holocene seafloor. Although the ages of these faults are unknown, <sup>14</sup>C dates of sediment in the Navarin basin province indicate accumulation rates of the upper 6 m of sediment to range from about **10** to 25 cm/10<sup>3</sup>yr (**Askren**, 1972; **Knebel**, 1972; **Carlson** and Karl, Chap. 4, this report). Therefore, faults that reach within 2-3 m of the seafloor may cut sediment as young as Holocene and are considered to be active. Faulting must be considered a potential hazard, but, like **seismicity**, the probability of fault-related damage to platforms and pipelines is certainly less than that in an area like southern California.

Gas-charged sediment can have a lower shear strength and bearing capacity than does equivalent gas-free sediment (Nelson and others, 1978; Whelan and others, 1976). An increase in the concentration of free or bubble-phase gas results in an increase of pore pressure and a concomitant decrease in shear strength until failure can occur. Such increases in bubble-phase gas can result from drilling into gas-charged sediment or disruption of the sediment by cyclic loading, and this may lead to failure of pipelines or platforms (U.S. Geological Survey, 1977). Examples of gas-charged sediment identified on high-resolution seismic-reflection profiles are shown in Carlson and others (1982; appendix F) and the hydrocarbon analysis of Navarin cores is discussed in Chapter 8 of this report. **The** potential hazard of gas-charged sediment will have to be assessed by the surveying of specific sites chosen for development.

Large **bedforms** are found in the heads of the submarine canyons incising the **Navarin** continental margin (Fig. 6; appendix H). The **bedforms** occur on a **substrate** of silty, very fine sand and have wavelengths of about 600 m and heights that vary between 5-15 m. We do not know if the sand waves are active. If the sand **waves** are active, they, as well as the processes responsible for them, could represent hazards.

A regional study of **geotechnical** properties of Navarin basin sediments are discussed in Chapter 7. It will be necessary to do **geotechnical** analyses on cores collected at specific sites chosen for development in order to determine design criteria for structures with foundations on the seafloor.

## References

- Askren, D. R., 1972, Holocene stratigraphic framework southern Bering Sea continental shelf: MS thesis, Univ. of Washington, 104 p.
- Carlson, P. R. and Karl, H. A.**, 1981, High-resolution seismic reflection profiles: Navarin basin province, northern Bering Sea, 1980: U.S. Geological Survey Open-File Report 81-1221, 4 p., 1 map, scale **1:1,000,000**.
- Carlson, P. R. and Karl, H. A.**, 1982, **High-resolutin** seismic reflection profiles: Navarin basin province, northern Bering Sea, 1981: Us. *Geological Survey* Open-File Report 82-786, 5 p., 1 map, scale **1:1,000,000**.
- Carlson, P. R.**, Karl, H. A., Fischer, J. M., and Edwards, B. D., 1982, Geologic hazards in Navarin basin province, northern Bering Sea: Proceedings Offshore Tech. **Conf.**, v. 1, p. 73-87.
- Karl, H. A. and **Carlson, P. R.**, 1982, Location and description of sediment samples: Navarin basin province, Bering Sea, 1980-81: U.S. Geological Survey **Open-File** Report 82-958, 5 p., 2 maps, scale **1:1,000,000**.
- Knebel, H. J.**, 1972, Holocene sedimentary framework of the east-central Bering Sea continental shelf: Ph.D. Thesis, Univ. Washington, Seattle, 186 p.
- Meyers, H., 1979, A historical summary of earthquake epicenters in and near Alaska: NOAA Tech. Memorandum EDS **NGSDC-1,80 P**.
- Nelson, H., **Kvenvolden, K. A.**, and **Clukey, E. C.**, 1978, Thermogenic gases in near-surface sediments of Norton Sound, Alaska: **In**, Proceedings of the 1978 Offshore Technology Society, p. 2623-2633.
- U.S. Geological Survey, 1977, **An** investigation of **Pennzoil's** blow-out and loss of platform: U.S. Geological Survey unpublished administrative report, 22p.
- Whelan, T., Coleman, J. M., Robert, H. Ho, and Sukayda, J. N., 1976. The occurrence of methane in recent deltaic sediments and its effect on soil stability: Bull. of the International Association of Engineering Geology, no. 14, p. 55-64.

## CHAPTER 3: TEXTURAL VARIATION OF SURFICIAL BOTTOM SEDIMENT

by

H. A. Karl and P. R. **Carlson**

### INTRODUCTION

A total of 278 sediment sampling stations **were** occupied during the 1980 POLAR STAR cruise and the 1980 and 1981 DISCOVERER cruises (Karl and **Carlson**, 1982, Appendix C, Fig. 5). The distribution of sediment types derived from visual descriptions of surface samples reveals that (1) silts and sandy silts generally characterize the shelf and slope, (2) zones of coarser sediment (coarse silt and sand) occur at the shelf edge, on the upper slope and in the heads of submarine canyons, (3) **surficial** sediment on the shelf tends to be coarser in the southeastern part of the area than elsewhere on the shelf, and (4) muds typify the lower slope and rise (see appendix C for plot of visual descriptions) .

### METHODS

**Subsamples** taken from the gravity cores and grab samples were soaked in **H<sub>2</sub>O<sub>2</sub> solution or acetone** solution to remove oxidizable organic matter. The samples were then wet sieved on a 63 micron screen to separate mud (<63 microns) and sand (>63 microns). **If** gravel (>2 mm) was present, it was separated from sand by dry sieving. The fine fraction (<63 microns) was analyzed by standard pipette method and the sand-size material analyzed by standard rapid settling tube (**RSA**) method. Statistical parameters were calculated as moment measures.

### RESULTS

Table 1 contains the results of detailed sediment analyses of eight cores and grab samples selected as typical examples of each textural **environment** listed above (Fig. 7). All the samples are poorly sorted (Table 1, Fig. 8). Mean grain-size of the rise and slope samples is in the very fine silt class. The distribution of sediment sizes in the rise and slope samples is very similar; the samples that happen to have been chosen are both weakly **bimodal** and differ only in that the dominant mode shifts from clay (**10.5 phi**) on the rise to fine silt (6.5 phi) on the lower slope (Fig. 9). Samples from the shelf edge are considerably coarser than samples from the slope and rise with mean grain-sizes of 0.02 mm and 0.07 mm. The finer of the shelf-edge samples overlaps mean grain diameters typical of the shelf (Fig. 8). Sediment in both shelf-edge samples is concentrated in the coarser silt and finer sand classes with modes in the coarse **silt** (4.5 phi) and fine sand (3.5 phi) classes (Fig. 9). Grain-size distribution of the sample (**80-G85**) from the southeastern part of the shelf resembles shelf-edge distributions in that sediment tends to be concentrated in the finer sand and coarser silt classes with a strong mode in the coarse silt (**4.5 phi**) class (Fig. 9). Sample **80-G23** from the northwestern part of the shelf differs from sample **80-G85** in that sediment particles are more uniformly distributed over the very fine sand

Table 1. Results of grain-size analysis on selected samples

Environment	Shelf		Shelf Edge		Slope	Rise	Canyon Head	
Sample number	80-G23	80-085	87-W40	81-G63	81-G13	81-G70	81-VV75	81-VV89
Sample type	gravity core	gravity core	Van Veen	gravity	gravity	gravity	Van Veen	Van Veen
Depth of subsample (cm)	10-12	10-12	sur.	23-33	10-15	40-50	sur.	sur.
% Gravel	0.00	0.00	0.00	0.00	0.00	0.00	0.00	19.05
% Sand	10.30	20.82	74.20	21.34	5.11	3.68	94.12	76.43
% silt	59.99	67.23	22.11	61.66	57.57	51.97	4.60	3.04
% clay	29.62	11.94	3.68	16.99	37.30	44.33	1.19	0.66
Mean grain size ( $\phi$ )	6.65	5*34	3.77	5*59	7.31	7.65	2.93	2.05
Mean grain size (nun)	0.010	0.025	0.07	0.02	0.006	0.005	0.13	0.24
Std. deviation ( $\phi$ )	2.26	1.90	1.46	2.17	2.07	2.11	0.96	1.92
Skewness ( $\phi$ )	0.27	1.12	2.23	0.94	0.03	-0.18	2.15	-0.50
Kartosis ( $\phi$ )	-1.01	0.70	5.63	-0.19	-0.98	-1.07	15.73	1.10

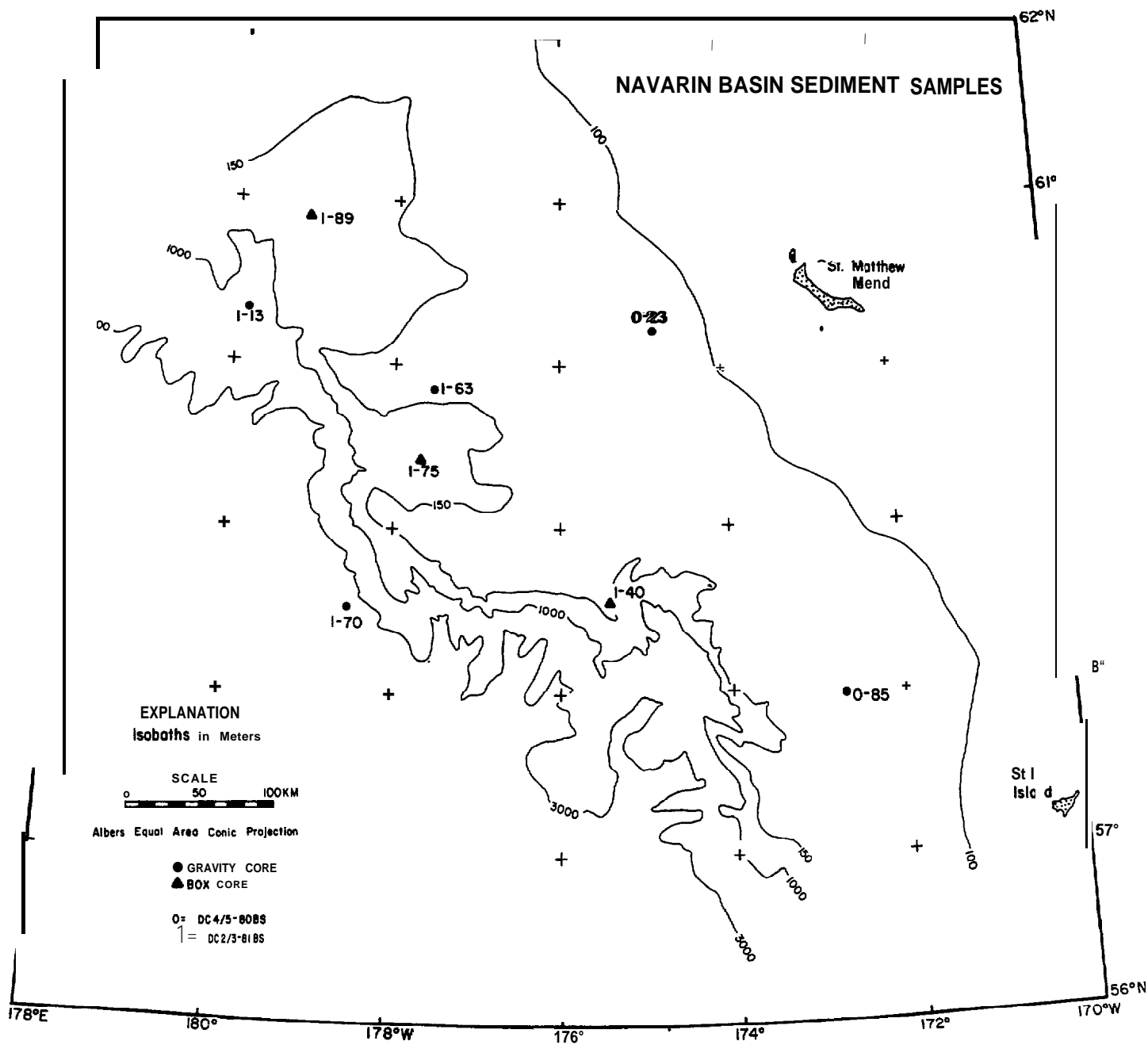


Figure 7. Location of sediment samples selected as typical examples of textural environments characterizing Navarin Basin province. (The solid triangle identifies Van Veen samples).

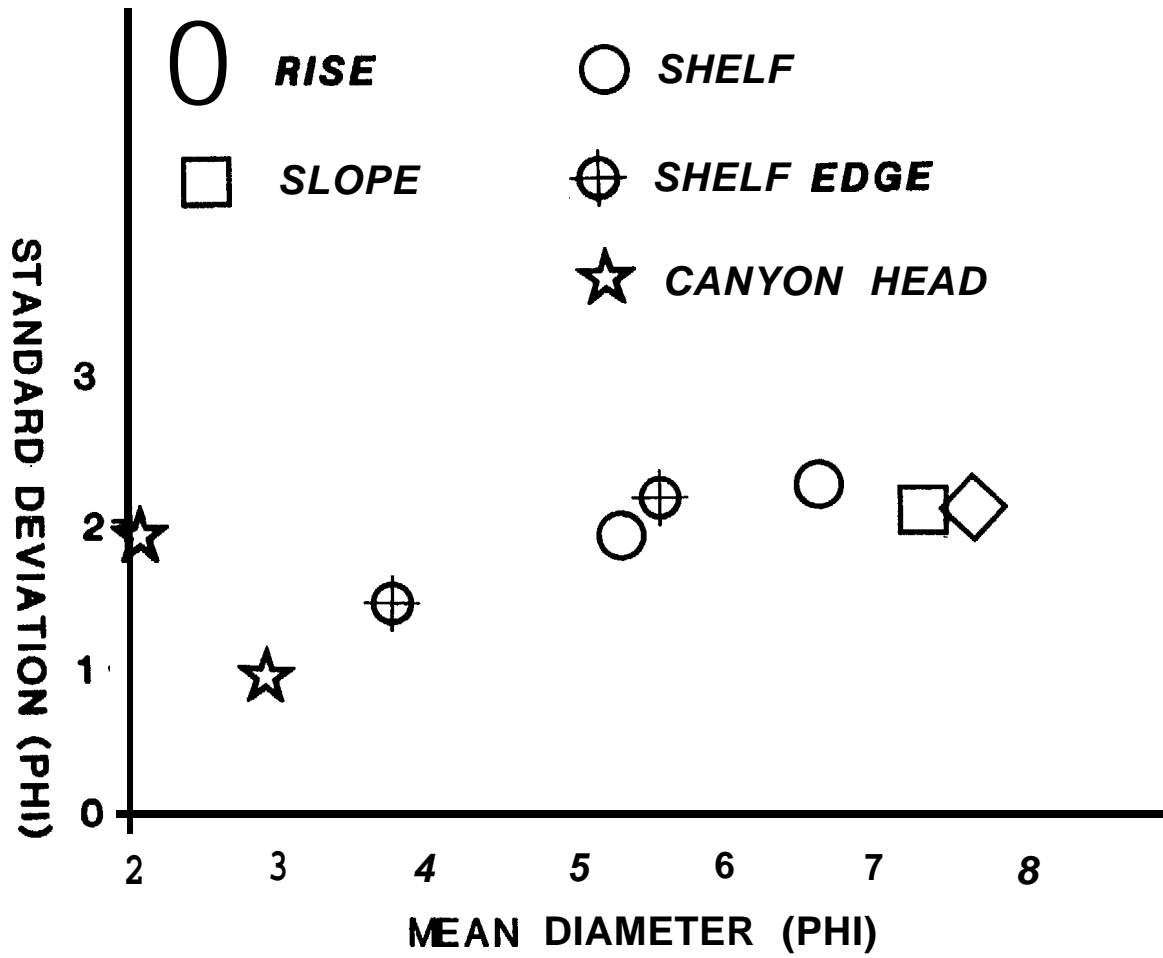


Figure 8. Plot of mean diameter vs. standard deviation.

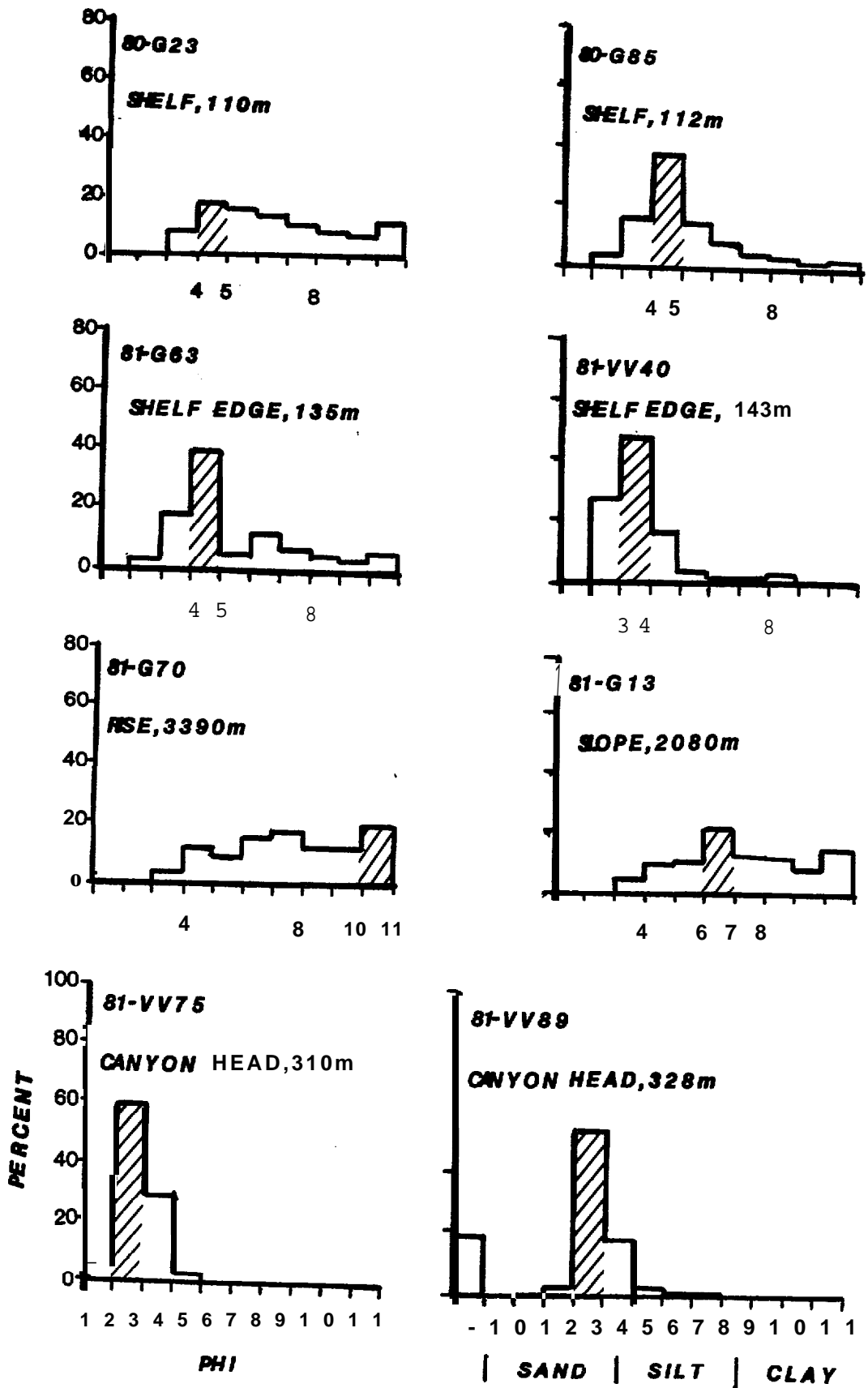


Figure 9. Histograms of selected samples. Modes identified by hachuring; dominant mode is hachured in bimodal samples.

through clay classes with a **weak** mode in the coarse silt class (Fig. 9). The coarsest mean grain-sizes occur in the heads of the submarine canyons. In the samples considered here, sediment particles are concentrated in the sand classes with a very strong mode in the fine sand (2.5 phi) class (Fig. 9).

#### DISCUSSION

Except for the samples from the rise and slope, the factors responsible for these grain-size distributions and regional textural variations are not obvious. The predominance of fine silt and clay size material in the rise and slope samples is typical of deep water environments. Depositional conditions in these environments during the low stands of sea level in the Pleistocene probably **would** not have been appreciably different than present-day conditions. This, however, is not true of the shelf and canyon heads. The zones of coarser sediment at the shelf edge and in the canyon heads could be due in part to lower sea levels when shorelines **were** at or near these areas. In **which** case coarser sediment was either supplied to the shelf edge and canyon heads by streams, for example, or energy levels were sufficiently high to **winnow** out the fines from sediment being deposited. Alternatively, the coarser sediment in these environments relative to the shelf and slope might reflect modern processes that supply sufficient energy to winnow sediment at the shelf edge and in the canyon heads. The Bering Slope Current, which flows **northward** parallel to the slope, and internal waves, which may be focused in and adjacent to the heads of the submarine canyons, are potential mechanisms to supply energy to winnow sediments. The finer shelf sediments in the northwestern section of the shelf relative to the southeastern part may indicate that relict sediment from lower sea levels is being diluted with finer material following flooding of the **shelf**; present sediment sources are over 400 km distant. These hypothesis are conjectures, however, as not enough textural data are available at present to **allow** us to choose between these interpretations.

#### REFERENCES

- Karl, H. A., and **Carlson**, P. R., 1982, Location and description of sediment samples: Navarin basin province, Bering Sea, 1980-81: U.S. Geological Survey Open-File Report 82-958, 5 p.

## CHAPTER 4: RATES OF SEDIMENT ACCUMULATION

by

Paul R. Carlson and Herman A. Karl

### INTRODUCTION

The **Navarin** basin province is located on the outer part of the flat, wide Bering continental shelf, a great distance (>300 km) from modern sources of detrital sediment. **However**, during low stands of sea level the ancestral **Anadyr** and Yukon Rivers must have transported vast quantities of sediment across the shelf to about the present-day 130 m isobath **where** the suspended and bottom sediments were entrained in the coastal currents that were sweeping through what is the present site of the Navarin basin. In order to understand the development of the Navarin continental margin, rates of accumulation of the sediment on the margin must be determined. This chapter presents some **preliminary** estimates of sediment accumulation rates based upon C-14 measurements of gravity core sub-samples from the **Navarin** shelf, slope, and rise.

### DATA COLLECTION AND ANALYSIS

Gravity cores (8 cm diameter) **subsampl**ed for radiocarbon dating **were** collected on two cruises of the NOAA ship DISCOVERER in 1980 and 1981 (Karl and **Carlson**, 1982). A total of 22 cores were selected for dating (Table 2; Fig. 10). The cores collected on both the 1980 and 1981 cruises were split longitudinally and described while at sea. After each cruise, preliminary studies of core descriptions (including X-radiographs) , **microfaunal** contents, organic carbon measurements, and interpretations of high-resolution seismic reflection records were utilized to select the cores for radiocarbon dating. The **working** half of each selected core was carefully sub-sampled to avoid the "smear-affect" along the core-liner. Sufficient sediment was collected to provide the analyst with about one gram of carbon from the "whole-core" samples. The intervals sampled from each core are listed in Table 2. Analyses **were** performed by the USGS radiocarbon dating lab in Menlo Park, California, for the 1980 cores and by Geochron Labs\* in Cambridge, Massachusetts for the 1981 cores.

Calculations of preliminary rates of sediment accumulation (Table 3) are based on the assumption of a constant rate of sediment deposition to a depth in the core of the mid-point of the sampled interval.

**\*Any use of trade names** in this publication is for descriptive purposes **only** and does not constitute endorsement by the **U.S.** Geological Survey.

Table 2. C-14 dates of Navarin samples

<u>Core No.*</u>	<u>Depth in core (cm)</u>	<u>C-14 date (yrs BP)</u>	<u>Water depth (m)</u>
o- 12	211-230	16,670 ± 100	3164
0- 13	188-228	5,580 * 45	2692
0- 13	245-270	34,520 * 490	"
0- 26	188-222	10,880 ± 80	3373
0- 26	235-260	33,990 ± 610	"
0- 26	322-333	33,300 ± 1800	"
0- 33	65- 90	28,980 ± 2200	210
0- 33	210-240	28,200 * 3000	"
0- 42	170-183	13,650 * 100	141
0- 44	125-145	14,900 ± 110	138
0- 66	65- 84	19,370 ± 160	1336
0- 66	325-335	37,500 * 1200	"
0- 66	380-385	>32,000	"
0-115	170-200	9,505 ± 300	2870
0-115	237-262	19,990 * 1400	"
1- 02	100-130	11,755 * 395	143
1- 03	0- 30	7,375 ± 270	133
1- 15	65- 90	5,330 ● 180	2750
1- 15	250-275	15,975 ± 850	"
1- 31	160-190	8,815 * 355	137
1- 32	160-190	7,500 * 305	130
1- 44	65- 90	4,460 ± 190	3400
1- 44	220-245	10,925 * 365	"
1- 58	25- 50	9,215 ± 310	179
1- 58	60- 88	>37,000	"
1- 58	240-265	>27,000	"
1- 65	25- 50	10,485 ± 355	436
1- 65	160-185	>32,000	"
1- 66	65- 90	>37,000	580
1- 67	65- 90	17,725 ± 680	167
1- 88	65- 90	>29,000	205
1- 88	350-375	>37,000	"
1-105	160-190	8,385 ± 310	144
1-106	160-190	8,700 ± 355	135
1-107	65- 90	8,900 * 290	116

\* o = DC 4/5-80 1 = DC 2/3-81

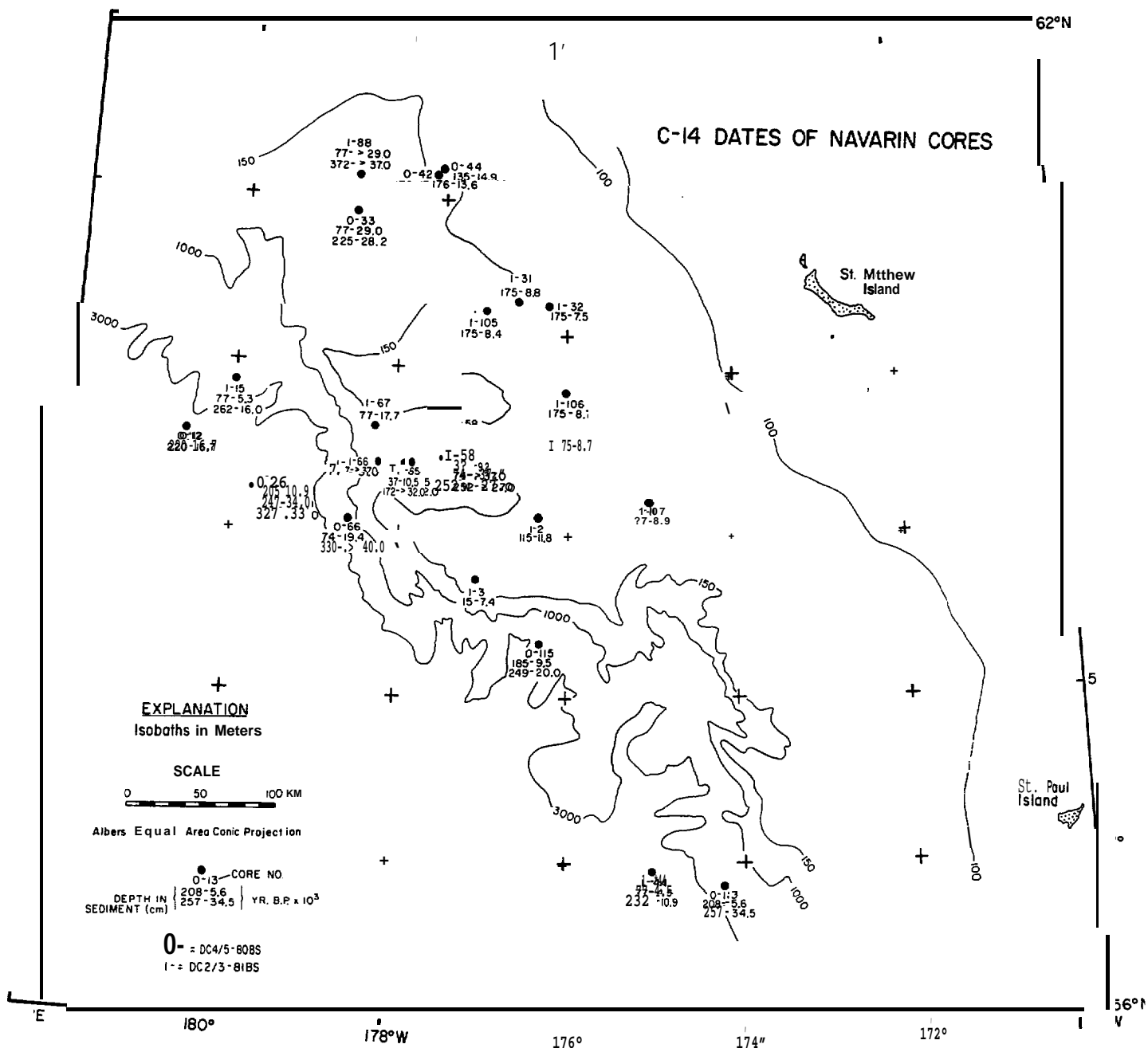


Figure 10. Location map of cores subsampled for C-14 dating.

Table 3. C-14 dates and rates of sediment accumulation listed by water depth.

	<u>Core No. *</u>	<u>Water Depth (m)</u>	<u>C-14 Date (yrs BP)</u>	<u>Depth in core (cm)</u>	<u>Rate of Accumulation (cm/1000 yrs)</u>
Shelf	1-107	<b>116</b>	8,900	77	8.8
	1- 32	<b>130</b>	7,500	175	23.3
	1- 03	<b>133</b>	7,375	15	2*0
	1-106	<b>135</b>	8,700	<b>175</b>	20.1
	0- 44	<b>138</b>	14,900	135	9.1
	1- 31	<b>137</b>	8,815	<b>175</b>	19.9
	0- 42	<b>141</b>	13,650	176	12.8
	1- 02	<b>143</b>	11,755	115	9.8
	1-105	<b>144</b>	8,385	175	20.9
<hr/>					
Slope (upper)	1- 67	<b>167</b>	17,725	77	4.4
	<del>1-</del> 58	<b>179</b>	9,215	37	4.1
	"	"	>37,000	74	<2.0
	"	"	>27,000	252	<9*4
	1- 88	205	>29,000	77	<2.7
	"	"	>37,000	363	<9.8
	<del>o-</del> 33	<b>210</b>	28,980	77	2.7
	"	"	28,200	225	8.0
	1- 65	436	10,485	37	3.6
	"	"	>32,000	172	5.4
1- 66	580	>37,000	77	<2.1	
<hr/>					
Slope (lower)	0- 66	<b>1,336</b>	<b>19,370</b>	74	3.9
	"	"	> <b>37,500</b>	330	8.8
	"	"	> <b>32,000</b>	382	11.9
	o- 13	2,692	<b>5,580</b>	208	37.1
	"	"	<b>34,520</b>	257	7.5
	1- 15	2,750	<b>5,330</b>	77	14.6
	"	"	<b>15,975</b>	262	16.5
	<b>0-115</b>	2,870	<b>9,505</b>	185	19.5
	"	"	<b>19,990</b>	249	12.5
	<hr/>				
Rise	o- 12	<b>3,164</b>	<b>16,670</b>	<b>220</b>	<b>13.3</b>
	0- 26	<b>3,373</b>	<b>10,880</b>	<b>215</b>	<b>19.8</b>
	"	"	<b>33,990</b>	<b>247</b>	<b>7.3</b>
	"	"	<b>33,300</b>	<b>327</b>	<b>9.9</b>
	1- 44	<b>3,400</b>	<b>4,460</b>	<b>77</b>	<b>17.5</b>
	"	"	<b>10,925</b>	<b>232</b>	<b>21.3</b>

\*o = DC 4/5-80; 1 = DC 2/3-81

## DISCUSSION

If we compare the rate of sediment accumulation with water depth (Table 3), some trends emerge for the various physiographic subdivisions of the Navarin continental margin. The average rate for all the shelf subsamples (<150 m water depth) analysed is 14.1 cm/10<sup>3</sup> yrs. However, a plot of these values (Fig. 11) shows that the samples make up two groups. A cluster of four cores located between the heads of Navarinsky and Pervenets canyons have an average rate of sediment accumulation of 21 cm/10<sup>3</sup> yrs, whereas shelf sediment north and south of the cluster averages 8.5 cm/10<sup>3</sup> yrs, including a low value of 2 cm/10<sup>3</sup> yrs from a core taken less than 10 kilometers from the shelf-slope break. The four cores that have an average rate of 21 cm/10<sup>3</sup> yrs plot near the center of greatest sediment thickness in Navarin basin (Chapter 6, this volume). Previous sedimentologic studies in the region illustrate the variable nature of the rates of sediment accumulation on the Bering shelf. Knebel (1972) reported rates ranging from 2.5 to 40 cm/10<sup>3</sup> yrs for cores collected northeast of Navarin basin. Askren (1972) reported rates ranging from 11 to 67 cm/10<sup>3</sup> yrs for cores collected along the southeastern edge of Navarin basin.

Accumulation rates of sediment cored on the upper slope range from 2 to nearly 10 cm/10<sup>3</sup> yrs, with an average value of 5 cm/10<sup>3</sup> yrs (Table 3). Eight of eleven of these subsamples yielded dates greater than 25,000 yrs BP, half of which came from sediment less than one meter deep in the core, suggesting either a very slow rate of deposition or erosion of some of the surficial sediment,

Cores from the lower slope range in accumulation rates from about 4 to 37 cm/10<sup>3</sup> yrs with an average of 15 cm/10<sup>3</sup> yrs (Table 3). Age dates from the upper meter of these cores, except O-66 which was obtained from mid-slope depths, are less than 10,000 yrs B.P. indicating a much more rapid rate of deposition than on the upper slope. An explanation for the large difference in rates between upper and lower slope may be the widespread mass movement that has been noted on the Navarin continental slope (Carlson, Karl, Fischer, and Edwards, 1982), resulting in removal of sediment from the upper slope and deposition on the lower slope and rise.

Continental rise sediment apparently has accumulated at rates ranging from about 7 to 21 cm/10<sup>3</sup> yrs, with an average rate of nearly 15 cm/10<sup>3</sup> yrs (Table 3). Some of the cores from lower slope and rise depths that are associated with the large submarine canyon systems contain coarse, graded layers attributed to turbidity current deposition (Carlson, Karl, and Quinterno, 1982). Deposition recorded by these cores that contain coarse layers interbedded with hemiplagic muds must be episodic, which very likely accounts for the variability in core O-26 for example (Table 3).

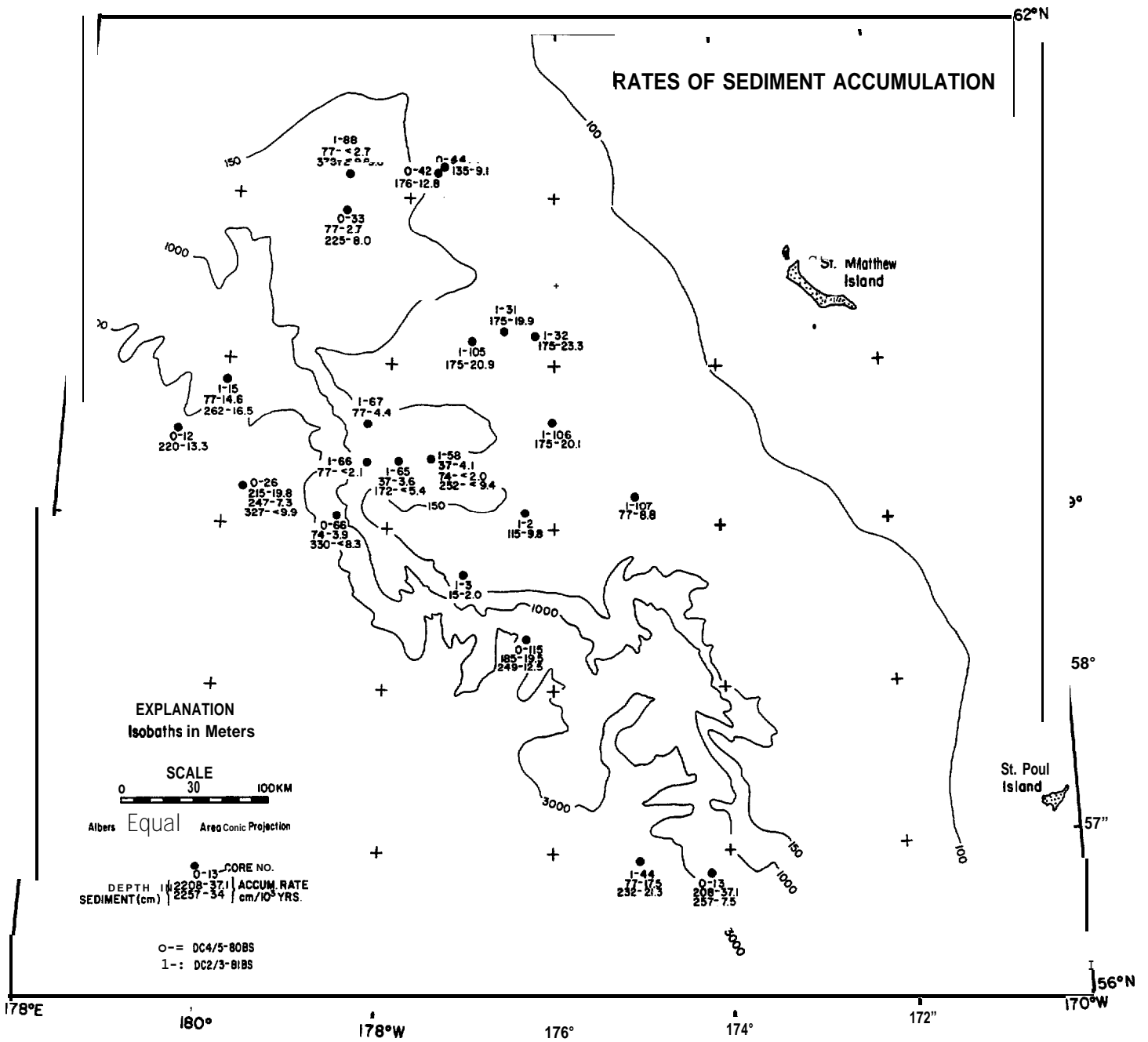


Figure 11. Map of dated cores showing calculated preliminary accumulation rates of sediment.

## REFERENCES

- Askren, D. R., 1972, Holocene stratigraphic framework - southern Bering Sea continental shelf: **M.S.** Thesis, Washington, Univ., Seattle, 104 p.
- Carlson, P. R., Fischer, J. M., Karl, H. A., and Larkin, C., 1983, **Isopach** map of unit A, youngest sedimentary sequence in **Navarin** basin, Bering Sea, in Karl, H. A. and **Carlson, P. R. eds.**, Surface and Near-surface Geology, **Navarin Basin** Province: Results of the 1980-81 Field Seasons: U.S. Geological Survey Open-File Report 83- , in press.
- Carlson, P. R.**, Karl, H. A., and Quinterno, P., 1982, **Sedimentologic** processes in world's largest submarine canyons, Bering Sea, Alaska: Geological Society of America, Abstracts with Programs, v. 14, no. 7, p. 459-460.
- Carlson, P. R.**, Karl, H. A., Fischer, J. M., and Edwards, B. D., 1982, Geologic hazards in Navarin Basin province, northern Bering Sea: 14th Offshore Technology Conference, Houston, Texas, Proceedings v. 1, p. 73-87.
- Karl, H. A. and **Carlson, P. R.**, 1982, Location and description of sediment samples: Navarin basin province, Bering Sea, 1980-81: U.S. Geological Survey **Open-File** Report 82-958, 5 p., 2 map sheets, scale **1:1,000,000**.
- Knebel, H. J.**, 1972, Holocene sedimentary framework **of the** east-central Bering Sea continental shelf: Ph.D. Thesis, Washington, Univ., **Seattle**, 186 p.

CHAPTER 5: **PRE-QUATERNARY** ROCKS AND SEMI-CONSOLIDATED SEDIMENT  
FROM THE NAVARIN CONTINENTAL MARGIN

by

Paul R. **Carlson**, Jack G. **Baldauf**, and Christopher Larkin

INTRODUCTION

The purpose of this chapter is to describe pre-Quaternary rocks and **semi-consolidated** sediment that have been collected from the outer shelf and slope of the Navarin basin province (see appendix D, Fischer and others, 1982, for a bathymetric map of the area). This chapter also compares these samples to rocks dredged from other parts of the Bering continental margin.

Although many of the samples **we** collected in 1980 and 1981 on cruises of the NOAA ship DISCOVERER (Karl and **Carlson**, 1982) are limited to the unconsolidated Holocene sediment blanket that covers most of the **Navarin** province, a few of the gravity cores penetrated through thin spots in the Holocene sediment *cover* into the underlying Pleistocene unit (**Baldauf**, 1982; **Quinterno**, 1981). Also, **two** gravity cores recovered semi-consolidated Tertiary-age strata that was cropping out on the continental slope. In addition to these cores, **we** also collected one chain-bag dredge of **pre-Quaternary** rocks from a steep scarp on the south side of **Zhemchug** Canyon. The locations of these three samples (1 dredge and 2 cores) are shown in figure 12.

**Pre-Quaternary** rocks also have been dredged from the Navarin margin from the USGS RV **S.P. LEE** (**Marlow** and others, 1979; Jones and others, 1981; see Fig. 12). Additional dredge samples were collected along the Bering margin south of Navarin basin from the RV **THOMAS G\* THOMPSON** (Hopkins and **others**, 1969) and from the USGS RV SEA SOUNDER (**Vallier** and others, 1980).

RESULTS

Preliminary analyses of samples **we** collected in the Navarin province in 1980 and 1981 show that **two** cores and a single dredge haul recovered **pre-Quaternary** age material.

Core 80-106 (DC 4/5-80-106). Core 106 was taken from the lower continental slope at a water depth of 1785 m on the north side of a ridge separating Middle and **Zhemchug** Canyons (Fig. 12). This gravity core recovered 55 cm of very stiff olive gray (5Y 3/2) clayey silt with shale chips scattered throughout the lower 15 cm of the recovered interval. Diatoms from this **semi-lithified** core **were** assigned to the *Denticulopsis seminae* var. *fossilis* - *D. kamtschatica* zone of Barron (1980) which is the age equivalent of early late-Pliocene. An organic carbon analysis of a **subsample** (10-12 cm depth) from this core produced a value of 0.36 percent.

Core 81-46 (DC 2/3-81-46). Gravity core 46 **was** collected from the base of the continental slope south of **Zhemchug** Canyon in water 2530 m deep (Fig. 12). The 70 cm long core contained the most distinctive color change of

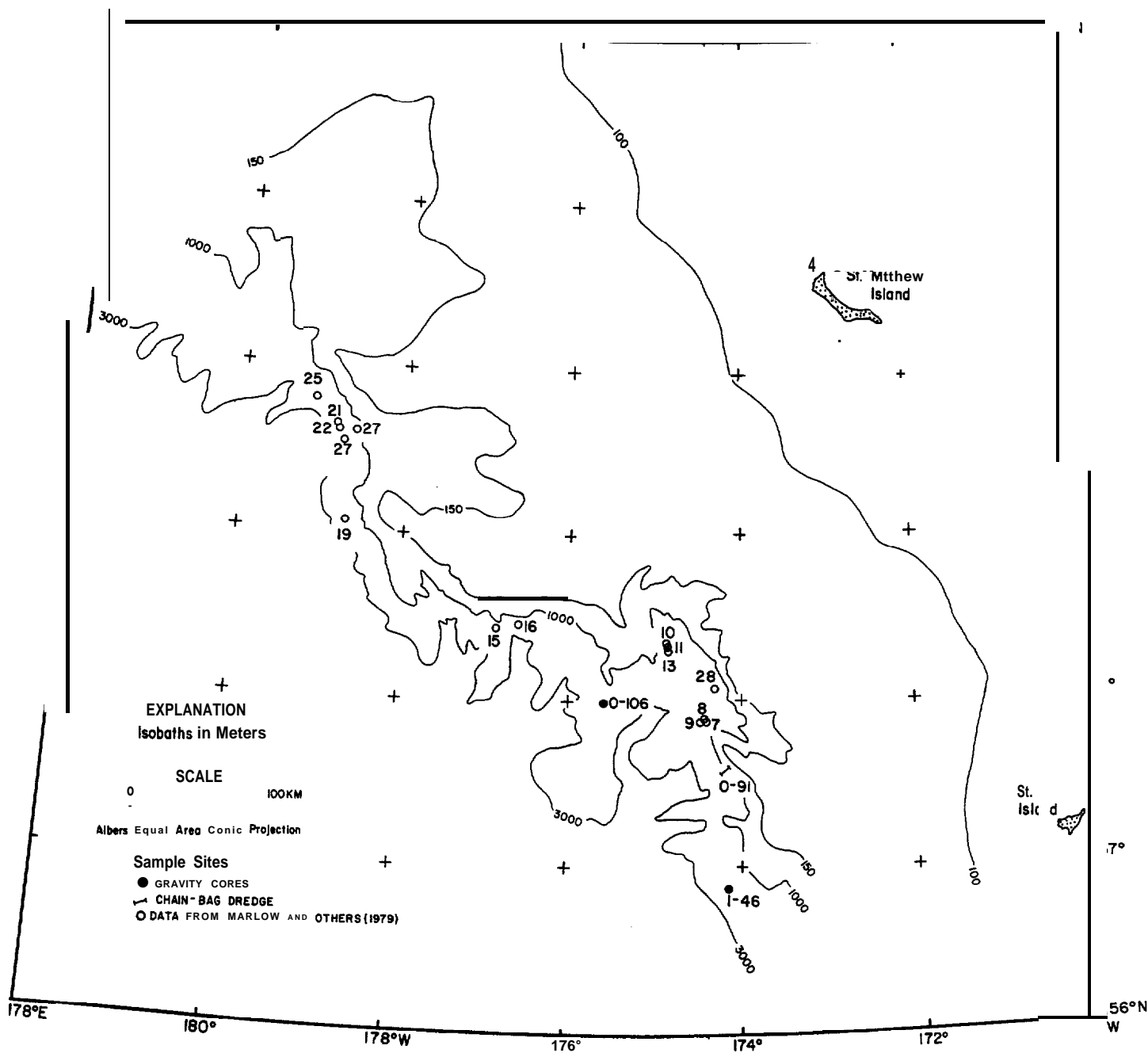


Figure 12. Locations of dredge hauls and gravity cores, Navarin margin.

any of the cores we collected. The upper 28 cm consisted of light olive brown (5Y 5/6) mud. At about 27-30 cm, there was an abrupt color change to a dark olive green gray (5GY 4/1) mud. There **was no** apparent textural change. Organic carbon contents of these two different colored muds was very similar, 0.41% at 11-15 cm and 0.48% at 45-49 cm. Clay mineral content in the two muds was quite different, however, with the upper unit containing 61% **smectite**, 18% **illite**, and 21% kaolinite plus chlorite compared to 46% smectite, 24% **illite**, and 30% **kaolinite** plus chlorite in the lower unit. Diatoms from both color units in this core are late Pliocene in age.

Dredge-1 (DC 4/5-80-91). A steep scarp on the **wall** of **Pribilof** Ridge, south of the main axis of **Zhemchug** Canyon (Fig. 12), was sampled by chain bag dredge in water depths between 2200 and 268 m. The excessive depth range of the dredge haul was due to a faulty tensiometer on the deep-sea winch, resulting in uncertainty of **when** the dredge was in contact with the seafloor. The dredge recovered a rather wide variety of rocks including one piece of ultra-basic rock (**Pyroxenite**), several small pieces of basalt, a large (40X28 cm) angular boulder of greenstone (probably metamorphosed basalt), several pieces of highly indurated conglomerate, an angular piece of black **argillite**, a small fragment of limestone, a small piece of **calcareous** siltstone, a small piece of **calcareous** sandstone, **and** many pieces of diatomaceous **mudstone**.

The cobble-size piece of limestone **was** found to be barren of **calcareous** nannofossils and of pollen and spores, thus not datable. The diatoms in the **numerous** pieces of mudstone provided age information ranging from early to late Miocene and the calcareous sandstone contained reworked mid-late Miocene diatoms.

Organic carbon contents of the mudstones range from 0.24% to 0.77% and average 0.56%. Carbonate carbon contents of the mudstones were all 0.01% or less. The **calcareous** siltstone has an organic carbon content of 0.79% and an inorganic carbon value of 3.63%. The limestone fragment consists of 0.72% organic and 7.28% inorganic carbon. The sandstone had the lowest organic carbon content of all samples measured (**0.12%**), but yielded an inorganic carbon value of 2.74%. Our carbon values agree quite closely with those reported by **Vallier** and others (1980), for rocks south of Navarin that yielded average organic carbon values of 0.52% and with Jones and others (1981) for mudstones from the northern half of the Bering margin, especially the Navarin margin, that have average organic carbon values of 0.55%. The inorganic carbon content of those mudstones averaged 0.08%. Jones and others (1981) also reported values from volcanic sandstones and tuffs that averaged 0.28% organic and 0.70% carbonate carbon, and from muddy and tuffaceous limestones that averaged 0.64% organic and 7.36% carbonate carbon. By way of comparison with the Tertiary **mudstone** samples dredged from the Bering margin, average organic carbon values of 93 **Quaternary-age** muds and sandy muds from cores **we** collected throughout the Navarin basin province was 0.83%, with the values ranging from 0.26% to 1.56%; inorganic carbon values also **were** higher than those of the Tertiary **mudstones**, averaging 0.13%, and ranging from 0.03% to 0.57% (Fischer, 1981).

A point count of 400 grains in a thin section of the mid-late Miocene sandstone (**DC4/5-80-91**) yielded a composition of quartz 37%, feldspar **17%**, rock fragments 40% (61% of **r.f.** are volcanic), **glauconite** 3%, heavy minerals 2%, and others 1% including diatoms, and forams. The grains are sub-angular to sub-rounded, poorly-sorted, and range in size from fine sand to granules; the intergranular cement consists of microcrystalline calcite and makes up about 30% of the sample. According to Folk (1974), this sandstone **would** be classified as a **submature calcareous** volcanic arenite.

#### REFERENCES

- Baldauf, J. G.**, 1982, Identification of the Holocene-Pleistocene boundary in the Bering Sea by diatoms: *Boreas*, v. 11, p. 113-118.
- Barron, J. A., 1980, Lower Miocene to Quaternary diatom biostratigraphy of Leg 57, off northeastern Japan, Deep Sea Drilling Project, **In, Honza, E.** and others, Initial Reports of the Deep Sea Drilling Project, p. 641-685: Washington, D. C. (U.S. Government Printing Office).
- Fischer, J. M., 1981, Carbon contents of Navarin basin sediments, **In, Carlson, P. R. and Karl, H. A. (eds.)**, Seafloor Geologic Hazards, **Sedimentology**, and Bathymetry: Navarin Basin Province, Northwestern *Bering Sea*: **U.S. Geological Survey Open-File Report 81-1217**, p. 44-57.
- Fischer, J. M., **Carlson, P. R.**, and Karl, H. A., 1982, Bathymetric map of Navarin continental margin, Bering Sea: **U.S. Geological Survey Open-File Report 82-1038**, 11 p., 1 map sheet **1:1,000,000**.
- Folk, R. L., **1974**, Petrology of sedimentary rocks: **Hemphill Publishing Co.**, Austin, Tex. 182 p.
- Hopkins, D., Scholl, D. **W.**, **Addicott, W. O.**, Pierce, R. L., Smith, P. **B.**, Wolfe, J., Gershenovich, D., **Kotenev, B.**, **Lohrman, J. E.**, **Lipps, J. H.**, and **Obradovich, J.**, 1969, Cretaceous, Tertiary, and early Pleistocene rocks from the continental margin in the Bering Sea: *Geological Society of America, Bull.* 80, p. 1471-1486.
- Jones, D. **M.**, Kingston, M. J., **Marlow, M. S.**, Cooper, A. K., Barron, J. A., Wingate, F. H., and **Arnal, R. E.**, 1981, Age, mineralogy, physical properties, and geochemistry of dredge samples from the Bering Sea continental margin: U.S. Geological Survey Open-File Report 81-1297, 68 p.
- Karl, H. A. and Carlson, **P. R.**, 1982, Location and description of sediment samples: **Navarin** Basin province, Bering Sea, 1980-81: U.S. Geological Survey **Open-File Report 82-958**, 5 p., 2 maps, scale **1:1,000,000**.
- Marlow, M. S.**, Cooper, A. K., Scholl, D. **W.**, **Vallier, T. L.**, and McLean, H., 1979, Description of dredge samples from the Bering *Sea* continental margin: U.S. Geological Survey Open-File Report **79-1139**.
- Quinterno, P. J.**, 1981, Preliminary report on benthic foraminifers from Navarin basin province, Bering Sea, Alaska, **In, Carlson, P. R. and Karl, H. A., (eds.)**, Seafloor Geologic Hazards, **Sedimentology**, and Bathymetry: Navarin Basin Province, Northwestern Bering Sea: **U.S. Geological Survey Open-File Report 81-1217**, p. 114-129.
- Vallier, T. L.**, **Underwood, M. B.**, Gardner, J. V., and Barron, J. **A.**, 1980, Neogene sedimentation on the outer continental shelf margin, southern Bering Sea: *Marine Geology*, v. 36, p. 269-287.

CHAPTER 6: **ISOPACH** MAP OF UNIT A, YOUNGEST SEDIMENTARY  
SEQUENCE IN NAVARIN BASIN

by

Paul R. **Carlson**, Jeffrey M. Fischer,  
Herman A. Karl, and Christopher Larkin

INTRODUCTION

**Navarin** Basin as defined by Marlow and others (1976) consists of a thick (>12 km) section of Mesozoic and Cenozoic sedimentary material that covers an area of **49,700** km<sup>2</sup> on the northwestern portion of the Bering continental shelf (Fig. 13). The main part of the basin, as delineated by the 2 km **isopleth**, is oriented northwest-southeast, parallel to the shelf-slope break.

The principal map in this chapter shows the thickness of only the uppermost unit, herein referred to as unit A, of the **Navarin** basin sedimentary sequence (Fig. 14). Figure 13 provides a comparison of the area covered by the **isopached** Unit A and the entirety of Navarin basin as mapped by Marlow and others (1979).

DATA COLLECTION AND REDUCTION

The high-resolution seismic-reflection data used in the development of the unit A **isopach** map were collected on cruises of the NOAA ship DISCOVERER in 1980 (DC 4/5-80) and 1981 (DC 2/3-81) (**Carlson** and Karl, 1981; 1982). Navigational control was by Loran C updated by satellite "fixes." Thicknesses of sediment seen on 3.5 kHz and **minisparker** records were measured on a digitizing table at five minute intervals. The Unit A was defined by a relatively flat-lying strong, persistent reflector that marked the base of the uppermost sedimentary unit (Fig. 15). This reflector could be traced with confidence throughout the mapped portion of the basin. The edges of the **isopached** area mark either an area where the reflector crops out at the seafloor (at least appears to do so within the limits of resolution of the high-resolution profiles) or the reflector cannot be traced further due to one of three factors (1) poor quality records, (2) disappearance or loss of strength of the reflector, or (3) insufficient track line coverage.

DISCUSSION

Unit A, the uppermost **seismic-stratigraphic** unit in the Navarin basin sequence, has been mapped over an area of 100,000 km<sup>2</sup> on the outer shelf in the northern Bering Sea (Fig. 14). This unit consists of unconsolidated sediment that ranges in type from clayey silt to muddy sand (Karl and **Carlson**, 1982) of Quaternary age (**Baldauf**, 1981). The average thickness of this unconsolidated unit is about 20 m. Unit A attains a maximum thickness of 45 m within a **narrow** (5-10 km wide) elongate trough located near the southeastern edge of **Navarinsky** Canyon, and just east of the deepest part of Navarin Basin (Fig. 13). This trough is part of a broader (40 km wide), shallower (30 m thick) depression filled with unit A sediment, that parallels

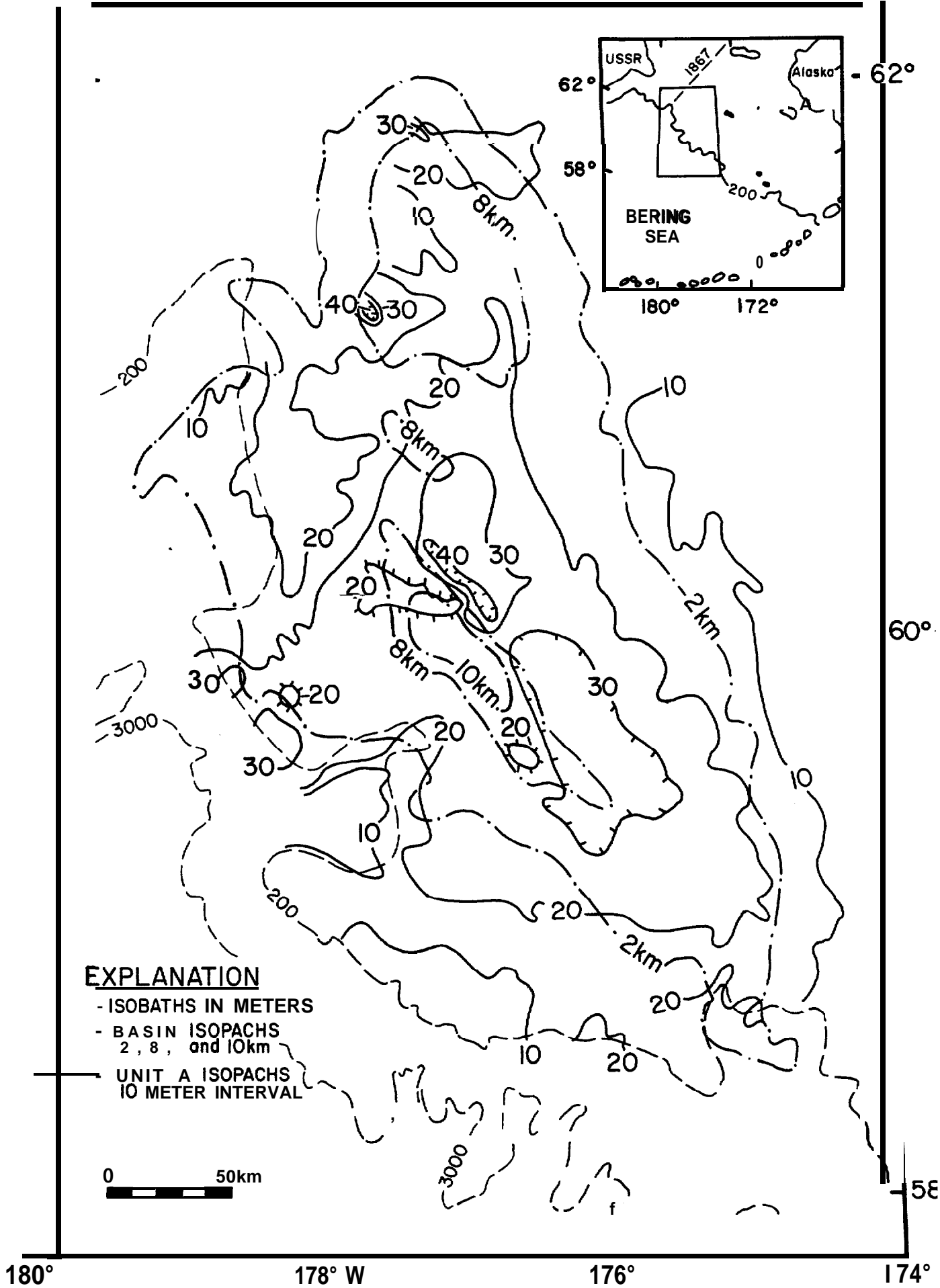


Figure 13. Isopach map of unit A superimposed on selected isopachs of strata above acoustic basement. Navarin Basin isopach above basement after Marlow and others (1979).

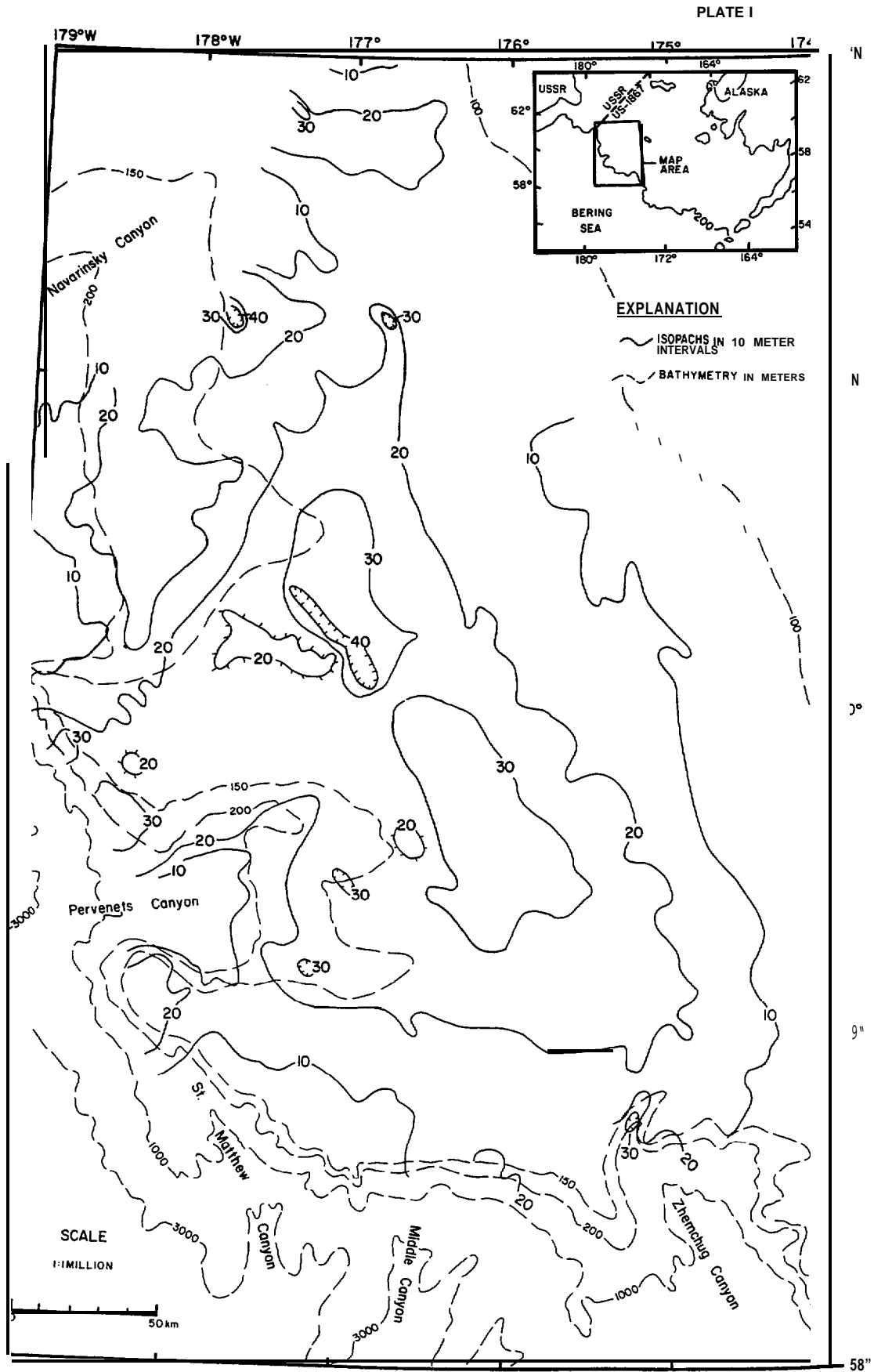


Figure 14. Isopach map of unit A, youngest stratigraphic sequence in Navarin Basin.

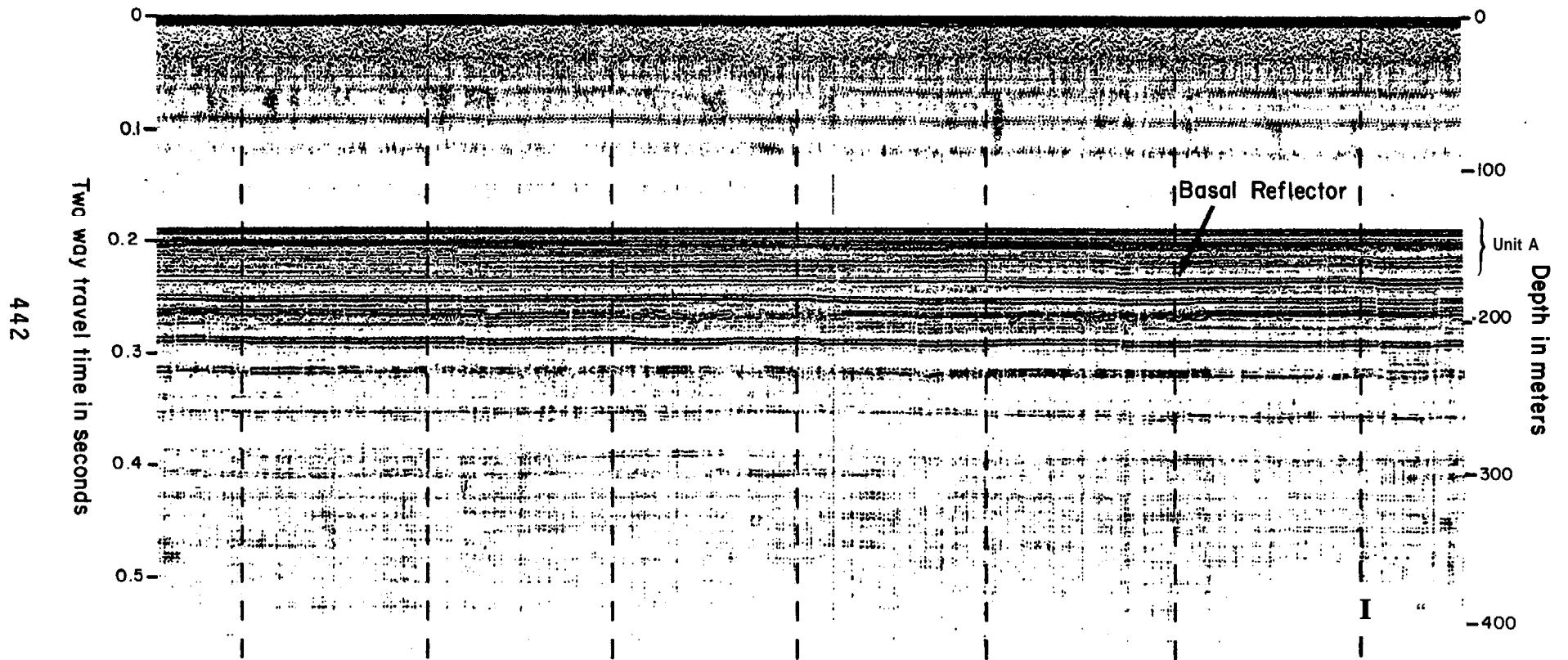


Figure 15. Minisparker profile (1000 J) showing seismic reflector (marked by arrow) that marks the base of isopached unit A. Vertical exaggeration  $\sim 8.5x$ .

the shelf break **in** present water depths of 130-150 m. The **isopached** unit pinches out to **the** northwest near the head of **Navarinsky** Canyon and also near the head of Pervenets Canyon. We have collected gravity cores near both canyons across **the** area of the outcropping reflector and are attempting to date this unit. At this **time**, we can only estimate that Unit A is less than 30,000 yrs **B.P.** based on C-14 dates and **faunal** data obtained from cores collected near the **"pinchouts"** {see Chapter 4).

#### REFERENCES CITED

- Baldauf, J. G.**, 1981, Diatom analysis of late Quaternary sediments from Navarin Basin province, Bering Sea, Alaska, **in** **Carlson, P. R.** and Karl, H. A., **eds.**, Seafloor geologic hazards, **sedimentology**, and **bathymetry**: Navarin Basin province, northwestern Bering Sea: U. S. Geological Survey Open-File Report 81-1217, p. 100-113.
- Carlson, P. R.** and Karl, **H. A.**, 1981, High-resolution seismic reflection profiles: Navarin Basin province, northern Bering Sea, 1980: U.S. Geological Survey Open-File Report 81-1221, 4 p., 1 map, scale **1:1,000,000.**
- Carlson, P. R.** and Karl, **H. A.**, 1982, High-resolution seismic reflection profiles collected in 1981 in Navarin Basin province, Bering Sea: U.S. Geological Survey open-File **Report** 82-786, 5 p., 1 map, **scale 1:1,000,000.**
- Karl, H. A. and **Carlson, P. R.**, 1982, Location and description of sediment samples: **Navarin** Basin province, Bering Sea, 1980-81: U.S. Geological Survey **Open-File** Report 82-958, 5 p., 2 map sheets, scale **1:1,000,000.**
- Marlow, M. S., Scholl, D. W., Cooper, A. K., and Buffington, E. C., 1976, Structure and evolution of Bering Sea shelf south of St. Lawrence Island: American Association of Petroleum Geologists Bulletin, v. 60, **p.** 161-183.
- Marlow, M. S.**, Cooper, A. K., Parker, A. W., and **Childs, J. R.**, 1979, **Isopach** map of strata above acoustic basement in the Bering Sea: **U.S.** Geological Survey Miscellaneous Field Studies Map **MF-1164.** 1 map sheet, scale **1:2,500,000.**

## CHAPTER 7: SUMMARY OF GEOTECHNICAL CHARACTERISTICS

by

Brian D. Edwards and Homa J. Lee

### INTRODUCTION

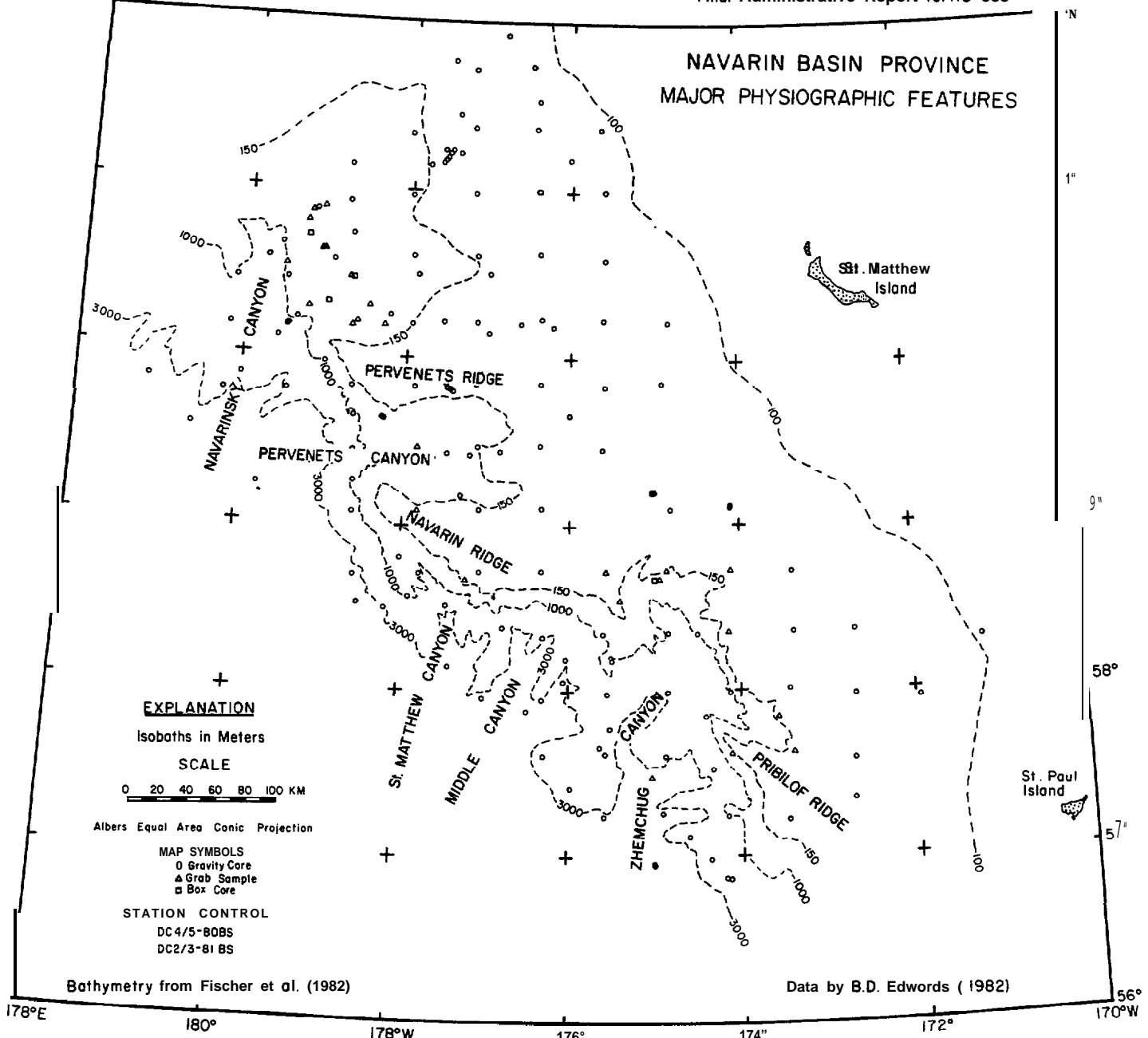
**Geotechnical** properties were determined on recovered cores as a means of assessing sedimentary processes of engineering importance. One such property, the estimated in-place shearing strength, is a critical sediment **geotechnical** property used **in** the evaluation of geologic hazards. Also determined were index properties and consolidation (i.e., relative degree of compaction) characteristics of the sediment. Index properties (e.g., undrained vane shear strength, water content, and grain-size distribution) were measured to classify the sediment and to correlate with advanced strength test results. Consolidation properties were measured to correlate with relative shearing strength (**Ladd** and **Foott**, 1974) and to determine the effects of past geologic events (e.g., erosion of overburden).

Figure 16 shows major **physiographic** features **in** the **Navarin** Basin province. Of the 212 gravity cores and grab samples collected from the R/V DISCOVERER in 1980 and 1981 (Fig. 16), 149 were analyzed for **geotechnical** information. The majority of these cores were analysed only for simple index properties (**vane** shear strength and water content). Seven cores from the 1980 R/V DISCOVERER cruise were taken as replicate cores at selected coring sites (**Fig. 17**). Each replicate core was **analysed** for the index properties listed above in addition **to** grain specific gravity, **Atterberg** limits, one-dimensional consolidation characteristics, and static and cyclic **triaxial** shear strength.

After collection, each core was cut into multiple sections onboard ship using a rotary knife blade cutter. Core sections, excluding those of replicate cores, were split longitudinally using a specially designed cutting system and a wire saw. Although sample disturbance is aggravated by such longitudinal splitting, this procedure allows more frequent **downcore** testing while maintaining sample integrity for other analyses (e.g., X-ray radiography, photography, and textural analysis). Testing for **undrained** vane shear strength and water content **subsampling** was conducted onboard ship.

The replicate cores collected for more advanced **geotechnical** testing were sectioned as described above, but were not split longitudinally. Vane shear tests were conducted and water content **subsamples** were taken **at** the top of each unsplit core section. End caps were sealed on both ends of each core section. The core sections were then wrapped in cheesecloth, sealed with a non-shrinking, microcrystalline wax, **labelled**, and stored vertically under refrigeration. The replicate cores were shipped by refrigerated air transport from Kodiak, Alaska, to refrigerated storage facilities at the U.S. Geological Survey laboratory in Palo Alto, California. These cores were subsequently shipped by refrigerated freight to **Ertec** Western, Inc., a commercial **geotechnical** testing laboratory in Long Beach, California, for advanced **geotechnical** analyses.

NAVARIN BASIN PROVINCE  
MAJOR PHYSIOGRAPHIC FEATURES



**EXPLANATION**

Isobaths in Meters

**SCALE**

0 20 40 60 80 100 KM

Albers Equal Area Conic Projection

**MAP SYMBOLS**

- Gravity Core
- ▲ Grab Sample
- Box Core

**STATION CONTROL**

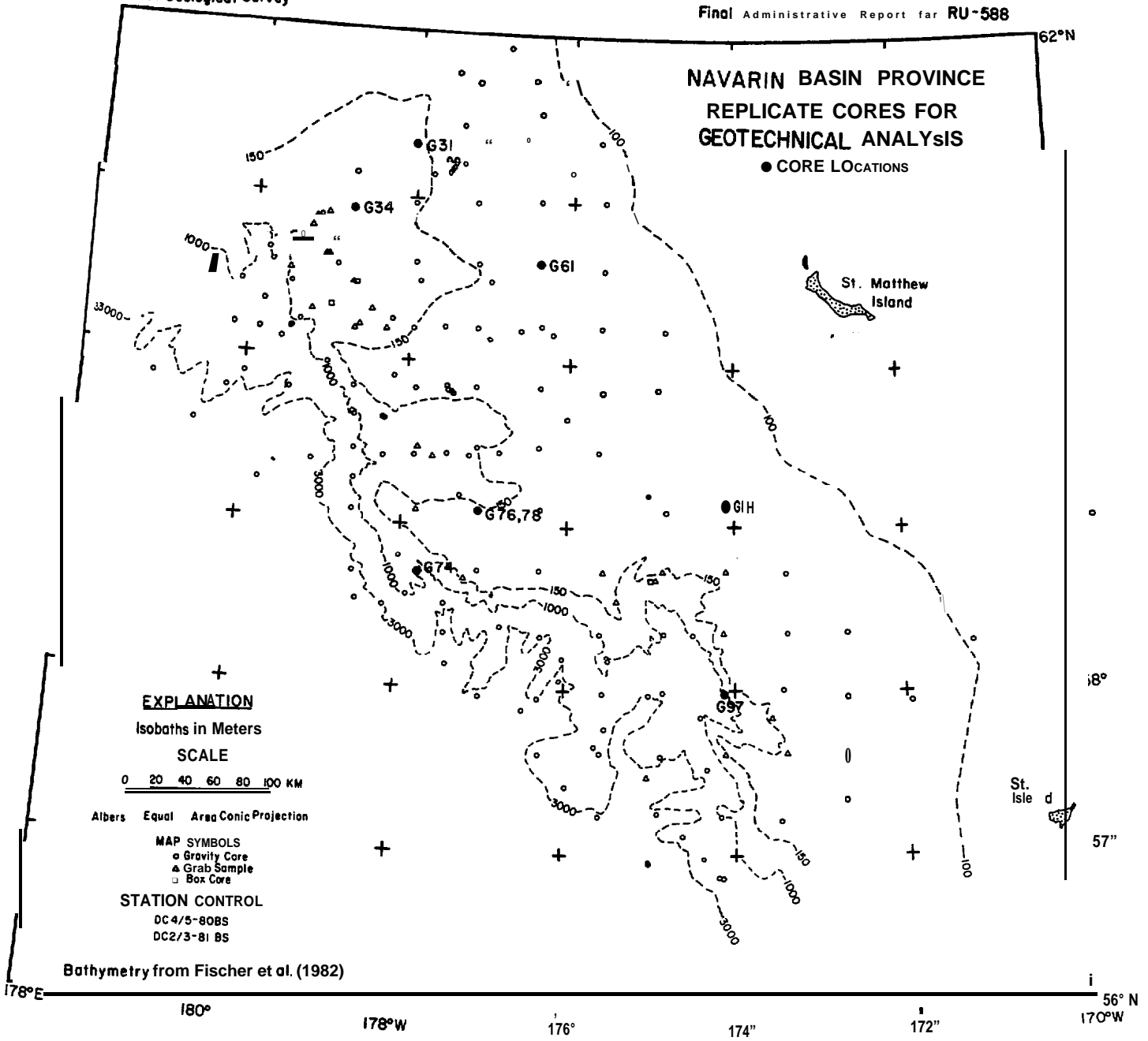
- DC 4/5-80BS
- DC 2/3-81BS

Bathymetry from Fischer et al. (1982)

Data by B.D. Edwards (1982)

THIS REPORT IS PRELIMINARY AND HAS NOT BEEN REVIEWED FOR CONFORMITY WITH U.S. GEOLOGICAL SURVEY EDITORIAL STANDARDS

Figure 16. Major **physiographic** features of **Navarin Basin province** {after Fischer et al., 1982), and core locations for 1980 and 1981 R/V DISCOVERER cruises.



THIS REPORT IS PRELIMINARY AND HAS NOT BEEN REVIEWED FOR CONFORMITY WITH U.S. GEOLOGICAL SURVEY EDITORIAL STANDARDS.

Figure 17. Location map of replicate cores collected for advanced geotechnical testing of Navarin Basin province sediment, 1980 R/V Discoverer cruise.

## TESTING PROGRAM

### Index Property Tests

#### Undrained Vane Shear Strength

Methods. Strength measurements were made using a motorized Wykeham-Farrance miniature vane shear device. Tests were made with a four-bladed 1/2 inch vane which was inserted into the cores so the top of the vane was buried by an amount equivalent to blade height. Torque was applied to the vane by either a torque cell that rotates the vane directly, or by a calibrated spring. Rotation rate of the torque cell and the top of the calibrated spring was a constant 90° per minute. When the spring system was used, torsion was measured and correlated directly with torque applied at the vane. Because of the spring's flexibility, rotation rate at the vane changed throughout the test. Tests were made on the ends of each core section and at 20 cm intervals on longitudinally split core sections.

Undrained vane shearing strength ( $S_v$ ), as determined with the Wykeham-Ferrance device, was calculated from peak torque by assuming that the sediment builds a peak shearing resistance everywhere, and at the same time, along a right-circular cylinder inscribed around the vane. This term ( $S_v$ ) is commonly equated with the undrained shear strength of the sediment ( $S_u$ ); tests were made in the triaxial testing program to assess the validity of this method.

Findings. Figure 18 presents a comparison of vane shear strength as determined on split and unsplit sections with the torque cell and calibrated spring. The method of torque measurement (spring vs torque cell) and the core state (split vs unsplit) appeared to have little impact on the general trend of the shear strength versus depth variation.

The Navarin Basin province can be divided into 3 morphologic zones: (1) the shelf, typically shallower than the 150 m isobath; (2) the shelf edge and uppermost slope (about 150 to 200 m); and (3) the continental slope and continental rise (about 200 m to 3600 m). The shelf edge and uppermost slope is typically a zone of sand and muddy sand (Karl and others, 1981). Because vane shear strengths of cohesionless sediments such as those at the shelf edge have little value due to pore water drainage during sampling and testing, the zone of cohesionless sediment has been identified and excluded from the data base for undrained vane shear strength.

The areal distribution of vane shear strength at subbottom depth intervals of 1 m is shown in Figures 19-23. Data control is shown by the large, solid circles. At a subbottom depth of 1 m on the shelf, undrained vane shear strengths range from 2 kPa to 22 kPa. A zone of relatively weak sediment (<10 kPa) occupies the shelf about 150 km west of St. Matthew Island. West of this zone, adjacent to Pervenets Ridge, is a zone of relatively high (>15 kPa) shear strength. To the southeast, near the head of Zhemchug Canyon, is another zone of relatively high (>10 kPa) shear strength.

The few cores that recovered more than 2 m of sediment on the shelf were all less than 3 m long and were concentrated in the northern part of the area



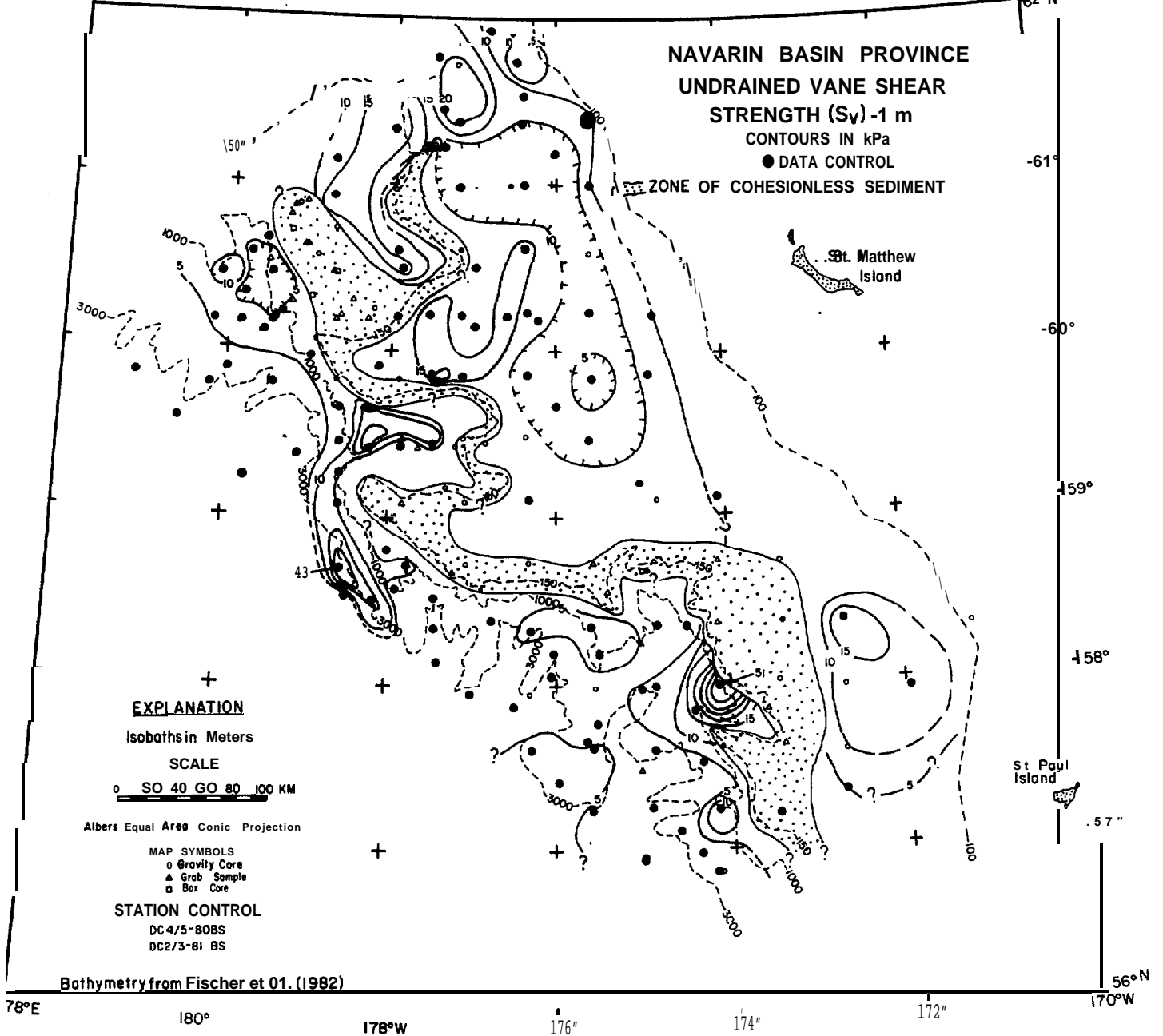
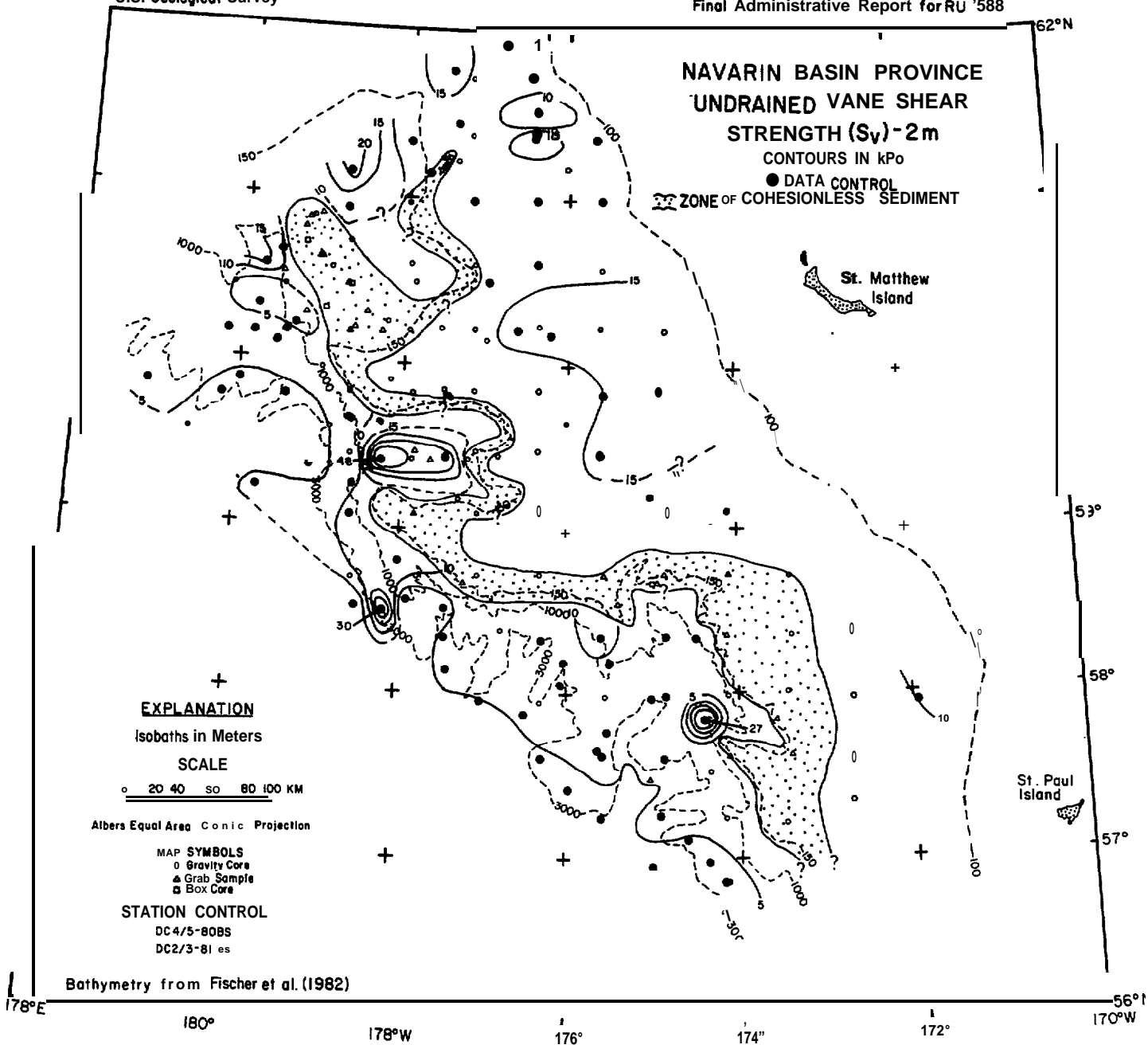
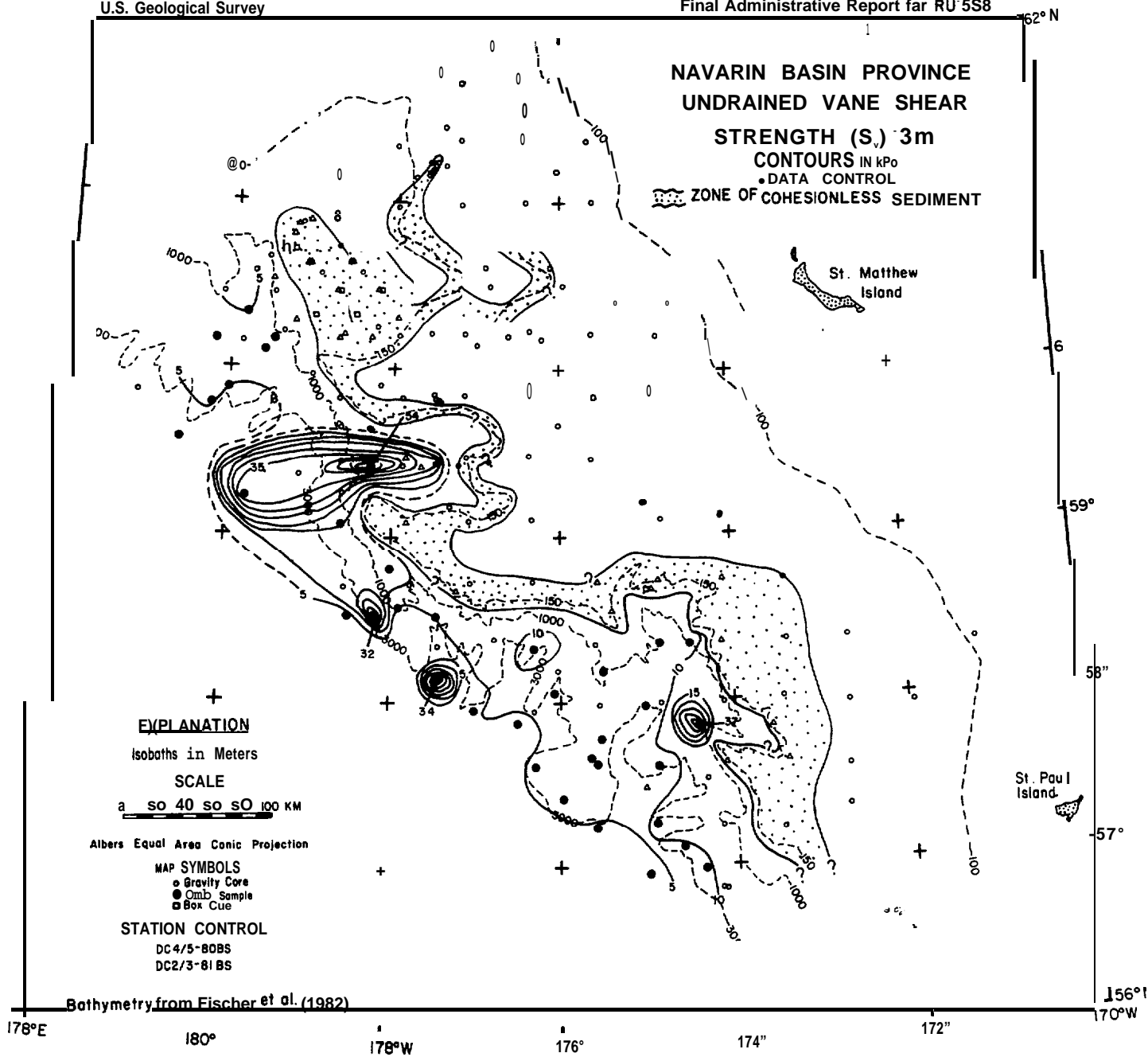


Figure 19. Areal distribution of peak undrained vane shear strength  $S_v$  at a subbottom depth of 1 m. Contour interval 5 kPa.



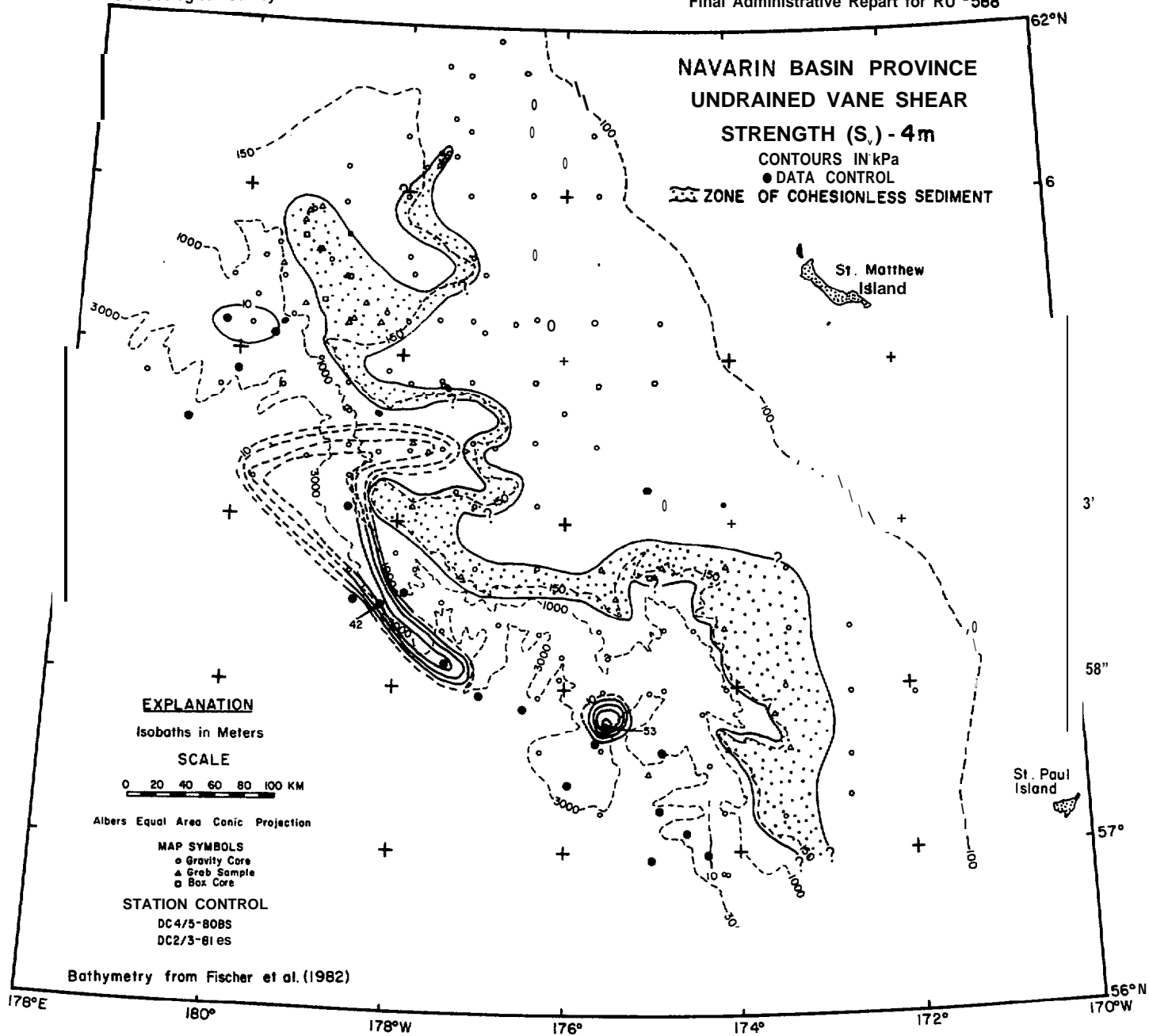
THIS REPORT IS PRELIMINARY AND HAS NOT BEEN REVIEWED FOR CONFORMITY WITH US GEOLOGICAL SURVEY EDITORIAL STANDARDS

Figure 20. Areal distribution of peak undrained vane shear strength  $S_v$  at a subbottom depth of 2 m. Contour interval 5 kPa.



THIS REPORT IS PRELIMINARY AND HAS NOT BEEN REVIEWED FOR CONFORMITY WITH U.S. GEOLOGICAL SURVEY EDITORIAL STANDARDS.

**Figure 21.** Areal distribution of peak undrained vane shear strength  $S_v$  at a subbottom depth of 3 m. Contour interval 5 kPa.



THIS REPORT IS PRELIMINARY AND HAS NOT BEEN REVIEWED FOR CONFORMITY WITH U.S. GEOLOGICAL SURVEY EDITORIAL STANDARDS.

Figure 22. Areal distribution of peak undrained vane shear strength  $S_v$  at a subbottom depth of 4 m. Contour interval 10 kPa.

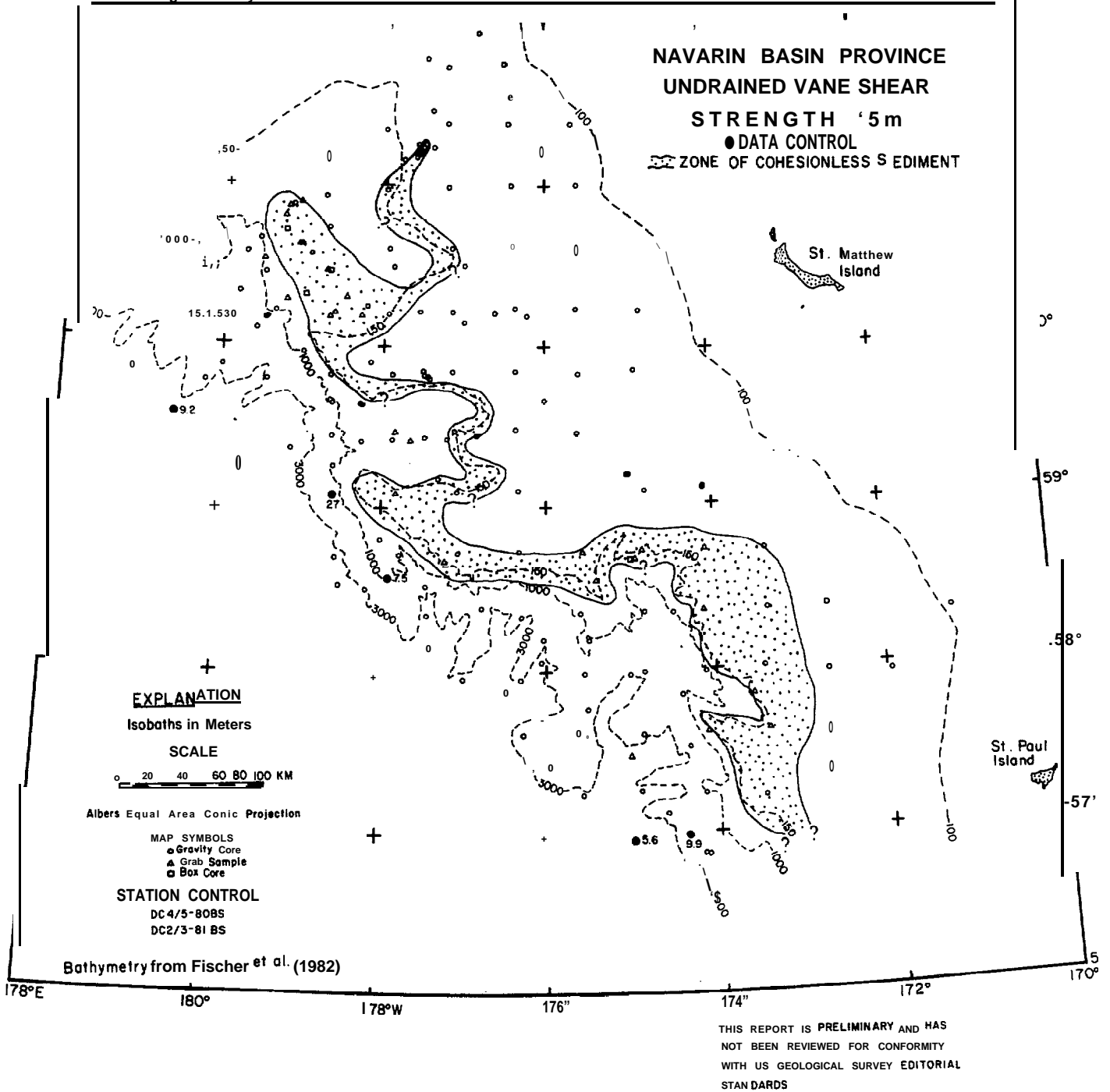


**Figure 23.** Areal distribution of peak undrained vane shear strength  $S_v$  at a subbottom depth of 5 m. Data values (in kPa) written beside appropriate core location.

(Figs. 20 and 21). At a **subbottom** depth of 2 m, shelf sediment **shear** strengths ranged from 7 kPa **to** 19 kPa. Distinct trends were not definable.

For slope cores, shear strengths ranged from 2 kPa **to** 51 kPa at a **subbottom** depth of 1 m (**Fig. 19**). Shear strengths were relatively **high** (>10 kPa) at the heads of canyons (**e.g., Navarinsky** Canyon). Most of the lower slope sediment, below **1500 m**, had shear strengths less than 5 kPa. Three sites, one in Pervenets Canyon, one below **Navarin** Ridge, and a third at the **headwall** of **Zhemchug** Canyon, had high shear strengths (ranging from **38** to 51 kPa). Evidence from one-dimensional consolidation tests conducted on a replicate core from the headwall of **Zhemchug** Canyon (**core G97**) shows that sediment **to be overconsolidated** and likely represents older sediments exposed due **to** slumping or erosion. **At** greater **subbottom** depth these isolated sites of high shear strength become **zones** of anomalously strong sediment (**cf., Figs. 19 through 23**) and likely represent older (possibly Pleistocene?) sediment exposed by slumping or erosion. Few (**7**) cores achieved penetrations of 5 m or more. These cores were all located on the slope or rise; shear strengths at 5 m **subbottom** depth ranged from 5 kPa **to** 27 kPa (**Fig. 23**).

Water Content

Methods. Water content (computed as percent dry weight of sediment) and bulk density **subsamples** were obtained from the location of the vane test immediately following strength testing. These samples were taken with a small tube sampler and stored in sealed sample bottles for subsequent analyses at the shorebased laboratory.

Water contents were determined following ASTM **D2216-80**. The data were salt corrected using an assumed salinity of 32.5 parts per thousand and the relationship:

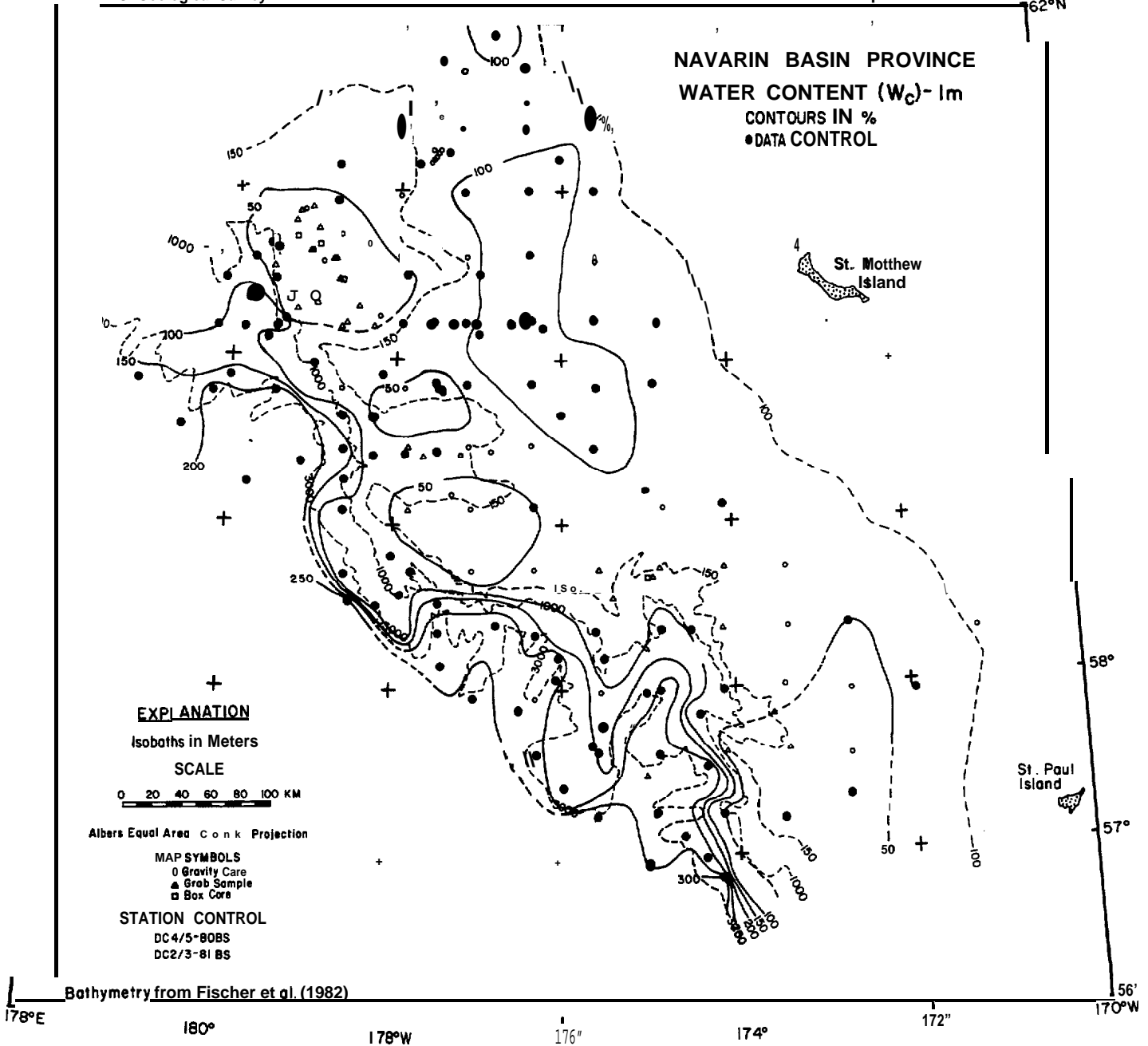
$$W_c = \frac{1.0325w}{1-0.0325w} \quad (1)$$

where  $W_c$  = corrected water content  
 $w$  = water content with no salt correction

Findings. Maps presenting water content are shown at **subbottom** depth intervals of 1 m **in** Figures 24 through 28. Shelf sediments at **1 m** have water contents ranging from 20% to 137% with the highest values being associated with **the** zone of weak sediment **150 km** west of St. Matthew Island. The lowest measured water contents at **1 m subbottom** depth are associated with the **Navarin** Ridge. Shelf sediment water contents at 2 m show an unremarkable distribution that ranges from 43% to 107%.

At a 1 m **subbottom** depth, slope sediment water contents increase to the south and with increasing water depth (**Fig. 24**). With increasing **subbottom** depth, water contents decrease across the entire area, but, at each horizon, the trend of increasing values to the south and with increasing water depth continues.

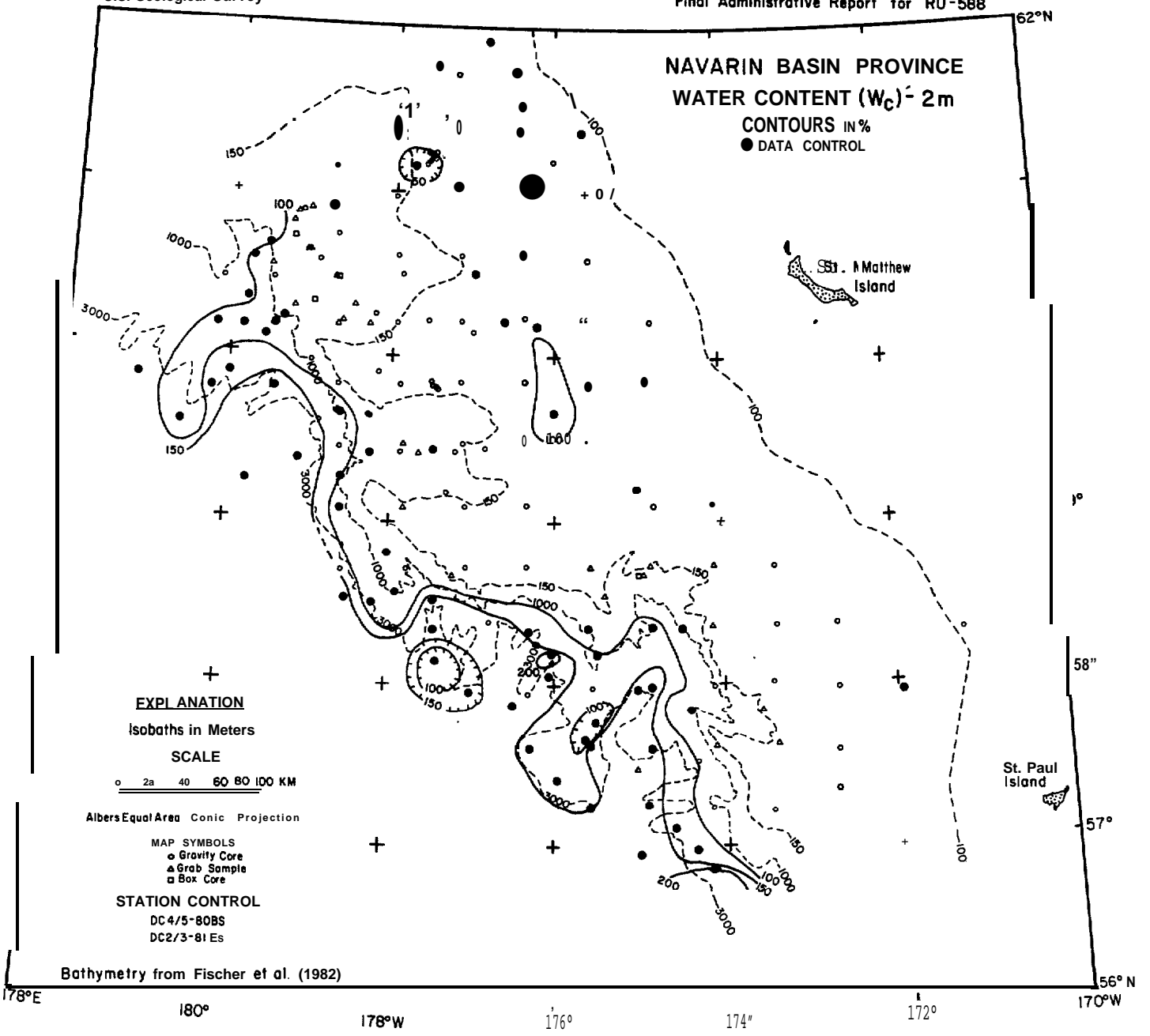
**NAVARIN BASIN PROVINCE**  
**WATER CONTENT ( $W_c$ )-1m**  
**CONTOURS IN %**  
**● DATA CONTROL**



THIS REPORT IS PRELIMINARY AND HAS NOT BEEN REVIEWED FOR CONFORMITY WITH U.S. GEOLOGICAL SURVEY EDITORIAL STANDARDS.

**Figure 24.** Areal distribution of salt corrected water content ( $W_c$ ) at a subbottom depth of 1 m. Contour interval 50% by dry weight.

NAVARIN BASIN PROVINCE  
WATER CONTENT ( $W_c$ ) - 2m  
CONTOURS IN %  
● DATA CONTROL



THIS REPORT IS PRELIMINARY AND HAS NOT BEEN REVIEWED FOR CONFORMITY WITH U.S. GEOLOGICAL SURVEY EDITORIAL STANDARDS

Figure 25. Areal distribution of salt corrected water content ( $W_c$ ) at a subbottom depth of 2 m. Contour interval 50% by dry weight.

NAVARIN BASIN PROVINCE  
WATER CONTENT ( $W_c$ )-3m  
CONTOURS IN %  
● DATA CONTROL

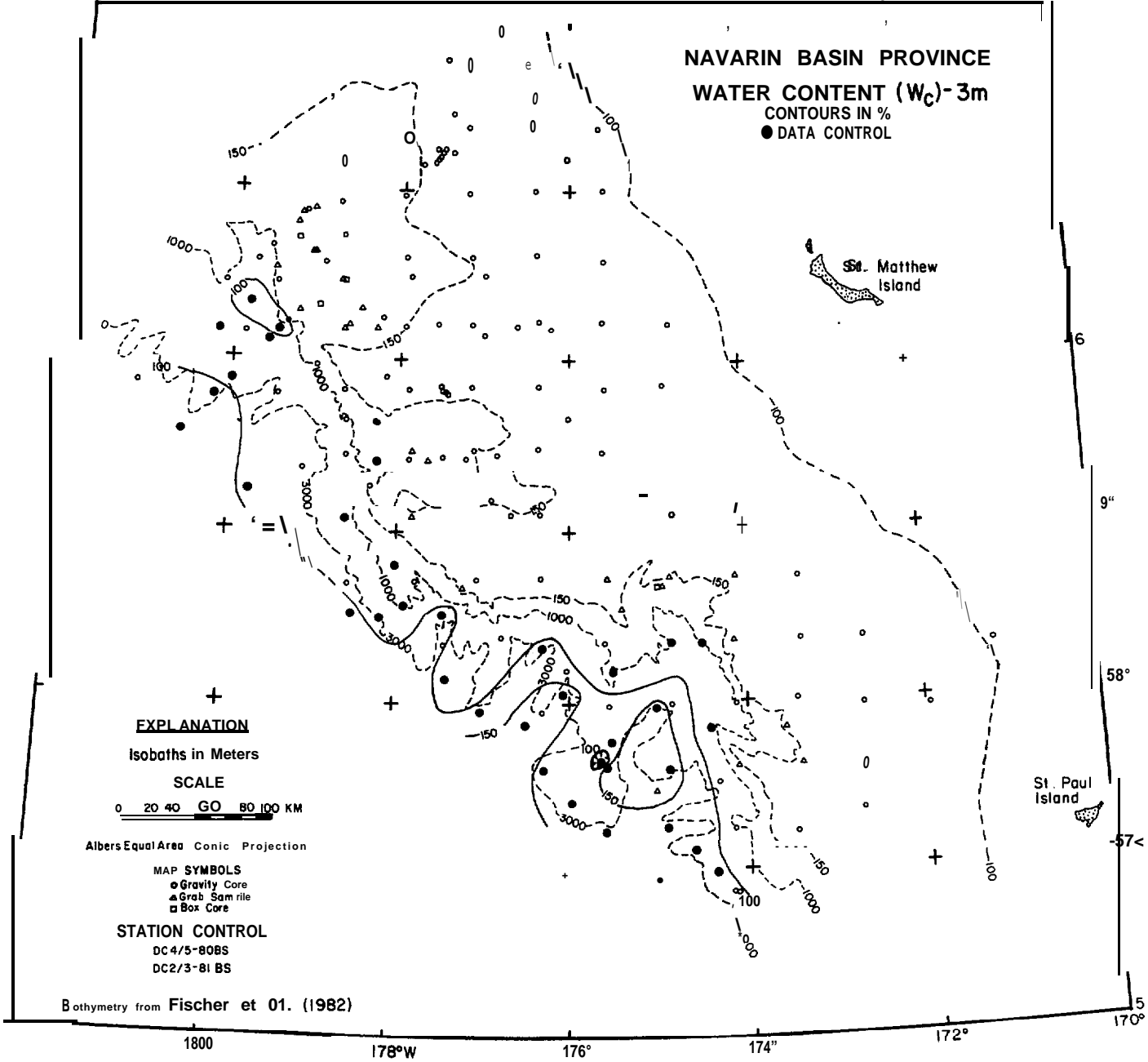


Figure 26. Areal distribution of salt corrected water content ( $W_c$ ) at a subbottom depth of 3 m. Contour interval 50% by dry weight.

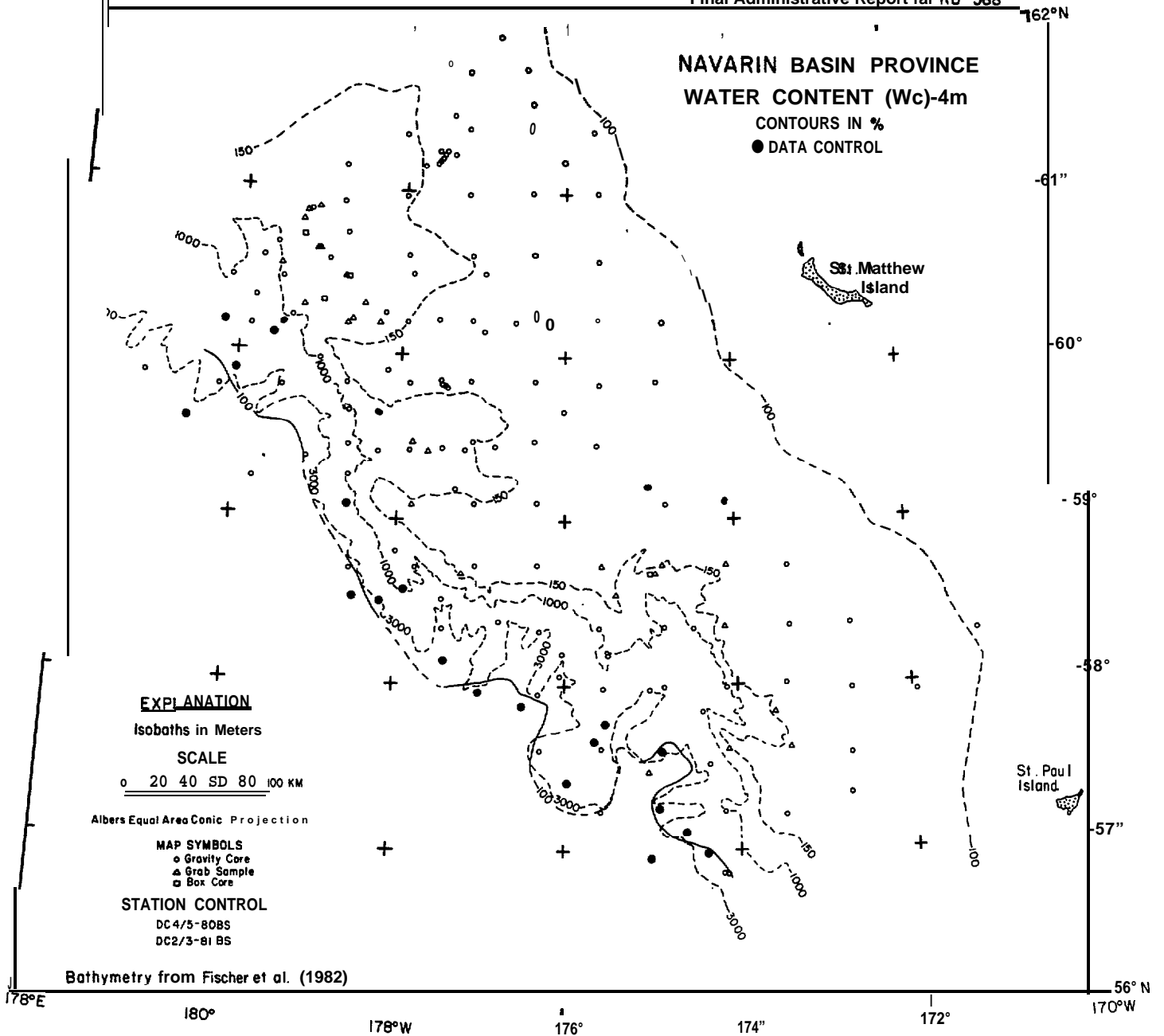
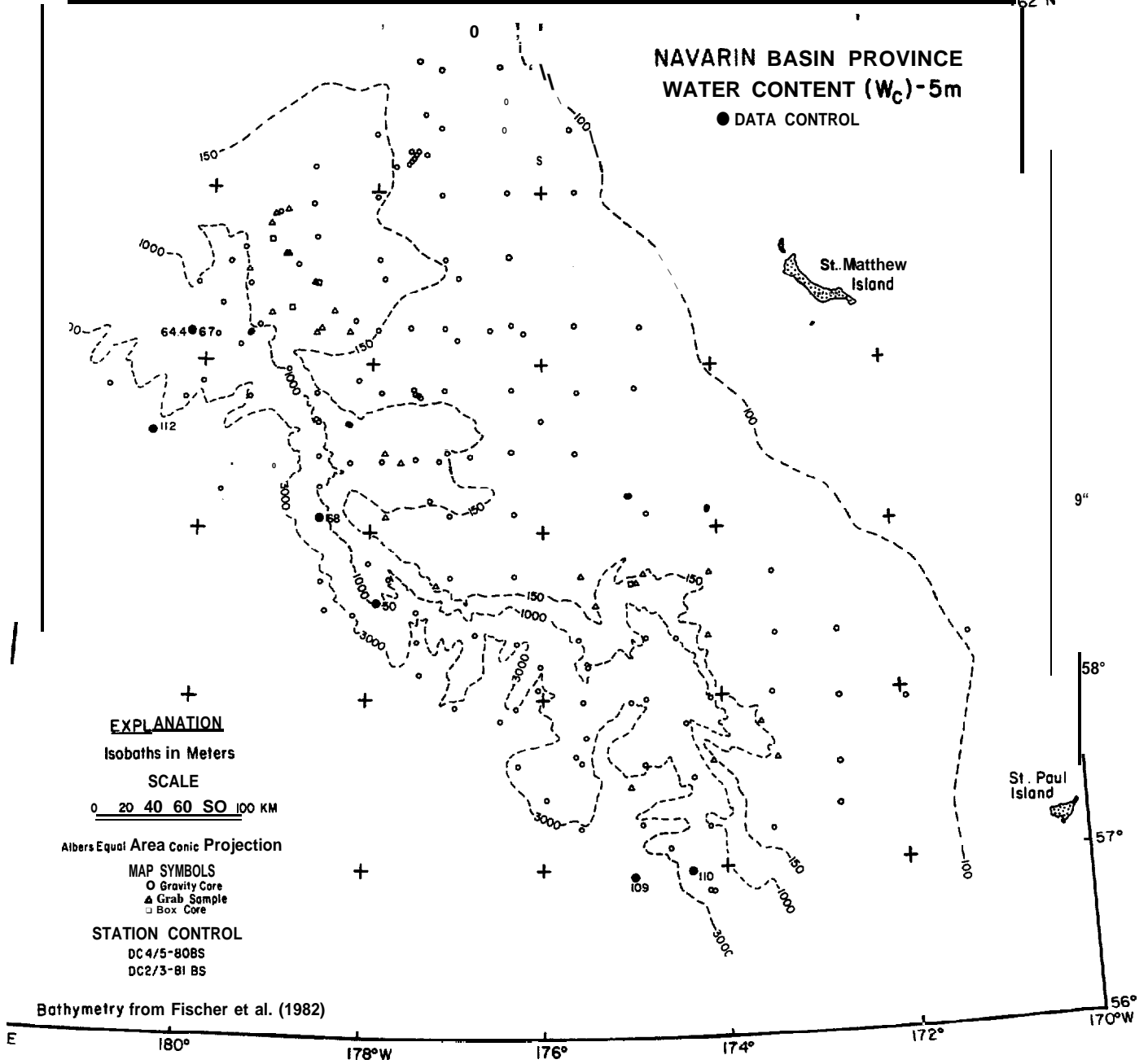


Figure 27. Areal distribution of salt corrected water content ( $W_c$ ) at a subbottom depth of 4 m. Contour interval 50% by dry weight.

### NAVARIN BASIN PROVINCE WATER CONTENT ( $W_c$ )-5m

● DATA CONTROL



THIS REPORT IS PRELIMINARY AND HAS NOT BEEN REVIEWED FOR CONFORMITY WITH U.S. GEOLOGICAL SURVEY EDITORIAL STANDARDS

Figure 28. Areal distribution of salt corrected water content ( $W_c$ ) at a subbottom depth of 5 m. Data values in  $\circ$  written beside appropriate core locations.

Bulk densities were computed directly from the water content data following standard formulas and assuming 100% saturation (e.g., Lambe and Whitman, 1969). In-place effective overburden stress ( $\sigma'_v$ ) was computed as:

$$\sigma'_v = \sum_0^z \gamma'_c \Delta z \dots \dots \dots (2)$$

where  $\gamma'_c$  = sediment submerged bulk density;  $\gamma'_c = \gamma_c - \gamma_{sw}$   
 $\gamma_c$  = sediment bulk density  
 $\gamma_{sw}$  = density of seawater  
 $z$  = subbottom depth in cm

Detailed **downcore** computations were made for most cores; values of  $\sigma'_v$  from the replicate cores agreed closely ( $\pm 2$  kPa) with this data set. For the short (**less than 4 m**) cores used in **this** study, effective overburden stress increased almost linearly with depth. Figure 29 shows linear regression fits for each of the replicate cores; correlation coefficients were better than **r=0.999** in **all** cases. This data set was combined with the one-dimensional consolidation data to estimate **overconsolidation** ratios (OCR'S) for the **near-surface** sediment of **Navarin Basin**.

Grain Specific Gravity

Twenty-one grain specific **gravity** tests were performed in accordance with ASTM **D854-58**. Most of the sample specimens were taken from trimmings of the **triaxial** test samples. **Salt** corrections were not applied in the computations. Values of grain specific gravity ranged from 2.55 to 2.77, with an average value of 2.64. The smaller values are lower than most continental shelf sediment grain specific gravity values and **likely** indicate the presence of diatoms.

Atterberg Limits

Methods. **Atterberg** Limits tests were performed on 50 samples following the procedures of ASTM **D423-66**, ASTM **D424-59**, and ASTM **D2217-66**. A salt correction assuming a salinity of 32.5 parts per thousand was applied in the computation.

Findings. The plasticity index (**PI**) ranged from 3 to 38 and the liquid limit (**LL**) ranged from 27 to 83. On a plot of liquid limit versus plasticity index (plasticity chart, Fig. 30), **Navarin** Basin province sediment varies dramatically. Within the Unified Soil Classification System (e.g., Mitchell, 1976), descriptive names are assigned to different parts of the plasticity chart based on empirical observations. According to this system, Navarin Basin shelf sediments {cores G61, **Gill**} are inorganic silts of medium to high compressibility and are more highly compressible (core **G61**) in the northern part of the province near **Navarinsky** Canyon. Sediment from Navarinsky Canyon, (**cores G31** and **G34**) however, is typically inorganic clay of low to medium plasticity combined with some inorganic silts of medium compressibility. Farther south, near the head of St. Matthew Canyon (**core G74**), the sediment behaves as a highly compressible inorganic silt or organic clay exhibiting a

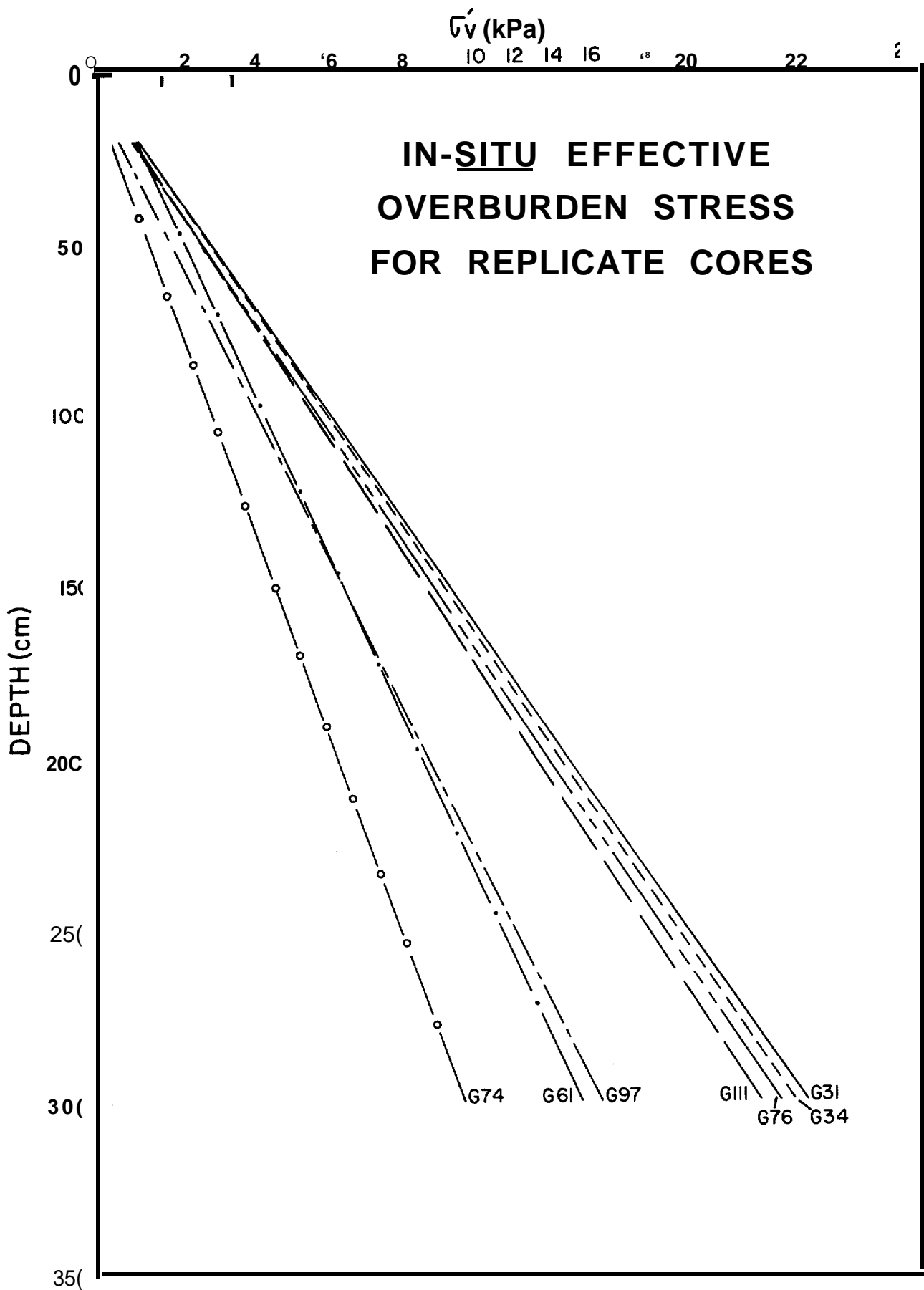


Figure 29. Linear regression best fit lines of the increase of in place effective overburden pressure ( $\sigma'_v$ ) with subbottom depth for replicate cores. Data from 1980 Discoverer cruise.

wide range of liquid limit and plasticity index values. This behavior likely reflects significant variations in diatom content. Slope sediment near the head of Zhemchug Canyon (core G97) behaves as a highly compressible inorganic silt.

Grain-Size Distribution

Procedures and results from grain-size analyses are summarized in Chapter 3, this report.

Advanced Geotechnical Tests

Consolidation Tests

Methods. One dimensional consolidation tests were performed in general accordance with ASTM D2435-70 on 15 specimens trimmed to a sample size of 6.35 cm in diameter by 2.54 cm in length. An initial or seating stress of 2.4 kPa and a pressure increment ratio of one were used in all tests. After reaching equilibrium under a vertical stress of 383 kPa, the sample was unloaded to 48 kPa and then reloaded until a vertical stress of 1532 kPa was reached. The specimens were unloaded in one step and removed from the consolidometers. Deformation versus time readings were recorded for each loading increment.

Maximum past overburden stress ( $\sigma'_{vm}$ ) was determined by the Casagrande procedure (Casagrande, 1936); values are summarized in Table 4. These maximum past stresses were used to determine consolidation pressures for triaxial tests and to estimate the amount of overburden removal due to slumping or erosion in some areas.

A useful consolidation state parameter is the excess past overburden stress ( $\sigma'_e$ ). The  $\sigma'_e$  parameter is determined from the one-dimensional consolidation tests used to determine  $\sigma'_{vm}$  and the in-situ effective overburden stress ( $\sigma'_v$ ) and is computed as:

$$\sigma'_e = \sigma'_{vm} - \sigma'_v \dots \dots \dots (3)$$

A more commonly reported variable is the overconsolidation ratio (OCR) which is the ratio of  $\sigma'_{vm}$  to  $\sigma'_v$ . For normally consolidated sediment,  $\sigma'_{vm} = \sigma'_v$  and thus OCR=1 and  $\sigma'_e=0$ .

Findings. All of the Navarin Basin sediment tested was overconsolidated ( $\sigma'_e > 0$ ) as shown in Figure 31 and Table 4. A characteristic of the Navarin replicate cores is very high OCR's at shallow (<30 cm) subbottom depths (e.g., see core G 78, 10-15 cm of Table 4). Such large OCR's are accentuated by the extreme contrast between  $\sigma'_{vm}$  and  $U'_v$  that characterizes the uppermost part of the cores. Such high levels of overconsolidation are unlikely, however, given the low surface strengths, lack of obvious depositional hiatuses, and uniform increase in vane shear strength with depth which all suggest normal consolidation. The  $\sigma'_e$  parameter is a useful compliment to OCR because  $\sigma'_e$  is not enlarged at very low (e.g., <1 kPa) values of  $\sigma'_v$ .

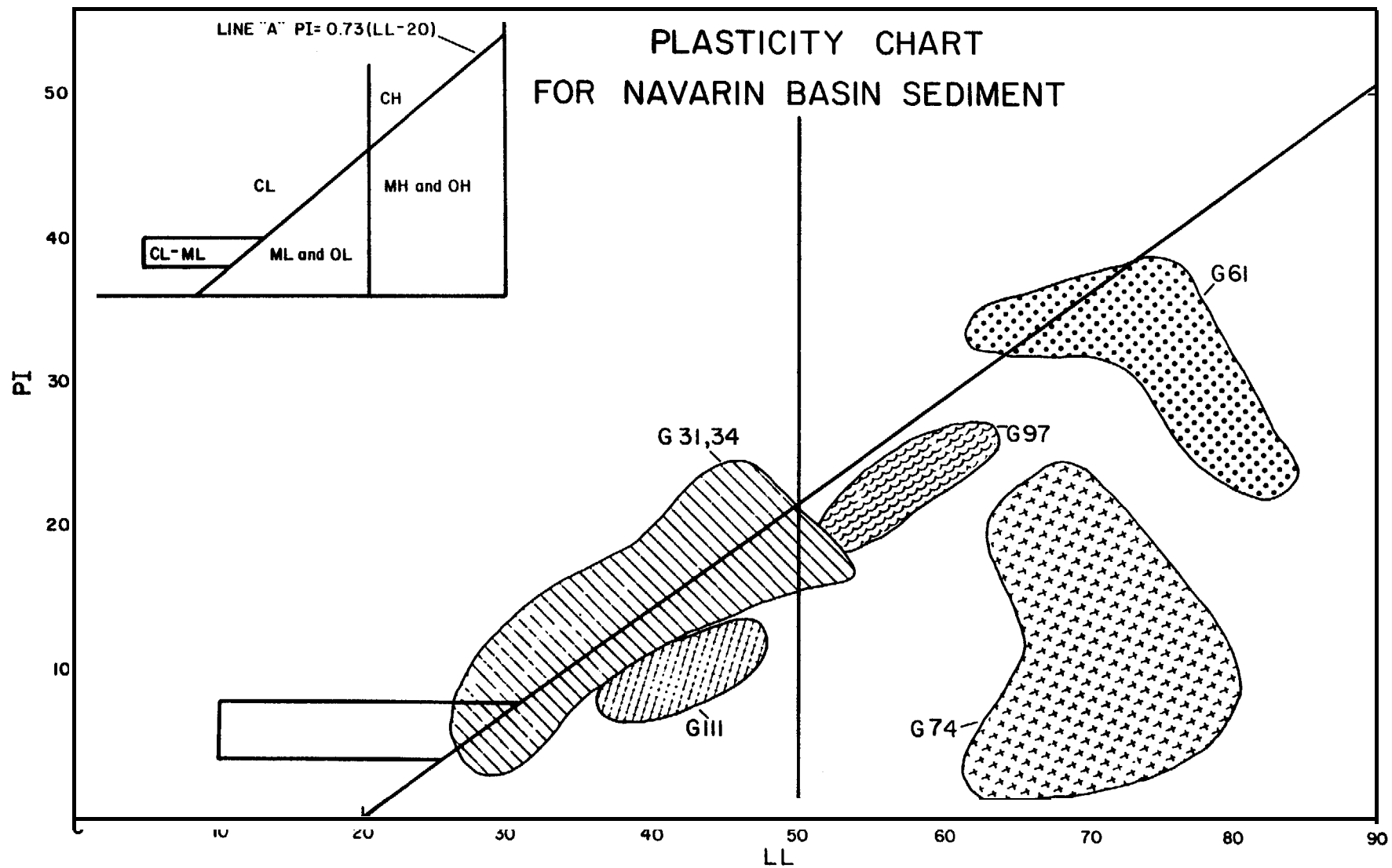


Figure 3°. Plasticity chart for Navarin Basin province replicate cores. Data from 1980 R/V Discoverer cruise.

# EXCESS PAST EFFECTIVE STRESS ( $\sigma'_e$ )

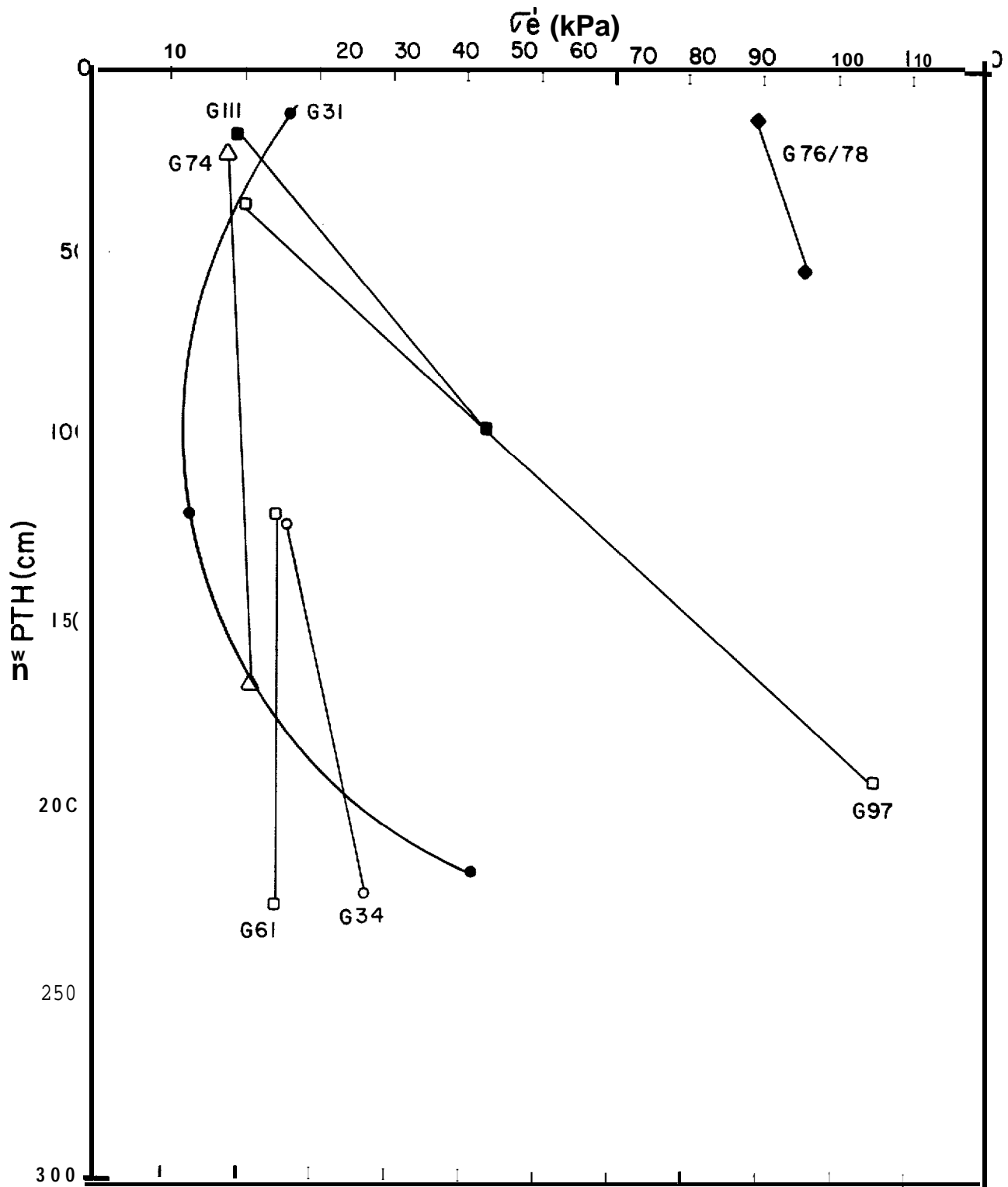


Figure 31. Plot of excess past effective stress  $\sigma'_e$  versus depth for Navarin Basin province replicate cores. Data from 1980 R/V Discoverer cruise.

Table 4. **Summary** of Consolidation **test** results

Core	z cm	$\sigma'_{vm}$ (kPa)	$\sigma'_v$ (kPa)	$\sigma'_e$ (kPa)	OCR
<b>G 31</b>	10-13	30	0.7	29	43
	119-122	20	8	12	2.5
	214-217	65	15	50	4.3
G 34	121-124	35	8	27	4.4
	220-223	52	15	37	3.5
<b>G 61</b>	<b>119-121</b>	<b>30</b>	<b>6</b>	<b>24</b>	<b>5</b>
	<b>223-226</b>	<b>35</b>	<b>11</b>	<b>24</b>	<b>3.2</b>
G 74	22-25	<b>19</b>	0.7	<b>18</b>	<b>27</b>
	<b>164-168</b>	<b>30</b>	<b>6</b>	<b>24</b>	<b>5</b>
G 78	10-15	90	0.8	89	112
G 76	50-55	100	3.3	96	30
G 97	35-40	22	2	20	11
	187-192	116	10	106	11.6
<b>G 111</b>	15-20	20	1.1	19	18
	95-100	60	6	54	10

Excluding the uppermost 30 cm, cores G31, G34, G61, and G74 are lightly to moderately **overconsolidated** (OCR 2-5). Core G76, taken from the shelf near **Navarin Ridge**, is heavily **overconsolidated** throughout (OCR~30). Core G97, recovered from the headwall of **Zhemchug Canyon**, is **overconsolidated** throughout (OCR~11) but a dramatic increase in  $\sigma'_e$  is seen at the base of the core (Fig. 31). The observed level of excess **overburden** pressure at the base of the core **likely** results from the removal of about 15 m of sediment. Core **Gill**, collected from the shelf about 60 km north of the head of **Zhemchug Canyon**, exhibits **overconsolidation** throughout (OCR~10). The cause of the observed **overconsolidation** is uncertain for the shelf cores. Sediment on the shelf can be subjected to a number of **loads** capable of inducing this **overconsolidation** state (e.g., erosion of overlying material, cyclic loading, cementation, ice loading, and **subaerial** exposure at low sea level stands). At present, we have insufficient data to evaluate these mechanisms.

### Strength Evaluation

#### Approach

The quality and usefulness of the strength data are limited by both the short core length (typically less than 5 m) and sediment disturbance during the coring process. Many features of **geotechnical** interest (e.g., basal shear surfaces of sediment failure zones) occur much deeper (50 m or more) than conventional coring devices can penetrate. Thus, the sediment involved at that horizon may not have the same properties as the sampled sediment. Further, the engineering properties of the sampled sediment can be modified by the coring process. That is, disturbance by thick-walled coring devices can alter **the** properties of the sampled **sediment** from **the** properties of **the** in place sediment. Both limitations (**short** corer penetration and sample disturbance) can reduce the validity of a **geotechnical** study.

As an approach to overcoming these limitations, we used the normalized soil parameter (**NSP**) method (Ladd and **Foott**, 1974; **Mayne**, 1980). The **NSP** method is based on empirical results that show certain engineering properties of a wide range of cohesive soils to be constant **if** normalized by appropriate consolidation stresses. The resulting data can be applied to a wide range of in place stress conditions. The most frequently used NSP is  $S_u/\sigma'_v$ . The  $S_u/\sigma'_v$  ratio is often a constant for a given value of OCR and can be used to construct strength profiles when overburden stresses are known. Thus, **the** overburden stresses and consolidation state of **the** sediment in question must be evaluated. By knowing the variation of OCR with depth in the sediment column, the strength profile can be predicted using the NSP derived equation (**Mayne**, 1980):

$$S_u/\sigma'_v = (\text{OCR})^A S_{nc} \dots \dots \dots (4)$$

- where
- $S_u$  = undrained shearing strength
  - $\sigma'_v$  = effective overburden stress
  - OCR = **overconsolidation** ratio

$\Lambda_o$  = Normalized strength parameter **that** is  
a constant for a given sediment

$s_{nc}$  = ratio of static undrained shearing strength  
**to** isotropic consolidation stress for  
normally consolidated conditions

As described **in** the preceding section on consolidation, OCR **is** evaluated from **the** determination of  $\sigma'_{vm}$  and  $\sigma'_{v}$ . **The** parameter  $\Lambda_o$  is simply the slope of **the** linear relationship between  $S_u/\sigma'_{v}$  (**overconsolidated**)/ $s_{nc}$  and the appropriate OCR on a log-log scale. **The** parameter  $s_{nc}$  is the **value** of  $S_u/\sigma'_{v}$  for normally consolidated sediment.

One advantage of the NSP approach is the determination of parameters that are independent **of** consolidation stress and depth in the sediment column. These normalized parameters can therefore be used as site properties that can be mapped. A second advantage of the approach is that the normalized parameters can circumvent the effect of coring disturbance by conducting all of the strength tests at consolidation **stresses** much greater than those experienced in place (**Ladd and Foott, 1974**). **That is, both** a relatively undisturbed sample and a disturbed sample produce approximately equivalent normalized soil parameters if each is consolidated (**in the triaxial cell**) to a high stress level before testing for shear. Once the normalized strength parameters have been determined at high stress levels, the data can be applied to any stress level including the low stress state that the sample experienced in place.

Methods. A **triaxial** testing program was designed to evaluate the strength characteristics, including strength degradation due to cyclic loading, of the Navarin Basin sediment. A total of 36 static, consolidated, undrained **triaxial** compression tests were performed in general accordance with procedures described by Bishop and **Henkel** (1962). **Sample** specimens were selected using X-ray radiograph interpretations **of** each core section. After hand trimming to a final size of 15 cm {length} by 6.35 cm (diameter), each specimen was enclosed in a thin latex membrane, placed in the **triaxial** cell, and flushed under low-gradient back pressure with fresh distilled water. **Tests requiring** OCR's greater than 1.0 were first consolidated to the specified consolidation stresses multiplied by the required OCR, and then rebounded to the final consolidation stresses under drained conditions. Failure was defined as **20%** axial strain.

Eighteen additional **triaxial** tests were performed to evaluate the behavior of **Navarin** Basin sediment under cyclic loading. Specimens were prepared, consolidated, and back-pressured according to the same procedures described for the 36 static **triaxial** tests.

Cyclic loads, beginning with compression, were applied **in** bursts with a sinusoidal, 1 Hz waveform for all **isotropically** consolidated samples. A series of cyclic loads consisted of three bursts of 10 cycles followed by two bursts of 35 cycles and two bursts of 100 cycles. Each burst was separated by about one hour to allow pore water pressure equalization. The cyclic loads were approximately 75 and 50 percent of the **static** deviator **stress** at failure.

All cyclic tests were terminated when either a single amplitude axial strain of 15 percent or a pore water pressure ratio of 80% was reached. In some cases, if samples did not fail within the first series of cyclic loads, a second series of cyclic loads with an amplitude of 100% of static strength was applied. If the samples did not fail after the second series, a monotonic load was applied until failure was reached.

The testing program (Table 5, Fig. 32) was divided into Special (S) and Routine (R) cores; the main distinction being that additional tests were performed on the Special cores. For the static suite, tests R1 and R2 were designed to measure the sample strength directly. Tests R3 and R4 were designed to estimate  $S_u$  for normally consolidated sediment ( $S_{nc}$ ) at stress levels well above the maximum past stress ( $\sigma'_{vm}$ ). Values of  $2.5 \sigma'_{vm}$  and  $4.0 \sigma'_{vm}$  were used to evaluate the NSP approach. Tests R8 and R5 were designed to determine  $S_u$  at elevated OCR's as a means of evaluating  $\Lambda_o$ .

For the cyclic suite, tests R6 and R7 were designed to evaluate the degree of strength degradation due to cyclic loading from earthquake or wave (surface or internal) sources. Stress levels were designed to assess failure in the vicinity of 10 cycles. Tests R9 - R11 were designed to assess the effect of induced OCR on cyclic strength degradation.

Findings. The triaxial test results are summarized in Table 6. A plot defining the normalized strength parameter  $\Lambda_o$  is presented in Figure 33.

Three approaches were used as estimates of  $S_u$ : (1) undrained vane shear tests,  $S_v$ , (2) direct triaxial cell tests at isotropic consolidation stresses of 1.0 kPa (R1) and  $\sigma'_v$  (R2), and (3) the NSP estimate following equation 4. In most cases the three methods gave similar estimates of  $S_u$  at the overburden stresses experienced in the upper 3 m of the sediment column. For example, Figure 34 shows a comparison of the  $S_u$  estimates from cores G31 and G32, collected from the head of Navarinsky Canyon. Note the close approximation of the three methods. Figure 35 presents similar data for cores G97 and G98 collected from the headwall of Zhemchug Canyon. In this case vane shear estimates for core G98 depart dramatically from vane and triaxial cell estimates from core G97. This difference probably results from slumping or erosion at the head of Zhemchug Canyon. As previously described, consolidation tests show that about 15 m of sediment has been removed from the site of core G97. The two cores were not collected from precisely the same location. Both sampled the overconsolidated layer but differing amounts of subsequent sedimentation overlies the slip surface. Although at a different scale, these data support the conclusion of slumping in the canyon head that is based on geophysical evidence (Carlson et al., 1982).

Undrained shear strengths were reduced to 51% to 80% of static strength (AD) during 10 cycles of dynamic loading (Table 6). Core G31 showed an increase in strength during cyclic loading that possibly was erroneous due to procedural difficulties with that test.

Table 5. **Triaxial** test specifications for Routine (R) and Special (S) cores(t)

Test or Number	Static Cyclic	Consolidation Stress	Induced OCR	Cyclic Deviator Stress
R-1	static	1 kPa	<b>1.0</b>	N/A*
R-2	static	$\sigma'_{vm}$	1.0	N/A
R-3	static	<b>2.5</b> $\sigma'_{vm}$	<b>1.0</b>	N/A
R-4	static	<b>4.0</b> $\sigma'_{vm}$	<b>1.0</b>	N/A
R-5	static	<b>2/3</b> $\sigma'_{vm}$	6.0	N/A
R-6	cyclic	<b>4.0</b> $\sigma'_{vm}$	1.0	<b>75%Su</b>
R-7	cyclic	<b>4.0</b> $\sigma'_{vm}$	1.0	<b>50%Su</b>
S-8	static	<b>4.0</b> $\sigma'_{vm}$	<b>3.0</b>	N/A
s-9	cyclic	2/3a $\sigma'_{vm}$	6.0	<b>75%Su</b>
<b>s-10</b>	cyclic	<b>2/3</b> $\sigma'_{vm}$	6.0	<b>50%Su</b>
<b>s-11</b>	cyclic	<b>4.0</b> $\sigma'_{vm}$	3.0	<b>75%Su</b>

t refer to **Figure 32** for location of tests in each core.

\* N/A indicates value is not applicable.

Table 6. Summary of **triaxial** test results -  
NSP estimate of undrained shearing strength.

Core	Depth in Core (cm)	Initial OCR	$\lambda_o^*$	$s_{nc}^*$	$\sigma'_v$ (kPa)	$S_u$ (NSP) (kPa)	OCR=1 $A_D$ %	OCR=6 $A_D$ %
G 31	10-13	43	0.87	0.36	0.7	6.6	162	
	119-122	2.5			8	6.4		
	214-217	4.3			15	19.2		
G 34	121-124	4.4	0.94	0.33	8	10.6	80	75
	220-223	3.5			15	16.1		
G 61	119-121	5*0	0.84	0.48	6	11.1	75	
	223-226	3.2			11	14.0		
G 74	22-25	27.0	0.74	0.57	0.7	4.6	63	
	164-168	5.0			6	11.2		
G 78	10-15	112	0.77	0.69	0.8	20.9	51	
G 76	50-55	30			3.3	31.2		
G 97	35-40	11.0	0.87	0.51	2	8.2	71	
	187-192	11.6			10	43.0		
G 111	15-20	18	0.85	0.60	1.1	7.7	75	
	95-100	10			6	25.5		

\*Values apply to entire core

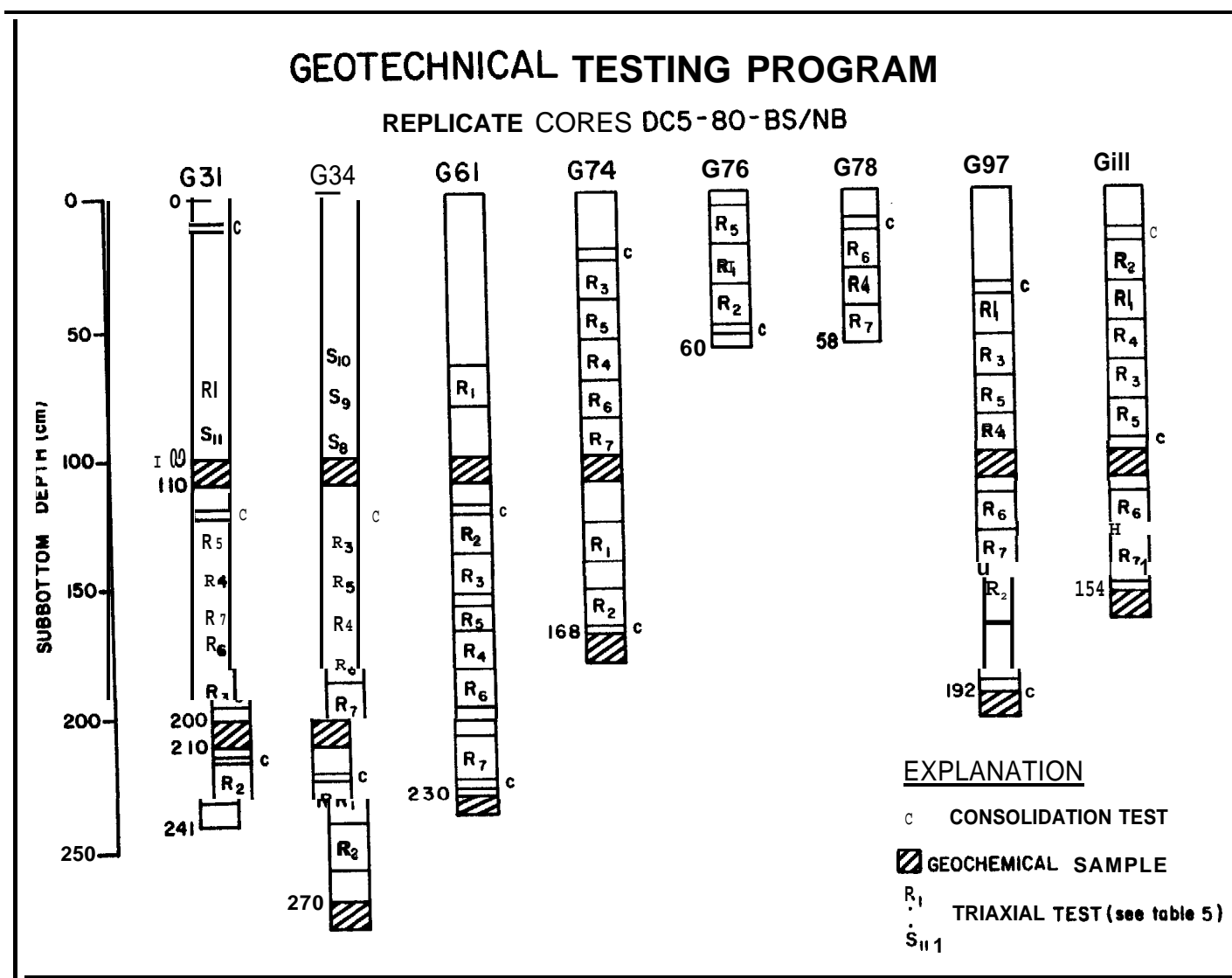


Figure 32. Location of tests for Navarin Basin province geotechnical testing program on replicate cores. Refer to Table 5 for summary of triaxial test specifications.

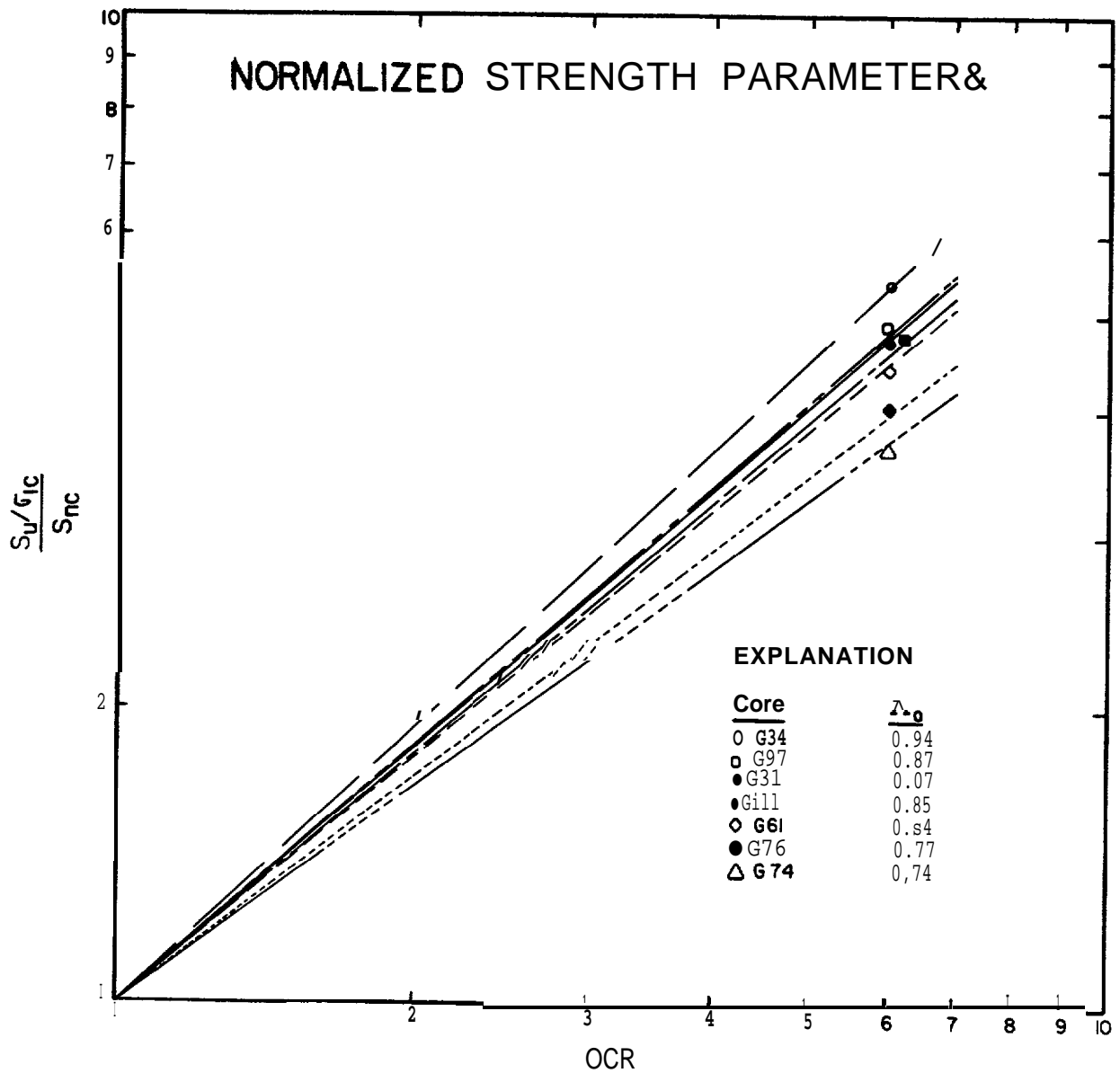


Figure 33. Plot of the normalized strength parameter  $\Lambda_{oc}$  as defined by a log-log plot of  $S_u/\sigma'_{vc}(\text{overconsolidated})/S_{nc}$  versus OCR for replicate cores collected on the 1980 R/V DISCOVERER cruise. See text for explanation.

# UNDRAINED SHEAR STRENGTH ESTIMATES

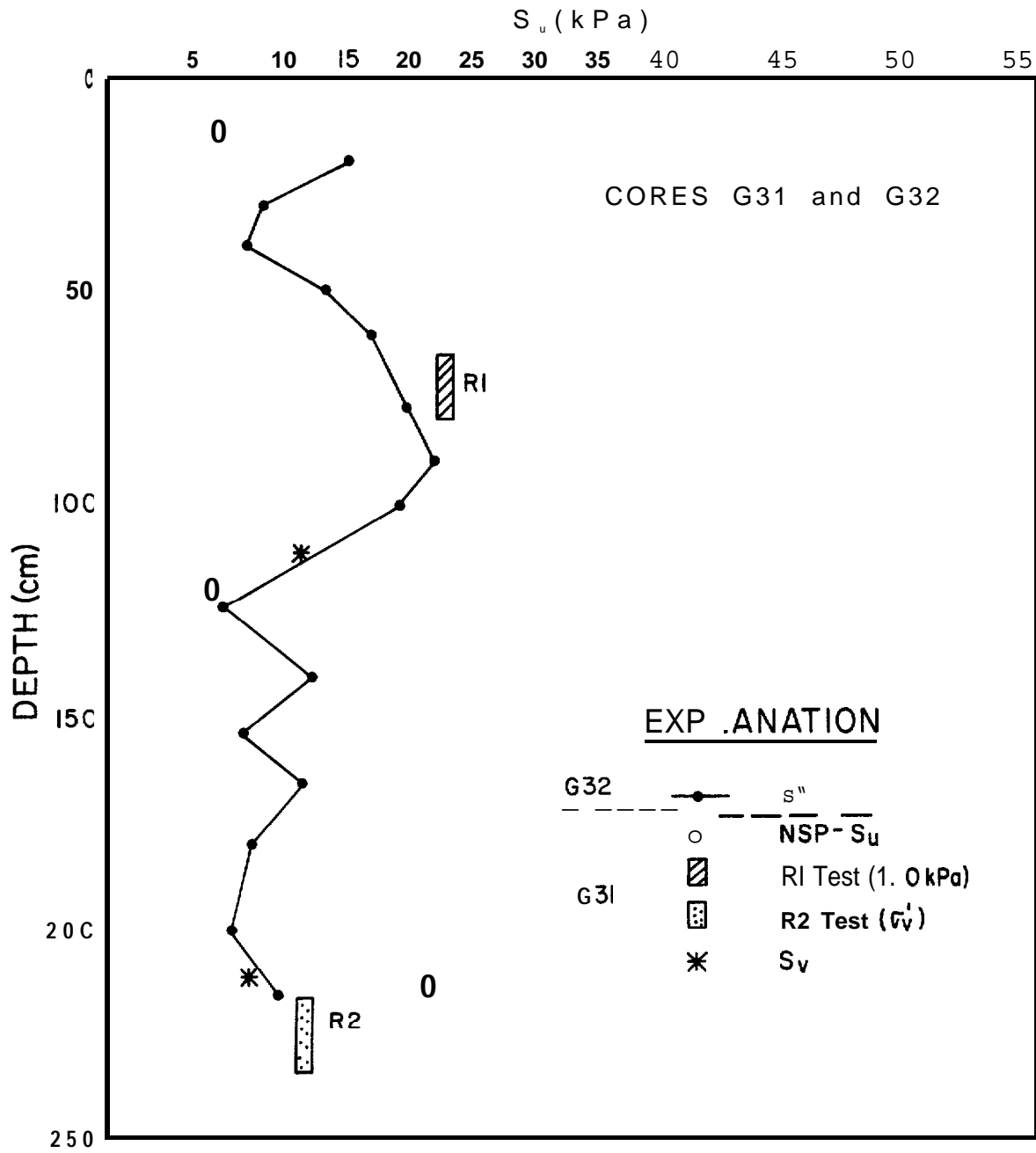


Figure 34. Example of multiple estimates of undrained shear strength ( $S_u$ ) for paired cores G31 and G32, 1980 R/V DISCOVERER cruise.

# UNDRAINED SHEAR STRENGTH ESTIMATES

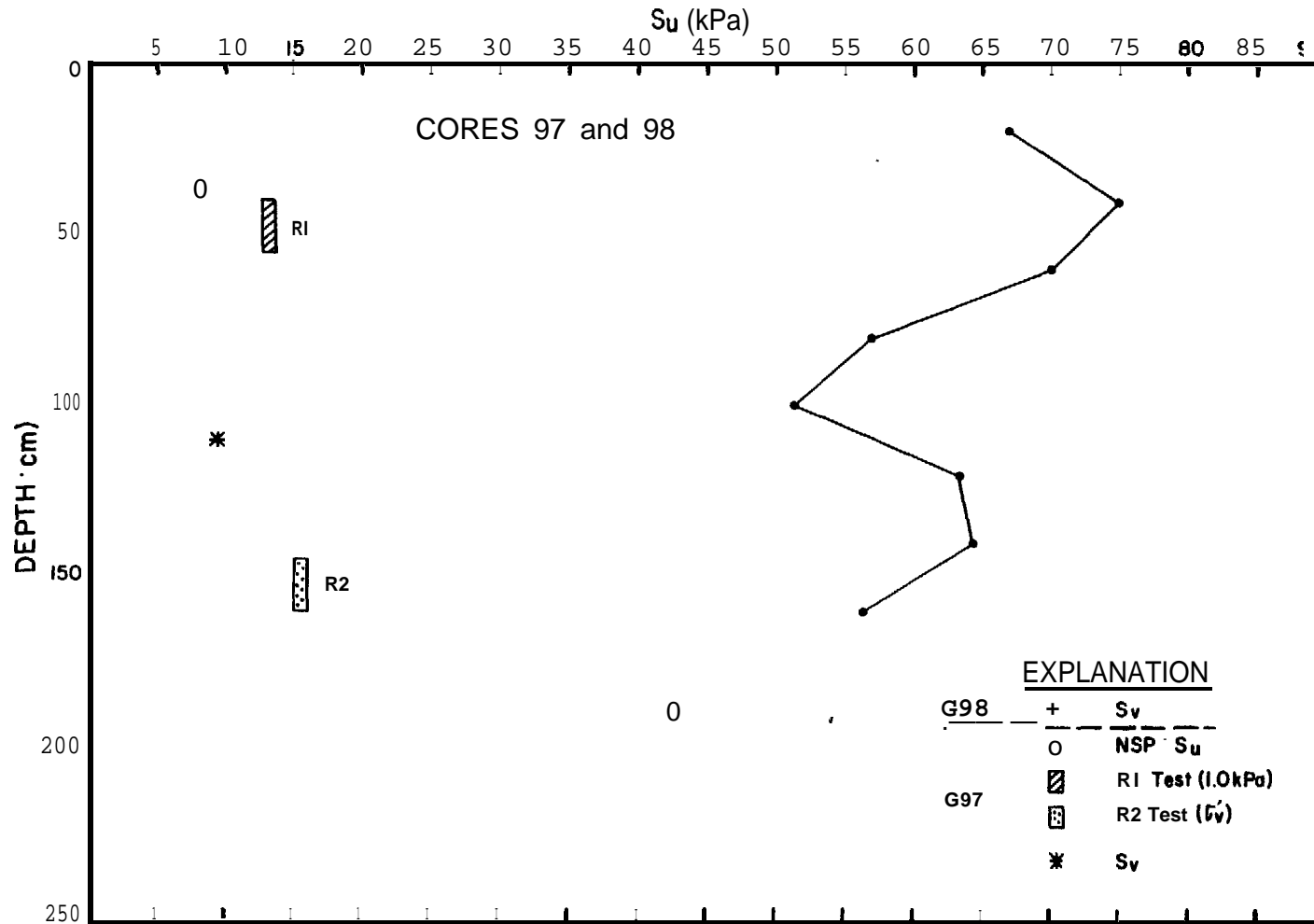


Figure 35. Example of multiple estimates of undrained shear strength ( $S_u$ ) for paired cores G97 and G98, 1980 R/V DISCOVERER cruise. Disparity between G97 and G98 strength estimates is due to the removal of approximately 15 m of sediment. See text for explanation.

## Stability Applications

The normalized cyclic **strength** (10 **cycles** to failure) for normal consolidation is the cyclic deccradation factor,  $A_p$ , times  $S_{nc}$ . Using values from Table 6, the normalized 10-cycle cyclic **strength** varies between 0.26 and 0.58, with a representative shelf value of 0.36. During a major storm the number of significant cycles **might range** from 100 to perhaps as many as 1000. From Lee and Focht (1976) such an increase in cycle number **might further degrade** the **strength by 50%**, **assuming no drainage**. Therefore, the representative normalized, storm-wave-degraded, **cyclic strength** for the shelf would be 0.18. For an assumed peak wave **height** of 22 m and a wave **length** of 400 m, the procedures of Seed and Rahman (1978) **yield** a peak normalized wave-induced **shearing** stress of 0.18 at a water depth of 57 m. At **greater** water depths, such as the entire Navarin **Basin** province, the level of **shearing** stress would be less and would be insufficient to cause failure in the cohesive sediments.

In sandy areas the level of **strength** degradation **resulting** from cyclic **loading** is probably **higher**. Seed and Idriss (in press) show that liquefaction during earthquakes has occurred at normalized shear stress levels of about 0.10. If storm waves produce a further 50% **strength degradation** beyond the influence of earthquakes, the critical normalized **shearing** stress for a sand subjected to wave **loading might** be as low as 0.05. Such a **shearing** stress level could be **generated** in water depths to 146 m for the storm waves assumed above. Some of the **cohesionless** sediment in the Navarin Basin province exists at this and shallower water depths and **might** be susceptible to liquefaction during major storm *waves*. Such *an occurrence is* fairly unlikely, however, because partial drainage from the pervious sediment would limit pore water pressure buildup.

## SUMMARY OF FINDINGS

- (1) A zone of **cohesionless** sediment exists at **the** shelf break.
- (2) Undrained vane shear strengths on the shelf are lowest on the central shelf **about** 150 km west **of St.** Matthew Island.
- (3) Undrained vane shear strengths are highly variable across the continental slope, possibly due to slumping, erosion, or changes in the depositional regime. In general, strengths increase **downcore**, and decrease **to** the south and with increasing water depth.
- (4) Water contents on the shelf **are** highest in the zone of weak shelf sediment.
- (5) Water contents in the slope province decrease with **subbottom** depth, and increase to the south and with increasing water depth.
- (6) Grain specific gravities ranged from 2.55 to 2.77 with an average value of 2.64. The variability likely results from changes in diatom content.
- (7) Where plastic behavior is exhibited, Atterberg Limits and the Unified Soil Classification System show the shelf sediment **to** be mostly inorganic silts of medium to high compressibility. Slope sediments are typically highly compressible inorganic silts or organic clays.
- (8) Navarin Basin sediment is typically **overconsolidated**, but not heavily except for a few locations. OCR values on the shelf are commonly greater than 10. Elsewhere in the province, values are OCR  $\sim$  2-5. About 15 m of sediment has been removed from the headwalls of **Zhemchug** Canyon {core G97 } .
- (9) Undrained vane shear determinations provide estimates of undrained shear strength in the upper 3 m of the sediment column that agree with **triaxial** strength determinations corrected for coring disturbance. Cyclic loading reduces static strength by 20 to 50%.
- (10) Navarin Basin province shelf **cohesionless** sediment may be susceptible to **liquefaction** by severe storm loading. The cohesive sediment is probably not susceptible to storm-wave-induced failure.

## NOMENCLATURE

- $\lambda_D$  = cyclic degradation factor applied to  $S_u$  as a result of cyclic loading
- LL = liquid limit from **Atterberg** Limit determinations
- NSP** = Normalized Soil Parameter method of shear **strength** determination
- OCR = overconsolidation ratio; defined as  $OCR = \sigma'_{vm} / \sigma'_v$
- PI = plasticity index of **Atterberg** Limits; defined as  $PI = LL - PL$
- PL = plastic limit of **Atterberg** Limit determinations
- $s_{nc}$  = ratio of static undrained **shearing strength** to isotropic consolidation stress for normally consolidated conditions
- $S_u$  = static undrained shear **strength**
- $S_v$  = undrained peak vane shear **strength**
- w = sediment water content by dry **weight**
- $W_c$  = sediment water content corrected for salt content
- z = **subbottom** depth in cm
- $\gamma_c$  = sediment bulk density
- $\gamma'_c$  = sediment bulk density corrected for the density of seawater;  
 $\gamma'_c = \gamma_c - \gamma_{sw}$
- $\gamma_{sw}$  = density of seawater
- $\sigma'_e$  = excess past overburden stress; defined as  $U'_e = \sigma'_{vm} - \sigma'_v$
- $\sigma'_v$  = in place effective overburden stress
- $\sigma'_{vm}$  = **maximum past** overburden stress
- $\Lambda_o$  = normalized **strength** parameter that is a constant for a **given** sediment

## REFERENCES

- ASTM, 1982, Annual Book of ASTM Standards, Part 19, Natural Building Stones, Soil and Rock; Philadelphia, 71 OP.
- Bishop, A.W., and D.J. Henkel, 1962, The Measurement of Soil Properties in Triaxial Test, Second Edition, Edward Arnold, Ltd., London, 228 p.
- Carlson, P.R., H.A. Karl, J.M. Fischer, and B.D. Edwards, 1982, Geologic hazards in Navarin Basin Province, Northern Bering Sea: OTC Paper 4172 14th Ann. Offshore Technology Conf., Houston, TX, May 3-6, p. 73-78.
- Casa Grande, Arthur, 1936, The determination of the preconsolidation load and its practical significance: Proc. First Int'l Conf. Soil Mech. Found. Eng., Cambridge, MA, p. 60.
- Fischer, J.M., P.R. Carlson, and H.A. Karl, 1982, Bathymetric map of Navarin Basin province, northern Bering Sea: U.S. Geological Survey Open-File Report 82-1038, 11p.
- Karl, H.A., P.R. Carlson, Jeff Fischer, Ken Johnson, and Beth Lamb, 1981, Textural variations and composition of bottom sediment: in P.R. Carlson and H.A. Karl, Seafloor geologic hazards, sedimentology, and bathymetry: Navarin Basin province, northwestern Bering Sea: U.S. Geological Survey Open-File Report 81-1217, 149p.
- Ladd, C.C., and Roger Foott, 1974, New design procedure for stability of soft clays: Am. Soc. Civil Eng., Jour. Geotech. Eng. Div., v. 100, no. GT7, p 763-786.
- Lamb, T.W., and R.V. Whitman, 1969, Soil Mechanics, John Wiley & Sons, Inc., New York, 553p.
- Lee, K.I., and J.A. Focht, Jr., 1976, Strength of the clay subjected to cyclic loading: Marine Geotechnology, v. 1, p. 165-185.
- Mayne, P.W., 1980, Cam-clay predictions of undrained strength: Am. Soc. Civil Eng., Jour. Geotech. Eng. Div., v. 106, no. GT11, p. 1219-1242.
- Mitchell, I.K., 1976, Fundamentals of Soil Behavior, John Wiley and Sons, Inc., New York, 422 p.
- Seed, H.B., and I.M. Idriss, in press, Evaluation of liquefaction potential of sand deposits based on observations of performance in previous earthquakes: Am. Soc. Civil Eng., Jour. Geotech., Eng. Div.
- Seed, H.B., and M.S. Rahman, 1978, Wave-induced pore pressure in relation to ocean floor stability of cohesionless soil: Marine Geotechnology, v. 3, p. 123-150.

CHAPTER 8: HYDROCARBON GASES IN SEDIMENTS --  
RESULTS FROM 1981 FIELD SEASON

by

Margaret Golan-Bat and **Keith A. Kvenvolden**

This study examines the distribution and origin of the hydrocarbon gases methane ( $C_1$ ), ethane ( $C_2$ ), ethene ( $C_2=$ ), ProPane ( $C_3$ ), ProPene ( $C_3=$ ), isobutane ( $i-C_4$ ), and normal butane ( $n-C_4$ ) in **surficial** sediments from the shelf, slope, and rise areas of the **Navarin** Basin province in the Bering Sea. The report covers results obtained on samples collected in 1981. **Results** for samples collected in 1980 have been reported previously (Vogel and Kvenvolden, 1981).

METHODS

Conventional gravity cores were taken from the shelf, slope, and rise areas of the Navarin Basin province. The 8 cm internal diameter core liner was cut into 10 cm sections at approximately 1 meter intervals (usually 90-100, 190-200, 290-300 cm, etc.). The sediment section was immediately extruded into one liter unlined paint cans which had two **septa-covered** holes on the side near the top. Each can was filled **with** helium-purged **salt** water and 100 ml of water was removed before the can was closed with a **double-friction-seal** lid. This resulting 100 ml headspace was then purged with helium through the septa, and the cans were immediately inverted and frozen. In the shore-based laboratory, the cans of sediment were brought to room temperature and shaken for **10** minutes by a mechanical shaker to equilibrate the hydrocarbon gases that are released from the sediment and are partitioned into the helium headspace. A sample of gas **in** this headspace was withdrawn through a septa with a gas-tight syringe. One milliliter of this sample was analyzed by gas chromatography using both flame ionization and thermal conductivity detectors. Concentrations of gases were determined by comparison **of** the integrated area of each hydrocarbon with the integrated area **of** a quantitative hydrocarbon standard. These values were then corrected for the different **solubilities** of the hydrocarbon gases in the interstitial water of the sediment sample by use of partition coefficients (0.8 for methane; 0.7 for **ethane**, propane, and butanes; 0.6 for ethene and **propene**).

The method of extraction yields semi-quantitative results; however, because all the samples were processed in the same manner, the results can be compared. The concentrations reported in Table 7 are rounded with respect to limitations of the analytical techniques. The detection limit is approximately **0.1  $\mu$ l** of methane/liter of wet sediment and **1 nl** of gas/liter of wet sediment for the other hydrocarbon gases. Error determined from analytical variation and repeat analysis is less than 20%.

RESULTS

Core locations, concentrations of hydrocarbon gas, and other relevant information for Navarin Basin province are listed in Table 7. This table is

Table 7. Hydrocarbon Gas (C<sub>1</sub>-nC<sub>4</sub>) Concentrations and Ratios from Sediment samples

from the Navarin Basin Province (1981)

Core No. and Interval (cm)	Water Depth (m)	Station No.	C <sub>1</sub> ul/l wet sediment	C <sub>2</sub>	C <sub>2</sub> :1	C <sub>3</sub>		i-C <sub>4</sub>	n-C <sub>4</sub>	$\frac{C_1}{C_2+C_3}$	$\frac{C_2}{C_2:1}$	Location	
						n1/1 wet sediment						Latitude	Longitude
<u>Shelf Sediment</u>													
<b>G1</b> 90-100 202-212	135	<b>1</b>	50 140	78 690	44 42	26 47	28 250	n.d. n.d.	n.d. n.d.	480 190	1.0 16	59°28.9'	175°35.7'
G2 90-100	143	1	47	270	150	170	68	12	33	110	1.8	59°05.6'	176°20.1'
G24 90-100 190-200	104	22	8.1 13	47 100	58 100	34 73	95 130	3 6	n.d. 14	99 73	0.82 1.0	61°31.6'	176°25.5'
G25 90-100 190-200	123	23	79 210	190 470	67 33	39 82	86 210	8 36	4 6	340 380	2.8 14.0	61°46.2'	177°30.2'
G26 90-100 190-200	122	24	7.8 18	43 66	57 81	31 44	81 200	11 6	n.d. 5	110 160	0.76 0.82	61°27.11	177°25.2'
G27 90-100 190-200	145	25	11 19	33 27	51 15	28 9	65 12	5 n.d.	4 n.d.	180 530	0.64 1.8	61°09.0'	177°47.0'
<b>G28</b> 90-100	128	26	29	42	66	31	83	4	3	400	0.64	61°13.5'	177°23.4'
G29 <b>90-100</b>	128	26	4.8	26	60	27	93	n.d.	5	90	0.44	61°13.5'	177°23.6"
<b>G31</b> 90-100 190-200	137	<b>28</b>	120 37	270 34	94 44	54 22	97 85	8 4	6 n.d.	380 660	2.9 0.76	60°12.1'	176° 35.5'
G32 90-100 190-200	130	29	34 62	120 70	210 61	100 30	130 20	21 4	22 n.d.	160 610	0.54 1.1	60°11.0'	176°13.1'
G33 90-100 190-200	130	29	47 160	43 340	86 91	26 80	89 81	3 8	n.d. 13	670 380	0.50 3.7	60°11.1'	176°13.1'
<b>G34</b> <b>90-100</b>	115	30	3.9	42	72	34	120	4	6	51	0.59	57°20.1'	172°42.7'
G35 90-100	115	30	7.5	34	39	24	67	4	n.d.	130	0.88	57°20.0'	172°42.7'
G60 90-100 190-200	140	56	23 11	270 390	40 55	34 62	34 71	5 15	6 n.d.	77 25	6.7 7.1	59°48.3'	177°24.6'
<b>G61</b> 90-100	141	57	36	230	30	28	98	n.d.	n.d.	140	7.4	59°48.3'	177°26.0'
G62 90-100 189-199	139	58	33 92	250 1300	38 56	36 52	63 120	4 6	n.d. n.d.	120 66	6.4 24	59°49.6'	177°29.8'
<b>G63</b> 90-100	135	59	28	180	17	23	65	18	2	140	11	59°51.2'	177°29.5'
<b>G73</b> 90-100	146	69	28	200	31	20	88	3	n.d.	130	6.5	59°27.1'	176°29.4'
G77 90-100	145	73	33	470	270	330	120	25	62	41	1.8	59°54.1'	178°09.1'
<b>G78</b> 90-100	139	74	18	420	430	360	190	66	26	23	0.96	60°13.1'	177°33.1'
G79 90-100 190-200	141	75	56 120	31 370	51 130	15 130	25 75	n.d. 13	n.d. 28	1200 240	0.6 2.7	60°30.1'	176°59.2'
G105 90-100 191-201	144	95	29 140	31 180	20 38	15 31	35 34	n.d. 5	n.d. n.d.	630 670	1.6 4.8	60°09.0'	176°59.3'
G106 90-100 190-200	135	96	57 180	40 540	38 27	18 26	36 57	n.d. 5	n.d. n.d.	970 320	1.1 20	59°40.0'	175°59.3'

Table 7. (Continued)

Core No. and Interval (cm)	Water Depth (m)	Station No.	C <sub>1</sub> ul/l wet sediment	C <sub>2</sub>	C <sub>2:1</sub>	C <sub>3</sub>	C <sub>3:1</sub> n1/1 wet sediment	i-C <sub>4</sub>	n-C <sub>4</sub>	$\frac{C_1}{C_2+C_3}$	C <sub>2</sub> C <sub>2:1</sub>	Location		
												Latitude	Longitude	
<u>Slope Sediment</u>														
G4	90-100	2816	5	8.2	n.d.	n.d.	23	34	n.d.	n.d.	360		58°31.3'	177°26.0'
	190-200			11	67	82	49	36	4	10	96	0.82		
	290-300			17	76	46	40	32	n.d.	8	150	1.6		
G7	95-105	173	7	53	420	140	110	55	16	21	99	3.0	59°38.3'	178°15.3'
G11	90-100	980	11	180	230	24	52	3400	170	170	630	9.8	60°39.2"	179°34.6'
	190-200			84000	950	110	3400	*	150	180	19000	8.7		
G12	90-100	1683	12	9.6	59	63	32	36	6	4	110	0.94	60°34.3'	179°45.1'
	190-200			17	150	41	410	25	180	46	30	3.6		
	262272			25	300	22	610	37	260	46	28	13		
G13	90-100	2080	13	5.8	38	36	34	29	n.d.	n.d.	81	1.0	60°19.3'	179°49.1'
	190-200			460	360	14	59	770	46	n.d.	1100	2?		
	290-300			49000	450	150	700	*	32	36	43000	3.1		
G14	90-100	1826	14	37	160	75	140	39	9	26	120	2.1	60°09.6'	179°50.1'
	190-200			230	300	19	610	120	65	49	260	16		
	290-300			780	430	22	690	130	84	59	700	20		
	390-400			12000	410	39	2700	*	34	26	3900	10		
	552-562			44000	270	420	1700	*	55	28	22000	0.63		
G15	90-100	2744	15	25	42	73	24	50	5	3	370	0.58	59°52.4'	179°59.5'
	190-200			57	33	74	19	31	4	n.d.	1100	0.44		
	290-300			150	640	40	49	33	5	n.d.	220	16		
	390-400			1400	1300	22	240	63	20	n.d.	900	61		
G17	90-100	900	17	1.2	26	50	18	29	1	n.d.	28	0.51	60°12.6'	179°21.5'
	190-200			4.5	57	45	28	45	4	n.d.	54	1.2		
	283-293			6.4	49	30	21	43	6	n.d.	92	1.6		
G18	90-100	884	17	2.8	37	36	18	23	3	n.d.	50	1.0	60°13.1'	179°21.51
	190-200			11	37	35	13	52	3	n.d.	230	1.1		
G19	90-100	1018	18	16	100	41	39	55	3	3	110	2.4	60°10.2'	179°27.9'
	190-200			13	270	190	130	70	9	17	34	1.4		
	290-300			170	1000	22	210	70	24	2	140	47		
	370-380			290	990	39	240	110	52	9	230	26		

n.d. = not detectable

= not reported

\* = concentration not reported due to methane interference

Table 7. (Continued)

Core No. and Interval (cm)	Water Depth (m)	Station No.	C <sub>1</sub> ul/1 wet sediment	C <sub>2</sub>	C <sub>2:1</sub>	C <sub>3</sub>	C <sub>3:1</sub>	i-C <sub>4</sub>	n-C <sub>4</sub>	C <sub>1</sub> C <sub>2</sub>		Location		
										C <sub>2</sub> +C <sub>3</sub>	C <sub>2:1</sub>	Latitude	Longitude	
Slope Sediment (continued)														
	90-100	1005	18	15	270	180	85	80	8	14	41	1.5	60°10.6'	179°26.9'
	190-200			27	510	200	130	83	12	17	43	2.6		
	290-300			47	710	93	150	48	12	19	55	7.6		
	364-374			52	780	180	270	97	30	36	50	4.3		
G21	90-100	1630	19	5.7	61	59	36	51	6	n.d.	58	1.0	60°06.1'	179°34.5'
	190-200			8.8	100	170	54	61	7	3	56	0.60		
G22	90-100	1670	19	5.7	150	200	120	75	12	20	21	0.76	60°06.1'	179°34.5'
	190-200			5.8	140	120	100	52	9	17	24	1.1		
	290-300			7.0	52	44	28	27	5	n.d.	89	1.2		
	390-400			8.5	65	36	26	36	3	n.d.	93	1.8		
G37	190-200	1100	32	5.7	91	52	32	68	7	n.d.	45	1.8	57°49.6'	174°23.5'
	290-300			8.9	160	130	46	120	9	10	42	1.2		
G38	90-100	1080	33	1.3	37	41	32	53	3	n.d.	18	0.91	58°10.1'	175°29.2'
	190-200			7.8	81	36	29	85	3	n.d.	71	2.3		
	290-300			130	1600	70	43	130	10	4	77	23		
G39	90-100	915	34	13	56	66	39	65	7	6	140	0.84	58°20.1'	174°29.1'
	190-200			32	60	56	32	84	8	4	350	1.1		
	290-300			39	250	36	35	31	4	n.d.	140	6.9		
G44	90-100	2530	39	5.4	20	54	16	86	3	n.d.	150	0.37	56°51.4'	174°08.5'
	190-200			13	26	52	17	61	n.d.	n.d.	310	0.50		
	290-300			14	54	63	39	63	4	n.d.	150	0.86		
	390-400			19	45	56	29	52	3	n.d.	260	0.80		
	490-500			17	41	86	26	67	3	n.d.	250	0.47		
G47	90-100	2760	41	2.7	36	87	23	81	3	n.d.	45	0.41	56°58.2'	174°21.2'
	190-200			7.5	150	240	120	130	19	20	27	0.64		
	290-300			6.8	39	59	21	86	3	n.d.	110	0.67		
	390-400			7.0	67	100	42	110	7	9	64	0.65		
	490-500			6.2	41	56	28	68	4	n.d.	91	0.73		
G49	90-100	1770	43	4.8	30	47	26	71	n.d.	n.d.	85	0.64	57°38.5'	175°38.0'
	190-200			7.8	45	75	28	57	n.d.	3	110	0.61		
	290-300			10	31	92	18	57	n.d.	rid.	210	0.34		
	390-400			14	57	51	23	92	4	n.d.	180	1.1		
	490-500			16	63	71	32	80	4	n.d.	170	0.89		

n.d. = not detectable

Table 7. (Continued)

Core No. and Interval (cm)	Water Depth (m)	Station No.	C <sub>1</sub> ul/l wet sediment	C <sub>2</sub>	C <sub>2</sub> :1	C <sub>3</sub>	C <sub>3</sub> :1	i-C <sub>4</sub>	n-C <sub>4</sub>	C <sub>1</sub> C <sub>2</sub> +C <sub>3</sub>	C <sub>2</sub> C <sub>2</sub> :1	Location		
												Latitude	Longitude	
Slope Sediment (continued)														
G52	90-100	1070	46	4.3	48	31	22	21	4	n.d.	61	1.5	58°33.6'	177°53.2'
	190-200			4.3	22	20	13	17	n.d.	n.d.	120	1.1		
	290-300			5.6	22	22	11	19	3	n.d.	170	1.0		
	390-400			5.1	15	28	11	12	n.d.	n.d.	180	0.53		
	490-500			5.3	26	17	16	25	n.d.	n.d.	130	1.6		
	570-580			5.3	30	23	14	30	3	n.d.	120	1.3		
G53	90-100	2676	47	3.0	53	72	45	32	3	9	31	0.74	58°23.2'	176°25.1'
G55	90-100	2320	49	5.2	27	12	13	10	n.d.	n.d.	130	2.3	57°45.7'	175°30.4'
	190-200			18	36	14	13	23	n.d.	n.d.	360	2.5		
	290-300			25	55	23	16	21	n.d.	n.d.	350	2.5		
	390-400			34	210	22	26	28	3	n.d.	140	9.5		
G58	90-100	179	53	11	44	39	41	22	n.d.	n.d.	130	1.1	59°26.1'	177°28.4'
	190-200			19	1400	250	350	110	25	61	11	5.5		
G65	90-100	436	61	6.3	35	24	22	23	3	n.d.	110	1.5	59°25.4'	177°51.2'
	190-200			7.3	34	28	24	56	5	n.d.	130	1.2		
G66	90-100	580	62	56	62	31	500	54	200	24	100	2.0	59°24.7'	178°14.5'
	190-200			110	4800	83	790	77	260	31	20	58		
	290-300			200	7300	17	970	110	320	26	24	440		
G67	90-100	167	63	74	540	71	80	66	8	11	120	7.6	59°38.7'	178°14.2'
G68	90-100	1048	64	19	130	23	20	75	n.d.	n.d.	130	5.7	59°38.6'	178°37.2'
	190-200			63	440	13	26	130	n.d.	n.d.	130	34		
G69	90-100	1230	65	1.6	76	62	57	90	n.d.	n.d.	12	1.2	59°15.8'	178°34.4'
	190-200			8.8	57	32	32	100	3	n.d.	99	1.8		
G71	90-100	520	67	18	180	38	22	130	7	n.d.	89	4.7	58°48.0'	178°00.0'
	190-200			71	1400	37	45	50	10	n.d.	47	39		
	290-300			170	93	16	120	57	10	n.d.	790	6.0		
G74	85-95	152	70	30	190	17	18	140	n.d.	n.d.	150	11	59°25.5'	177°11.9"
G80	90-100	152	76	16	180	180	150	73	9	31	48	1.0	60°29.4'	177°53.3'
G82	90-100	860	78	5.6	61	37	23	33	5	n.d.	66	1.6	60°27.2'	179°29.1'
G83	90-100	1120	79	2.4	38	48	27	49	n.d.	4	37	0.8	60°26.2'	179°53.4'
G84	90-100	780	80	23	74	33	31	68	4	n.d.	220	2.2	59°57.9'	178°59.2'
G85	90-100	1745	81	6.4	28	41	21	52	4	n.d.	130	0.68	59°51.9'	179°09.7'
	190-200			10	49	41	34	51	5	n.d.	130	1.2		
G86	90-100	2195	82	64	90	150	74	80	4	18	390	0.59	60°09.21	179°51.4'
	190-200			320	930	38	120	170	21	7	310	24		
	280-290			34000	1900	54	1700	*	54	n.d.	9400	35		
G88	90-100	205	83	4.8	120	32	52	31	8	8	2a	3.6	61°08.1"	178°46.1"
	190-200			9.2	290	86	120	47	n.d.	14	23	3.3		

n. d. . not detectable

\* = concentration not reported due to methane interference

Table 7. (Continued)

Core No. and Interval (cm)	Water Depth (m)	Station No.	C <sub>1</sub> ul/l wet sediment	v <sub>2</sub>	C <sub>2:1</sub>	C <sub>3</sub>	C <sub>3:1</sub>	i-C <sub>4</sub>	n-C <sub>4</sub>	-C <sub>1</sub> C <sub>2</sub> +C <sub>3</sub>	C <sub>2</sub> . C <sub>2:1</sub>	Location		
												Latitude	Longitude	
<u>Rise Sediment</u>														
G6	90-100	3395	6	4.1	39	140	49	58	5	11	47	0.29	58°08.3'	177°23.5'
	190-200			8.5	41	58	27	34	5	n.d.	120	0.71		
	290-300			3.5	120	310	95	120	8	19	16	0.39		
	390-400			7	29	23	8	33	n.d.	n.d.	190	1.3		
G42	90-100	3150	37	8.4	20	34	19	50	1	n.d.	210	0.59	57°57.8'	175°00. 0'
	190-200			17	43	66	32	77	3.	n.d.	220	0.65		
	290-300			21	48	4s	22	69	2	n.d.	300	0.99		
G48	90-100	2910	42	7.7	24	39	22	81	n.d.	n.d.	170	0.62	57°06.6'	174°035.5'
	190-200			13	45	88	26	59	3	n.d.	190	0.50		
	290-300			15	23	52	16	77	3	n.d.	380	0.44		
	390-400			20	37	100	24	65	5	n.d.	320	0.37		
G50	90-100	3430	44	4.4	21	55	22	89	3	n.d.	100	0.39	57°52.2'	176°28.5'
	190-200			6.3	36	69	28	74	2	n.d.	98	0.52		
	290-300			7.9	47	62	30	75	3	n.d.	100	0.77		
	390-400			12	26	43	17	97	n.d.	n.d.	290	0.60		
	490-500			19	100	91	54	29	5	73	120	1.1		
G51	90-100	3220	45	4.3	1s	26	13	28	n.d.	n.d.	140	0.71	58°20.4"	177°25.1'
	190-200			7.5	20	24	16	24	n.d.	n.d.	210	0.53		
G54	90-100	3220	48	10	60	32	24	19	n.d.	n.d.	120	1.9	58°08.4'	176°02.9'
	190-200			18	29	28	15	32	n.d.	n.d.	420	1.0		
	290-300			16	30	25	16	28	n.d.	n.d.	350	1.2		
G56	90-100	2925	50	6.0	19	34	14	70	n.d.	n.d.	1s0	0.55	58°11.6'	176°00.1'
	190-200			16	27	44	16	96	4	n.d.	360	0.60		
G57	90-100	3395	51	3.9	14	25	10	25	n.d.	n.d.	160	0.5s	57°57.3'	176°58. s'
	190-200			6.9	24	32	16	54	4	n.d.	170	0.77		
	290-300			13	240	270	200	110	15	39	30	0.90		
	390-400			12	190	320	170	130	15	39	33	0.59		
	470-480			26	520	18	71	22	7	n.d.	44	29		
G70	90-100	3390	66	6.5	13	22	41	22	n.d.	n.d.	300	0.61	58°31.6'	178°28.0'
	190-200			8	1s	25	16	62	n.d.	n.d.	230	0.72		
	290-300			12	51	3s	25	89	4	n.d.	160	1.3		
	390-400			8.7	15	20	16	46	n.d.	n.d.	2s0	0.76		
G76	90-100	3210	72	4.4	36	74	39	42	n.d.	5	59	0.49	59°21.5'	179°06.6'
	190-200			11	130	170	110	79	8	19	45	0.72		

n. d. = not detectable

divided into three sections, namely, cores taken from the outer shelf (water depths from 100 to 250 m), the slope (water depths from 150 to 2800 m), and the rise (water depths from 2800 to approximately 3600 m). These three areas are delineated by the 150 m and 2800 m contour lines, and in Figure 36 samples are identified by **their** core number.

Information **relative** to the ranges of concentrations of hydrocarbon gases found in sediments of the shelf, slope, and rise are summarized in Table 8. Methane is the most abundant hydrocarbon gas in all the sediment samples analyzed and **is** typically present in concentrations that are 2 to 3 orders of magnitude greater than the concentrations of the other low molecular weight hydrocarbons (**LMWH**).

**Areal** distributions of maximum concentrations of  $C_1$ ,  $C_2+C_3$  and  $n-C_4+i-C_4$  are shown in Figures 37, 38 and 39, respectively. These maximum concentrations generally reflect results of analyses of the deepest samples obtained at a given core location, because the deepest samples usually have the highest concentrations of gas (Table 7). In five cores (11, 13, 14, 15 and 86), all located on the slope, the maximum concentrations of  $C_1$  exceed 1000  $\mu\text{l/l}$  and range from 1400 to 84000  $\text{Pi/l}$ . In each of these cores  $C_1$  concentrations increase 2 to 4 orders of magnitude with depth (Table 7).

Concentrations of  $C_2$  exceed 1000  $\text{nl/l}$  in samples from seven cores of slope sediment (15, 19, 38, 58, 66, 71 and 86) and from one core of shelf sediment (62). In these cores,  $C_2$  concentrations increase 1 to 2 orders of magnitude with depth (Table 7). Concentrations of  $C_3$  are usually less than concentrations of  $C_2$ , but the distributions of these gases tend to be parallel. **Figure 38** shows locations of eleven cores where the maximum concentrations of  $C_2 + C_3$  exceed 1000  $\text{nl/l}$ . These cores include numbers 11, 13 and 14 in addition to the **eight** cores listed above.

Butane ( $n-C_4$  and  $i-C_4$ ) is generally the least abundant **LMWH** in **shelf**, **slope** and **rise** sediment. Wherever detected,  $i-C_4$  is generally more abundant than  $n-C_4$ ; in samples  $n-C_4$  could not be measured. The highest concentrations of  $n-C_4+i-C_4$  are found in slope sediment. Core 66 had the highest amount of  $i-C_4$  (320  $\text{nl/l}$ ) and core 11 had the most  $n-C_4$  (100  $\text{nl/l}$ ).

The **alkenes** ( $C_2=$  and  $C_3=$ ) are present in most sediment samples in amounts less than  $C_2$  but generally greater than  $C_3$ . Concentrations of  $C_2=$  and  $C_3=$  show no discernible trends with depth. In those samples where  $C_1$  concentrations exceeded about 12000  $\mu\text{l/l}$ ,  $C_3=$  could not be measured because of interference resulting from our method of analysis.

#### Biogenic Methane

The most abundant gas in sediments of **Navarin** Basin province is  $C_1$ , and in five cores (11, 13, 14, 15, 86), all located in **Navarinsky** Canyon, maximum concentrations exceed 1000  $\text{Pi/l}$  (Table 7 and Figure 37). During the 1980 season, the only core (G-37) analyzed with concentrations of  $C_1$  exceeding 1000  $\mu\text{l/l}$  (1900  $\mu\text{l/l}$ ) was from the rise near the mouth of **Navarinsky** Canyon (**Vogel** and **Kvenvolden**, 1981). Concentrations for four of the **five** cores (11, 13, 14, and 86) taken during 1981 approach or exceed the saturation of the

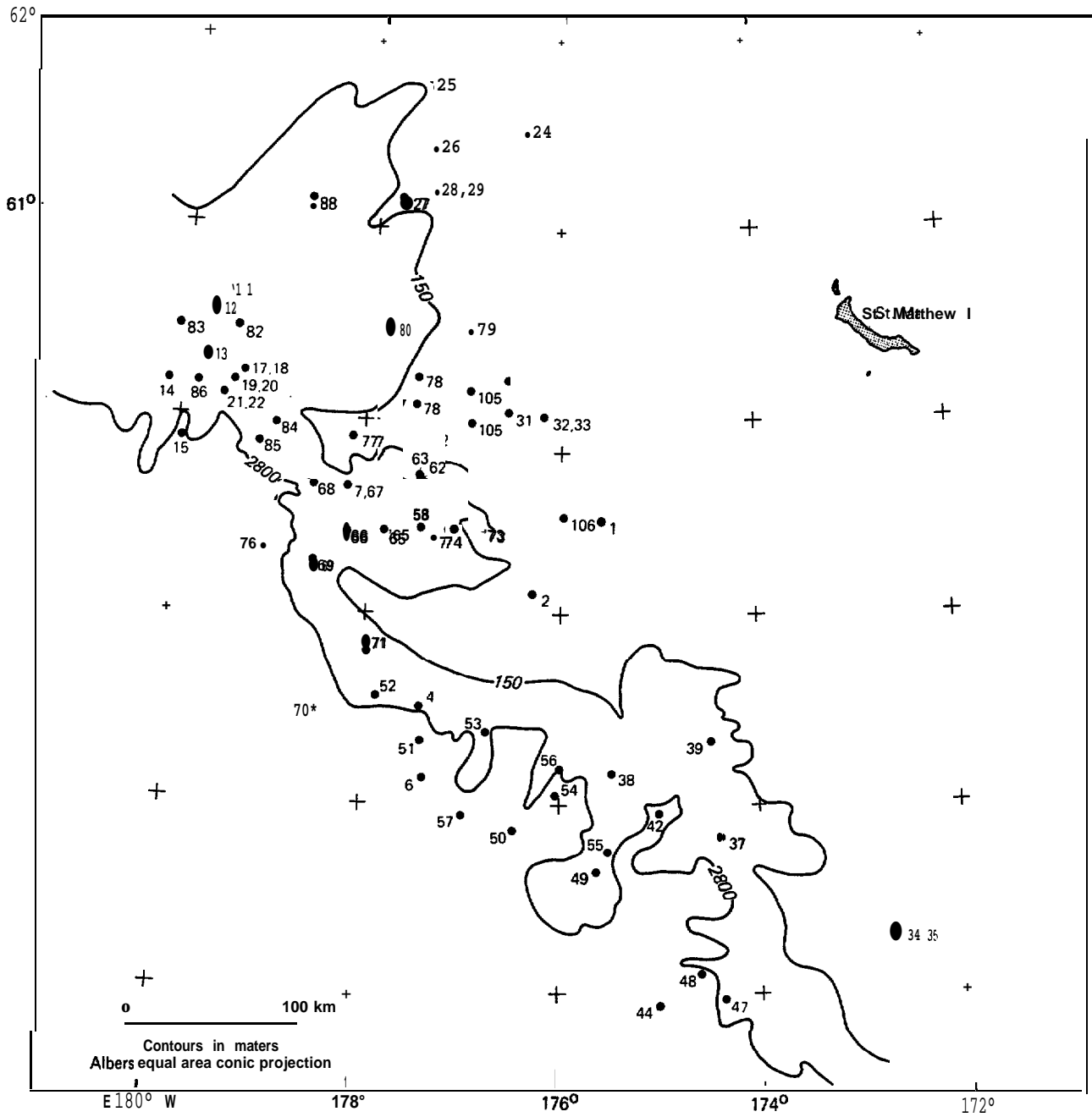


Figure 36. Location of hydrocarbon gas sampling sites in the Navarin Basin province. Sites are designated with core numbers.



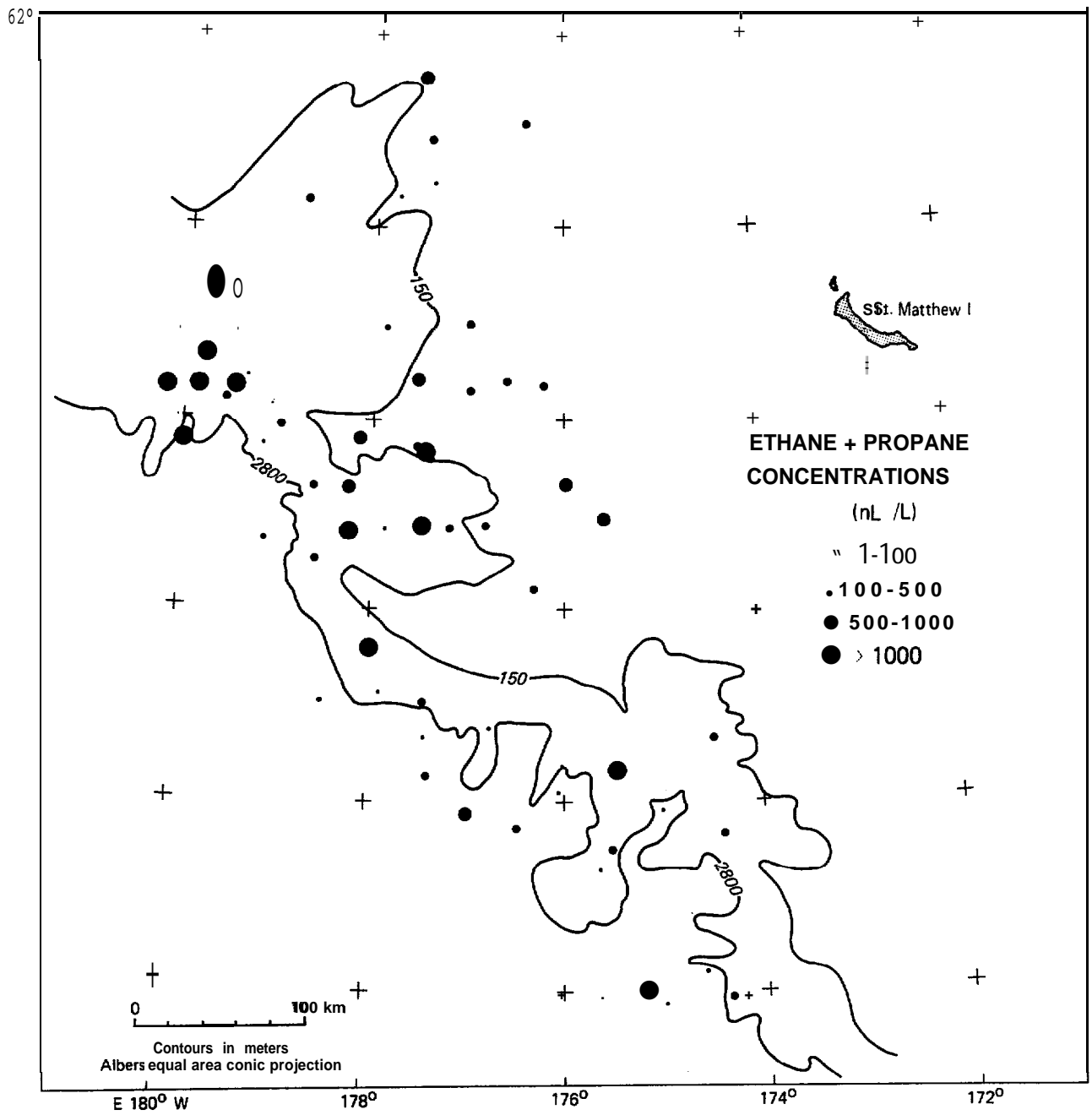


Figure 38. Distribution of maximum concentrations of ethane plus propane in **nL/l** of wet sediment.

interstitial water at atmospheric pressure and temperature (about 40 ml of Cl per liter of seawater according to Yamamoto et al., 1976). Because Cl volubility increases with increasing pressure, the measured concentrations only represent minimum values; some quantity of gas likely escaped during the sampling procedure. In fact, core descriptions for three of the five cores include remarks about cracks attributed to escape of gas. The possibility that Cl is present at concentrations exceeding its volubility in the interstitial water at depth may lead to high pore-water pressures and hence, sediment instability; seismic evidence indicates slumping of the sediments in the Navarinsky Canyon region (Carlson et al, 1982) which may be due in part to the high concentrations of gas present. Cl concentration profiles with depth for these five cores are shown in Figure 40A. The rapid increase in amount. of Cl with depth can be attributed to the presence of Cl-producing bacteria operating under anoxic conditions. A zone of low Cl concentration probably exists between the sediment-water interface and about 100 cm depth where the first measurements were made. This zone is generally referred to as the zone of sulfate reduction, where the low Cl concentrations have been attributed to bioturbation and oxidation by molecular oxygen (Reeburgh, 1969), sulfate inhibition of methanogenesis (Martens and Berner, 1974), and to anaerobic Cl oxidation by sulfate-reducing bacteria (Barnes and Goldberg, 1976; Reeburgh and Heggie, 1977). Below the zone of sulfate reduction is the zone of Cl production where high concentration of Cl occurs. Here the Cl is being generated by the anaerobic microbial decomposition of the organic-rich mud which ranges from 0.7 to 1.43% organic carbon (Fischer, 1981). Those samples having high Cl concentrations (greater than 1000  $\mu\text{l/l}$ ) also have large  $C_1/(C_2+C_3)$  values ranging from 900 to 43,000 (Table 7). These ratios indicate a biogenic source for Cl according to criteria defined by Bernard et al. (1977).

At most stations in Navarin Basin the Cl concentrations are less than 1000  $\mu\text{l/l}$  (Table 7 and Fig. 37). For these stations  $C_1/(C_2+C_3)$  values are usually low. In fact, for many samples the ratio is less than 50, which is the upper limit of the range of values assigned by Bernard et al. (1978) to gas from thermogenic sources. However, as pointed out by Kvenvolden and Redden (1980), use of this ratio for assigning source is equivocal where gas concentrations are low. In the case of Navarin Basin, we believe that most of the  $C_1$  and other hydrocarbon gases present are from biogenic sources and not from thermogenic sources. The low  $C_1/(C_2+C_3)$  ratios are attributed to preferential loss of Cl during sampling from sediments in which the original concentrations of Cl are much lower than 1000  $\mu\text{l/l}$ .

#### Other Biogenic Hydrocarbons

Other LMWH besides Cl may be biologically produced, as suggested by Emery and Hoggan (1958) and Bernard et al. (1978). The relationship of  $C_1$  to these other hydrocarbon gases may provide a clue to their origin. At the eleven sites with  $C_2+C_3$  concentrations greater than 1000  $\text{nl/l}$  (11, 13, 14, 15, 19, 38, 58, 62, 66, 71, and 86), five sites (11, 13, 14, 15, and 86) show a strong correlation between increasing Cl concentrations and increasing  $C_2+C_3$  concentrations with depth (Figure 41). This correlation suggests that the microbiological processes that produced Cl may be operating in parallel with the process responsible for  $C_2$  and  $C_3$ . Samples at all five sites also have

anomalously high butane values (Table 7, Figs. 39 and 42) which suggest butane may also result from microbiological processes.

The production of alkenes is controlled by biological processes and has been produced by microbes in the laboratory (Davis and Squires, 1954), by marine organisms (Hunt, 1974), and by bacteria in soils (Primrose and Dilworth, 1976). In the Navarin Basin province, alkene concentrations vary with depth but generally remain at about the same level of concentration throughout the area.

#### Thermogenic Hydrocarbons

Two ratios ( $C_1/(C_2+C_3)$  and  $C_2/C_{2=}$ ) were used by Kvenvolden et al. (1981) to attempt to distinguish biogenic and thermogenic hydrocarbon gases in sediments. Extrapolating from the work of Bernard et al. (1976) and from Cline and Holmes (1977) they proposed that samples containing gases with  $C_1/(C_2+C_3)$  values less than 50 and with  $C_2/C_{2=}$  values greater than 1 may have thermogenic sources.

of the thirteen sites (12, 19, 20, 22, 38, 57, 58, 60, 62, 66, 71, 77, and 88) where  $C_1/(C_2+C_3)$  ratios are low and  $C_2/C_{2=}$  ratios are high (Table 7), core 66 is of particular interest. The  $C_1/(C_2+C_3)$  values in core 66 are 20 and 24 at 200 and 300 cm depth. These values are comparable to the ratios of possible thermogenic gas in cores from St. George Basin (Kvenvolden and Redden, 1980) and core 36 from the 1980 work in Navarin Basin (Vogel and Kvenvolden, 1981). The  $C_2/C_{2=}$  ratio of 440 in Core 66 is the highest in the sampling area and in fact, is two orders of magnitude greater than most of the other ratios in the region. The value of the ratio is one order of magnitude greater than the highest value (50) at a minor anomaly observed on the Bering Shelf of St. George Basin (Kvenvolden and Redden, 1980; Kvenvolden et al., 1981). The value of the  $C_2/C_{2=}$  ratio in core 66 is almost a factor of three greater than the highest value (160) obtained from the 1980 Navarin Basin study from core 36 (Vogel and Kvenvolden, 1981).

Figure 42 summarizes the cores with anomalous concentrations of  $C_1$ ,  $C_2$ , and/or  $C_3$  and with  $C_1/(C_2+C_3)$  and  $C_2/C_{2=}$  values indicating a possible thermogenic origin. Of the thirteen cores mentioned above, where the  $C_1/(C_2+C_3)$  values are less than 50 and the  $C_2/C_{2=}$  values are greater than 1, the majority are not of special interest for various reasons. For example, concentrations from core 12 did not increase particularly rapidly with depth. Core 38 has mostly background concentration levels, with only one anomalous concentration (ethane) at the 300-cm depth, the deepest sample analyzed in the core. Core 77 was only sampled at the 90-100 cm depth interval and also had high concentrations of alkenes. Core 88 has background concentrations and cores 22, 57, and 71 have erratic concentration versus depth profiles. Cores 19 and 20 are at almost the same coring location and have mostly high amounts of ethane. A longer core is needed here to determine if these high values continue to increase with depth. Cores 60 and 62 on the shelf and core 58 on the slope are of some interest, but due to the short cores obtained from these locations, it is difficult to predict and interpret the concentration gradient with depth.

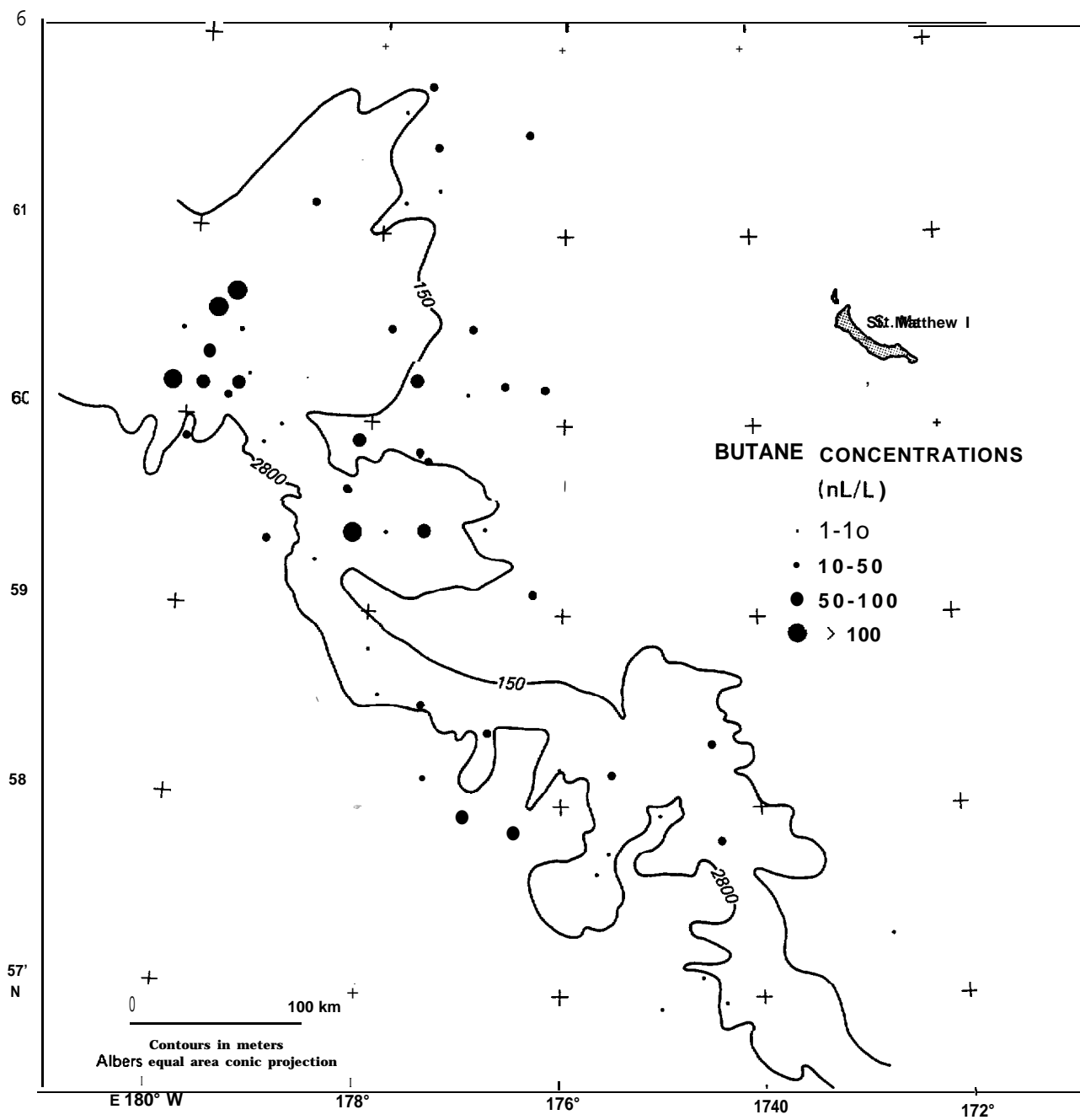


**Figure 39.** Distribution of maximum concentrations of butane in **nl/l** of wet sediment.

CONCENTRATIONS OF C<sub>1</sub>

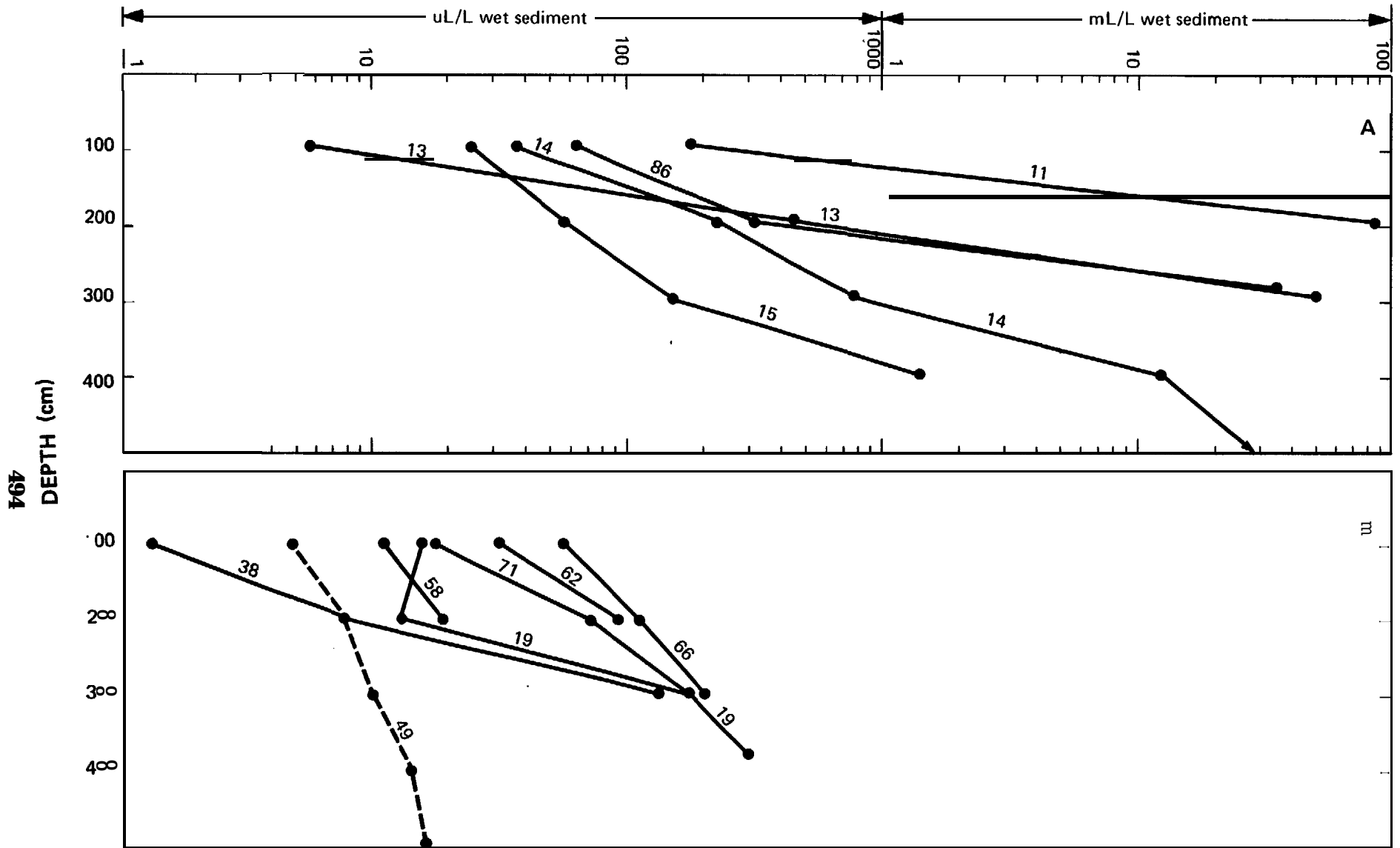
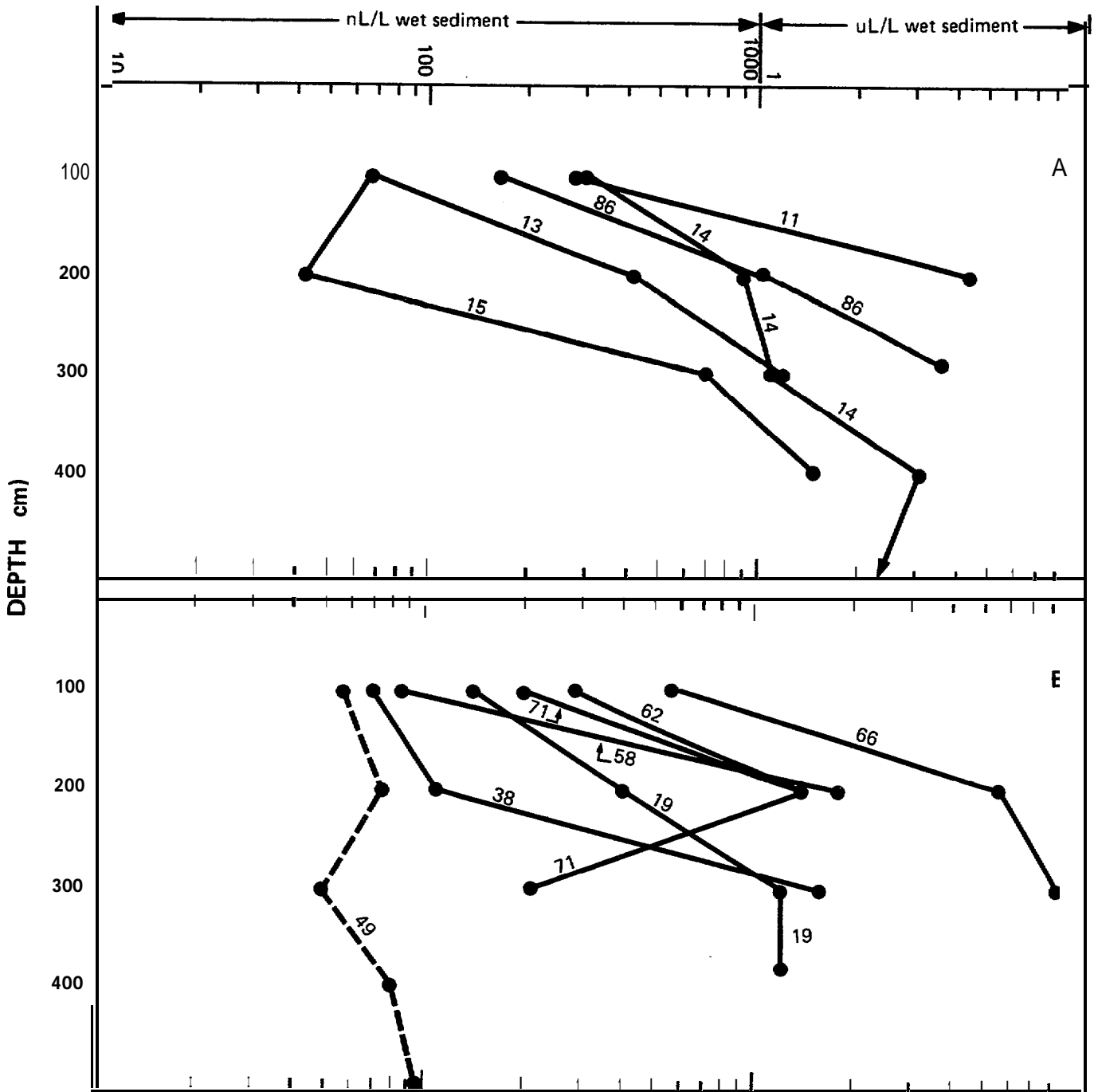


Figure 40. Graph of concentrations of C<sub>1</sub> in µl/l and ml/l wet sediment vs. depth in centimeters for sediment samples from the eleven sites in the Navarin Basin Province where C<sub>2</sub>+C<sub>3</sub> concentrations reach or exceed 1 µl/l wet sediment at some depth interval. Figure A groups those profiles whose C<sub>1</sub> concentrations exceed 1 ml/l wet sediment at some depth interval while Figure B groups the remaining cores. The dashed line in Figure B is the profile of a core which represents background concentration levels.

### CONCENTRATIONS OF C<sub>2</sub> + C<sub>3</sub>



"Figure 41. Graph of concentrations of C<sub>2</sub>+C<sub>3</sub> in nl/l and µl/l wet sediment vs. depth in centimeters for sediment samples from the eleven sites in the Navarin Basin Province where C<sub>2</sub>+C<sub>3</sub> concentrations reach or exceed 1 µl/l wet sediment at some depth interval. Figure A groups those profiles whose C<sub>1</sub> concentrations exceed 1 ml/l wet sediment at some depth interval while Figure B is the profile of a core which represents background concentration levels.

Anomalous* Parameters				Core #		
C1	C2	C3	R	Shelf	Slope	Basin
•				61,73,79	7,67	
		•		32		6,76
			•		22,88	
•	•			1,25,31,33, 105,106		
•		•			13,14	
•	•			2,78		
•			•	60		
		•	•		12	
•	•	•			11,15, 86	
•	•		•	62	3 8 , 7 1	
•	•	•	•	77	20,58	57
•	•	•	•		19,66	

\* Concentrations of C1 (methane) , C2 (ethane) , C3 (propane) that are above background for the region indicated and R (ratios) that indicate a **thermogenic** origin (C1/(C2+C3) values that are low and C2/C3= values that are high).

Figure 42. Tally of anomalous parameters for **cores** in the regions indicated.

## RELATIONSHIP TO GEOPHYSICAL ACOUSTIC ANOMALIES

Geophysical evidence shows that extensive areas in the northern shelf areas of the **Navarin** Basin province may contain gas-charged sediment (**Carlson** and others, 1982). **Geochemical** data from the same areas on the shelf show that gas is present in cores collected where seismic anomalies suggest **gas-charged** sediment. However, the amount of gas observed **is** not large enough to be responsible **for the** seismic anomalies. Actually, the **anomalies occur at depths below** which sediment samples could be recovered (i.e. greater than about 15 m). **Thus**, a correlation between our **geochemical** data and the occurrence of geophysical anomalies attributed to gas-charging of sediment cannot be **firmly** established.

## CONCLUSIONS

Hydrocarbon gases are common **in** the upper **five** meters of sediment **in** the Navarin Basin province. Locations with highest concentrations of gases are found **in** the slope sediment, followed by sediment of the shelf and rise, respectively. **Cl** **is** the most abundant hydrocarbon gas in all three regions and is generally present in concentrations that are two to three orders of magnitude greater than the higher molecular weight hydrocarbon gases. In four cores, all from the slope, the concentration of **C<sub>1</sub>** ranged from **12,000 to 84,000  $\mu$ l/l** and is probably being generated from the microbial decomposition of **organics** in the anoxic **mud** found in Navarinsky Canyon. Ratios of **C<sub>1</sub>/(C<sub>2</sub>+C<sub>3</sub>)** are very large for these samples, ranging from 900 to 43,000, indicating mainly a **biogenic** source. These concentrations may be near or exceed the **solubility** of **Cl** in interstitial water at depth and thus the gas may affect the stability of the sediment.

**C<sub>2</sub>+C<sub>3</sub>** concentrations are greater than 1000 **nl/l** **in** eleven cores taken at nine locations on the slope and two on the shelf. In seven of these cores, the trends of increasing **C<sub>2</sub>+C<sub>3</sub>** concentration strongly correlate with increasing concentration of **Cl** down the core. Therefore, the microbiological processes that account for the **Cl** concentrations may be related to the processes producing the high **C<sub>2</sub>+C<sub>3</sub>** concentrations in these cores.

Low concentrations of **i-C<sub>4</sub>** and **n-C<sub>4</sub>** are present but are not detectable **in** many samples. The highest **i-C<sub>4</sub>+n-C<sub>4</sub>** concentrations are found in the **slope** sediment. **Anomalously** high **i-C<sub>4</sub>+n-C<sub>4</sub>** concentrations were found in **all** five cores that had concentrations of **C<sub>2</sub>+C<sub>3</sub> > 1000 nl/l** and **Cl > 1000  $\mu$ l/l**.

The **alkenes** are generally present **in** all the samples and are likely the result of biological activity in the sediment. Concentrations are generally low and average about **50 nl/l** in the sediment of the shelf and slope and are slightly higher in the rise sediment, averaging about **70 nl/l**. Concentrations of the alkenes do not show distinctive trends with depth.

One core in the Navarin **Basin** province **is** of particular interest with respect to **geochemical** prospecting. Core 66 has a mixture of gases that suggest a **thermogenic** source. The **C<sub>1</sub>/(C<sub>2</sub>+C<sub>3</sub>)** ratios are 20 and 24 at the 200 and 300 **cm** depths, respectively, and the **C<sub>2</sub>/C<sub>2=</sub>** ratios are **58 and 440**. **C<sub>2</sub>+C<sub>3</sub>** has the highest concentration (**>8000 nl/l**) of any measured in the 1981 study

Table 8. Hydrocarbon Gas ( $C_1$ - $nC_4$ ) Concentration and Ratio Ranges from Sediment Samples from the Navarin Basin Province (1981). Methane ( $C_1$ ) concentrations are in  $\mu\text{l/l}$ ; the other hydrocarbon concentrations are in  $\text{nl/l}$ .

	Shelf	Slope	Rise
$C_1$	<b>4</b> - 200	1 - 84000	4 - 2 6
$C_2$	27 - 1300	n.d.- 7300	13 - 520
$C_3$	10- 360	<b>11</b> - 3400	8 - 200
$C_2=C_3$	15 - 430	n.d.- 420	18 - 320
$C_3=C_4$	12 - 250	n.d.- <b>3400</b>	<b>19 - 130</b>
$i-C_4$	<b>n.d.-</b> 66	n.d.- 320	<b>n.d.-</b> 15
$n-C_4$	<b>n.d.-</b> 62	n.d.- 180	<b>n.d.-</b> 73
$C_1/C_2+C_3$	23 - <b>1200</b>	11 - 43000	16 - 420
$C_2/C_2=C_3$	0.44- 24	0.44- 440	0.29- 29

n.d. - not detectable

area.  $C_4$ 's are also present in anomalously high concentrations: for example, the amount of the  $i-C_4$  (320  $\text{nl/l}$ ) is the highest measured in the study area.

#### ACKNOWLEDGMENT

We thank T. M. Vogel and D. J. Blunt for collecting the samples and helping with some preliminary analyses.

## References

- Barnes, R. O., and Goldberg, E. D., 1976, Methane production and consumption in anoxic marine sediments: **Geology**, V. 4, p. 297-300.
- Bernard, B. B., Brooks, J. M., and Sackett, W. M., 1976, Natural gas seepage in the Gulf of Mexico: **Earth and Planet. Sci. Lett.**, 31, p. 48-54.
- Bernard, B. B., Brooks, J. M., and Sackett, W. M., 1977, A geochemical model for characterization of hydrocarbon gas sources in marine sediments: **Proc. 9th Offshore Tech. Conf.**, 1, p. 435-438.
- Bernard, B. B., Brooks, J. M., and Sackett, W. M., 1978, Light hydrocarbons in recent continental shelf and slope sediments: **Jour. Geophys. Res.**, 83, p. 4053-4061.
- Carlson, P. C., Karl, H. A., Fischer, J. M., and Edwards, B. D., 1982, Geological hazards in Navarin Basin Province, Northern Bering Sea: **Proc. 14th Offshore Tech. Conf.**, OTC 4172, p. 73-87.
- Cline, J. D., and Holmes, M. L., 1977, Submarine seepage of natural gas in Norton Sound, Alaska: **Science**, no. 198, p. 1149-1153.
- Davis, J. B., and Squires, R. M., 1954, Detection of microbially produced gaseous hydrocarbons other than methane: **Science**, no. 119, p. 381-382.
- Emery, K. O., and Hoggan, D., 1958, Gases in marine sediments: **Am. Assoc. Petrol. Geol. Bull.**, no. 42, p. 2174-2188.
- Fischer, J. M., 1981, Carbon contents of Navarin Basin sediments: In Carlson, P. R., and Karl, H. A., (eds.), **Seafloor Geologic Hazards, Sedimentology, and Bathymetry: Navarin Basin Province, Northwestern Bering Sea**: U.S. Geological Survey Open-File Report 81-1217, p. 44-57.
- Hunt, J. M., 1974, Hydrocarbon geochemistry of Black Sea: In **The Black Sea - Geology, chemistry, and Biology**, Am. Assoc. Pet. Geol. Mere., no. 20, p. 499-504.
- Kvenvolden, K. A., and Redden, G. D., 1980, Hydrocarbon gas in sediment from the shelf, slope, and basin of the Bering Sea: **Geochim. Cosmochim. Acta**, vol. 44, p. 1145-1150.
- Kvenvolden, K. A., Vogel, T. M., and Gardner, J. V., 1981, Geochemical prospecting for hydrocarbons in the outer continental shelf, southern Bering Sea, Alaska: **Jour. Geochem. Expl.**, 14, p. 209-219.
- Martens, C. S., and Berner, R. A., 1974, Methane production in the interstitial waters of sulfate-depleted marine sediments: **Science**, 185, p. 1167-1169.
- Primrose, S. B., and Dilworth, M. J., 1976, Ethylene production by bacteria: **Jour. General Microbiology**, no. 93, p. 177-181.
- Reeburgh, W. S., 1969, Observations of gases in Chesapeake Bay sediments: **Limnol. Oceanogr.**, no. 14, p. 368-375.
- Reeburgh, W. S., and Heggie, D. T., 1977, Microbial methane consumption reactions and their effect on methane distributions in fresh water and marine environments: **Limnol. Oceanogr.**, no. 22, p. 1-9.
- Vogel, T. M., and Kvenvolden, K. A., 1981, Hydrocarbon gases in Navarin Basin province sediments: In Carlson, P. R., and Karl, H. A., (eds.), **Seafloor Geologic Hazards, Sedimentology, and Bathymetry: Navarin Basin Province, Northwestern Bering Sea**: U.S. Geological Survey Open-File Report 81-1217, p. 80-99.
- Yamamoto, S., Alcauskas, J. B., and Crozier, T. E., 1976, Volubility of methane in distilled water and seawater: **Jour. Chem. and Eng. Data**, vol. 21, no. 1, p. 78-80.

## CHAPTER 9. BENTHIC FORAMINIFERS

by

Paula Quintero

### INTRODUCTION

Samples collected by the U.S. Geological Survey from the Navarin Basin province were analyzed for **benthic foraminifers**. This study is a continuation of previous work (Quintero, 1981) and includes samples collected during both 1980 and 1981 (Fig. 43).

Other studies of **benthic** foraminifers in the Bering Sea have been in areas to the north and west (Saidova, 1967; Lisitsyn, 1966) and in shallow waters to the east and northeast of the study area (Anderson, 1963; Knebel and others, 1974).

The purpose of this study is to determine the distribution of **benthic** foraminifers in the surface sediments and to record **faunal** changes with depth in the cores.

### METHODS

Samples were processed by washing the sediment over a 62 micron-mesh sieve to remove silt and clay. In samples with much sediment, foraminifers were concentrated by floating in carbon **tetrachloride**. A **microsplitter** was used to obtain a representative split of approximately 300 benthic **foraminifers**. The actual number of benthic **foraminifers** in the splits ranged from 3 to 2,860.

Foraminifers were mounted on cardboard slides, identified, and the relative frequency percentage of each species calculated.

### SURFACE DISTRIBUTION

Samples from the approximate upper 2 cm of forty-two gravity cores or grab samples were examined for benthic foraminifers; the relative frequency percentages of the species present are listed in Table 9. Table 10 is the key to abbreviations for species. In order to recognize **faunal** trends that might be related to water depth, stations were arranged from left to right in order of increasing water depth and the relative frequency percentages of the most abundant species were plotted (Fig. 44). To simplify plotting and to make Figure 44 more legible, the species abundances for samples having similar water depths were averaged and the average plotted. Although percentages fluctuate with depth, some general trends are apparent.

The peak abundances of Reophax arctica (35 and 37%) are at depths of 91 and 99 m. At depths greater than 150 m, the abundance decreases to 5% or less (Fig. 44). Anderson (1963) reports R. arctica in the Bering Sea as dominant

N AVARIN BASIN SEDIMENT SAMPLES

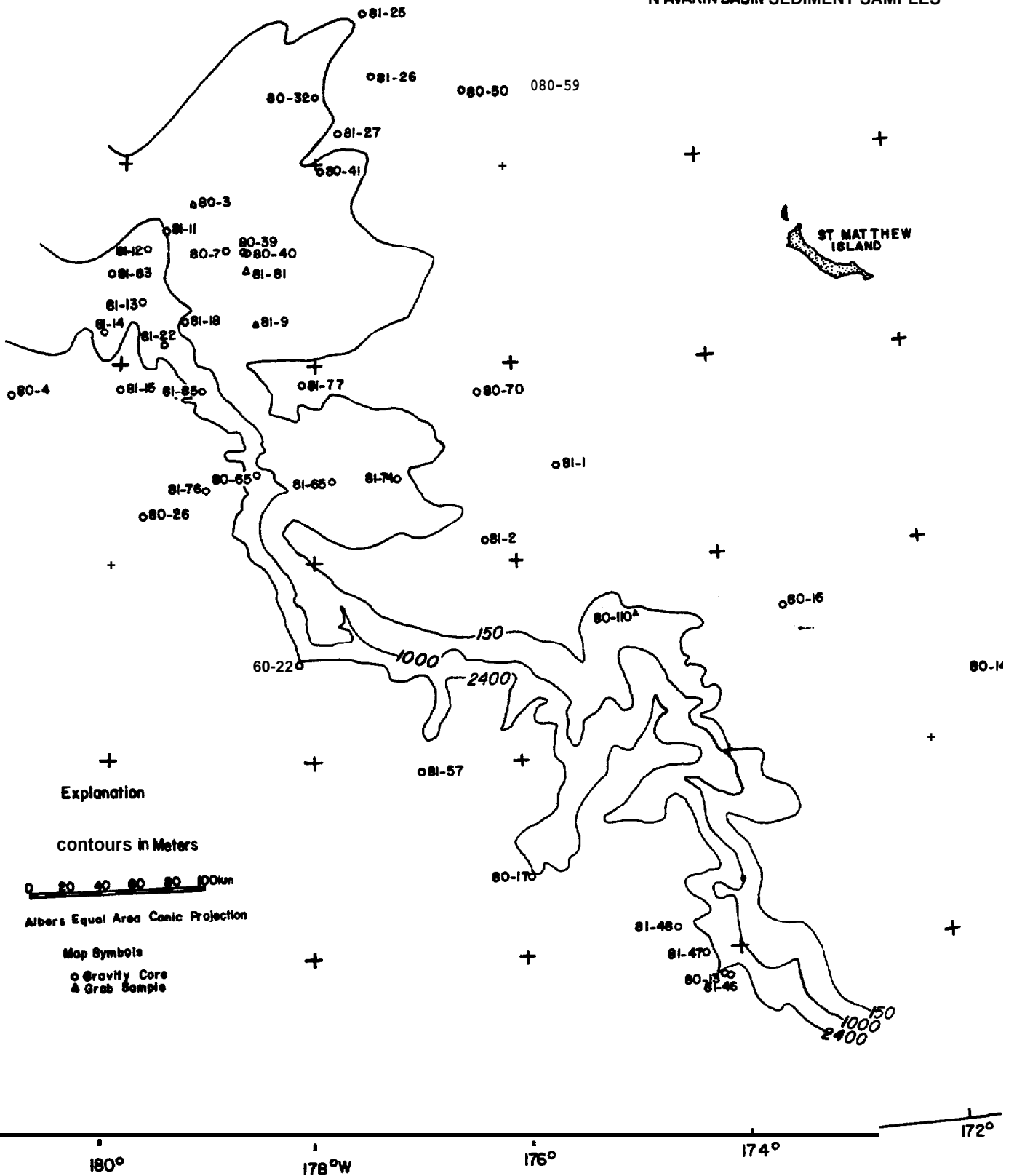


Figure 43. Sample locations.

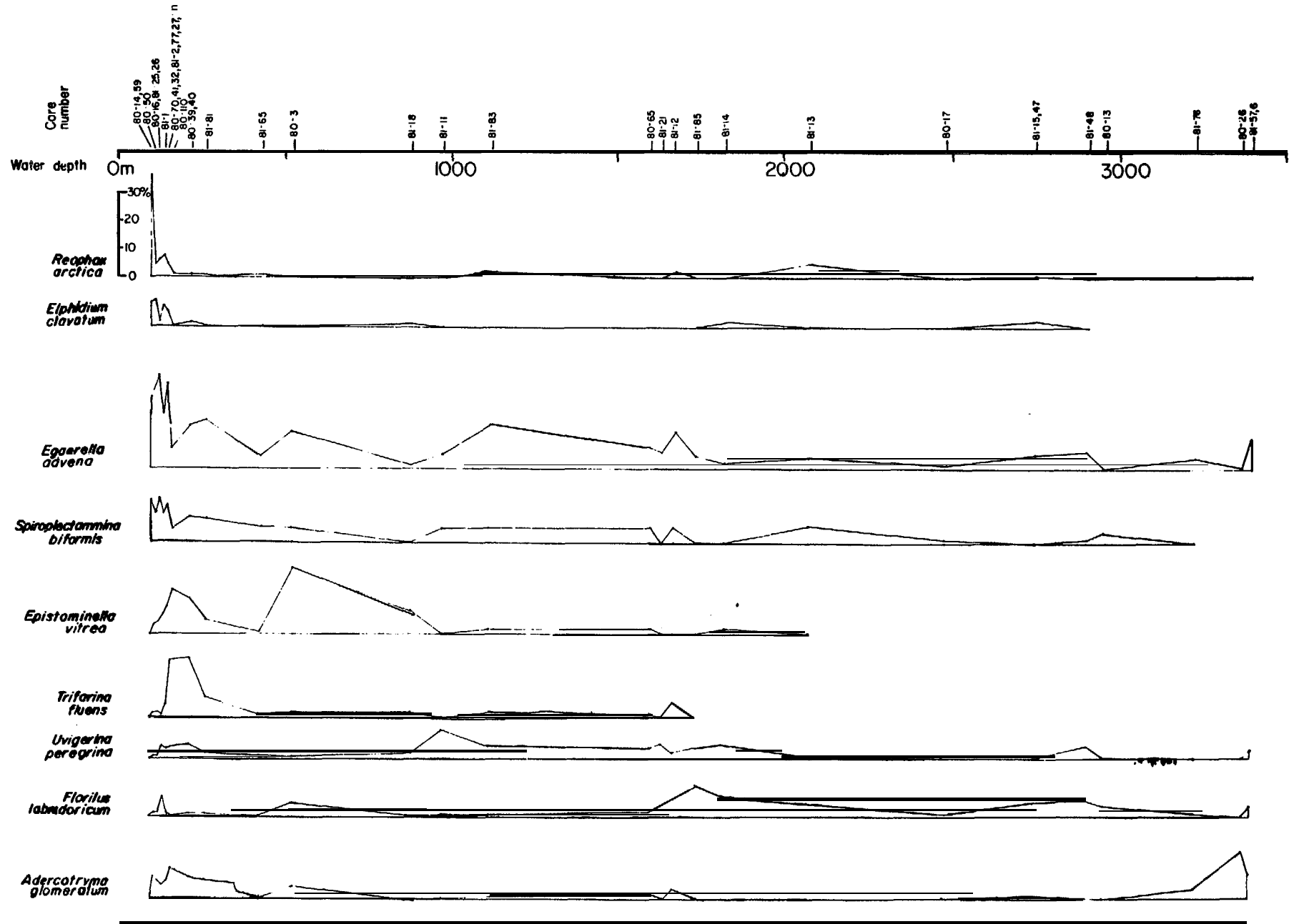


Figure 44. Relative frequency percentages of the most abundant species in surface samples plotted against increasing water depth.

in his Central Shelf fauna (48-100 m) with very low percentages in deeper water. **Knebel** and others (1974) report the maximum abundance for this species in the *Bering* Sea between 35-105 m.

Percentages of **Elphidium clavatum** are low throughout my samples with the peak abundance of 15% occurring at 99 m. This species is absent at most stations having water depths greater than 150 m (Fig. 44). This agrees with previous studies which show that **E. clavatum** is typical of shelf environments (**Knebel** and others, 1974; Anderson, 1963; Matoba, 1976).

Peak abundances of **Eggerella advena** and **Spiroplectammina biformis** occur in water depths shallower than 150 m; there is a general decrease in abundance with increasing water depth (Fig. 44). Anderson (1963) reports the maximum abundance of **E. advena** on the Inner Shelf (22-48 m) but finds it present in lesser numbers in the Central and Outer Shelf faunas (48-200 m).

**Epistominella vitrea** and **Trifarina fluens** reach maxima between approximately 150 m and 900 m water depth and disappear below 1,800 m (Fig. 44).

**Fursenkoina spp.**, **Reophax spp.**, **Textularia torquata**, **Bolivina pacifica**, and **Elphidium batialis** are most abundant below 900 m (Fig. 44).

Several species of **Fursenkoina** were grouped together as **Fursenkoina spp.**, because the tests are extremely small and fragile and are difficult to separate into species. Further subdividing into species might show more clearly-defined depth trends.

**Elphidium** is usually considered a shelf species with highest abundance in water less than 200 m deep. However, there have been reports of a deep-water species, **Elphidium batialis** (Saidova, 1961; Matoba, 1976). This large, robust species has a sharp periphery and makes up more than 6% of the fauna at 9 stations with water depths greater than 1,100 m in the Navarin Basin province (Fig. 44). with one exception, (80-110) it is absent in water shallower than 975 m (Table 9).

The depth trends noted above may be dependent on one or more environmental factors (such as salinity, dissolved oxygen, temperature, and sediment type); however, detailed measurements of these parameters are not available at this time. Furthermore, the distribution of some tests has been affected by bottom currents, storm waves, and downslope transport.

#### DOWN-CORE STUDIES

Relative frequency percentages for benthic foraminiferal species which are present at various intervals in core 81-12 are listed in Table 11, and graphs showing down-core distribution of species are presented in Fig. 45.

Gravity core 81-12 is 262 cm in length and was collected from the floor of Navarinsky Canyon in 1683 m of water. A pronounced faunal and lithologic break exists between 130 cm and 140 cm within the core (Fig. 45). Visual inspection of the greater than 62 micron portion of sediment from 5 samples above 130 cm shows it to be fine sand. The eleven samples below 130 cm are

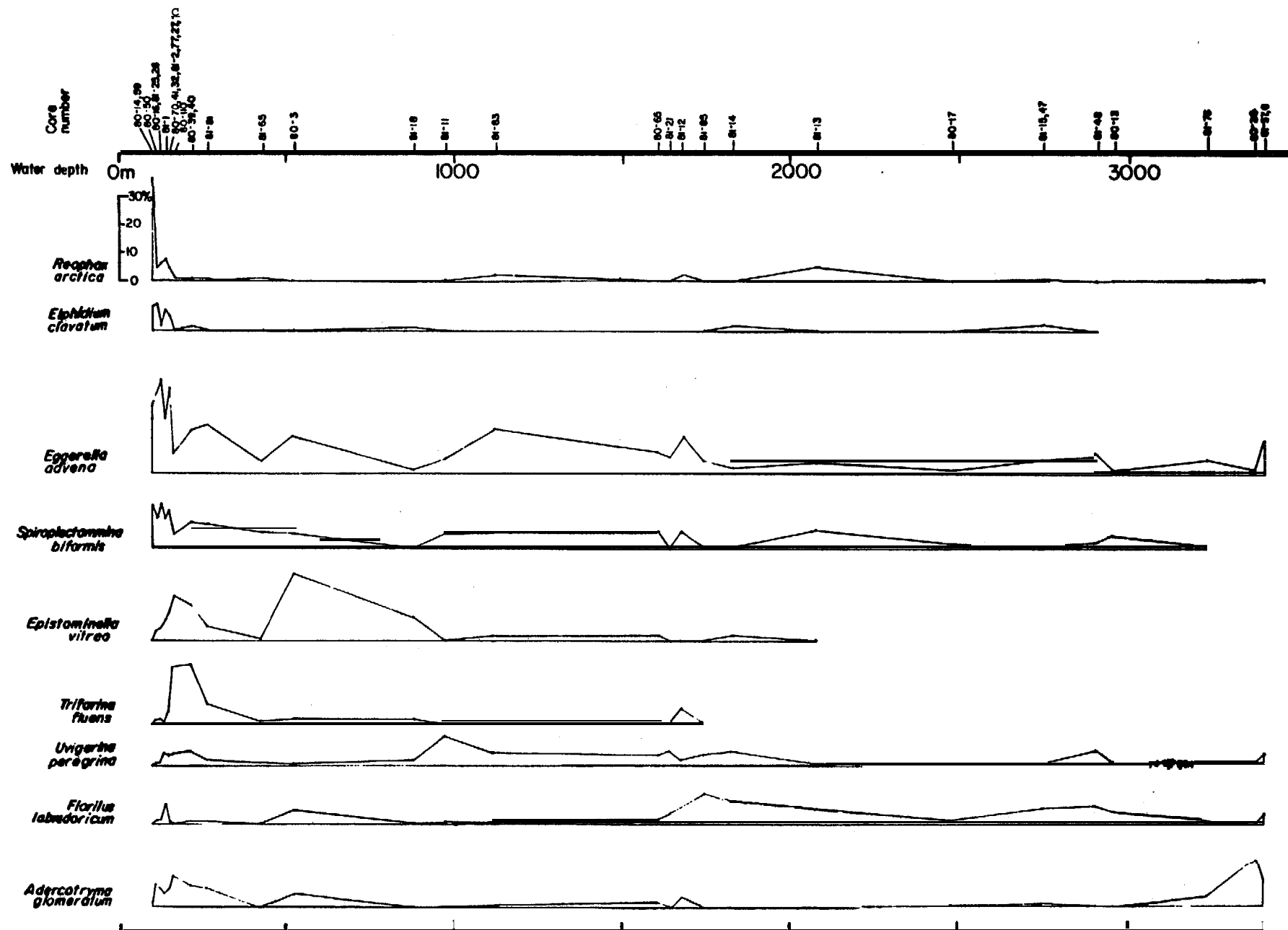


Figure 44. Relative frequency percentage of the most abundant species in surface samples plotted against increasing water depth.

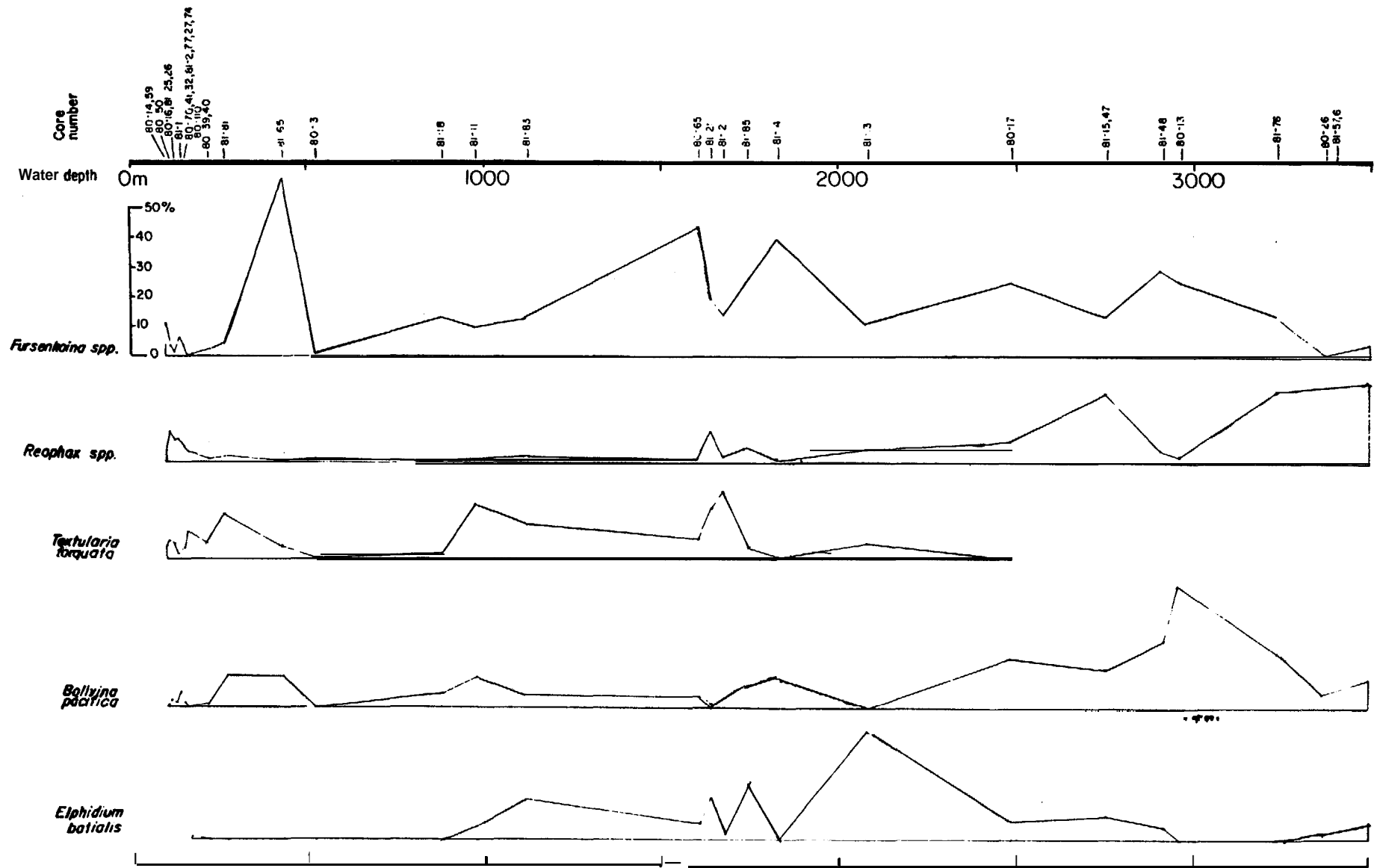


Figure 44 (continued) .

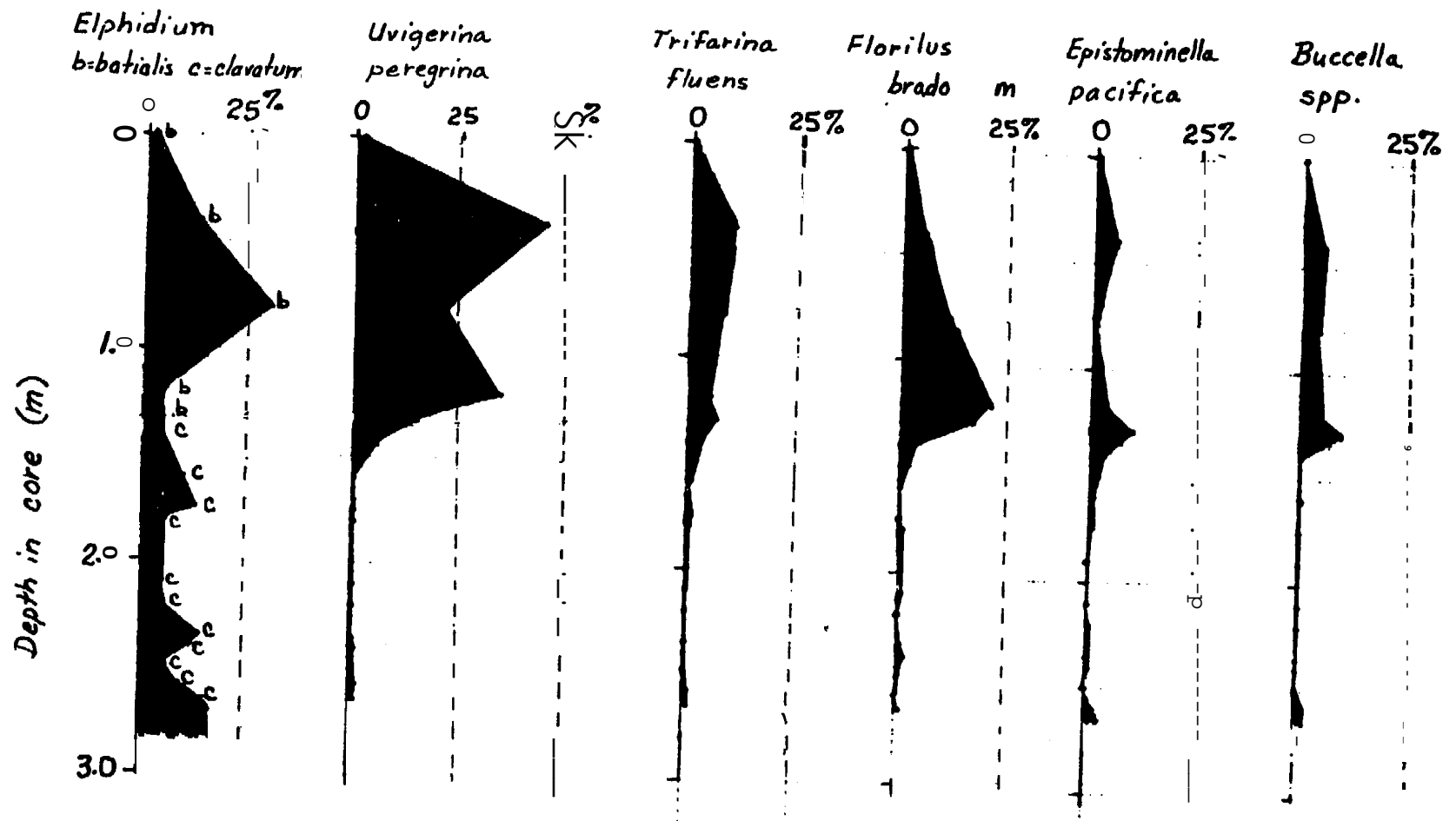


Figure 45. Relative frequency percentages of the most abundant benthic foraminiferal species plotted against depth in core 81-12.

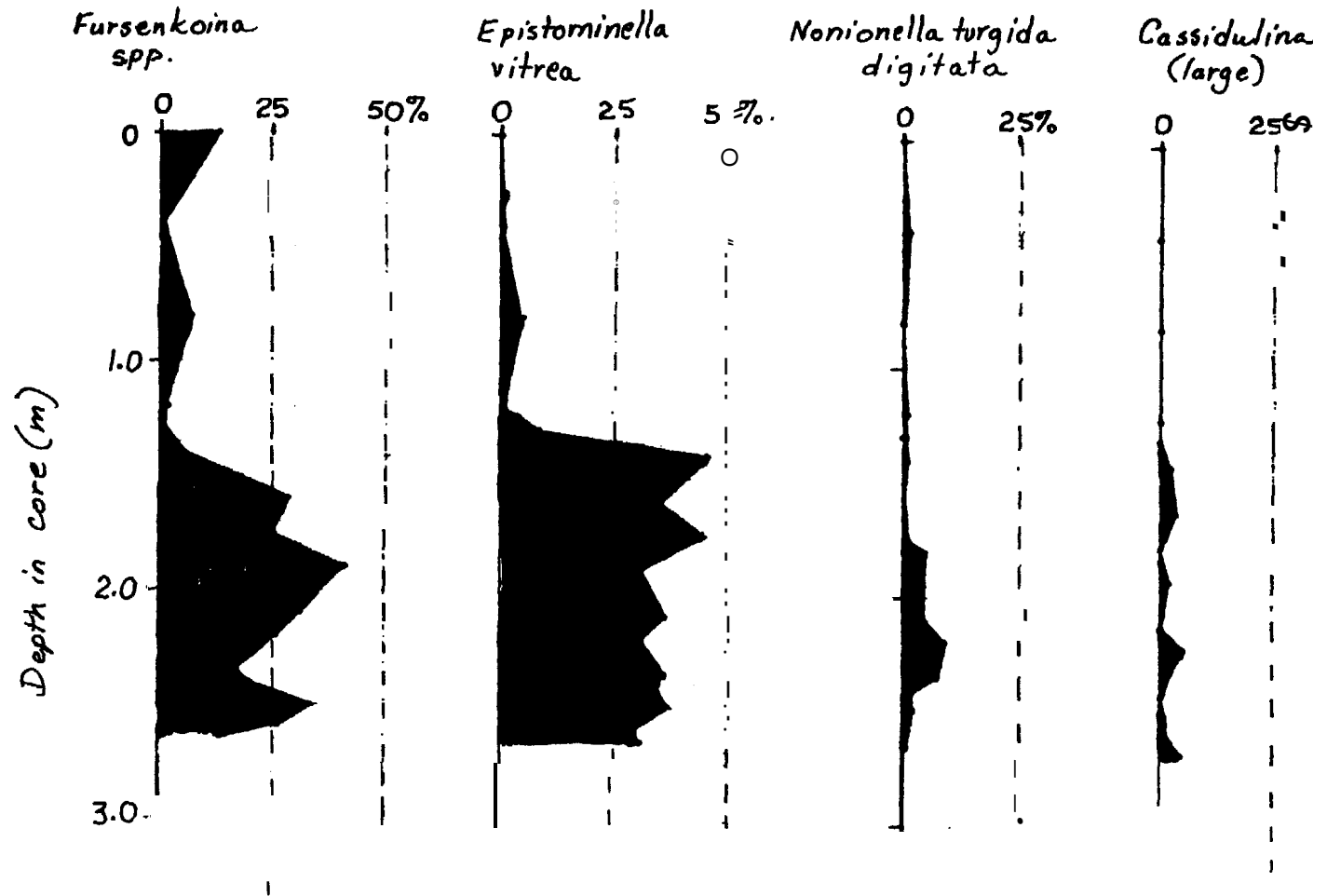


Figure 45 (cont nued).

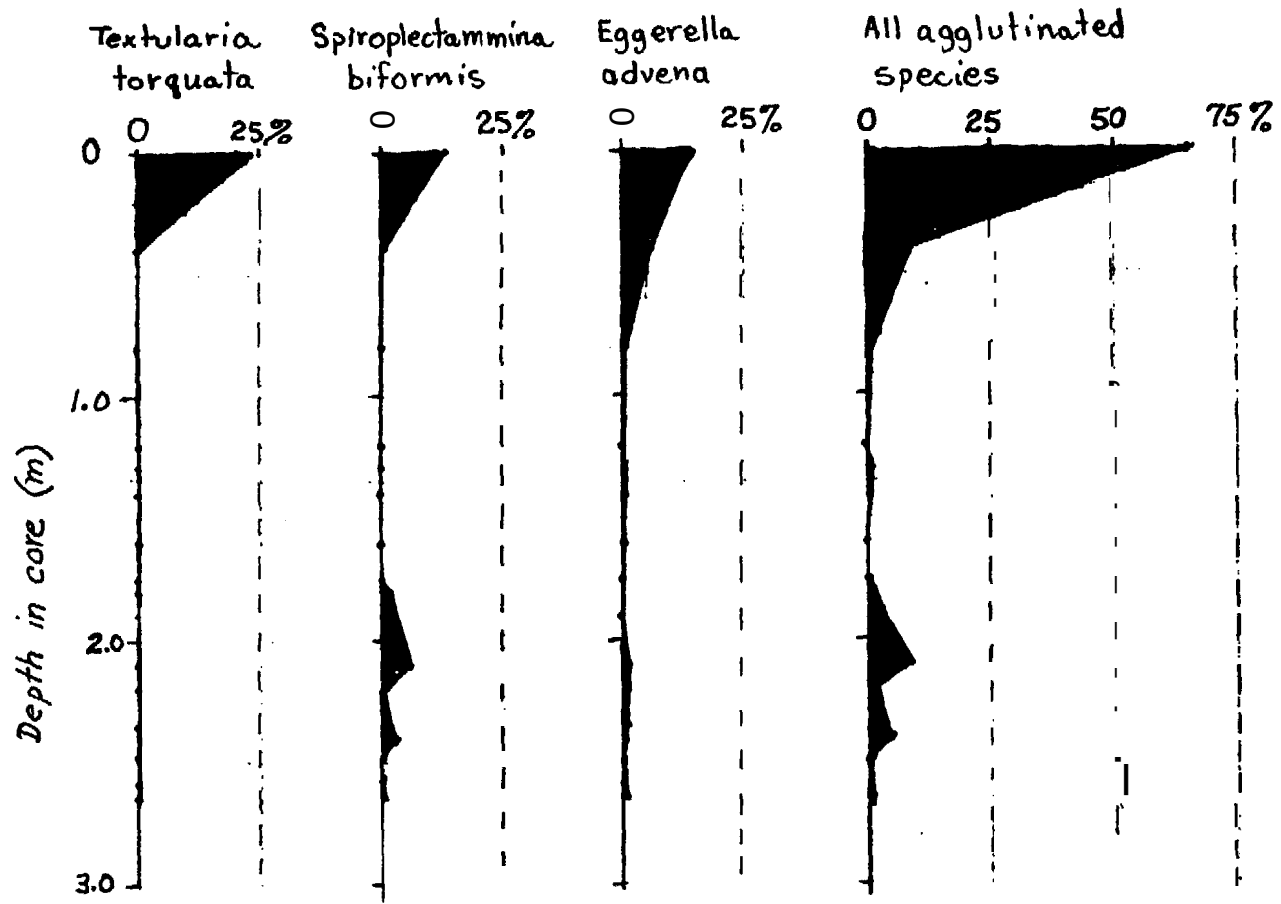


Figure 45 (continued).

generally coarser (most contain pebbles or pebble-sized **silt** aggregates), and contain **glauconite** and/or iron-stained grains. The sample at 180 cm contains several irregularly-shaped iron-sulfide plates up to 8 mm long.

Relative frequency percentages of the deep-water species **Elphidium batialis** range from 2-30% in the 5 uppermost samples (0-130 cm) of the core. The shallow-water species **E. clavatum** is not present in these 5 samples (Fig. 45). However, **E. batialis** is absent in all eleven samples below 130 cm, whereas **E. clavatum** is present in abundances ranging from 4-15%. Based on the present-day distribution of **E. clavatum** with respect to water depth, it is unlikely that this species could live at station 81-12 (1,683 m). Even with glacially lowered sea level, the water depth would be too great. Downslope transport of **E. clavatum** tests is a possible explanation for the presence of this species in deep water.

The following species have peak abundances above 130 cm in core 81-12 and decrease markedly below: **Uvigerina peregrina**, **Epistominella pacifica**, **Buccella spp.**, **Trifarina fluens**, and **Florilus labradoricum**. The following species show the opposite trend--low abundances above 130 cm and peak abundances below: **Fursenkoina spp.**, **Epistominella vitrea**, **Nonionella turgida digitata**, and large, poorly-preserved specimens of **Cassidulina** (probably reworked) (Fig. 45).

The pronounced faunal and lithologic break between 130 and 140 cm in core 81-12 may reflect physical and chemical changes in the environment resulting from a change from glacial to interglacial conditions and may represent the Pleistocene/Holocene boundary. With lowered sea level during Pleistocene glaciation, a wide area of the continental shelf was subaerially exposed, and the submerged portion of the shelf was much narrower than at present. During these times, rivers dissected the shelf and transported sediment to the present-day outer shelf (Nelson, Hopkins, and Scholl, 1974). Turbidity currents and debris flows also contributed to down-slope transport (Vallier, Underwood, Gardner, and Barron, 1980; Carlson, Karl, and Quintero, 1982). Under these conditions, coarser sediment and shallow-water, an organism, such as **E. clavatum**, could easily be transported into deeper water.







SPECIES	SAMPLE	
	80-14 (91m)	80-59 (99m)
VALCON	0	0
VALGLA	0	0
VIRSP	0	0
OTHAGG	0	0
OTHCAL	0	0
OTHMIL	0	0
	80-50 (110m)	80-16 (120m)
VALCON	0	0
VALGLA	0	0
VIRSP	0	0
OTHAGG	0	0
OTHCAL	0	0
OTHMIL	0	0
	81-25 (123m)	81-26 (125m)
VALCON	0	0
VALGLA	0	0
VIRSP	0	0
OTHAGG	0	0
OTHCAL	0	0
OTHMIL	0	0
	81-01 (135m)	80-70 (142m)
VALCON	0	0
VALGLA	0	0
VIRSP	0	0
OTHAGG	0	0
OTHCAL	0	0
OTHMIL	0	0
	81-97 (145m)	81-27 (145m)
VALCON	0	0
VALGLA	0	0
VIRSP	0	0
OTHAGG	0	0
OTHCAL	0	0
OTHMIL	0	0
	81-41 (150m)	80-32 (150m)
VALCON	0	0
VALGLA	0	0
VIRSP	0	0
OTHAGG	0	0
OTHCAL	0	0
OTHMIL	0	0
	81-74 (152m)	80-110 (164m)
VALCON	0	0
VALGLA	0	0
VIRSP	0	0
OTHAGG	0	0
OTHCAL	0	0
OTHMIL	0	0
	80-39 (220m)	80-40 (220m)
VALCON	0	0
VALGLA	0	0
VIRSP	0	0
OTHAGG	0	0
OTHCAL	0	0
OTHMIL	0	0
	81-81 (269m)	81-09 (290m)
VALCON	0	0
VALGLA	0	0
VIRSP	0	0
OTHAGG	0	0
OTHCAL	0	0
OTHMIL	0	0
	81-65 (436m)	80-03 (524m)
VALCON	0	0
VALGLA	0	0
VIRSP	0	0
OTHAGG	0	0
OTHCAL	0	0
OTHMIL	0	0
	81-18 (884m)	81-11 (975m)
VALCON	0	0
VALGLA	0	0
VIRSP	0	0
OTHAGG	0	0
OTHCAL	0	0
OTHMIL	0	0
	81-83 (1120m)	
VALCON	0	0
VALGLA	0	0
VIRSP	0	0
OTHAGG	0	0
OTHCAL	0	0
OTHMIL	0	0

Table 9 (continued).



SPECIES	SAMPLE		SAMPLE		SAMPLE																	
	80-65 (1609m)	81-21 (1640m)	81-12 (1683m)	81-85 (1745m)	81-14 (1826m)	81-13 (2080m)	80-17 (2481m)	81-46 (2530m)	81-15 (2750m)	81-47 (2760m)	80-22 (2842m)	81-48 (2910m)	80-13 (2962m)	80-04 (3222m)	81-76 (3230m)	80-26 (3373m)	81-57 (3395m)	81-06 (3395m)				
CYCSP	0	3	0	0	0	3	0	0	0	0	0	0	0	0	0	0	0	0	0	0	0	
DENSPP	0	0	0	0	0	0	0	0	0	0	0	0	0	0	0	0	0	0	0	0	0	
EGGADV	70	60	130	40	2	30	10	80	30	50	0	60	0	20	30	0	10	10	0	0	0	
EGGSCR	20	10	10	4	0	0	0	0	0	0	0	0	0	0	0	0	0	0	0	0	0	
EGGSUB	0	0	0	0	0	0	0	0	0	0	0	0	0	0	0	0	0	0	0	0	0	
ELPBAT	60	140	20	190	0	370	60	0	140	20	10	40	0	150	0	20	100	10	0	0	0	
ELPCLA	0	0	0	0	20	0	0	0	50	0	0	0	0	0	0	0	0	0	0	0	0	
ELPSPP	0	0	0	0	2	0	0	0	0	0	0	0	0	0	20	0	0	0	0	0	0	
EPIPAC	0	0	0	0	2	0	0	0	0	0	0	0	0	0	0	10	0	0	0	0	0	
EPIVIT	20	3	0	0	20	3	0	0	0	0	4	0	0	0	0	0	0	0	0	0	0	
EPOLEV	4	0	0	0	0	0	70	0	20	90	190	10	0	0	10	90	10	30	0	0	0	
EPOSPP	0	0	0	0	0	0	0	0	0	0	0	0	20	0	0	0	0	0	0	0	0	
FISSPP	0	3	0	0	0	0	0	0	10	14	20	4	0	0	20	0	3	3	0	0	0	
FLOLAB	20	30	3	100	70	40	10	0	10	70	0	50	30	50	10	0	50	20	0	0	0	
FURSPP	430	190	130	250	391	110	250	0	124	130	110	290	260	20	130	10	60	15	0	0	0	
GLOSPP	24	10	8	70	40	10	10	0	4	40	0	10	50	50	0	0	43	12	0	0	0	
GYRSPP	0	0	0	0	0	0	10	0	0	0	0	0	0	0	0	0	0	0	0	0	0	
HAPBRA	0	3	0	0	0	0	0	0	4	10	0	10	0	0	0	0	0	10	0	0	0	
HAPCOL	0	0	0	0	0	0	0	0	0	0	0	0	0	0	0	0	0	0	0	0	0	
HAPSPP	0	10	0	0	1	0	0	0	0	0	0	0	0	0	0	0	0	0	0	0	0	
HYPSP	0	0	0	0	0	0	0	0	0	0	0	0	0	0	0	0	0	0	0	0	0	
ISTRNR	0	0	0	2	1	40	0	0	20	10	0	0	0	0	0	0	3	0	0	0	0	
KARBAC	0	0	0	0	0	0	0	5	0	4	0	0	0	0	0	0	0	2	0	0	0	
LAGSPP	2	0	3	0	4	3	3	0	10	0	0	0	0	0	0	0	0	2	0	0	0	
MAROB	0	0	0	0	0	0	0	0	0	0	0	0	0	0	10	0	0	0	0	0	0	
MARSPP	0	0	0	0	0	0	0	0	0	0	0	0	0	0	0	0	0	0	0	0	0	
MELPDM	0	0	0	0	0	0	3	0	0	10	0	4	0	0	0	0	0	0	0	0	0	
NONPUL	0	0	0	0	0	0	0	0	0	0	0	0	0	0	0	0	0	0	0	0	0	
NONTGD	40	20	0	40	40	20	120	0	10	40	50	80	0	0	0	40	10	0	0	0	0	
NONSP	0	0	70	0	0	0	0	0	0	0	0	0	0	0	0	0	0	0	0	0	0	

Table 9 (continued)

SPECIES	SAMPLE																	
	80-65 (1609m)	81-21 (1640m)	81-12 (1683m)	81-85 (1745m)	81-14 (1826m)	81-13 (2080m)	80-17 (2481m)	81-46 (2530m)	81-15 (2750m)	81-47 (2760m)	80-22 (2842m)	81-48 (2910m)	80-13 (2962m)	80-04 (3222m)	81-76 (3230m)	80-26 (3373m)	81-57 (3395m)	81-06 (3395m)
OOLSPP	0	0	0	0	0	0	0	0	0	0	0	0	0	0	0	0	0	0
PATCOR	0	0	0	0	0	0	0	0	0	0	0	0	0	0	0	0	0	0
PELVAR	0	0	0	0	0	0	0	0	0	0	0	0	0	0	0	0	0	0
PRTORB	0	0	0	0	0	0	0	0	0	0	0	0	0	0	0	0	0	0
PSENON	0	0	40	0	0	0	0	0	0	0	0	0	30	0	10	10	10	2
PULSPP	0	0	0	0	0	0	0	0	0	4	0	0	0	0	0	0	0	0
PYRSPP	0	0	0	0	0	0	0	0	0	0	0	0	0	0	0	10	0	2
QNSPP	0	0	0	0	0	0	0	0	0	0	0	0	0	0	0	10	0	0
RECSPP	0	0	0	0	0	0	0	10	0	0	0	0	0	0	0	10	0	0
REOARC	0	0	20	0	0	50	0	20	0	0	0	10	0	0	10	10	10	0
REOCUR	2	80	10	30	10	20	0	490	0	0	0	0	0	0	0	0	0	0
REODIF	4	0	0	0	0	0	50	30	100	160	50	40	0	0	140	230	120	210
REOFUS	0	0	0	20	0	0	20	0	30	0	0	0	0	100	50	10	20	0
REOSCO	0	0	0	0	0	10	0	0	40	0	0	0	0	0	0	20	30	20
REOSPP	0	20	13	0	0	10	0	110	88	34	0	0	20	80	0	60	30	90
RHSBPP	0	0	0	0	0	0	0	0	0	0	0	0	0	0	0	0	0	0
SACSPH	0	0	0	0	0	0	3	0	0	10	0	0	0	0	10	0	0	30
SPRBIF	60	0	50	0	0	60	10	0	0	0	0	10	30	0	0	0	0	0
SPRSPP	0	30	80	10	0	0	0	190	0	10	0	0	30	0	0	20	10	20
TEXTOR	70	170	230	30	3	50	0	30	0	10	0	0	0	0	0	0	0	2
TEXSPP	10	0	0	0	0	0	20	0	0	0	40	0	0	80	0	0	0	0
TRIFLU	10	0	5	0	0	0	0	0	0	0	0	0	0	0	0	0	0	0
TRLTRI	0	0	0	0	3	0	0	0	0	0	0	0	30	0	0	0	0	0
TROGLO	0	0	0	0	0	0	3	0	0	0	0	0	0	0	0	10	0	0
TRONIT	0	0	0	2	0	0	0	0	50	0	0	0	0	0	50	0	0	40
TROPAC	0	0	50	0	0	30	0	0	60	40	0	20	0	0	50	100	40	120
TROSPP	2	23	0	0	4	0	13	0	0	0	30	10	0	20	10	0	0	10
UVGPRG	30	50	20	30	40	10	0	0	0	0	0	4	0	0	0	50	0	0
UVGSEN	0	10	0	0	0	0	0	0	0	10	10	0	0	50	0	10	0	0
UVGSPP	0	0	0	0	0	0	0	0	0	0	0	0	0	0	0	0	0	5

Table 9 (continued).



Table 10. List of Benthic **Foraminiferal** Species.

ADRGLO	<i>Adercotryma glomeratum</i>
ALVSPP	<i>Alveolophragmium</i> spp.
AMOBAC	<i>Ammobaculites</i>
AMDSPP	<i>Ammodiscus</i> spp.
AMSSPP	<i>Ammoscalaria</i> spp.
AMTCAS	<i>Annotium cassis</i>
ASTSPP	<i>Astrononion</i> spp.
BTYSI P	<i>Bathysiphon</i>
BOLDEC	<i>Bolivina decussata</i>
BOLPAC	<i>Bolivina pacifica</i>
BOLPSE	<i>Bolivina pseudobeyrichi</i>
BOLSEM	<i>Bolivina seminuda</i> and <i>B. seminuda</i> var. <i>foraminata</i>
BOLSPI	<i>Bolivina spissa</i>
BOLSPP	<i>Bolivina</i> Spp.
BUCSPP	<i>Buccella</i> spp.
BULELE	<i>Buliminella elegantissima</i>
BULTEN	<i>Buliminella tenuata</i>
CALSP1	small, transparent calcareous foram
CASCAL	<i>Cassidulina californica</i>
CASDEL	<i>Cassidulina delicata</i>
CASLIM	<i>Cassidulina limbata</i>
CASLRG	<i>Cassidulina lomitensis</i> and <i>C. Z. elegantula</i>
CASMIN	<i>Cassidulina minuta</i>
CASSPP	<i>Cassidulina</i> spp.
CSDSPP	<i>Cassidulinoides</i> spp.
CHISPP	<i>Chilostomella</i> spp.
CHNFIM	<i>Chilostomellina fimbriata</i>
CIBLOB	<i>Cibicides lobatulus</i>
CIBSPP	<i>Cibicides</i> spp.
CRBSPP	<i>Cribrostomoides</i> spp.
CYCSPP	<i>Cyclammina</i> Spp.
DENSPP	<i>Dentalina</i> spp.
EGGADV	<i>Eggerella advena</i>
EGGSCR	<i>Eggerella scrippsi</i>
EGGSUB	<i>Eggerella subadvena</i>
ELPBAT	<i>Elphidium batialis</i>
ELPCLA	<i>Elphidium clavatum</i>
ELPSPP	<i>Elphidium</i> Spp.
EPIPAC	<i>Epistominella pacifica</i>
EPIVIT	<i>Epistominella vitrea</i>
EPOLEV	<i>Eponides leviculus</i>
EPOSPP	<i>Eponides</i> spp.
FISSPP	<i>Fissurina</i> Spp.
FLOLAB	<i>Florilus labradoricum</i>

FURSPP	<i>Fursenkoina</i> spp.
GLOSPP	<i>Globobulimina</i> spp.
GYRSPP	<i>Guroidina</i> spp.
HAPBRA	<i>Haplophragmoides bradyi</i>
HAPCOL	<i>Haplophragmoides columbiense</i>
HAPSPP	<i>Haplophragmoides</i> spp.
HYPSP	<i>Hyperammia</i> spp.
ISTRNR	<i>Islandiella teretis/norcrossi</i>
KARBAC	<i>Karrerella baccata</i>
LAGSPP	<i>Lagena</i> spp.
MAROBS	<i>Marginulina obesa</i>
MARSPP	<i>Martinottiella</i> spp.
MELPOM	<i>Melonis pompiliodes</i>
NONPUL	<i>Nonionella pulchella</i>
NONTGD	<i>Nonionella turgida digitata</i>
NONSPP	<i>Nonionella</i> spp.
OOLSPP	<i>Oolina</i> spp.
PATCOR	<i>Patellina corrugata</i>
PELVAR	<i>Pelosina variabilis</i>
PRTORB	<i>Protelphidium orbiculare</i>
PSENON	<i>Pseudononion</i> spp.
PULSPP	<i>Pullenia</i> spp.
PYRSPP	<i>Pyrgo</i> Spp.
QNSQSP	<i>Quinqueloculina</i> spp.
RECSPP	<i>Recurvoides</i> spp.
REOARC	<i>Reophax arctica</i>
REOCUR	<i>Reophax curtus</i>
REODIF	<i>Reophax difflugiiformis</i>
REOFUS	<i>Reophax fusiiformis</i>
REOSCO	<i>Reophax scorpiurus</i>
REOSPP	<i>Reophax</i> spp.
RHBSPP	<i>Rhabdammina</i> Spp.
SACSPH	<i>Saccammina sphaerica</i>
SPRBIF	<i>Spiroplectammina biformis</i>
SPRSPP	<i>Spiroplectammina</i> spp.
TEXTOR	<i>Textularia torquata</i>
TEXSPP	<i>Textularia</i> spp.
TRIFLU	<i>Trifarina fluens</i>
TRLTRI	<i>Triloculina</i> spp.
TROGLO	<i>Trochammina globigerinaformis</i>
TRONIT	<i>Trochammina nitida</i>
TROPAC	<i>Trochammina pacifica</i>
TROSPP	<i>Trochammina</i> spp.
UVGPRG	<i>Uvigerina peregrina</i>
UVGSEN	<i>Uvigerina senticosa</i>
UVGSPP	<i>Uvigerina</i> spp.
VALCON	<i>Valvulina conica</i>
VALGLA	<i>Valvulineria glabra</i>
VIRSPP	<i>Virgulina</i> spp.
OTHAGG	Other agglutinated species
OTHCAL	Other calcareous species
OTHMIL	<i>Miliollids</i>

SPECIES	Sample number and depth interval within core														core catcher	
	81-12	TOP (~2cm)	40-42cm	80-82cm	120-122cm	129-132cm	140-142cm	160-162cm	175-177cm	180-183cm	210-212cm	220-222cm	235-237cm	240-242cm		248cm
ADRGLO	30	0	0	0	0	0	0	0	0	0	0	0	0	0	0	0
ALVSPP	0	0	0	0	0	0	0	0	0	0	0	0	0	0	0	0
AMOBAC	0	0	0	0	0	0	0	0	0	0	0	0	0	0	0	0
AMDSPP	0	0	0	0	0	0	0	0	0	0	0	0	0	0	0	0
AMSSPP	0	0	0	0	0	0	0	0	0	0	0	0	0	0	0	0
AMTCAS	0	0	0	0	0	0	0	0	0	0	0	0	0	0	0	0
ASTSPP	0	0	0	0	2	0	0	3	0	1	0	0	0	1	0	2
BTYSIP	0	0	0	0	0	0	0	0	0	0	0	0	0	0	0	0
BOLDEC	0	0	20	0	6	10	10	10	4	3	5	0	10	20	20	20
BOLPAC	30	20	10	20	20	40	60	30	20	40	30	20	40	50	40	30
BOLPSE	0	0	0	2	6	3	0	2	0	0	0	0	1	0	0	0
BOLSEM	0	0	0	0	3	0	0	0	2	0	0	0	0	0	1	0
BOLSPI	0	0	0	0	0	3	0	0	0	0	0	0	0	0	0	0
BOLSPP	0	0	0	0	0	0	0	0	0	0	0	0	0	0	0	0
BUCSPP	6	50	30	50	90	10	10	4	1	6	10	10	10	0	20	20
BULELE	0	0	0	10	3	3	1	0	0	10	0	10	1	0	0	10
BULTEN	0	3	0	10	6	40	4	4	10	10	10	10	20	10	20	20
CALSPI	0	0	0	0	0	0	0	0	0	0	0	0	0	0	0	0
CASCAL	0	0	0	0	0	20	30	0	0	0	0	0	0	0	0	0
CASDEL	0	0	0	2	0	0	0	0	0	0	0	0	0	0	2	0
CASLIM	0	0	0	0	0	0	0	0	0	0	0	0	0	0	0	0
CASLRG	0	0	0	0	0	0	0	4	20	3	50	10	4	0	20	40
CASMIN	20	30	90	20	70	30	0	30	30	40	60	50	60	30	50	70
CASSPP	0	0	0	0	0	0	0	0	0	0	0	0	0	10	0	0
CSDSPP	0	0	0	50	30	0	0	2	1	0	0	0	0	0	0	0
CHISPP	0	0	0	0	0	0	0	0	0	0	0	0	0	0	0	0
CHNFIM	3	0	0	10	10	10	4	10	10	0	20	30	10	5	20	10
CIBLOB	0	0	0	0	0	0	10	0	0	0	5	0	0	10	10	20
CIBSPP	0	0	3	10	0	10	1	0	0	3	0	0	10	0	1	0
CRBSPP	0	0	0	0	0	0	0	0	0	0	0	0	0	0	0	0

Table 11. Relative frequency percentages of benthic foraminiferal species in core 81-12.

SPECIES	Sample number and depth interval within core														core catcher	
	81-12	TOP(-2cm)	40-42cm	80-82cm	120-122cm	129-132cm	140-142cm	160-162cm	175-177cm	180-183cm	210-212cm	220-222cm	235-237cm	240-242cm		248cm
CYCSPP	0	0	0	0	0	0	0	0	0	0	0	0	0	0	0	0
DENSPP	0	0	0	0	0	0	0	0	0	0	0	0	0	0	0	0
EGGADV	130	60	5	0	3	10	0	0	2	10	10	10	10	2	2	10
EGGSCR	10	0	0	0	0	0	0	0	0	0	0	0	0	0	0	3
EGGSUB	0	0	0	0	0	0	0	0	0	0	0	0	0	0	0	0
ELPBAT	20	130	30	0	50	40	0	0	0	0	0	0	0	0	0	0
ELPCLA	0	0	0	0	6	50	100	120	60	40	60	140	110	60	90	150
ELPSP	0	0	0	0	6	0	3	10	2	6	3	0	10	0	20	20
EPIPAC	0	50	5	40	100	30	10	10	0	3	10	3	10	4	20	30
EPIVIT	0	10	40	10	80	450	350	440	310	360	310	360	340	370	290	310
EPOLEV	0	0	10	0	3	3	0	10	1	0	0	0	0	0	1	0
EPOSP	0	0	0	0	0	0	0	0	0	0	0	0	0	0	0	0
FISSPP	0	0	0	2	3	0	2	2	2	3	4	0	1	10	5	0
FLOLAB	3	50	100	210	170	30	2	0	10	10	5	10	20	2	2	10
FURSP	130	10	70	30	20	63	280	250	412	323	260	170	202	330	261	140
GLOSP	8	10	10	30	20	40	20	10	10	3	10	3	20	10	10	30
GYRSP	0	0	0	0	0	0	0	0	0	0	0	0	0	0	0	0
HAPBRA	0	0	0	0	0	0	0	0	0	3	0	0	0	0	0	0
HAPCOL	0	0	0	0	0	0	0	0	0	0	0	0	0	0	0	0
HAPSP	0	0	0	0	0	0	0	0	0	0	0	0	0	0	0	0
HYPSP	0	0	0	0	0	0	0	0	0	0	0	0	0	0	0	0
ISTRNR	0	0	0	5	10	3	4	4	2	10	10	10	10	4	10	20
KARBAC	0	0	0	0	0	0	0	0	0	0	0	0	0	0	0	0
LAGSP	3	6	3	5	15	0	4	2	0	0	0	0	0	2	1	0
MAROBS	0	0	0	0	0	0	0	0	0	0	0	0	0	0	0	0
MARSP	0	0	0	0	0	0	0	0	0	0	0	0	0	0	0	0
MELPOM	0	0	0	0	0	0	0	0	0	0	0	0	0	0	0	0
NONPUL	0	0	0	0	0	0	0	0	0	0	0	0	0	0	0	0
NONTGD	0	10	0	10	0	10	0	10	40	40	80	70	20	20	0	0
NONSPR	70	0	0	0	0	0	10	0	0	0	0	0	0	10	0	0

Table 11 (continued)

SPECIES	Sample number and depth interval within core																
	81-12	16-20cm	40-42cm	80-82cm	120-122cm	129-132cm	140-142cm	160-162cm	175-177cm	180-183cm	210-212cm	220-222cm	235-237cm	240-242cm	248cm	257-260cm	Core catcher
OOLSPP	0	0	0	0	0	0	0	0	0	0	0	0	0	0	0	0	0
PATCOR	0	0	0	0	0	0	0	0	0	0	0	0	0	0	0	0	0
PELVAR	0	0	0	0	0	0	0	0	0	0	0	0	0	0	0	0	0
PRTORB	0	0	0	0	0	0	0	0	0	0	0	0	0	0	0	0	0
PSENON	1	0	0	0	0	2	0	0	0	1	0	1	0	0	0	0	0
PULSPP	0	0	0	0	2	0	0	0	0	0	0	0	0	0	0	0	0
PYRSPP	0	0	0	0	0	0	0	0	0	0	0	0	0	0	0	0	0
QNOQSP	0	0	0	0	0	0	0	0	0	0	0	0	0	0	0	0	0
RECSPP	0	0	0	0	0	0	0	0	0	1	0	0	0	0	0	0	0
REOARC	2	0	0	0	0	0	0	0	0	5	0	0	0	0	0	0	0
REOCUR	1	0	3	0	0	0	0	0	0	0	6	0	0	0	0	0	0
REODIF	0	0	0	0	0	0	0	0	0	0	0	0	0	0	0	0	0
REOFUS	0	0	0	0	0	0	0	0	0	0	0	0	0	0	0	0	0
REOSCO	0	0	0	0	0	0	0	0	0	0	0	0	0	0	0	0	0
REOSPP	1	3	0	0	0	0	0	0	0	0	0	0	0	0	0	0	0
RHBSPP	0	0	0	0	0	0	0	0	0	0	0	0	0	0	0	0	0
SACSPH	0	0	0	0	0	0	0	0	0	0	0	0	0	0	0	0	0
SPRBIF	5	0	10	0	0	0	0	0	0	2	6	1	2	3	0	4	0
SPRSPP	8	0	0	0	0	0	0	0	0	0	0	0	0	0	0	0	0
TEXTOR	2	3	0	0	0	0	0	0	0	1	0	0	0	4	0	0	0
TEXSPP	0	0	0	0	0	0	0	0	0	0	0	0	0	0	0	0	0
TRIFLU	5	10	0	8	5	6	3	1	1	2	0	0	3	0	0	1	1
TRLTRI	0	0	0	0	0	0	0	0	0	0	0	0	0	0	0	0	0
TROGLO	0	0	0	0	0	0	0	0	0	0	0	0	0	0	0	0	0
TRONIT	0	0	0	0	0	0	0	0	0	0	0	0	0	0	0	0	0
TROPAC	5	0	0	0	0	0	0	0	0	0	0	0	0	0	0	0	0
TROSPP	0	3	0	3	0	3	0	0	0	0	0	0	0	0	0	0	0
UVGPRG	2	0	45	0	2	10	35	18	0	7	10	1	0	0	0	2	0
UVGSEN	0	0	0	0	0	0	0	0	0	0	0	0	0	0	0	0	0
UVGSPP	0	0	0	0	0	0	0	0	0	0	0	0	2	0	0	0	0

Table 11 (continued).

	SPECIES	Sample number and depth interval within core
		81-12
VALCON	0	TOP (~2cm)
VALGLA	0	
VIRSPP	0	40-42cm
OTHAGG	0	
OTHCAL	0	80-82cm
OTHMIL	0	
		120-122cm
	0	
	0	129-132cm
	0	
	0	140-142cm
	0	
	0	160-162cm
	0	
	0	175-177cm
	0	
	0	180-183cm
	0	
	0	210-212cm
	0	
	0	220-222cm
	0	
	0	235-237cm
	0	
	0	240-242cm
	0	
	0	248cm
	0	
	0	257-260cm
	0	
	0	core catcher

## REFERENCES

- Anderson, G. J., 1963, Distribution patterns of Recent foraminifera of the Bering Sea: *Micropaleontology*, v. 9, no. 3, p. 305-317.
- Carlson, P. R., Karl, H. A., and Quintero, Paula**, 1982, **Sedimentologic** processes in world's **largest** submarine canyons, Bering Sea, Alaska: Geological Society of America Abstracts with Programs, v. 14, no. 7, p. 459-460.
- Knebel, H. J., Creager, J. s., and Echols, R. J.**, 1974, Holocene sedimentary framework, east-central Bering Sea continental shelf, **in** Herman, Y. (cd.), *Marine Geology and Oceanography of the Arctic Seas*: New York, Springer-Verlag, p. 157-172.
- Lisitsyn, A. P., 1966, Recent sedimentation **in** the Bering Sea (in Russian): Inst. **Okeanol.** Akad. Nauk, USSR, (translated by Israel Program Sci. **Transl.**, Jerusalem), Washington, D.C., U.S. Department of Commerce: National Science Foundation, 614 p.
- Ma toba, **Yasumochi**, 1976, Recent **foraminiferal** assemblages off Sendai, Northeast Japan, **in** Schafer, C. T. and **Pelletier, B. R.**, First International **Symposium** on Benthonic Foraminifera of Continental Margins: *Maritime Sediments*, Special Publication no. 1, p. 205-220.
- Nelson, C. H., Hopkins, D. M., and Scholl, D. W., **1972**, Cenozoic sedimentary and tectonic history of the Bering Sea, **in** Hood, D. W. and **Kelley, E. J. (eds.)**, *Oceanography of the Bering Sea: Occasional Publication no. 2*, Institute of Marine Science, University of Alaska, Fairbanks, p. 485-516.
- Quintero, P. J.**, 1981, Preliminary report on **benthic** foraminifera from Navarin Basin province, Bering Sea, Alaska, **in** Carlson, P. R. and Karl, H. A. (eds.), *Seafloor geologic hazards, sedimentology and bathymetry: Navarin Basin Province, northwestern Bering Sea*: U.S. Geological Survey Open-File Report 81-1217, p. 135-149.
- Saidova, Kh. M., 1961, **Ekologiia foraminifer paleogeografiia dal'nevostochnykh morei** (in Russian): Moscow, **Academy of Sciences of the Soviet Union**, 232 p., 31 plates.
- \_\_\_\_\_ 1967, Depth changes in Bering Sea during the Upper Quaternary, **as** indicated by benthonic foraminifera, in Hopkins, D. (cd.), *The Bering Land Bridge*: Stanford University Press, p. 364-368.
- Vallier, T. L., Underwood, M. B., Gardner, J. V., and Barren, J. A.**, **1980**, Neogene sedimentation **on** the outer continental margin, southern Bering Sea: *Marine Geology*, v. 269-287.

CHAPTER 10: DIATOM ANALYSIS OF SURFACE SAMPLES  
RECOVERED FROM PERVENETS CANYON

by

Jack G. Baldauf

INTRODUCTION

The Navarin Basin province within the Bering Sea (Fig. 46) is geographically divided into a shallow shelf, steep slope, and a deep marginal basin. Five major submarine canyons (**Zhemchug**, Pervenets, St. Matthew, Middle, and Navarinsky) occur within this region (Fisher and others, 1982).

Previously, **Baldauf** (1982) analyzed thirty surface samples from this region and documented the existence of two distinct diatom assemblages separated from each other by the shelf-slope break. The basin-slope assemblage is characterized by the species Denticulopsis seminae which typically comprises 20-40 percent of the entire assemblage. Other species within this group include; Coscinodiscus marginatus, Coscinodiscus oculus-iridis, Rhizosolenia hebatata forma hebatata, and Thalassiosira oestrupii. Most basin-slope species, although most abundant in the deeper waters, are present on the shelf. For example, Denticulopsis seminae composes less than 10 percent of the overall assemblage on the continental shelf compared to 20-40 percent in the basin-slope region.

The shallow water assemblage is dominated by Nitzschia grunowii (previously referred to as Nitzschia oceanica in **Baldauf** (1981, 1982)) which composes greater than 20 percent of the shelf assemblage. Additional species in this assemblage include: Nitzschia cylindrus, Thalassiosira nordenskioldii, and an increase in abundance of both benthonic and brackish water species.

The presence of these two assemblages within the surface sediment may be useful in determining the effect that secondary processes such as sediment transport or winnowing have on surface sediment within the canyon and slope regions of the Navarin basin province. The very abundant occurrence of shelf species within the surface samples examined from the canyon regions would suggest the erosion and transportation of sediment from the shelf and deposition of these sediments in the canyon.

To examine the usefulness of diatoms for interpreting the effect of sedimentary processes, thirty-three surface samples were examined within the region of Pervenets Canyon (Fig. 47). Pervenets Canyon was selected for this preliminary study due to its relatively small size in comparison to the dimensions of **Zhemchug** and Navarinsky Canyons. An additional motive for selecting **Pervenets Canyon**, was the occurrence of Rhizosolenia curvirostris and Thalassiosira nidulus in sample G-80-66 recovered from within this canyon. The presence of these species suggests that sample G-80-66 has an age greater than 0.26 Ma, the age cited by Donahue (1970) and Schrader (1976) for the last occurrence of Rhizosolenia curvirostris.

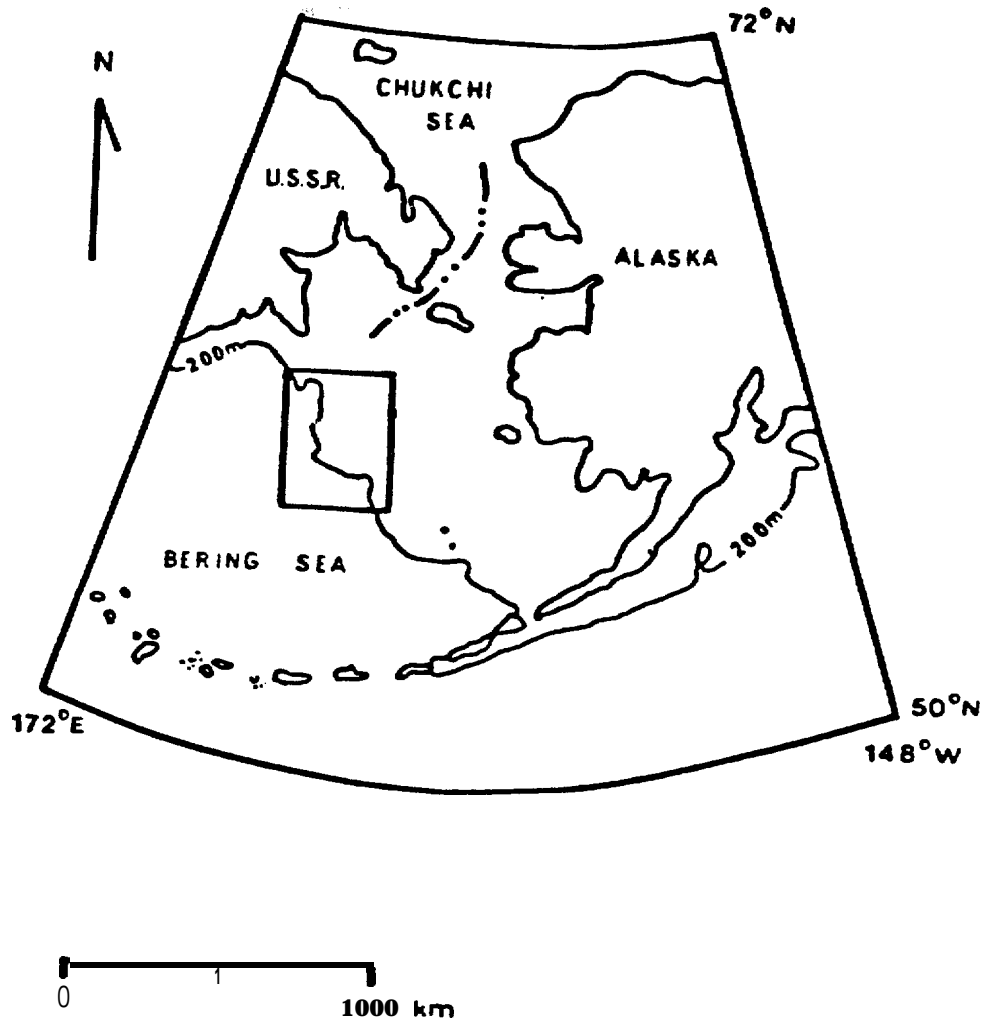


Figure 46. Index map of the Navarin Basin Province, Bering Sea.

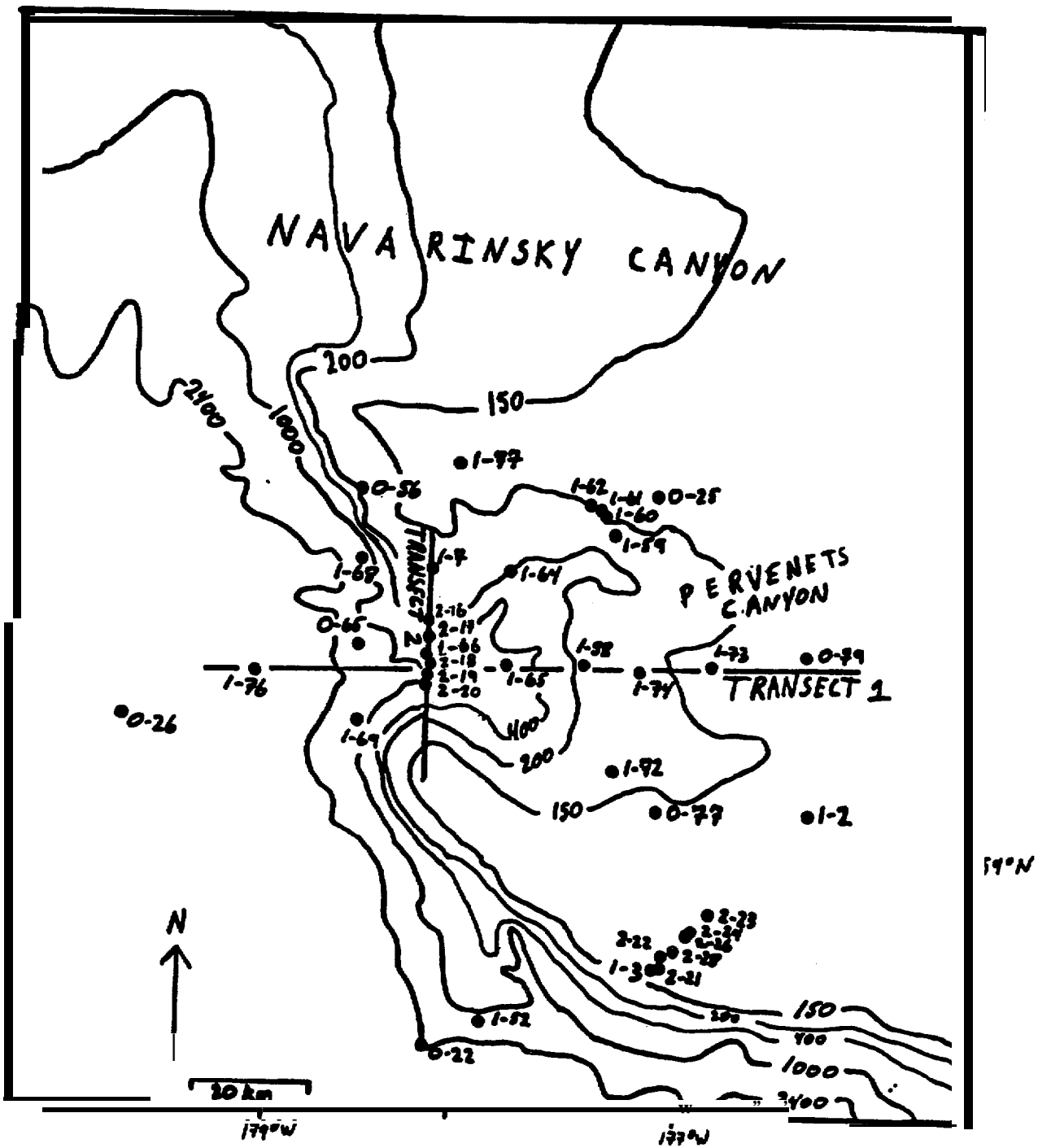


Figure 47. Location of surface samples collected from Pervenets Canyon (0 = 1980; 1 = 81; 2 = 82).

**Pervenets** Canyon, located within the central portion of the Navarin Basin province, is approximately **125 kilometers** long and heads in a water depth of approximately 150 meters. The mouth of this canyon occurs at an approximate water depth of 3000 meters. Pervenets Canyon is approximately 30 kilometers wide at the shelf break, which is narrow when compared to both **Zhemchug** and Navarinsky Canyons which have an approximate width of 100 kilometers. **Two** main tributaries **which** form a right angle at the head of Pervenets Canyon are 80-90 kilometers long and have an approximate gradient of 0.30 degrees.

#### METHODS AND PROCEDURES

In addition to samples previously examined (**Baldauf** 1981, 1982), **thirty-three** surface samples **were** obtained from cores collected in and around Pervenets Canyon by the NOAA research vessel DISCOVERER during the summers of 1980, 1981, and from the U.S. Geological Survey vessel **S.P. LEE** during the summer of 1982. Strewn slides of unprocessed sediment were prepared for each sample and examined at 500x for age diagnostic species. Samples of Quaternary age **were** further examined at 1250x with the first 300 specimens tabulated to determine the abundance of individual species within each sample.

The preservational quality of each sample is based on the presence and absence of delicate forms such as **Thalassiosira hyalina**, **Pseudopodosira elegans**, and **Asteromphalus robustus** and heavily **silicified** forms such as **Coscinodiscus marginatus**, **Rhizosolenia hebatata** forma **hebatata**, **Stephanopyxis turris**, **Bacteriosira fragilis**, and **Thalassiosira gravida**. The occurrence of both robust and delicate species suggests well preserved samples whereas the presence of only robust forms indicated poorly preserved samples.

#### RESULTS

With the exception of samples G-82-18, **G-82-20** and G-81-66 all samples examined are latest Quaternary in age. Samples **G-82-18** and G-82-20 are equivalent in age with previously examined sample G-81-66, based on the presence of **Rhizosolenia curvirostris** and **Thalassiosira nidulus**. The occurrence of these **two** species suggests that these samples are older than 0.26 Ma. Samples G-81-66, G-82-18, and G-82-20 are located in Pervenets Canyon at a water depth of 580, 625, and 739 meters, respectively (Fig. 47).

Sample **G-82-19**, which is located between samples G-82-18 and G-82-20 (Fig. 47) at a water depth of 852 meters, is latest Quaternary in age, as it lacks both **Rhizosolenia curvirostris** and **Thalassiosira nidulus**. This suggests that material is swept clean of the canyon walls and deposited on the canyon floor. However, the sediment associated with core G-82-19 also could be derived from the adjacent continental shelf.

A seismic profile perpendicular to the canyon's axis (Figs. 47 and 48) shows surface exposures of **stratigraphically** older seismic reflectors within the upper canyon **walls**. A portion of these reflectors occur in proximity of samples **G-81-66**, **G-82-18**, and G-82-20 **which** suggests an age greater than 0.26 Ma for these reflectors. Although exact correlation **between** these samples and specific seismic reflectors is uncertain, the water depth of each sample

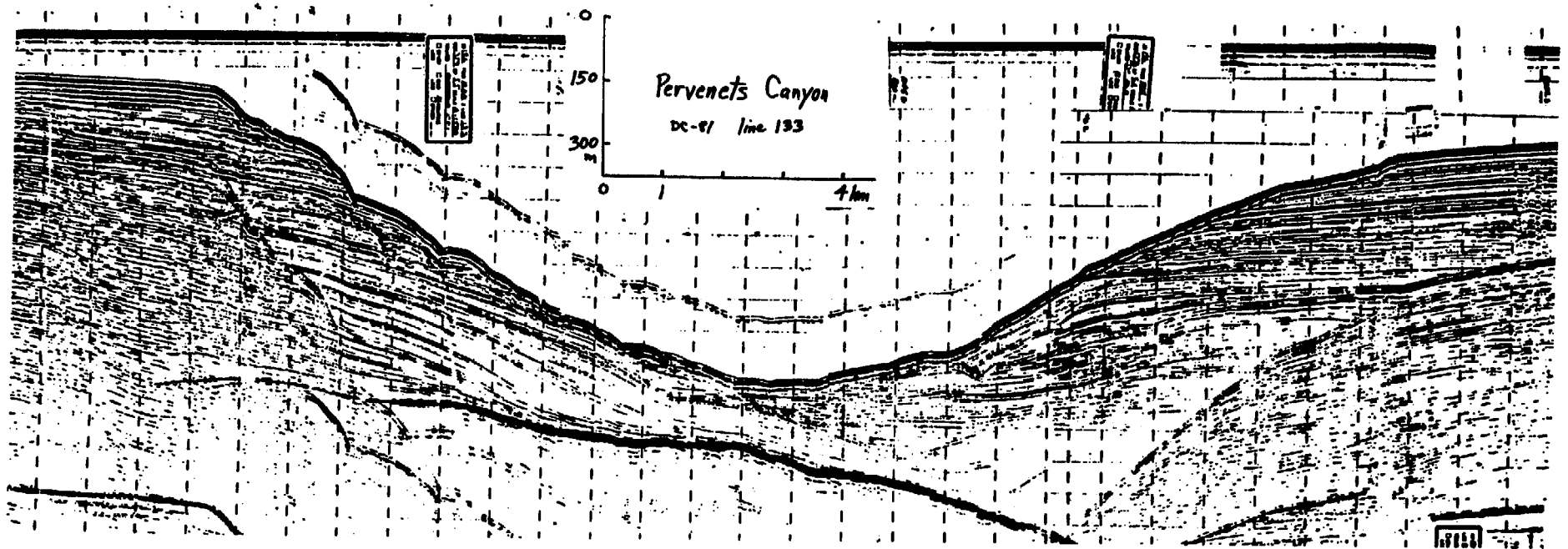


Figure 48. Seismic reflection profile across Pervenets Canyon showing surface exposures of stratigraphically older reflectors. Line 33, DC4-81-BS/NB. See Fig. 47, transect 2 for profile location.

allows approximate correlation and suggests that the reflectors of interest are exposed **surficially between** the depths of 580-739 meters.

Table 12 shows the occurrence of species encountered during the examination of the latest Quaternary age surface sediment from Pervenets Canyon. The over-all species distribution agrees **well** with the previous conclusions of **Baldauf** (1982) in which **two** assemblages separated by the **shelf-slope break** were observed. The deeper water assemblage is dominated by *Denticulopsis seminae* from the shelf, to mid-slope, to **lower** slope and basin *Nitzschia grunowii*.

The latest Quaternary samples from the Pervenets Canyon area (Fig. 47) range in water depth from 145 meters to 3230 meters. One major transect from the shelf (sample G-80-79, 128 meters) to the basin (sample G-81-76, 3230 meters; Fig. 47 transect 1) shows an increase in the abundance of *Denticulopsis seminae* from the shelf, to mid slope, to lower slope and basin (Fig. 49). In sample G-80-65, water depth 1609 meters, *D. seminae* composes approximately **33** percent of the assemblage. This **unusually** high concentration of *D. seminae* is the probable result of either high productivity within a very restricted microenvironment or sediment transport. The abundance of other species within this sample is equivalent to their abundance within nearby samples.

The abundance of *Denticulopsis seminae* in samples from transect 2 (Figs. 47 and 48) perpendicular to the canyon axis (samples G-82-16,17,19, and G-81-67; Fig. 49) is similar to the above results. *D. seminae* composes approximately 15-17 percent of the assemblage **at a** depth between 100-500 meters, and increases in abundance to 23-26 percent of the assemblage at a water depth greater than 500 meters. Although samples G-80-76,77 are exceptions to this trend for presently unknown **reasons**, the conformity of all other samples to this trend suggest that depth either directly or as a secondary factor is responsible for the distribution of *D. seminae* within the Navarin Basin province.

To determine the abundance of shelf species **in** the surface sediments of Pervenets Canyon, the same samples used in the transects for determining the distribution of *Denticulopsis seminae*, were also used to compare the **abundance** of the shelf species *Nitzschia grunowii*.

The abundance of *Nitzschia grunowii* within surface samples from Pervenets Canyon (**Fig. 50**) shows more irregularities than that observed in the distribution pattern of *Denticulopsis seminae*. as a general trend, *Nitzschia grunowii* increases in abundance as *one* proceeds from the slope region to the inner shelf (see **Baldauf**, 1982).

The abundance of *Nitzschia grunowii* within Pervenets Canyon, however, disagrees with this pattern. *N. grunowii* in most samples within the canyon **between** the depths of 150-2400 meters constitutes approximately 10-17 percent of the entire assemblage. No trend in abundance vs. depth is observed. Furthermore, in sample G-80-26, *Nitzschia grunowii* composes 19 percent of the assemblage **which** is equivalent elsewhere in the Navarin Basin to its abundance within water depths of less than 125 meters.

Table 12. Abundance (in percent) of species encountered during the examination of surface sediments from the Pervenets Canyon region

SAMPLE	80-04	80-12	80-13	80-22	80-25	80-26	80-28	80-30	80-35	80-36	80-50	80-51	80-52	80-56	80-65	80-77	80-79	80-81	80-83	80-84	80-89	
<b>SPECIES</b>																						
<i>Actinocyclus curvatus</i>	-	-	0.3	-	0	6	-	-	-	-	-	-	0	6	1	0	-	-	-	-	0.6	0.3
<i>A. divisus</i>	0.6	0.6	0.3	0.3	1.6	0.3	2.6	0.3	1.0	0.6	1.0	1.0	0.3	1.6	-	0.6	0.6	2.0	2.3	2.3	1.0	
<i>A. ochotensis</i>	-	-	-	1.0	-	-	-	0.6	0.6	-	-	-	1.0	1.6	-	-	-	-	-	-	1.0	1.0
<i>Actinoptychus undulatus</i>	-	-	-	-	0.6	-	0.3	-	-	-	0.6	-	-	-	0.3	-	0.3	0.3	0.6	-	-	
<i>A. vulgaris</i>	-	0.3	-	-	-	-	-	-	-	0.3	-	-	-	-	-	-	-	-	-	-	-	
<i>Asteromphalus robustus</i>	-	0.6	-	-	-	-	-	-	0.6	-	-	-	-	-	-	-	-	-	-	-	-	
<i>Bacteriosira fragilis</i>	6.0	6.6	2.6	3.0	4.3	4.3	7.3	7.3	3.3	6.0	9.3	9.0	10.6	7.0	3.0	7.6	7.0	7.3	6.0	5.3	3.0	
<i>Biddulphia aurita</i>	3.0	1.6	2.6	1.0	1.0	2.0	1.0	1.6	2.3	1.3	2.0	1.3	1.6	1.3	0.3	1.3	0.6	1.0	1.6	2.3	2.3	
<i>Coscinodiscus lacustris</i>	-	-	-	0.3	-	-	-	0.3	-	-	0.6	-	-	-	-	-	0.3	0.3	-	-	-	
<i>c. marginatus</i>	0.6	2.0	0.3	0.6	-	1.6	1.0	0.3	1.3	0.3	-	0.3	1.6	1.3	2.3	2.3	0.3	2.0	1.0	1.3	1.3	
<i>c. oculus-iridis</i>	1.0	1.3	1.3	0.3	-	1.3	0.6	0.3	1.3	1.3	0.6	1.6	0.6	0.3	2.6	-	0.6	0.6	0.3	1.6	2.0	
<i>c. radiatus</i>	-	-	-	-	-	-	-	-	-	-	-	-	-	-	-	-	-	-	-	-	-	
<i>c. tataricus</i>	-	-	-	-	-	-	-	-	-	-	-	-	-	-	-	-	-	-	-	0.3	0.3	
<i>c. tabularis</i>	0.3	0.3	-	-	0.6	-	0.3	-	-	-	0.3	0.6	0.3	-	-	-	-	-	-	-	0.6	
<i>Denticulopsis seminae</i>	28.0	27.0	31.3	38.3	4.0	26.0	7.3	3.0	17.0	29.0	7.0	6.3	6.0	14.3	33.0	27.6	10.0	10.6	13.0	11.3	37.0	
<i>Melosira "GROUP"</i>	1.0	1.0	0.6	1.0	9.3	1.0	2.6	5.3	4.0	2.6	3.6	5.3	4.0	4.6	1.6	2.3	5.3	11.6	-	9.0	2.3	
<i>Navicula</i> sp. 1.	0.3	0.3	-	0.3	2.0	0.6	5.0	4.3	1.6	0.6	3.3	2.6	2.3	0.3	1.0	0.3	1.6	2.3	0.3	1.3	0.3	
<i>Navicula</i> sp. 2.	-	0.3	0.3	0.3	1.0	-	0.6	-	1.3	1.6	0.6	1.3	0.6	0.6	0.6	-	0.6	-	0.3	1.0	0.6	
<i>Navicula</i> sp. 3.	0.3	0.3	-	-	-	-	-	-	0.6	0.3	0.3	0.3	1.0	0.3	-	-	0.3	1.0	1.0	-	0.3	
<i>Nitzschia cylindrus</i>	4.0	3.0	3.6	3.1	9.0	5.6	10.6	13.6	10.0	7.0	9.0	10.3	10.6	8.3	7.3	6.6	9.3	6.0	6.6	7.6	1.0	
<i>N. grunowii</i>	16.3	10.6	9.6	11.0	26.3	19.0	19.3	36.0	18.6	15.0	25.6	24.3	20.6	20.3	11.3	16.6	16.6	17.6	15.3	9.0	5.6	
<i>Pleurosigma</i> Sp.	-	-	-	0.3	-	-	0.6	-	-	0.3	-	0.3	-	-	-	-	0.6	-	0.3	-	-	
<i>Porosira glacialis</i>	1.0	2.0	1.3	1.6	2.3	3.0	4.6	2.6	3.6	3.6	2.0	1.3	6.0	3.3	4.0	1.3	3.3	1.3	3.3	4.0	2.6	
<i>Pseudopodosira elegans</i>	1.3	3.0	-	1.3	1.3	0.6	0.6	-	0.6	-	-	1.0	-	2.6	-	2.0	1.0	0.6	0.3	1.0	-	
<i>Rhaphoneis sachalinensis</i>	-	-	-	0.3	0.6	-	-	-	1.0	0.3	-	0.3	-	-	0.3	0.3	1.3	0.3	0.6	-	-	
<i>R. surirella</i>	-	0.3	-	-	1.3	-	-	1.3	2.3	-	0.6	-	0.3	-	0.3	-	-	-	-	-	2.0	
<i>Rhizosolenia hebatata</i>	2.6	3.0	4.6	3.0	1.6	3.3	1.6	0.3	2.0	1.6	0.3	1.6	2.6	2.3	2.3	2.3	3.0	2.0	0.3	1.3	2.3	
<i>R. styliformis</i>	1.3	2.3	-	1.0	0.3	-	0.6	0.3	0.3	0.3	1.3	1.6	0.6	2.6	1.6	1.3	0.3	1.3	1.3	2.3	2.0	
<i>Stephanopyxis turris</i>	-	-	-	-	0.6	-	-	-	0.3	-	-	-	-	-	0.3	-	-	-	-	-	-	
<i>Thalassionema nitzschoides</i>	-	-	1.6	1.0	3.6	0.3	2.0	2.6	2.6	1.0	1.3	0.6	3.0	2.6	2.0	0.6	1.6	-	2.6	4.6	4.0	
<i>Thalassiosira decipiens</i>	2.3	3.3	2.0	2.0	1.3	2.6	2.6	1.6	2.6	1.0	3.3	2.3	2.6	3.3	2.0	3.3	4.3	2.3	3.3	3.6	1.6	
<i>T. eccentrica</i>	-	-	-	-	-	-	-	-	-	-	-	-	-	-	-	-	-	-	-	-	-	
<i>T. gravida</i>	7.3	6.6	2.3	3.0	3.6	2.3	4.6	8.6	1.6	4.3	10.0	12.3	3.0	2.6	2.6	5.6	6.3	10.0	7.0	1.0	2.3	
<i>T. hyalina</i>	10.0	8.0	11.0	5.6	5.6	7.6	8.6	0.6	6.6	5.0	7.0	5.0	5.0	6.0	5.3	3.0	5.3	5.0	3.6	4.0	6.3	
<i>T. leptopus</i>	1.0	-	0.3	-	0.6	-	0.3	0.3	0.3	-	0.3	1.0	0.6	0.3	-	-	-	0.3	-	0.3	-	
<i>T. nordenskiöldii</i>	3.0	-	6.0	5.6	3.6	4.6	8.0	4.6	1.6	6.3	4.0	3.6	5.3	4.3	4.0	6.0	4.6	4.6	1.6	5.3	4.0	
<i>T. oestrupii</i>	-	1.3	2.0	2.0	-	1.3	2.0	-	2.6	2.6	-	1.0	-	2.6	0.3	2.0	2.0	1.3	2.3	2.6	1.0	
<i>T. trifulta</i>	6.6	8.3	10.0	7.3	4.6	10.3	3.3	2.0	5.3	6.0	3.3	2.3	3.0	3.3	5.3	7.3	6.6	5.6	6.0	8.3	10.3	
<i>T. undulosa</i>	-	1.6	1.0	1.6	0.6	1.6	-	-	0.6	1.3	0.6	0.6	1.0	1.6	1.3	0.6	1.3	0.3	-	0.6	0.3	
<i>Thalassiothrix longissima</i>	1.0	0.6	3.0	1.6	1.0	1.6	1.0	0.6	1.6	0.3	0.3	-	0.6	1.0	0.3	-	-	-	1.0	0.6	1.3	
<i>Xathlopyxis ovalis</i>	0.6	0.3	0.3	0.6	-	0.3	-	-	-	0.3	-	-	-	-	0.6	0.6	-	-	-	-	0.6	
<b>FRESH WATER SPECIES</b>	-	-	-	-	-	-	-	-	-	-	-	-	-	-	-	-	-	-	0.3	-	-	

Table 12. cent' d

SAMPLE	80-94	80-96	80-98	80100	80101	80105	80-10'	80110	80112	81-3	81-2	81-7	81-51	81-58	81-59	81-60	81-61	81-62	81-64	81-65	81-66	81-68	
<b>SPECIES</b>																							
<i>Actinocyclus curvatus</i>		1.0	0.3	-	0.6	0.6	-	-	-	-	-	-	0.3	-	-	-	-	-	-	-	-	-	-
<i>A. divisus</i>	0.6	0.6		1.0	1.0	1.0	3.0	2.0	2.3	-	-	-	0.6	-	0.3	0.6	-	-	-	-	-	0.3	-
<i>A. ochotensis</i>	0.6	2.0	0.3	-	1.0	1.0	-	0.6	0.6	0.6	-	0.6	-	-	0.3	1.3	-	0.3	-	-	-	0.6	-
<i>Actinoptychus undulatus</i>	0.6	1.0	-	-	-	0.3	-	-	-	-	-	-	-	-	-	-	-	-	-	-	-	-	-
<i>A. vulgaris</i>	-	-	-	-	-	-	-	-	-	-	-	-	0.3	-	-	0.3	-	-	0.3	0.3	-	-	-
<i>Asteromphalus robustus</i>	-	-	0.6	-	-	-	-	-	-	0.3	-	-	-	0.3	-	-	-	-	-	-	-	-	0.3
<i>Bacteriosira fragilis</i>	7.0	6.0	4.3	4.3	3.6	4.6	4.3	6.6	5.6	4.3	8.0	6.6	1.3	5.0	6.0	5.0	4.6	7.3	5.6	2.3	3.6	5.0	-
<i>Biddulphia aurita</i>	1.3	1.3	1.0	0.3	2.3	2.0	1.6	3.3	0.6	2.0	2.3	0.6	1.6	2.3	2.0	1.0	1.6	0.3	2.3	3.3	1.0	0.6	-
<i>Coccinodiscus lacustris</i>	-	-	-	-	0.3	-	-	-	0.3	-	0.3	0.3	-	-	0.6	0.3	0.6	-	-	-	1.0	-	-
<i>c. marginatus</i>	0.3	0.6	1.3	1.6	0.6	0.6	1.6	-	1.0	2.0	0.3	1.3	0.3	-	0.3	2.6	1.0	-	1.3	0.3	2.3	1.3	1.3
<i>c. oculus-iridis</i>	1.0	1.0	1.0	0.6	1.3	1.3	1.3	0.6	0.6	1.0	-	1.0	-	1.3	-	0.6	-	-	0.3	2.6	2.0	-	-
<i>C. radiatus</i>	-	-	-	-	-	-	-	-	-	-	0.6	-	-	-	-	1.0	-	-	-	-	-	-	-
<i>c. stellaris</i>	-	-	-	-	-	-	-	-	-	-	-	-	-	0.3	0.3	-	-	-	-	-	-	-	0.3
<i>c. tabularis</i>	-	-	0.3	1.3	-	1.0	-	-	0.3	-	-	-	0.3	0.6	-	-	-	0.3	1.0	-	-	-	1.3
<i>Denticulopsis seminae</i>	9.6	10.3	17.6	28.0	24.0	22.3	33.3	15.0	14.6	11.3	17.6	17.6	40.6	15.7	6.6	14.0	9.6	9.6	14.0	16.3	24.3	24.0	-
<b>Melosira GROUP</b>	12.0	6.0	4.6	2.0	2.6	7.0	1.0	4.0	10.3	2.3	5.3	2.0	0.3	5.5	4.0	3.3	3.6	3.6	3.6	1.0	1.3	2.0	-
<i>Navicula</i> sp. 1.	1.0	3.0	1.6	1.0	0.3	2.0	-	-	-	4.3	0.3	1.3	0.6	-	1.3	1.0	0.3	2.0	1.3	2.0	1.0	0.3	-
<i>Navicula</i> sp. 2.	0.3	-	1.3	-	-	-	-	-	-	0.6	-	-	-	1.3	-	-	1.0	0.3	-	0.3	0.3	-	-
<i>Navicula</i> sp. 3.	-	0.3	0.3	-	-	0.3	-	-	-	0.3	0.3	0.6	-	0.3	-	0.6	0.3	-	1.3	-	0.3	0.6	-
<i>Nitzschia cylindrus</i>	8.0	9.6	9.3	3.0	3.0	6.6	4.6	5.6	4.3	5.6	4.3	9.0	1.3	6.0	9.3	4.3	9.6	8.0	6.0	9.0	6.6	0.6	-
<i>N. grunowii</i>	21.0	15.6	17.6	13.0	11.0	13.0	7.0	21.0	21.6	8.2	12.0	12.3	6.6	11.0	17.3	16.0	16.6	14.6	16.3	16.6	8.6	13.6	-
<i>Pleurosigma</i> sp.	-	-	0.3	-	-	-	-	-	-	0.6	-	-	-	-	-	-	-	0.6	-	-	-	-	-
<i>Podosira glacialis</i>	4.0	3.3	3.6	2.0	2.6	1.6	4.0	1.6	2.0	2.0	5.0	1.6	2.6	1.3	1.3	3.3	1.7	1.0	1.0	1.6	1.0	-	-
<i>Pseudopodosira</i> sp. legana	2.6	-	-	1.0	1.6	0.6	0.6	1.0	0.6	1.6	1.0	1.0	1.0	0.3	1.0	0.6	0.3	2.0	0.6	0.6	0.6	0.6	-
<i>Rhaphoneis sachalinensis</i>	0.3	0.3	-	-	-	-	-	-	-	0.3	-	0.6	-	0.3	1.3	0.3	-	1.3	-	-	0.3	1.0	-
<i>Rh. surirella</i>	2.0	1.3	2.0	-	0.3	0.6	-	-	1.6	-	0.3	-	-	-	-	0.6	-	-	-	-	-	-	-
<i>Rhizosolenia hebatata</i>	2.3	0.6	2.3	2.6	5.3	1.3	3.0	1.3	2.3	4.6	3.6	1.6	7.3	1.6	1.0	5.0	1.3	3.6	2.3	1.0	2.0	2.0	-
<i>R. styli formis</i>	1.6	0.6	2.0	3.3	1.6	2.0	0.6	0.6	0.3	-	0.6	-	0.3	0.3	-	0.3	-	-	-	-	-	-	-
<i>Stephanopyxis turris</i>	-	-	-	0.3	-	-	-	-	-	-	-	-	-	-	-	-	-	-	-	-	-	-	-
<i>Thalassionema nitzschoides</i>	2.3	4.0	3.0	0.6	3.0	3.3	1.6	0.6	4.0	8.3	2.6	7.3	4.3	6.6	10.0	4.6	7.6	8.3	7.6	10.3	7.6	6.0	-
<i>Thalassiosira decipiens</i>	1.3	2.6	3.0	3.0	1.0	2.3	1.2	2.3	2.3	1.0	0.6	-	-	1.6	3.3	0.3	2.3	0.6	1.0	1.0	0.6	-	-
<i>T. eccentricus</i>	-	-	-	-	-	-	-	-	-	3.0	2.6	0.6	1.0	1.6	3.0	-	1.0	3.0	1.6	0.6	1.6	4.3	-
<i>T. gravida</i>	3.6	4.3	1.3	2.6	4.0	3.3	4.3	5.3	3.0	3.0	12.0	11.6	5.6	8.2	3.0	12.6	8.0	7.6	5.6	3.6	7.3	6.6	-
<i>T. hyalina</i>	2.6	4.0	7.6	7.6	5.3	7.0	7.3	4.6	6.0	9.0	3.0	4.6	4.3	5.3	9.6	4.0	6.6	5.0	5.0	6.0	9.3	5.3	-
<i>T. leptopus</i>	0.3	-	0.3	0.3	-	0.6	0.6	-	-	0.3	1.0	0.6	0.3	-	0.3	-	-	0.6	0.3	-	0.3	-	-
<i>T. nordenskioldii</i>	3.0	5.6	1.6	6.6	6.0	4.3	3.6	3.3	5.6	9.4	6.6	2.3	2.6	6.3	8.0	6.0	6.3	5.0	6.6	8.0	5.0	5.3	-
<i>T. ostrupii</i>	1.0	1.6	0.6	1.0	0.3	1.3	2.6	0.6	0.6	0.6	-	0.3	0.3	0.6	-	0.6	-	1.0	1.0	0.3	0.6	1.3	-
<i>T. trifurca</i>	5.0	6.0	6.0	7.3	17.0	6.3	8.3	2.6	4.3	3.3	4.3	5.0	5.0	7.3	2.3	3.3	2.3	5.0	3.6	4.0	6.6	4.0	-
<i>T. undulosa</i>	0.6	1.3	0.6	0.6	0.3	1.6	1.6	0.6	1.3	2.3	-	2.3	-	3.0	1.0	3.0	2.3	1.3	-	2.3	2.3	3.3	-
<i>Thalassiothrix longissima</i>	1.0	1.0	0.6	1.6	0.6	1.3	1.0	0.3	0.6	1.0	0.6	1.0	-	2.0	1.3	1.3	2.3	2.0	2.3	0.3	1.6	-	-
<i>Xanthiopyxis ovalis</i>	-	-	-	0.3	0.6	0.3	1.0	0.3	0.3	-	-	-	0.3	0.3	-	0.3	-	-	0.3	0.6	-	0.3	-
<b>FRESH WATER SPECIES</b>	-	-	-	-	-	-	-	-	-	0.6	0.3	-	-	-	0.3	-	0.3	-	0.3	-	-	-	-

Table 12. cent' d

SAMPLE	81-72	81-73	81-74	81-76	81-77	82-16	82-19	82-21	82-22	82-23	82-24	82-26	82-28
SPECIES													
Actinocyclus curvatus	-	-	-	-	-	-	-	-	-	-	-	-	-
A. divisus	0.3	-	-	-	-	0.3	-	0.6	-	1.0	1.0	1.3	0.6
A. octanerus	-	-	0.3	-	-	-	-	-	0.3	-	0.3	-	-
Actinoptychus undulatus	-	-	-	-	-	0.6	-	0.3	-	-	-	0.3	0.3
A. vulgaris	-	-	-	-	-	0.3	0.3	-	-	-	0.3	-	0.3
Asteromphalus robustus	-	-	-	-	0.6	0.3	0.3	0.3	-	0.3	0.6	-	-
Bacteriosira fragilis	5.0	9.6	5.0	6.0	5.0	2.3	2.0	2.6	4.3	7.3	5.0	5.3	4.6
Biddulphia aurita	1.3	1.3	2.0	0.6	1.0	3.0	1.0	1.6	3.0	1.6	0.6	2.3	1.0
Coccinodiscus lacustris	-	-	-	-	-	0.3	1.0	0.3	0.3	0.3	-	-	0.6
C. marginatus	0.6	1.0	2.3	-	1.3	2.6	2.3	2.0	2.3	2.3	2.6	1.0	2.0
C. oculus-iridis	0.3	0.3	1.0	-	-	1.0	-	1.6	1.3	0.3	2.0	0.6	1.0
C. radiatus	0.6	-	-	-	-	0.6	-	1.6	0.3	0.6	-	0.3	-
C. stellaris	-	-	0.3	0.3	0.3	-	-	-	-	-	-	-	0.3
C. tabularis	-	-	-	-	0.3	-	0.3	0.3	0.3	-	0.3	-	0.3
Denticulopsis seminae	9.3	12.4	14.3	22.3	14.0	23.3	26.3	18.6	20.6	13.3	18.3	23.3	20.3
Melosira "GROUP"	2.0	3.6	1.6	1.3	3.3	2.0	2.6	2.3	2.6	2.3	3.6	3.0	2.3
Navicula sp. 1.	0.3	1.3	2.3	0.6	0.6	0.6	1.3	1.0	-	1.6	0.3	0.6	-
Navicula sp. 2.	-	-	0.3	1.0	0.3	0.6	0.6	-	-	-	-	-	0.3
Navicula sp. 3.	-	0.3	0.6	-	0.3	1.0	-	0.3	-	-	-	-	0.3
Nitzschia cylindrus	5.0	8.3	5.0	5.6	6.3	2.3	3.0	4.0	5.0	3.6	7.6	4.3	3.6
N. grunowii	6.3	17.3	14.0	15.6	17.0	10.3	10.0	16.6	16.6	10.6	18.0	15.6	15.3
Pleurosigma sp.	0.3	-	-	-	-	0.6	-	-	-	-	-	-	-
Podosira glacialis	3.0	0.6	1.3	-	1.3	1.6	2.0	2.6	1.3	3.0	2.6	1.0	1.3
Pseudopodosira elegans	-	0.6	0.6	0.3	1.3	1.3	2.6	-	-	-	0.3	0.3	1.0
Rhaphoneis sachalinensis	-	0.3	0.3	0.3	0.6	0.3	1.0	1.3	1.0	0.3	-	-	-
R. surirella	0.3	0.6	0.6	-	-	0.6	1.3	-	0.3	0.3	-	0.3	0.3
Rhizosolenia hebatata	-	2.6	2.3	1.3	1.3	1.6	3.3	4.3	4.6	3.6	2.3	5.3	3.0
R. styli formis	1.3	-	-	-	0.3	-	-	-	0.3	-	-	-	0.3
Stephanopyxis turris	-	-	-	-	-	-	-	0.3	-	-	-	-	-
Thalassionema nitzschoidea	2.6	5.6	5.0	10.6	13.0	3.0	5.0	4.3	4.0	4.3	4.0	5.3	6.0
Thalassiosira decipiens	1.0	0.6	0.3	1.0	0.3	0.6	1.6	-	1.0	0.6	1.3	0.3	1.3
T. eccentricus	-	0.3	2.0	0.6	1.3	3.3	3.0	1.0	-	1.0	0.3	1.6	2.6
T. gravida	9.6	7.0	9.3	2.6	6.0	7.6	6.0	9.6	8.6	10.0	5.6	7.3	9.0
T. hyalina	5.0	3.6	5.3	6.0	2.6	5.6	4.0	4.0	3.6	4.6	5.0	3.3	7.6
T. leptopus	0.3	-	-	1.0	-	0.6	0.3	0.3	-	0.6	-	0.3	0.6
T. nordenskioldii	7.0	6.6	6.0	6.6	5.6	4.3	6.0	5.0	4.0	4.6	3.6	3.0	3.3
T. oestrupii	1.0	0.6	0.3	0.3	0.6	0.6	1.3	1.0	0.6	0.6	0.3	1.0	0.6
T. trifulta	5.0	6.3	6.0	4.0	4.6	7.6	6.6	4.6	6.6	7.3	4.0	4.3	3.0
T. undulosa	2.0	3.6	2.0	0.6	2.3	2.3	1.6	3.0	3.3	5.0	3.0	1.6	2.6
Thalassiothrix longissima	1.0	1.0	1.0	1.6	1.3	1.3	2.0	0.6	1.0	1.3	1.0	1.3	0.6
Xanthiopyxis ovalis	0.6	-	0.3	-	-	-	-	0.6	-	-	-	-	0.3*
FRESH WATER SPECIES	0.3	1.0	-	-	-	-	-	-	-	-	-	-	-

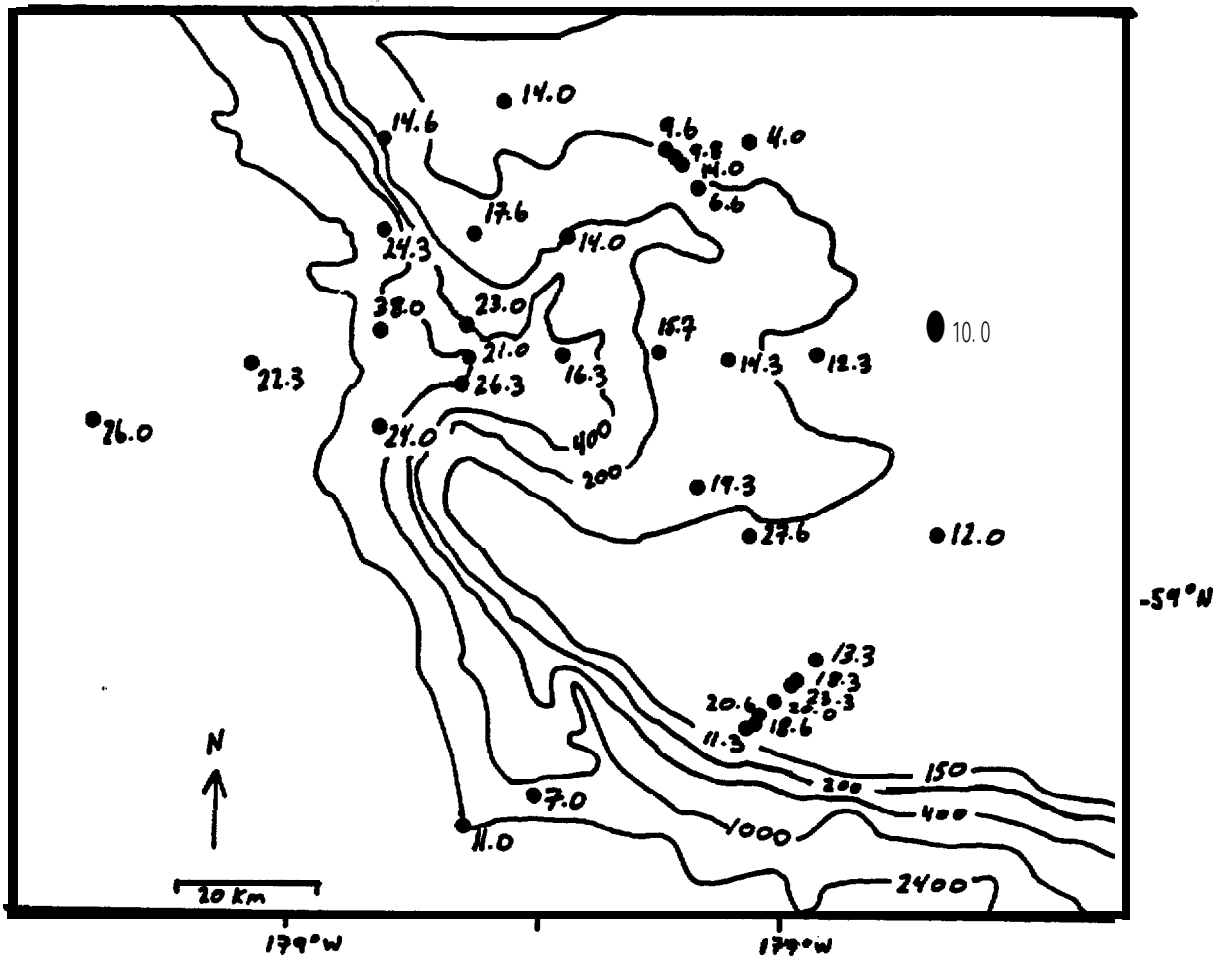


Figure 49. Distribution of *Denticulopsis seminae* in the surface sediments (values are in percent) .

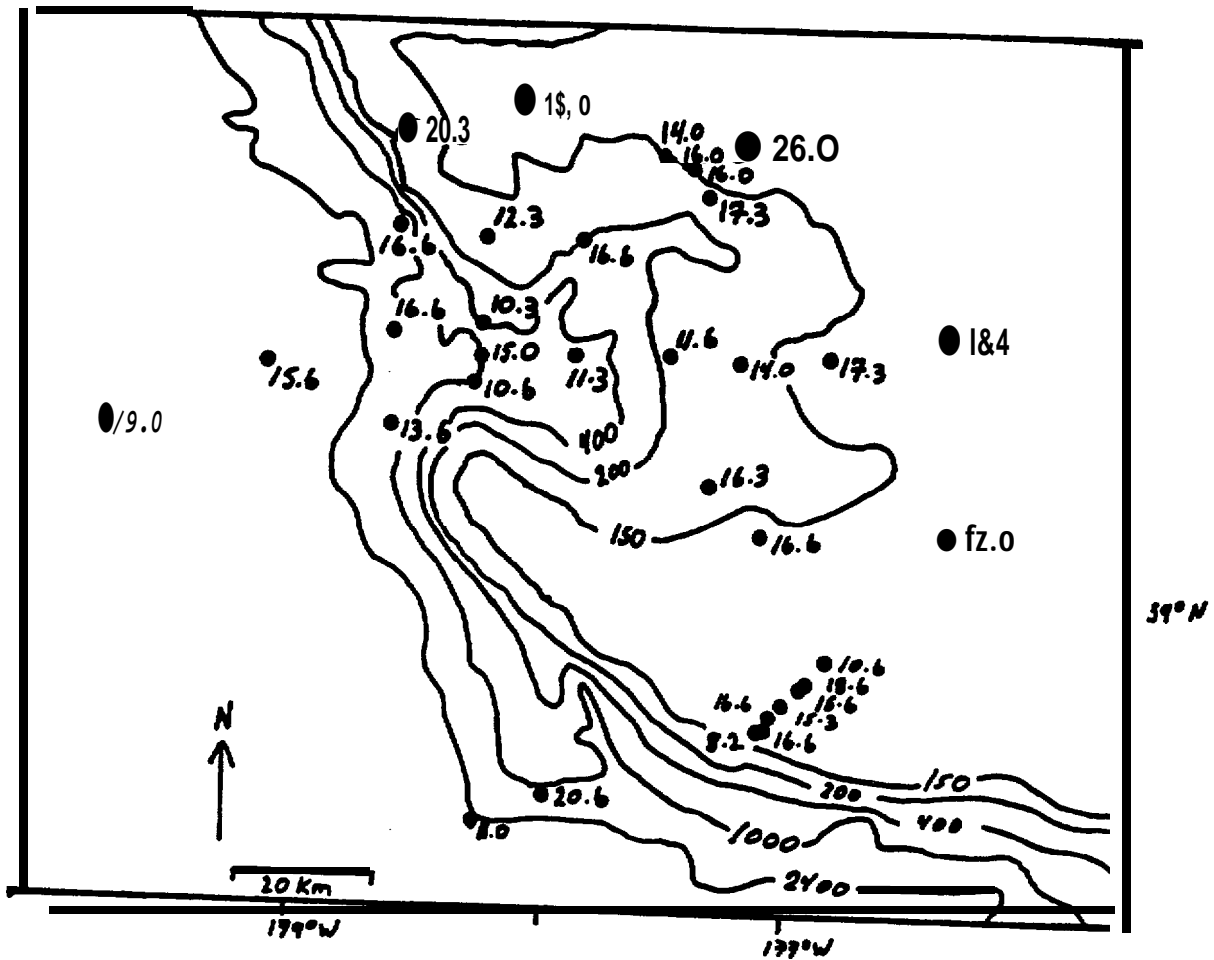


Figure 50. Distribution of *Nitzschia grunowii* in the surface sediment (values are in percent).

The difference in abundance patterns of *N. grunowii* between samples within Pervenets Canyon and elsewhere within the Navarin Basin (see Baldauf, 1982) suggests that sediments within the canyon may be under the influence of post depositional processes of which sediment transport of shelf sediments in to the canyon may be a primary factor.

However, further studies are required to determine all factors which influence this process as well as to examine in detail additional distribution patterns of species not only restricted to shelf environments but also to the slope and basin regions as well.

#### REFERENCES

- Baldauf, J. G., 1981, Diatom analysis of late Quaternary sediments from the Navarin Basin Province, Bering Sea. In Carlson, P. R. and Karl, H. A. (eds.), Seafloor geologic hazards, **Sedimentology**, and **Bathymetry**: Navarin Basin Province, Northeastern Bering Sea. U.S. Geological Survey Open-File Report 82-1217, p. 100-113.
- Baldauf, J. G., 1982, Identification of the Holocene-Pleistocene Boundary in the Bering Sea by diatoms. **Boreas**, volume 11, p. 113-118.
- Donahue, J. G., 1970, Pleistocene diatoms as climatic indicators in North Pacific sediments. Geological Society of America Memoir 126, p. 121-138.
- Fischer, J. M., Carlson, P. R., and Karl, H. A., 1982, Bathymetric map of Navarin Basin province, northern Bering Sea; U.S. Geological Survey Open-File Report 82-1038, 11 p., 1 map, scale 1:1,000,000.
- Schrader, H. J., 1973, Cenozoic diatoms from the Northeastern Pacific, Leg 18. In Kulm, D., von Huene, R., et al., Initial Reports of the Deep Sea Drilling Project, Volume 18, Washington (U.S. Government Printing Office), p. 673-797.

## CHAPTER 11: ASPARTIC ACID GEOCHRONOLOGY OF MOLLUSKS

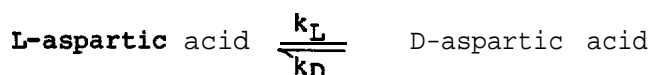
by

David J. Blunt and Keith A. Kvenvolden  
U.S. Geological Survey, Menlo Park, CA 94025

This report considers relative and absolute ages of fossil mollusks from the Navarin Basin Province, Bering Sea, as estimated by the method of **amino-acid geochronology**. Blunt and Kvenvolden (1981) first reported **leucine geochronology** of fossil mollusks from the Navarin Basin province (Fig. 51). In the present study, aspartic acid is used for the purpose of establishing the age of fossil mollusks.

### THEORY

Individual amino acids that are no longer being biologically reproduced in the protein of shell matrix undergo a **stereochemical** change from the **L**-enantiomeric to a mixture of the **L**- and **D**-enantiomeric configurations during natural hydrolysis. The process of interconversion of enantiomers is called racemization and takes place over geologic time. The kinetics of racemization can be expressed as a reversible first-order reaction:



where  $k_L$  and  $k_D$  are the respective reaction rate constants for the **L**- and **D**-aspartic acid enantiomers. The integrated rate expression for the **racemization** reaction as derived by Bada and Schroeder (1972) is:

$$\ln \frac{1 + D/L}{1 - D/L} - \ln \frac{1 + D/L}{1 - D/L} \Big|_{t=0} = 2 kt \quad (1)$$

where  $k$  is the racemization rate constant,  $D/L$  is the ratio of **D**- and **L**-aspartic acid enantiomers, and  $t$  is time. The logarithmic term at  $t = 0$  is evaluated by measuring the  $D/L$  value obtained from modern specimens. **Aspartic acid** has a  $D/L$  value of about 0.06 in modern mollusks (Kvenvolden and others, 1980; Blunt, unpublished data).

### RESULTS

Fossil mollusks recovered from the Bering Sea have been analyzed for **aspartic acid**  $D/L$  values by the method of Kvenvolden and others (1973). Further characterization of the amino acid content in some of the **molluscs** is reported by Blunt and Kvenvolden (1981). Twenty-four specimens from ten genera of **Mollusca** (nine **pelecypods** and one gastropod, Neptunea) are reported in Table 13. These specimens occur within the top two meters of the sedimentary column. The aspartic acid values range from 0.06 in Panomya (DC-5-80, G-71) to 0.43 in Neptunea (DC-5-80, G-98). Radiocarbon analyses of organic

Table 13.--Summary of aspartic acid D/L values in mollusks from the Navarin Basin province

Specimen <sup>1</sup>	Cruise <sup>2</sup>	Station	Core	SO <sup>3</sup> Depth (cm)	D/L	Age	<sup>14</sup> C	Comment <sup>5</sup>
<u>Macoma</u> sp.	DC-4-80	3	G-6	10	0.07			
<u>Macoma</u> sp.	DC-3-81	58	G-62	18	0.07			
<u>Macoma</u> sp.	DC-5-80	47	G-59	13-14	0.08			
<u>Macoma calcarea</u>	DC-3-81	95	G-105	100	0.14		8,385 ± 310	160-190 cm
<u>Macoma</u> sp.	DC-2-81	28	G-31	38-39	0.14		8,815 ± 355	160-190 cm
<u>Macoma prota</u>	DC-5-80	49	G-62	214-220	0.21			
<u>Macoma</u> cf. <u>M. obliqua</u>	DC-5-80	34	G-44	203	0.23		14,980 ± 110	125-145 cm
<u>Nuculana fossa</u>	DC-2-81	22	G-24	205	0.23			
<u>Nuculana radiata</u>	DC-5-80	39	G-50	219-230	0.23			
<u>Nuculana fossa</u>	DC-5-80	34	G-44	125	0.24	•	14,980 ± 110	125-145 cm
<u>Nuculana fossa</u>	DC-5-80	32	G-42	170	0.30	•	13,650 ± 100	170-183 cm
<u>Nuculana radiata</u>	DC-5-80	20	G-26	223-230	0.30	22,000	10, BBO ± 80 to 33,900 ± 610	188-222 cm 235-260 cm
<u>Neptunea</u> sp.	DC-3-81	76	G-50	164	0.26	21,000		
<u>Neptunea neptunea</u>	S-4-76		G-116	90-98	0.33	•	29,197 ± 320	90-98 cm on shell <sup>6</sup>
<u>Neptunea</u> sp.	DC-5-80	79	G-9B	140	0.43	41,000		
<u>Yoldia myalis</u>	DC-3-81	71	V. V.-75	0-2	D.07			
<u>Yoldia myalis</u>	DC-5-80	20	G-26	223-230	0.23 ± .01	14,000	10,800 * 80 to 33,990 * 610	18 B-222 cm 235-260 cm
<u>Yoldia myalis</u>	DC-5-00	53	G-66	60	0.30	•	19,370 * 160	65-64 cm
<u>Clinocardium</u> sp.	DC-2-81	29	G-32	220	0.20	•	7,500 * 305	160-190 cm
<u>Clinocardium nuttallii</u>	DC-5-80	32	G-42	97	0.21	8,000	13,650 ± 100	170-103 cm
<u>Cyclocardia crebricostata</u>	DC-5-80	21	G-28	8	0.10			
<u>Mya truncata</u>	DC-5-80	19	G-25	173	0.21			
<u>Serripes groenlandicus</u>	DC-2-81	36	SC-41	0-2	0.08			
<u>Panomya</u> sp.	DC-5-80	60	G-71	1-6	0.06			

<sup>1</sup> Fossil mollusks are identified by L. Marincovich, USGS, Menlo Park

<sup>2</sup> DC, NOAA Research Vessel DISCOVERER; S, USGS Research Vessel SEA SOUNDER

<sup>3</sup> G, gravity core; V V., Van Veen sampler; B. C., box core

<sup>4</sup> ASP, D-aspartic acid/L-aspartic acid

<sup>5</sup> Depths of radiocarbon analysis differs from depths of mollusk occurrence

<sup>6</sup> Sample from southern Bering Sea, radiocarbon analysis on shell carbonate (Jim Gardner, personal communication)

• Sample used for determination of calibrated rate constant for amino acid dating

carbon in the bulk sediments **range** from 7,500 to **33,990** years.

## DISCUSSION

### Relative Age

Relative ages for the same genera of mollusks are inferred by the order of extent of aspartic acid **racemization** (column 6, Table 13). Older fossils have progressively larger D/L values. For example, Macoma of Dc-4-80 G-6 has an **aspartic** acid D/L value of 0.07 at 10 cm depth, whereas, Macoma of DC-5-80 G-44 has an aspartic acid D/L value of 0.23 at 203 cm depth. Yoldia from DC-3-81 **V.V.-75** and DC-5-80 G-66 has aspartic acid D/L values that range from 0.07 at 0.2 cm to 0.30 at 60 cm, respectively.

In **several** instances, however, samples with similar D/L values occur at quite different sediment-depths. For example, Macoma specimens from DC-3-81 G-105 and DC-2-81 G-31 have aspartic acid D/L values of 0.14 and sample depths of 100 cm and 38-39 cm, respectively. Specimens of Yoldia from DC-5-80 G-26 and DC-5-80 G-66 have D/L values and depth relationships of  $0.23 \pm .01$  at 223-230 cm and 0.30 at 60 cm, respectively. Possible explanations for samples having relatively high D/L values and shallow sample depths are: 1) specimens may have been reworked; 2) sediment accumulation rates may be different at the sites.

### Absolute Ages

Absolute ages of specimens are determined with equation 1, the expression of linear first-order racemization kinetics. Samples which have radiocarbon ages measured immediately next to them are used for the calculation of a calibrated rate constant (Bada and **Protoch**, 1973). The measured aspartic acid D/L value, radiocarbon age and correction at  $t = 0$  are inserted into equation (1), and the equation is solved for  $k$ , the calibrated rate constant. The calibrated rate constant represents the integrated temperature history of the mollusk over the radiocarbon span of time. A calibrated rate constant cannot be calculated for Macoma, because radiocarbon ages are not available adjacent to these specimens. Calibrated rate constants for four general of mollusks are:

<u>Nuculana</u>	$k_{asp} = 1.53 * 0.30 \times 10^{-5} \text{ yr}^{-1}$
<u>Neptunea</u>	$k_{asp} = 9.69 \times 10^{-6} \text{ yr}^{-1}$
<u>Yoldia</u>	$k_{asp} = 1.29 \times 10^{-5} \text{ yr}^{-1}$
<u>Clinocardium</u>	$k_{asp} = 1.90 \times 10^{-5} \text{ yr}^{-1}$

These rate constants permit age estimations to be made for other specimens-of the same genera that lack radiocarbon age control (Table 13). The age of Nuculana in G-26 from DC-5-80 is calculated to be 22,000 years by this method. This value is in agreement with the range of 10,880 to 33,990 years based on radiocarbon dates that bracket an erosional surface close to where the Nuculana was recovered. Yoldia from the same interval in G-26 gives an age of 14,000 years which also is in agreement with the radiocarbon range of

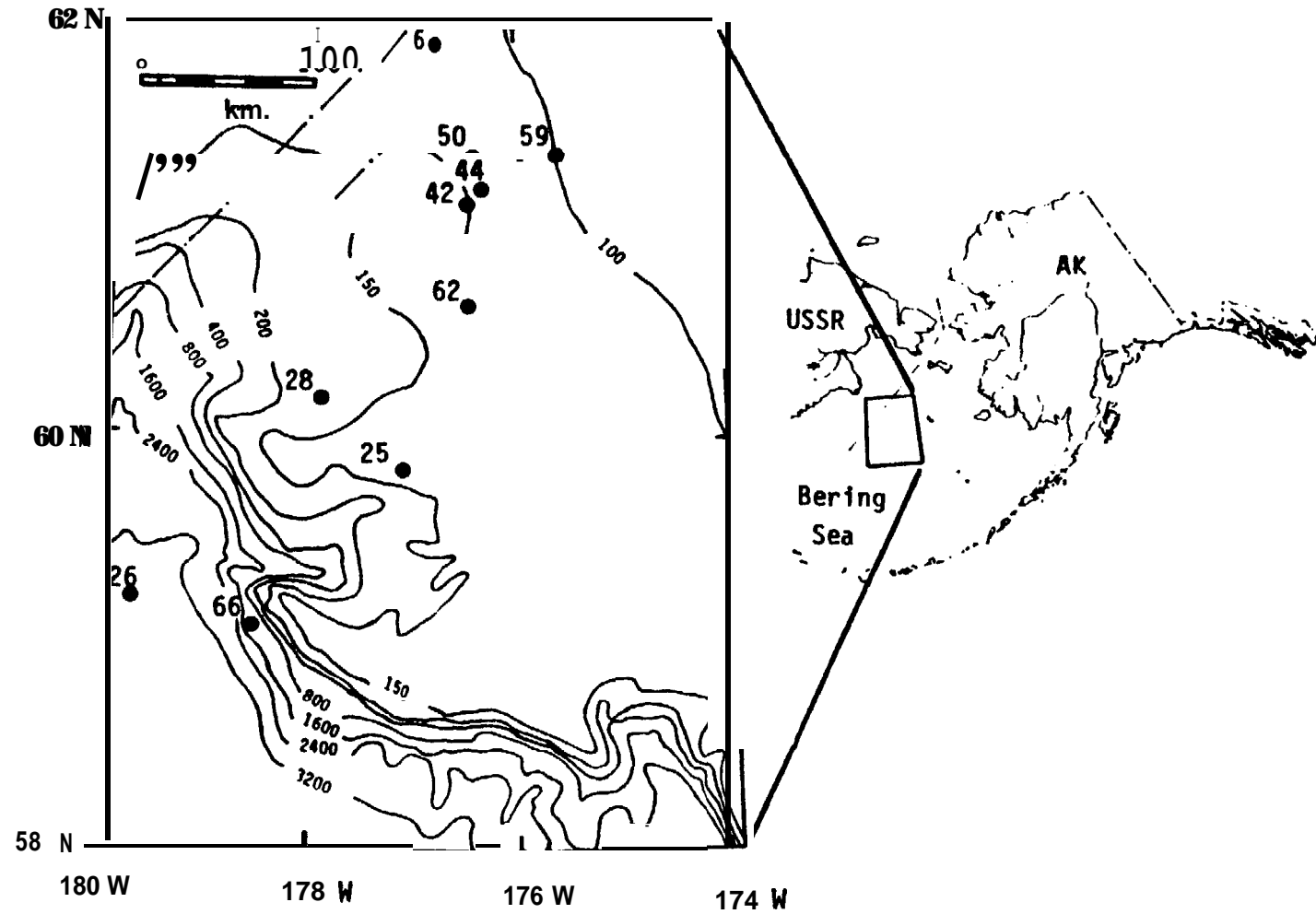


**Figure 51.** Location of gravity cores in the northern Navarin Basin province where fossil mollusks were studied. Bathymetry is in meters.

**10,880 to 33,990 years.** In core G-42 from DC-5-SO Clinocardium at 97 cm has an age of 8,000 years which is in general agreement with the radiocarbon date of 13,650 at 170-183 cm depth. Neptunea from DC-3-81 G-80 has a calibrated age of 21,000 years. The Neptunea from DC-5-80 **G-98** has an age of 41,000 years at a depth of 140 cm. This is the oldest sample measured in this investigation.

#### Summary

Aspartic acid enantiomeric ratios were used to establish the age of five **molluscan** samples collected from sediment cores from the **Navarin** Basin province. These samples range in age from 8,000 to 41,000 years old. In general, the ages given by the amino acid method agree with radiocarbon dates.

#### References

- Bada, J. L. and Protsch, R., 1973, Racemization** reaction of aspartic acid and its use in dating fossil bones: Proceedings of the National Academy of Science, v. 70, p. 1331-1334.
- Bada, J. L. and Schroeder, R. A., 1972, Racemization of isoleucine in calcareous marine sediments: kinetics and mechanism:** Earth and Planetary Science Letters, v. 15, p. 223-231.
- Blunt, D. J. and **Kvenvolden, K. A., 1981, A preliminary report on amino acid diagenesis in fossil mollusks recovered from the Navarin Basin Province, Bering Sea:** in **Carlson, P. R. and Karl, H. A. (eds) Seafloor Geologic Hazards, Sedimentology, and Bathymetry:** U.S. Geological Survey **Open-File Report 81-1217**, p. 138-149.
- Kvenvolden, K. A., Blunt, D. J., and H. E. Clifton, 1979, Amino acid racemization in Quaternary "shell deposits at Willapa Bay, Washington:** **Geochimica Cosmochimica, Acts**, v. 43, p. 1505-1520.
- Kvenvolden, K. A., Blunt, D. J., McMenamin, M. A., and Strahan, S. E., 1980, Geochemistry of amino acids in shells of the clam Saxidomus:** in Douglas, A. G., and Maxwell, J. R. (eds), **Advances in Organic Geochemistry 1979:** Pergamon Press, Oxford, p. 321-332.

CHAPTER 12: APPENDED REPORTS

- A. **Carlson**, P. R. and Karl, H. A., 1981, High-resolution seismic reflection profiles: Navarin Basin province, northern Bering Sea, 1980: U.S. Geological Survey Open-File Report 81-1221, 4 p., 1 map, scale **1:1,000,000.**
- B. CarlSon, P. R. and Karl, H. A., 1982, High-resolution seismic reflection profiles: Navarin Basin province, northern Bering Sea, 1981: U\*S. Geological Survey Open-File Report 82-786, 5 p., 1 map, scale **1:1,000,000.**
- c. Karl, H. A. and **Carlson**, P. R., **1982, Location** and description of sediment samples: Navarin Basin province, Bering Sea, 1980-81: U.S. Geological Survey **Open-File** Report 82-958, 5 p., 2 maps, scale **1:1,000,000.**
- D. Fischer, J. M., **Carlson**, P. R., and Karl, H. A., 1982, Bathymetric map of Navarin Basin province, northern Bering Sea: U.S. Geological Survey Open-File Report 82-1038, **11** p., **1** map, scale **1:1,000,000.**
- E. **Carlson**, P. R., Fischer, J. M., and Karl, H. A., **1983**, Two newly discovered submarine canyons on Alaskan continental margin of Bering Sea: U.S. Geological Survey Open-File Report 83-24, 36 p., 1 map, scale **1:250,000.**
- F. **Carlson**, P. R., Karl, H. A., Fischer, J. M., and Edwards, B. D., 1982, Geologic hazards **in Navarin** Basin province, northern Bering Sea: 14th Offshore Technology Conference, Houston, Texas, Proceedings, v. 1, 73-87.
- G. **Carlson**, P. R., Karl, H. A., and Edwards, B. D., Puzzling features **in** the head of the **Navarinsky** Canyon, Bering Sea: submitted to Gee-Marine Letters, 13 ms. p., (1983).
- H. Karl, H. A. and **Carlson**, P. R., Large sand waves in submarine canyon heads, Bering Sea: preliminary hypothesis of their depositional history: **submitted** to Gee-Marine Letters, 15 ms. p., (1983).

APPENDIX A:

HIGH-RESOLUTION SEISMIC REFLECTION PROFILES:  
NAVARIN BASIN PROVINCE, NORTHERN BERING SEA, 1980

by

Paul R. **Carlson** and Herman A. Karl

U.S. Geological Survey

## INTRODUCTION

In June and **July** 1980, the U.S. Geological Survey conducted a high resolution geophysical and seafloor sampling cruise (DC 4/5-80 **BS/NB**) in the northern Bering Sea to obtain data *on* seafloor hazards pertinent to OCS oil and gas lease sale activity. **This** report contains a list of the seismic reflection records that are publicly available and includes a **trackline** map of the Navarin Basin province. Microfilm copies of the seismic reflection records are available for viewing:

- (1) U.S. Geological Survey  
Pacific-Arctic Branch of Marine Geology, Room **B171**  
Menlo Park, CA 94025

or for purchase:

- (2) National Geophysical and Solar  
Terrestrial Data Center  
**EDS/NOAA**  
Boulder, CO 80302

## DATA COLLECTION

DISCOVERER cruise DC 4/5-80 **BS/NB** left Kodiak July 2, 1980, for **work in** OCS lease sale are 83 (Navarin Basin). The first leg, **which** was 75 percent geophysics and 25 percent sampling, ended at Adak July 24, 1980. The second leg of the cruise **which** began July **28, 1980, consisted of 60** percent sampling and 40 percent geophysics, and ended at Kodiak August 17, 1980.

Navigation positions were determined by satellite and Loran C. Position accuracies are probably on the order of 0.5 km.

Three separate seismic reflection systems **were** operated simultaneously, throughout much of the study area, providing high and intermediate frequency acoustic records. The systems **were:** 3.5 kHz transducer (12,842 km), 400-800 Joule minisparker (4624 km), and **two** 40 in<sup>3</sup> airguns (6757 km). The 3.5 kHz system was operated continuously throughout the **cruise**, including transit lines to and from the study area and to and from St. Paul Island for three medivacs. The airguns were deployed along all except transit and sampling **lines**. The minisparker system was operated in shelf and upperslope **water** depths (to about 800 m). (See Table A1 and Figure A1 for **line numbers along** which the various systems were operational).

## ACKNOWLEDGMENTS

**We** appreciate the assistance provided by the scientific personnel on the cruise (Brian Edwards, Jeff Fischer, George Ford, Sarah Griscom, Ken Johnson, Beth Lamb, Grant **Lichtman**, Paula **Quinterno**, Jeff Rupert, John **Saladin**, Rick Vail, Tim Vogel, Pat **Wiberg**, Bob Wilson, and Mark Yeats), the ship's captain and crew, and the marine logistics group.

The cruise was supported jointly by the **U.S.** Geological Survey and by the Bureau of Land Management through interagency agreement with the National Oceanic and Atmospheric Administration, under which a multi-year environmental hazards study of the Alaskan continental shelf is managed by the OCSEAP office.

Table A1. Track **lines** along which seismic systems were operational.

	<b>3.5 only*</b>		<b>Minisparker</b>	<b>Airguns</b>
	<b><u>Transit</u></b>	<b><u>Study Area</u></b>		
Leg 1 (DC-4-80)	T-1, 1, 26, 27, 32, 33, 38	None	1-3, 4-14, 18, 22-25, 28-29 31, 34-37	1-25, 28-31 34-37
Leg 2 (DC-5-80)	30, 98, 99	48-51 53-62 72-74 81-86 93-95 100 105-108 114-115 121-123	40-43, 45-47, 63-67, 69, 76-79, 87-91 97, 102-103 110, 117, 125-126	40-47, 52 63-71, 75-80, 87-92, 96-97, 101-104, 109-113, 116-120, 124-127

---

\*3.5 kHz system was operated continuously during both legs of cruise.

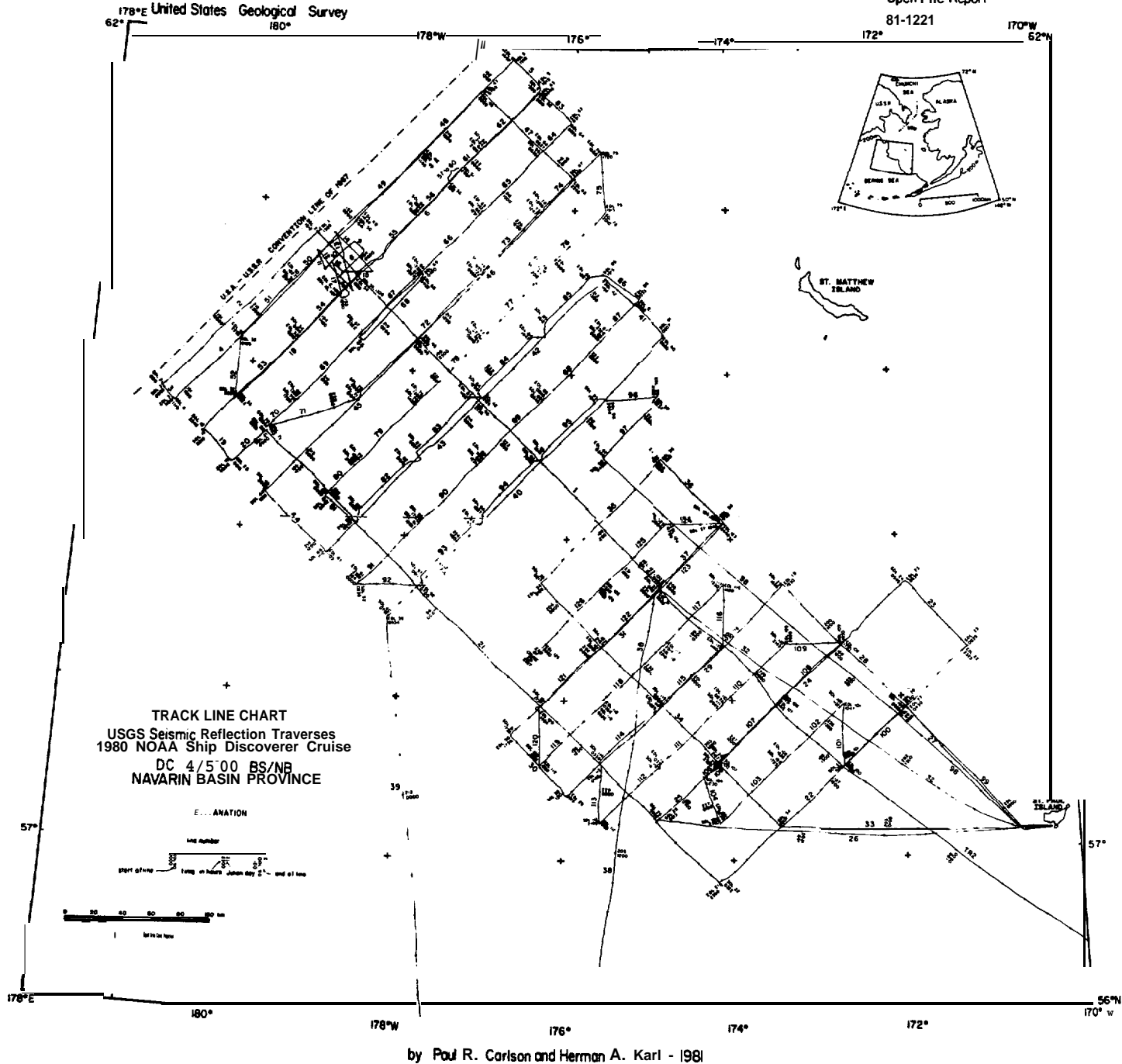


Figure A1. Track line chart for 1980 DISCOVERER Cruise DC 4/5-80 BS/NB.

APPENDIX B:

HIGH-RESOLUTION SEISMIC REFLECTION PROFILES:  
NAVARIN BASIN PROVINCE, NORTHERN BERING SEA, 1981

by

Paul R. **Carlson** and Herman A. Karl

U.S. Geological Survey

## INTRODUCTION

In June and July 1981, the U.S. Geological Survey conducted a high resolution geophysical and seafloor sampling cruise (DC 2/3-82 **BS/NB**) in the northern Bering Sea to obtain data on seafloor hazards pertinent to OCS oil and gas lease sale activity. This report contains a list of the seismic reflection records that are publicly available and includes a **trackline** map of the Navarin Basin province. Microfilm copies of the seismic reflection records are available for **reviewing**:

- (1) U.S. Geological Survey  
Pacific-Arctic Branch of Marine Geology, Room B164  
Deer Creek Facility  
Menlo Park, CA 94025

or for purchase:

- (2) National Geophysical and Solar  
Terrestrial Data Center  
**EDS/NOAA**  
Boulder, CO **80302**

## DATA COLLECTION

DISCOVERER cruise **DC2/3-81 BS/NB** left Kodiak June 8, 1981, for **work** in OCS lease sale area 83 (**Navarin Basin**). The first leg, **which** was 65 percent geophysics and 35 percent sampling, ended at Adak **July 2, 1981**. The second leg of the cruise **which** began July 6, 1981, consisted of 55 percent geophysics **and** 45 percent sampling, and ended at Dutch Harbor July **29, 1981**.

Navigation positions were determined by satellite and Loran C. Position accuracies are probably on the order of 0.5 km.

Three separate seismic reflection systems were operated simultaneously throughout much of the study area, providing high and intermediate frequency acoustic records. The systems were: 3.5 kHz transducer (10,143 km), 400-800 **Joule minisparker** (5247 km), and **two** 40 in<sup>3</sup> **airguns (8050 km)**. The 3.5 kHz systems as operated continuously throughout the cruise, including transit lines to the study area and part of the **way** to and from **St. Paul Island for two medivacs**. The airguns were deployed along all except transit and sampling lines. The **minisparker** system was operated in shelf and upper-slope water depths (to **about 800 m**). {See **Table B1** and Figure A-f? for line numbers along **which the** various systems were operational.)

## ACKNOWLEDGMENTS

We appreciate the **assistance** provided by the scientific personnel on the cruise (Jack **Baldauf**, Neal Barnes, Mike **Bennett**, Dave Blunt, Drew Comer, Merid Dates, Jon Erickson, Jeff Fischer, Dan **Hurlbert**, Ken Johnson, Jim Joyce, Larry Kooker, Beth Lamb, Larry **Lawver**, Sue **McGeary**, Jim Nicholson, Robert Patrick, Paula **Quinterno**, Robin Ross, Jeff Rupert, John Saladin, Dennis Thurston, Tim

Vogel, Hal Williams, and Mark Yeats) the ship's captain and crew, and the marine logistics **group**.

The cruise was supported jointly by the U.S. Geological Survey and by the Bureau of Land Management through interagency agreement with the National Oceanic and Atmospheric Administration, under which a multi-year environmental hazards study of the Alaskan continental shelf is managed by the OCSEAP office.

Table B1. Track lines along which seismic systems were operational.

	<u>3.5 only*</u>		<u>Minisparker</u>	<u>Airguns</u>
	<u>Transit</u>	<u>Study Area</u>		
<b>Leg 1</b> <b>(DC-2-81)</b>	<b>T1-T4</b>	48,49,63,70	<b>T2,T4,1-5,</b> 8-20,24-28 31-47, 50-60 62, 64-68 73-82	<b>1-47,</b> 50-62 64-69, 71-92
<b>Leg 2</b> <b>(DC-3-81)</b>	None	<b>111, 119-122</b>	<b>106-110,</b> <b>112-118,</b> <b>123-137,</b> <b>141-153,</b> <b>159-188</b>	<b>95-110, 112-118,</b> <b>123-188</b>

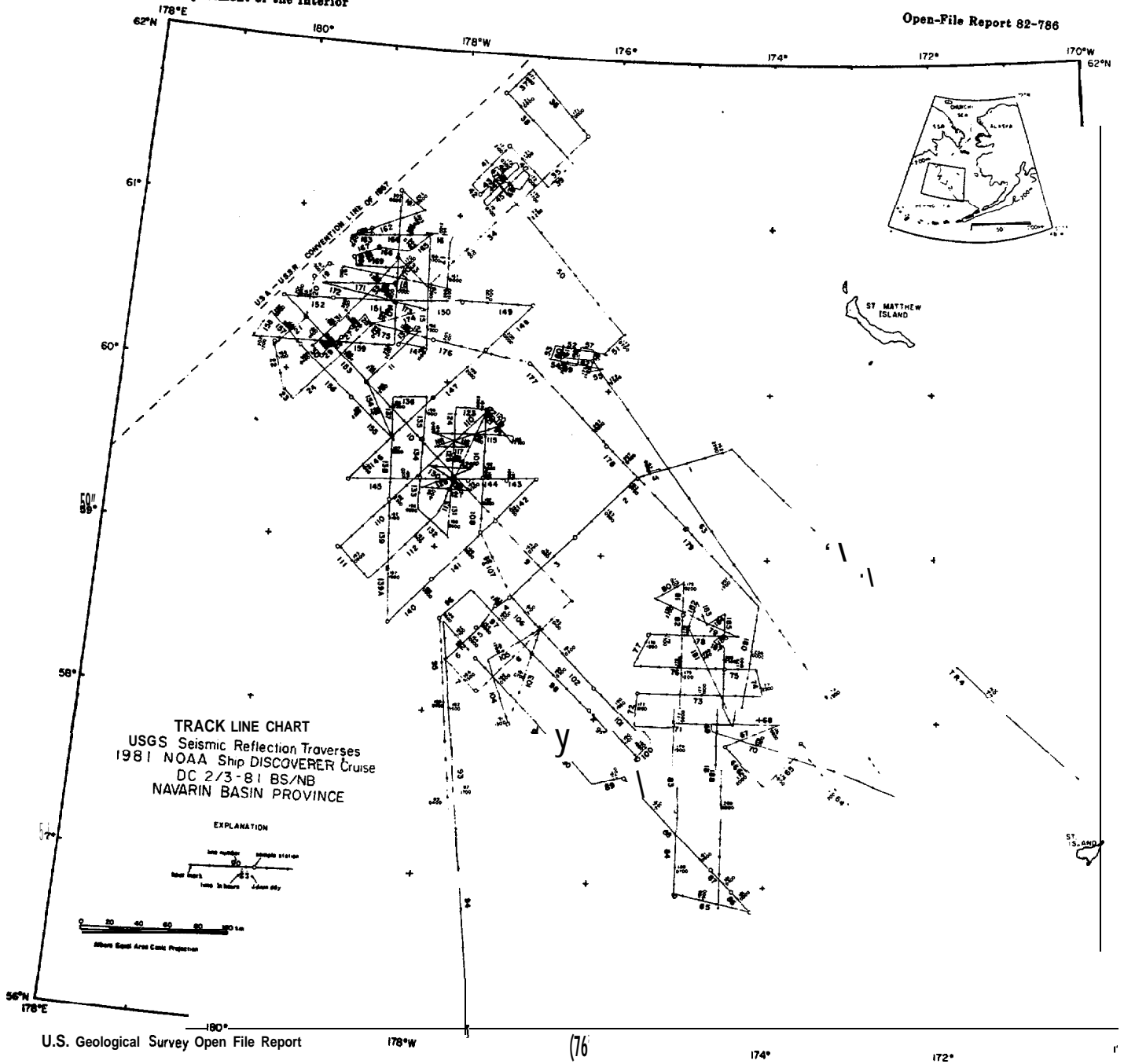


Figure B1. Track line chart for 1981 DISCOVERER Cruise DC 2/3-81 BS/NB.

APPENDIX C:

LOCATION AND DESCRIPTION OF SEDIMENT **SAMPLES**:

**NAVARIN** BASIN PROVINCE, BERING SEA, 1980-1981

by

Herman A. Karl and Paul R. **Carlson**

U.S. Geological Survey

## INTRODUCTION

Three cruises have been conducted in the Navarin Basin province (lease sale area 83) in the northern Bering Sea to obtain data on seafloor hazards pertinent to OCS oil and gas lease sale activity. This report summarizes the information that is presently available regarding sediment samples collected during those cruises. Included in this report are a station location map (Figure C1) and a map of sediment types (Figure C2) derived from qualitative visual descriptions of surface samples. Microfilm copies of the visual core description logs are available for viewing:

- (1) U.S. Geological Survey  
Pacific-Arctic Branch of Marine Geology, **Room B 171**  
Menlo Park, CA 94025

or for purchase:

- (2) National Geophysical and Solar Terrestrial Data Center  
**EDS/NOAA**  
Boulder, CO 80302

## DATA COLLECTION

USCG Ice breaker POLAR STAR followed the ice in spring (**May 2-29**) 1980 and 22 gravity cores and 33 grab samples **were** collected during this cruise designated **PST-80-BS**; 104 **gravity cores**, 10 **grab samples** and 1 **dredge sample** were collected in summer (July 2 - August 17) 1980 during NOAA ship DISCOVERER cruise **DC 4/5-80-BS/NB**; and 88 **gravity cores**, 10 **grab samples**, 6 **box cores**, and 5 vibracores **were** collected in summer (June 8 - July 29) 1981 during DISCOVERER cruise **DC2/3-81-BS/NB**.

Cores collected on USCG POLAR STAR during cruise **PST-80-BS** cores were stored at **Adak**, Alaska from late May to late July and then transferred to NOAA ship DISCOVERER for **study**. **PST-80-BS**, **DC4/5-80-BS/NB**, and **DC2/3-81-BS/NB** cores were split and described and **subsamples** were collected for grain-size, **geochemical**, **faunal**, clay mineral, carbon, and **geotechnical** analyses at onshore laboratories. The split cores **were** placed in D-tubes and kept with **subsamples** in cold storage and are archived at the **U.S.** Geological Survey refrigerated core locker in Menlo Park.

Navigation was by Loran C and satellite; position accuracies are probably on the order of 0.5 km.

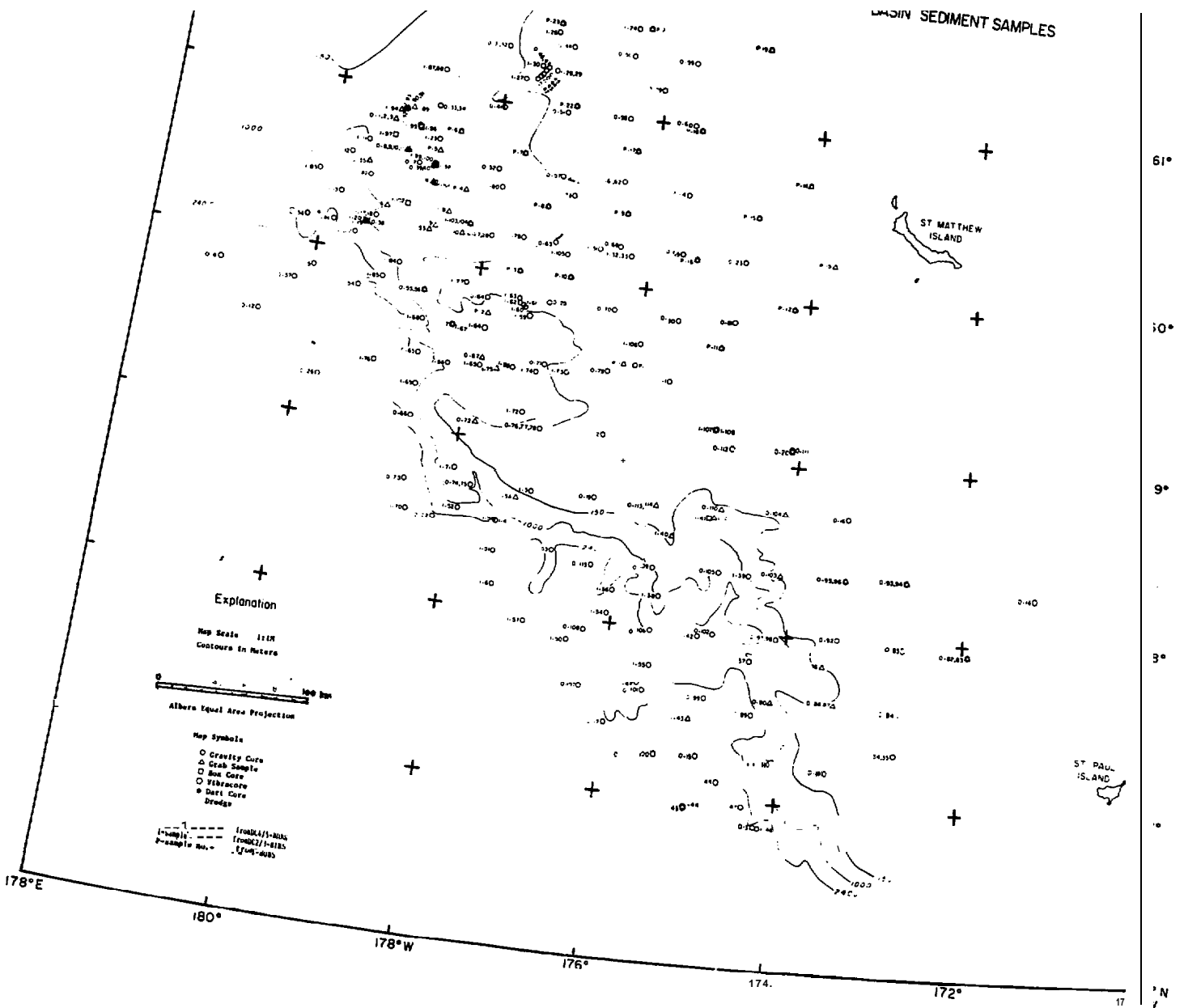


Figure C1. Station location map.

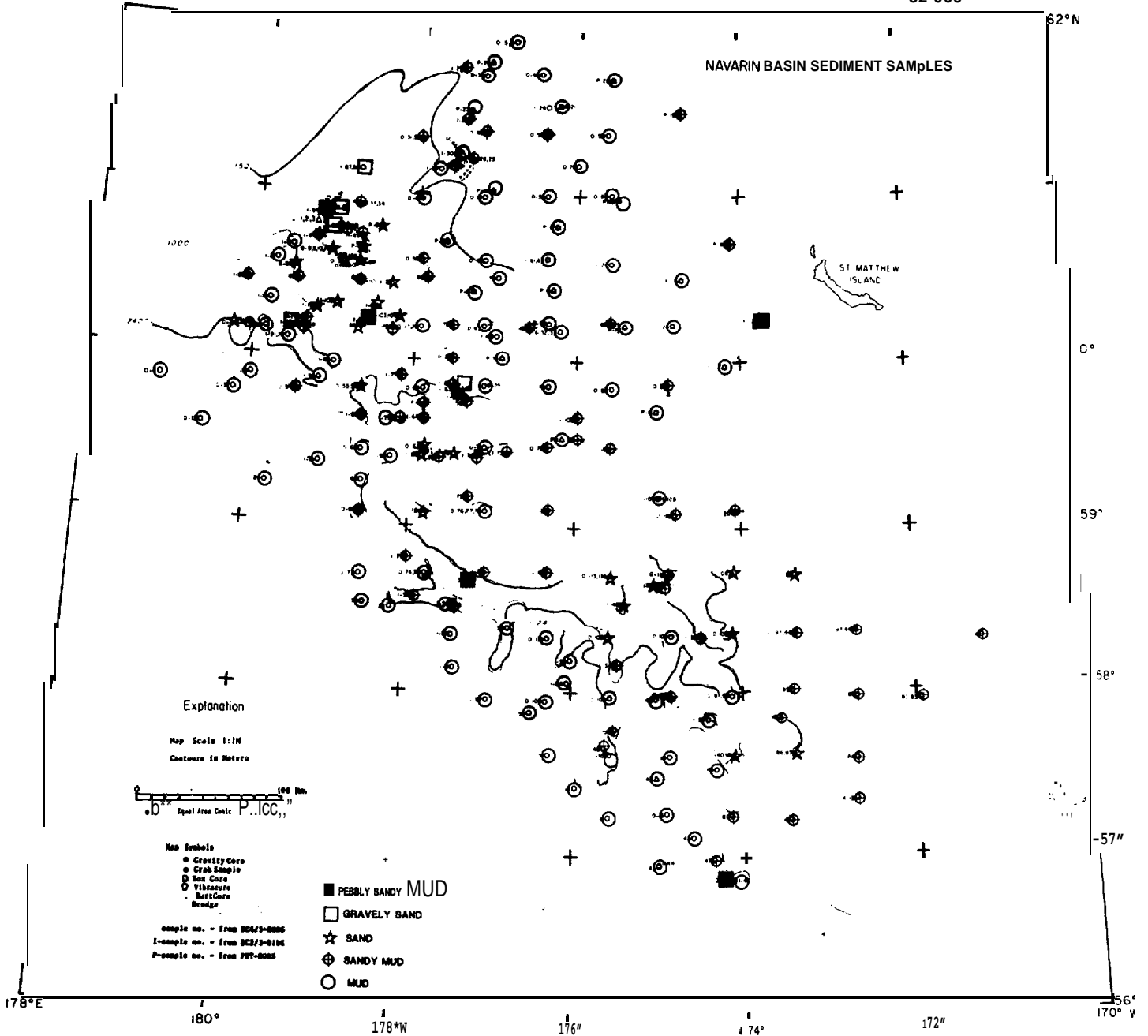


Figure C2. Map of sediment types.

## OBSERVATIONS

Sediment sampling stations are plotted in Figure C1. Figure C2 shows the distribution of sediment types derived from qualitative visual descriptions of surface samples, defined as bulk **subsamples** from grab samples and discrete **subsamples** from the upper 35 cm of gravity cores. Silts generally characterize the shelf and slope, but there are zones of coarser sediments at the shelf break, *on* the upper slope, and in the heads of submarine canyons. **Surficial** sediment on the shelf tends to be coarser in the southeastern part of the area than **elsewhere**.

## ACKNOWLEDGMENTS

We appreciate the assistance provided by the scientific personnel on each of the cruises (Jack **Baldauf**, Neal Barnes, Mike Bennett, Dave Blunt, Drew Comer, Merid Dates, Brian Edwards, Jon Erickson, Jeff Fischer, George Ford, Sarah **Griscom**, Rick Herrera, Dan Hurlbert, Ken Johnson, Jim Joyce, Larry Kooker, Beth Lamb, Larry Lawver, Grant **Lichtman**, Sue McGeary, Jim Nicholson, Robert Patrick, Paula **Quinterno**, Robin Ross, Jeff **Rupert**, John **Saladin**, Dennis Thurston, Rick Vail, Tim Vogel, Pat Wiberg, Hal Williams, Bob Wilson, and Mark Yeats) and by the **ship's** captains and crew and the marine logistics group. .

The cruises **were** supported jointly by the U.S. Geological Survey and by the Bureau of Land Management through interagency agreement with the National Oceanic and Atmospheric Administration, under which a multi-year environmental hazards study of the Alaskan continental shelf is **managed** by the OCSEAP office.

APPENDIX D:

BATHYMETRIC MAP OF NAVARIN BASIN PROVINCE,  
NORTHERN BERING SEA

by

Jeffrey M. Fischer, Paul R. **Carlson**, and Herman A. Karl

U.S. Geological Survey

## INTRODUCTION

This bathymetric map of the Navarin basin province is part of the ongoing research in preparation for OCS Lease Sale 83 which is scheduled for the spring of 1984. The intended use of this map, in addition to showing the morphology of the Navarin continental margin, is for the plotting of geologic and geophysical data. It is not intended for use in navigation. Names used herein for seafloor features are from historical and general usage and have not been formally approved.

**Navarin** Basin province includes an area of over 150,000 km<sup>2</sup> and contains the large, deep, sediment-filled Navarin Basin named by Marlow and others (1976). The study area is located in the northern Bering Sea (see index map) and extends to within 100 km of St. Matthew Island on the northeast and to within 100 km of St. Paul Island on the southeast. To the southwest, the boundary of the study area is the 3600 m isobath, and to the northwest, the U.S.-Russia Convention Line of 1867; however, the basin itself continues to within 150 km of the Siberian Coast (Marlow, Cooper, Parker, and Childs, 1981).

Previous studies of the Bering Sea have concentrated on the Siberian and Alaskan coasts, in addition to the Aleutian Arc and portions of the southeastern Bering continental margin. Within the **Navarin** Basin province, few studies were conducted previous to the 1960's. Maps by Baranov and others (1967), Pratt and Walton (1974), Scholl and others (1974), and Schumacher (1976) improved coverage, but the Navarin basin area has received little detailed attention, and consequently inaccuracies abounded, especially northwest of **Zhemchug** Canyon. The present study improves coverage up to the U.S.-Russia Convention Line of 1867 and makes significant changes in the published **bathymetry**, especially in the Navarinsky Canyon area.

## DATA COLLECTION

The data base for the map consists of over 23,000 kms of 3.5 kHz **tracklines** obtained on U.S. Geological Survey cruises from 1976 to 1982 (see Fig. D1 and Table D1). Navigation was based on Loran C, updated with satellite fixes. On the continental shelf the trackline grid spacing averages about 30 km. Digitized depths along each **trackline** were spaced 2 km apart on the continental shelf and rise and depths were spaced 0.2 km or less apart on the continental slope. We assumed a water velocity of 1500 meters/see with no correction for tides, temperature, or salinity. Tides in the Bering Sea, although poorly understood, are generally less than a meter (Lisitsyn, 1966) and waves during the survey periods were negligible. The depth data and navigation data were computer merged, contoured by hand, and compared with a computer contoured map as a **final** check. Contour intervals range from 200 m for depths **below** 200 m, to 25 m between 150 to 200 m, to 10 m from 0 to 150 m water depths. Contours shallower than 100 m are taken from Pratt and Walton (1974).

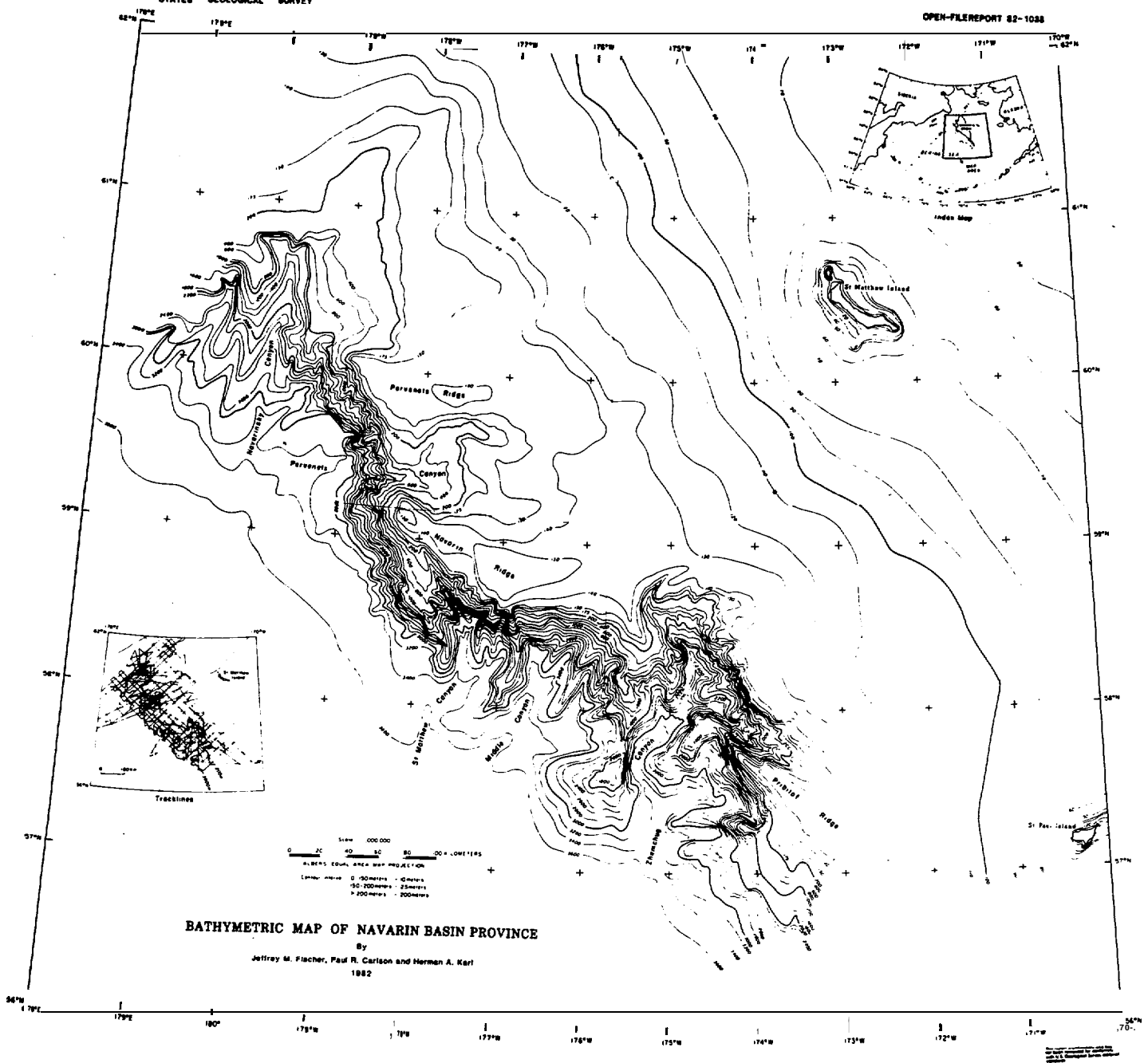


Figure D1. Bathymetric map of Navarin Basin province and inset showing tracklines.

Table III. Sources of bathymetric data

<u>Cruise*</u>	<u>km of tracklines</u>
L-5-76	800
s-3-77	700
L-5-77	<b>1,000</b>
L-8-77	2,300
DC-4/5-80	6,800
DC-2/3-81	10,100
L-10-82	1,600

\*cruise identifier includes ship (**L=S.P. Lee**, **S=Sea Sounder**, **DC=Discoverer**), consecutive cruise **number** and year.

#### GEOLOGY

A tectonic model of the Bering shelf margin proposed by Scholl and others (1975) suggests that during the Mesozoic era the ocean plate boundary was a subduction zone of **small** convergence angle which ran along the present Bering shelf margin. As a result of subduction, **fore-arc-eugeosynclinal** rocks were uplifted and an inner **magmatic** arc formed (Marlow and others, 1976). Remnants of these **fore-arc-magmatic-arc** facies can be traced southeast from Siberia through St. **Matthew** and St. Lawrence Islands, where they change trend to the northeast and extend into Alaska (Patton and others, 1976). Sometime in Cretaceous or earliest Tertiary time, the subduction zone either jumped or migrated to its present position at the Aleutian Trench (Scholl and others, 1975; Patton and others, 1976). With the cessation of subduction, both **fore-arc** and **magmatic-arc** rocks were uplifted and eroded. About the same time, the **compressional** deformation ceased and changed to extensional rifting (Marlow and others, 1976). Extension, erosion, and subsequent subsidence have continued during much of the Cenozoic, creating the Navarin basin, among others, and influencing much of the present **bathymetry**. Navarin basin contains as much as 12 km of fill in **places** beneath the continental shelf (Marlow, Cooper, Parker, and Childs, 1981; Marlow, Carlson, Cooper, Karl, McLean, McMullin, and Lynch, 1981). The sedimentary fill consists of **semi-consolidated to unconsolidated**, generally flat-lying, relatively undeformed, **hemipelagic** deposits of Cenozoic age (Scholl and others, 1968; Marlow and others, 1979; Karl and Carlson, 1982).

#### GEOMORPHOLOGY

The Navarin basin province is an area of great contrasts, including the very flat continental shelf with its subtle structures, to the steep continental slope with its spectacular precipices and large canyons, and the gentle continental rise crossed by turbidity current channels and buried **deep-sea** fan channels. These morphologic features are influenced by, if not directly related to, the tectonic history of the region.

The continental **shelf** within the Navarin Basin province is extremely flat and encompasses an area of 100,000 km<sup>2</sup> between the 100 m and 150 m isobaths. The width of the **shelf** in the province *varies* from 100 km to 250 km and gradients range from 0.04° to 0.01°. Compared to Shepard's (1963) worldwide average shelf gradient of 0.12°, the Bering shelf appears to be one of the

flattest in the world. The most prominent features are large canyons incised into the shelf and large submarine ridges oriented parallel to and located next to the shelf break. **Two** large submarine ridges, Navarin and **Pribilof** (**Marlow** and others, 1976), are each outlined by the 130 m isobath and are south of Pervenets and **Zhemchug** Canyons respectively. These ridges appear to be surface expressions of structural highs where acoustic basement rises to within less than one kilometer of the seafloor (Cooper and others, 1981) . A few protrusions of probable acoustic basement crop out along these ridges, but are too **small** to show at this scale. Three such protruding knobs crop out on Navarin Ridge just north of Middle Canyon. Another knob, just south of **Zhemchug** Canyon, on **Pribilof** Ridge, rises to within 100 meters of the surface. The third and smallest ridge north of Pervenets Canyon, herein called Pervenets Ridge, is somewhat anomalous since shallow acoustic basement is not discernible on the seismic records.

The shelf break in Navarin Basin province occurs between the 150-175 m isobaths. Around the canyons, the break varies somewhat; Navarinsky Canyon has no distinct shelf break, in Pervenets the break is very gentle, and in **Zhemchug** the break is very abrupt. In general, from northwest to southeast, the depth of the break decreases until at **Zhemchug** Canyon the shelf break occurs at about 150 m.

The continental slope, an area of 40,000 km<sup>2</sup>, begins at about the 150 m isobath and extends to the 2800 m isobath. The slope is dissected by five large submarine canyon systems which from north to south are Navarinsky, Pervenets, St. Matthew, Middle, and **Zhemchug** Canyons. It should be noted that all the above are large canyon systems, composed of numerous tributary canyons many of which are too small to resolve at our present grid spacing and map scale. The slope within the Navarin Basin province **has a length of 600 km** and varies in width from 200 km near Navarinsky Canyon to 15 km near **st. Matthew** Canyon. The Navarin continental slope ranges in gradient from 3° to 10°, compared to a world-wide average of 4.3° (**Shepard**, 1963) .

Navarinsky Canyon has a width of 150 km at the shelf break, an axial length of 200 km, and an approximate volume of 4900 km<sup>3</sup>. The **Navarinsky** system consists of **two** main branches, the western which is oriented roughly north-south and the eastern which trends northeast-southwest. Above the 400 m isobath, these branches form large, broad, gently sloping shelf valleys that have axial gradients of less than **0.2°**. Between 400 m and 3600 m, where these **two** branches merge into a single deep-sea fan channel, the gradients are about **1.2°**. The gradient of the fan channel between 3200 and 3600 m is approximately 0.3°. Still, both of these gradients are gentle compared to the other Navarin margin canyons.

The next major canyon to the southeast, Pervenets, is incised perpendicular to the slope and trends east to west. Pervenets Canyon has a width of 70 km at the shelf break, a downslope length of 120 km, and a volume of 1200 km<sup>3</sup>; the major portion of this volume is above the 1000 m isobath. Above 1000 m the canyon bifurcates into two branches which can be traced to the 150 m isobath. Each of these main branches has an axial gradient of **0.4°**. The larger northern branch located just south of Pervenets Ridge is well-defined, whereas the smaller southern branch of Pervenets Canyon is

poorly developed and has little expression above 600 meters. Below 1000 meters the canyon system is less well-developed than any of the Navarin margin canyons. Between 1000 m and 3000 m the canyon **thalweg** attains a gradient of **3.8°**.

The St. Matthew Canyon system, the smallest of the five canyons, contains some of the steepest relief in the Navarin basin area and is located south of the Navarin Ridge. St. Matthew Canyon consists of at least two main branches and several tributaries, the west branch with a gradient of 2.5° being the longer and the east the shorter and steeper with a gradient of 5° (**Carlson** and others, in press). The upper part of St. Matthew Canyon is parallel to Navarin Ridge and bounded to the southwest by the steep continental slope that reaches declivities of greater than 15°. Adjacent to St. Matthew Canyon is a large broad ridge about 30 km **long** and 20 km wide in water depths between 400 m and 1000 m. Another large linear ridge over 80 km long extends along the 1770 W meridian and separates St. Matthew and Middle Canyons.

Directly to the east of St. Matthew Canyon lies the Middle Canyon system which is very similar to the St. Matthew system, but twice as large (**Carlson** and others, in press). The east and west branches of Middle Canyon are roughly equal in size and each branch has two large and several smaller tributaries. The west branch is the steeper attaining a **thalweg** gradient of 4.1° **compared** to a gradient of 3.2° for the east branch.

Neither the St. Matthew or Middle Canyon systems are incised into the shelf, perhaps due to the moderately well-consolidated nature of the sedimentary rocks and the apparent young age of both canyon systems.

**Zhemchug** Canyon, located in the southeast corner of the Navarin Basin province, is perhaps the most spectacular of all the Navarin margin canyons. With a length of 160 km and a width of 40 km, this canyon has a volume of over 6300 **km<sup>3</sup>**. The upper half of the **Zhemchug** Canyon system is incised deeply into the continental shelf between Navarin Ridge and **Pribilof** Ridge. The main **thalweg** of this giant canyon cuts deeply through the structural high formed at the shelf break by **Pribilof** Ridge and debouches onto the continental rise at a depth of about 2600 m. The axial gradient of this canyon is about 2° and the gradient of the fan channel is 1°. Numerous **small** tributaries run into the main canyon and numerous small slumps occur on its sides. A long ridge, total length of 130 km separates **Zhemchug** and Middle canyons. This ridge has a maximum relief of about 1200 m (1800-3200 m), and extends from the shelf edge across the slope and intersects the rise.

The continental rise begins at the 2800 m isobath at the base of the slope and continues beyond the 3600 m isobath, the limit of our bathymetric data. The rise varies in width from 25 km to 100 km and gradient from 0.5° to 1.8°. Many deep-sea channels dissect the rise and all five of the previously mentioned canyon systems have well developed channels that extend across the continental rise. Cores taken in and near these channels contain sand lenses and graded sand beds suggesting turbidity current deposition (**Carlson** and others, 1981b).

REFERENCES CITED

- Baranov**, A. N., and others, **eds.** , 1967, **The World Atlas:** Chief Administration of Geodesy and Cartography, under the Council of Ministers of the U.S.S.R., 2nd cd., **Moscow**, 250 p. (English edition).
- Carlson, P. R., Karl, H. A., Johnson, K. A., and Fischer, J. M., 1981, Submarine canyons flanking Navarin Basin, Bering Sea, in U. S. Geological Survey in Alaska: Accomplishments during 1980: U. S. Geological Survey Circular 844, p. 139-141.
- Carlson**, P. R., Fischer, J. M., and Karl, H. A., in press, Two newly discovered submarine canyons on the Alaskan Continental Margin of the Bering Sea: U. S. Geological Survey Open-File Report 82-
- Cooper, A. K., **Marlow**, M. S., Parker, A. W., and **Childs**, J. R., 1981, Structure contour map on acoustic basement in the Bering Sea: U. S. Geological Survey Miscellaneous Field Studies **Map MF-1165**.
- Karl, H. A. and **Carlson**, P. R., 1982, Location and description of sediment samples: Navarin Basin province, Bering Sea, 1980-81: U. S. Geological Survey **Open-File** Report 82-958, 5 p., 2 map sheets **scale 1:1,000,000**.
- Lisitsyn, A. P., 1966, Recent sedimentation in the Bering Sea: Akad. Nauk SSR Inst. **Okean., Moskva**, (Israel Program for Sci. Translations, 1969; U. S. Dept. of Commerce, Clearinghouse for Federal **Sci. Tech. Info.**, Springfield, va, 614p.).
- Marlow**, M. S., Scholl, D. W., Cooper, A. K., and Buffington, E. C., 1976, Structure and evolution of Bering Sea shelf south of St. Lawrence Island: American Association Petroleum Geologist **Bull.**, v. 60, p" 161-183.
- Marlow**, M. S., Cooper, A. K., Scholl, D. W., **Vallier**, T. L., and **McLean**, H., 1979, Description of dredge samples from the Bering Sea continental margin: U. S. Geological Survey **Open-File** Report 79-1139, 5 p.
- Marlow**, M. S., Carlson, P. R., Cooper, A. K., Karl, H. A., **McLean**, H., **McMullin**, R., and Lynch, M. B., 1981, Resource Report for proposed OCS sale number 83 Navarin Basin, Alaska: U. S. Geological Survey Open-File Report 81-152, 82 p.
- Marlow, M. S., Cooper A. K., Parker, A. W., and **Childs**, J. R., 1981, **Isopach** map of strata above acoustic basement in the Bering Sea: u. s. Geological Survey Miscellaneous Field Studies Map **MF-1164**.
- Patton, W. W., Lanphere, M. **A.**, Miller, T. P., and Scott, R. A., 1976, Age and tectonic significance of volcanic rocks on St. Matthew Island, Bering Sea, Alaska: U. S. Geological Survey, Journal of Research, v. 4, p. 67-73.
- Pratt, R., and Walton, F., 1974, Bathymetric Map of the Bering Shelf: Geological Society of America, Inc., Boulder, **Colo.**
- Shepard, F. P. , 1963, Submarine geology, 2nd cd.: Harper and Row, New York, 557 p.
- Scholl, D. W., Buffington, E. C. and Hopkins, D. M., 1968, Geologic history of the continental margin of North America in the Bering Sea: Marine Geology, v. 6, p. 297-330.
- Scholl, D. W., Alpha, T. R., **Marlow**, M. S., and Buffington, E. C., 1974, Base map of the Aleutian-Bering Sea region: U. S. Geological Survey Miscellaneous Investigation Series **Map I-879**, scale **1:2,500,000**.

Scholl, D. W., Buffington, E. c., and Marlow, M. s., 1975, Plate tectonics and the structural evolution of the Aleutian Bering Sea region, in Forbes, R. v., cd., Contributions to the geology of the Bering Sea Basin and adjacent regions: Geological Society of America Special Paper 151, p" 1-32.

Schumacher, G. M., 1976, Bathymetric map of the Aleutian Trench and Bering Sea: U. S. Geological Survey Open-File Map 76-821, scale 1:2,500,000.

APPENDIX E:

TWO NEWLY DISCOVERED SUBMARINE CANYONS  
ON ALASKAN CONTINENTAL MARGIN OF BERING SEA

by

Paul R. **Carlson**, Jeffrey M. Fischer, and Herman A. Karl

U.S. Geological Survey

Two Newly Discovered Submarine Canyons, on Alaskan Continental  
Margin of Bering Sea

by

Paul R. Carlson, Jeffrey M. Fischer, and Herman A. Karl

INTRODUCTION

The search for new energy resources by the U. S. Geological Survey has focused increasing attention on the Alaskan continental margin in the Bering Sea, sometimes called the Beringian margin. Although there has been emphasis on the Aleutian Islands and the Bering Strait, partly due to their strategic locations, there has been limited oceanographic and geologic coverage of the Beringian margin until the last decade. The bathymetric and geophysical track line coverage across the northern part of the margin was, until 1980, very sparse. However, regional studies by **Marlow** and others (1976; in press) and Scholl and others (1976), resulted in the discovery of large basins filled with thick sequences of sedimentary material of Cenozoic and perhaps **Mesozoic** age. These thick sedimentary sequences have become **the** targets of several petroleum lease sales planned for the next few years. In preparation for the scheduled sales, we collected the first publicly available, detailed, bathymetric and high-resolution geophysical data over the northern Beringian margin in the summer of 1980 (**Carlson** and Karl, 1981). From these data, we developed a better understanding of the margin, and in particular the three large submarine canyons, **Navarinsky**, **Pervenets**, and **Zhemchug** Canyons (Plate 1 and **Carlson** and others, 1981). The data collected in 1980 also suggested the presence of another moderate-size canyon between **Pervenets** and **Zhemchug** Canyons. A second cruise, conducted in 1981 (**Carlson** and Karl, 1982) provided additional data on the northern Beringian margin that showed two canyon systems to be present between **Pervenets** and **Zhemchug** Canyons (Fischer and others, 1982).

The purpose of this paper is to describe, delineate and compare these newly-discovered submarine canyons. Included in the report are a detailed bathymetric map of the two canyon systems and sketches of seismic profiles showing the canyons and the **subbottom** units into which they were carved. We also speculate briefly on the mode and time of formation of these canyons.

Data Collection

Data used to develop "**smooth sheets**" are taken primarily from 3.5 kHz transducer records complimented by simultaneously collected airgun seismic profiles collected in 1980 and 1981 (**Carlson** and Karl, 1981, 1982). These data *are* supplemented by depth data from several other cruises (**Marlow** and Cooper, 1979, 1980; Scholl, Buffington, and **Marlow**, 1976; Scholl and **Marlow**, 1970). Navigational control was obtained from Loran C updated with satellite positions. Water depths for the Navarin study area were digitized assuming 1500 km/sec for speed of sound in water. Records were corrected for the **hull-**depth of transponder systems but no other corrections were made of the depth data.

## MORPHOLOGY OF THE BERINGIAN CONTINENTAL MARGIN

Three **physiographic** provinces make up the Beringian continental margin. These are the flat, wide, continental shelf, the steep, rugged continental slope, and the gently sloping continental rise that extends from the base of the slope to the 3600-m isobath. Large submarine canyons deeply dissect the **outer** shelf and slope. Coalescing fans at the mouths of these canyons form part of the wedge of sediment of the continental rise. The continental shelf, one of the widest and flattest in the world, is about 450 km wide and has a gradient of  $0.02^\circ$  seaward of the Yukon River delta. By comparison, Shepard (1963) reported a world-wide average continental-shelf gradient of  $0.12''$ . The continental slope begins at about the 150-m isobath and extends to a depth of about 2800 m. The width of the continental slope is about 50 km. The gradients of the Navarin slope range from  $3^\circ$  to  $8^\circ$  and even steeper gradients exist locally (Fischer and others, 1982). These slopes compare fairly well with the world-wide average gradient for continental slopes of about  $4.3^\circ$  (Shepard, 1963). The continental rise begins at the base of the slope at a depth of about 2800 m and extends to the 3600-m isobath that appears to mark the beginning of the **abyssal** plain. The average width of the rise is about 75 **km** and the gradients across the rise range from  $0.5''$  to  $1.8^\circ$  (Fischer and others, 1982). Deep-sea channels cross the rise in the area of the canyon mouths and apparently are connected to the submarine canyons.

### Descriptions of Newly Discovered Canyons

The Beringian continental slope between the Aleutian Island chain to the southeast and Cape **Navarin**, U.S.S.R. to the northwest, is dissected by seven large submarine canyon systems. They are from north to south Navarinsky, Pervenets, St. Matthew, Middle, **Zhemchug**, **Pribilof** and Bering Canyons. Five of these canyons have been known for at least 17 years (**Kotenev**, 1965). The names of St. Matthew and Middle canyons are proposed for the two canyons that have just been discovered.

The name St. **Matthew** Canyon is taken from St. Matthew Island located about 300 km northeast of the canyon head. Middle Canyon is the name proposed for the other canyon system for two reasons: (1) it is the middle-most canyon of the seven large slope canyons and (2) it is located at a midway point on the continental slope between the Aleutian Islands to the southeast and the U.S.S.R., to the northwest.

#### A. St. Matthew Canyon system

This complex dendritic canyon system, consisting of two main branches, heads near the shelf break in about 140 m of water (Plate 1). **The west thalweg trends southeast obliquely across the continental slope for about 65 km** where it bends to the south and continues another **12 km** where the canyon debouches onto a deep-sea fan at a depth of 3200 m. St. Matthew Canyon west has an average **thalweg** gradient of  $2.5^\circ$  and reaches a gradient of  $3.3''$  over the steepest part of the canyon (Fig. E1; Table E1). Below 3200 m, as the canyon morphology changes to that of a deep-sea fan channel, the gradient changes to  $0.4^\circ$  and the channel extends at least another 55 km across the fan. Selected cross-canyon profiles show a V-shaped canyon that has **maximum**

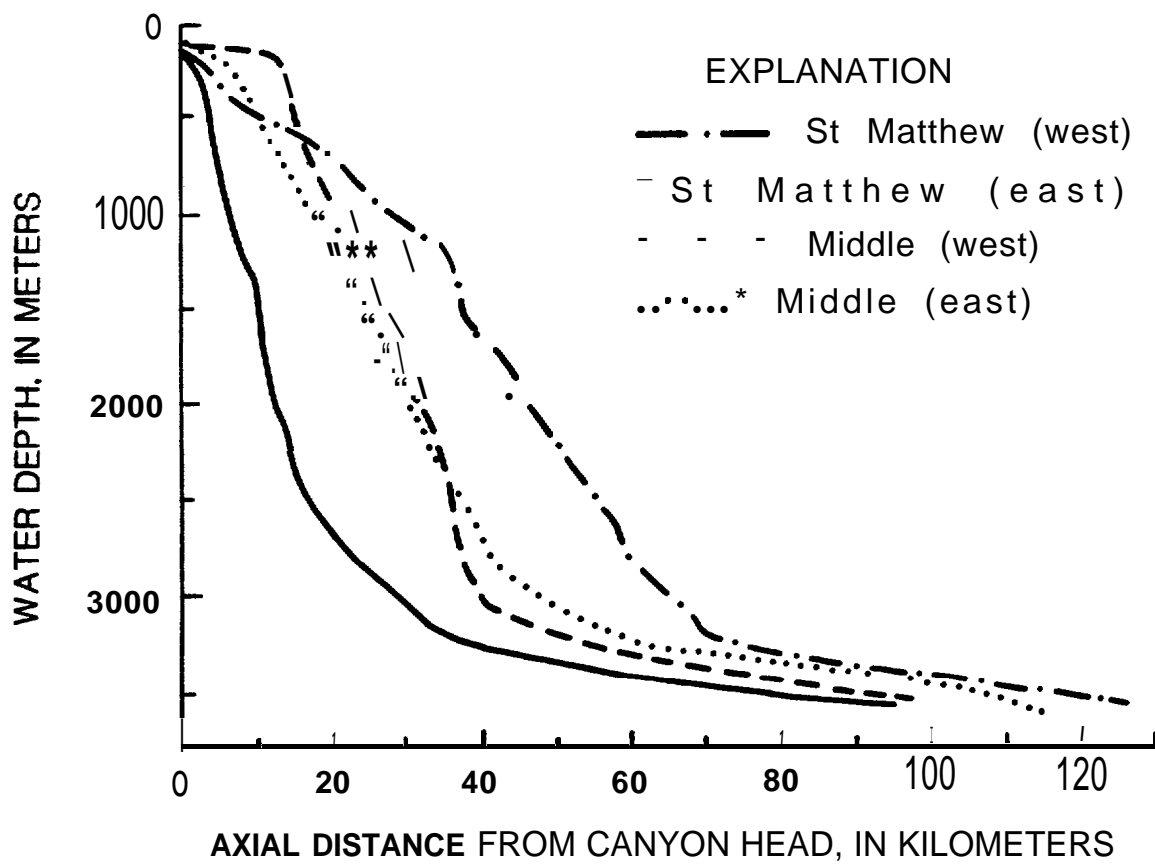


Figure E1. Thalweg profiles of main branches of St. Matthew and Middle Canyons.

Table E1. Principal Canyons and Fan Channels of the St. Matthew and Middle Systems

<u>Canvon</u>	<u>Length(km)</u>	<u>Head(m)</u>	<u>Mouth(m)</u>	<u>Gradient</u>	<u>Steepest Gradient</u>
<u>St. Matthew</u>					
West Branch	<b>70</b>	<b>150</b>	3000	2.5°	<b>3.3°</b>
East Branch	<b>34</b>	<b>150</b>	3000	<b>5.1°</b>	7.60
<u>Middle</u>					
West Branch	40	130	3000	<b>4.1°</b>	<b>6.4°</b>
East Branch	60	140	3200	<b>2.90</b>	<b>4.3°</b>
<u>Fan Channel</u>					
<u>St. Matthew</u>					
West Branch	<b>55</b>	<b>3200</b>	3600*	<b>0.4°</b>	
East Branch	<b>64</b>	<b>3200</b>	3600*	<b>0.4°</b>	
<u>Middle</u>					
West Branch	<b>67</b>	<b>3000</b>	3600*	<b>0.5°</b>	
East Branch	<b>60</b>	<b>3200</b>	3600*	<b>0.4°</b>	

\* Marks extent of deepest contour; channel extends further onto fan. see Figure E3 for location of canyon systems.

relief of 2200 m on the northeast wall and 1250 m on the southwest wall (Fig. E2). The walls of the canyon have average declivities of  $8.1^\circ$ , ranging from as steep as  $16^\circ$  (profile G-H, northeast wall) to as gentle as  $2^\circ$  (profile O-P, east wall; Table E2a). The western branch of St. Matthew Canyon has at least nine tributaries (Fig. E3) that average 23 km in length and  $5.2^\circ$  in gradient, ranging in length from 6 to 42 km and in gradient from  $8.5^\circ$  to  $2.9^\circ$  (Table E3a).

The eastern branch of the St. Matthew Canyon system begins at a water depth of about 150 m and trends south-southwest for a distance of about 34 km where the canyon discharges onto a deep-sea fan at 3000 m (Plate 1). The average axial gradient of the eastern branch is about  $5^\circ$  and reaches a gradient of  $7.6^\circ$  over the steepest part of the canyon (Fig. E1; Table E1). The deep-sea channel that extends from the east branch canyon about 64 km across the fan to the 3600 m isobath, has a gradient of  $0.4^\circ$ . The eastern and western branches of the St. Matthew Canyon system merge on the fan at a depth of about 3600 m.

Selected cross-canyon profiles of the eastern branch of St. Matthew Canyon are much less v-shaped than those of the west branch and show maximum wall relief of 1100 m (Fig. E2b; Table E2b). The walls have average declivities of  $8.2^\circ$ , ranging from as steep as  $16.7^\circ$  (profile C-D, west wall) to as gentle as  $1.1^\circ$  (profile I-J, west wall). The east branch of St. Matthew Canyon has three good-sized tributaries that range in length from 26.5 to 30 km and in axial gradient from 2.3 to  $4.8^\circ$  (Table E3b).

#### B. Middle Canyon system

This complex canyon system consisting of two main branches and numerous tributaries (Plate 1), has a dendritic pattern similar to the St. Matthew system, but has approximately twice the areal extent. (St. Matthew =  $3290 \text{ km}^2$  and Middle Canyon =  $6620 \text{ km}^2$ ). The west branch of Middle Canyon, has cut a shallow valley about 20 km into the shelf. The west branch heads in 130 m of water and trends southerly across the slope about 40 km where it debouches onto a deep-sea fan at a water depth of 3000 m. The average thalweg gradient of the west branch of Middle Canyon is  $4.1^\circ$  and this thalweg attains a gradient of  $6.4^\circ$  over the steepest part of the canyon (Fig. E1; Table E1). The contiguous deep-sea fan channel extends at least 67 km across the fan at a gradient of  $0.5^\circ$ . Selected cross-canyon profiles are V-shaped on the slope and open up dramatically to broad channels (12-20 km wide) on the deep-sea fan (Fig. E4a). The canyon has a maximum relief of 1100 m on the west wall and 650 m on the east wall (Table E4a). The walls of the west branch canyon attain an apparent maximum steepness of  $20.6^\circ$  (east wall, profile C-D, Fig. E4a; Table E4a) and as low a gradient as  $1.6^\circ$  on the fan channel east wall (profile K-L). The walls have an average slope of  $9.3^\circ$ . The west branch of Middle Canyon has seven tributaries that join the canyon above a depth of 3200 m and four that merge with the fan channel between 3200 and 3600 m (Fig. E3). The longest of these eleven valleys measures 79 km (32 km above 3000 m) and the shortest is about 6 km in length (Table E5a). The gradients range from  $11.3^\circ$  for a slope tributary to  $0.8^\circ$  for a fan valley.

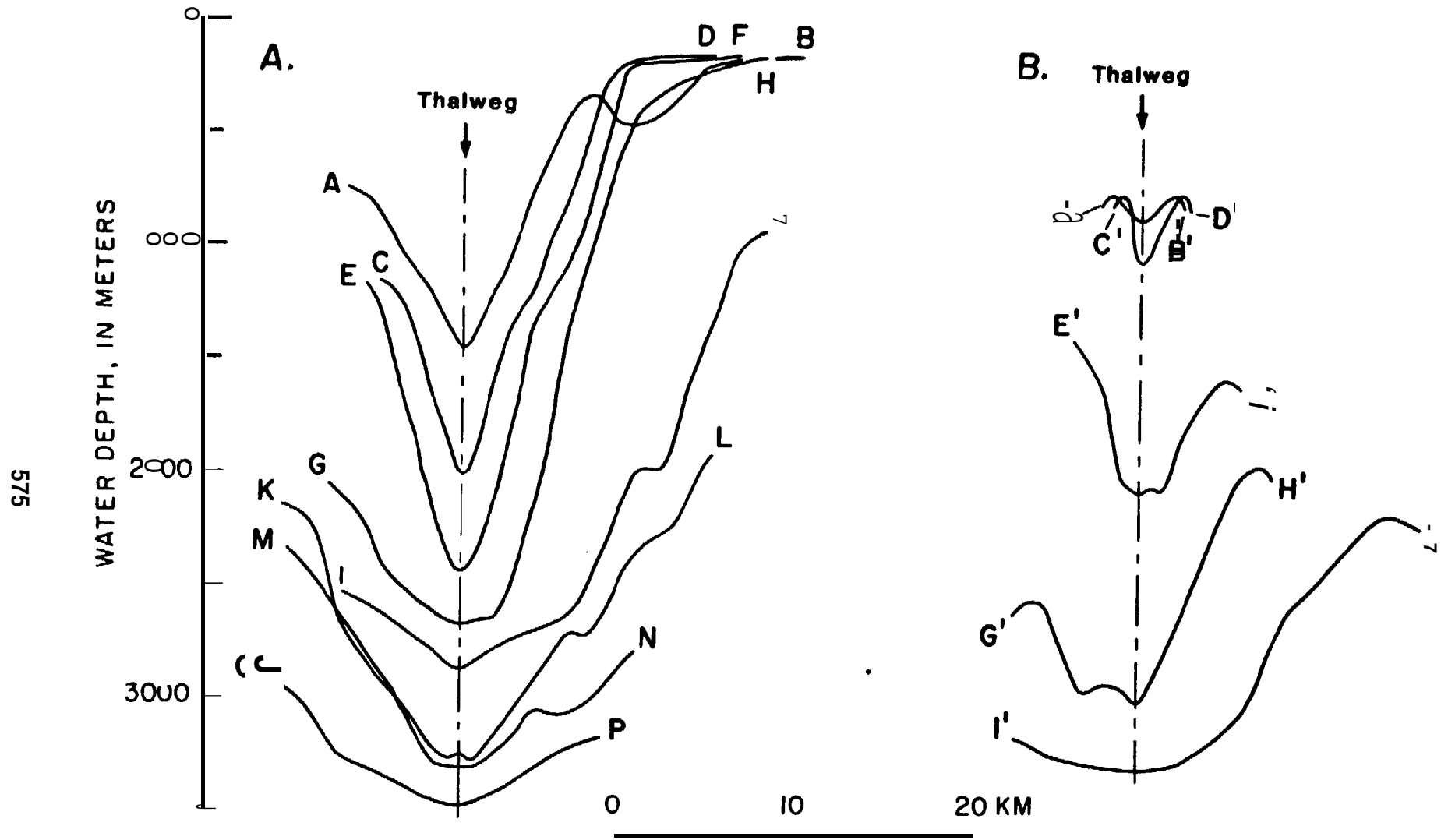


Figure E2. Transverse profiles of west (a) and east (b) branches of St. Matthew Canyon (see Fig. E3 for traverse locations).

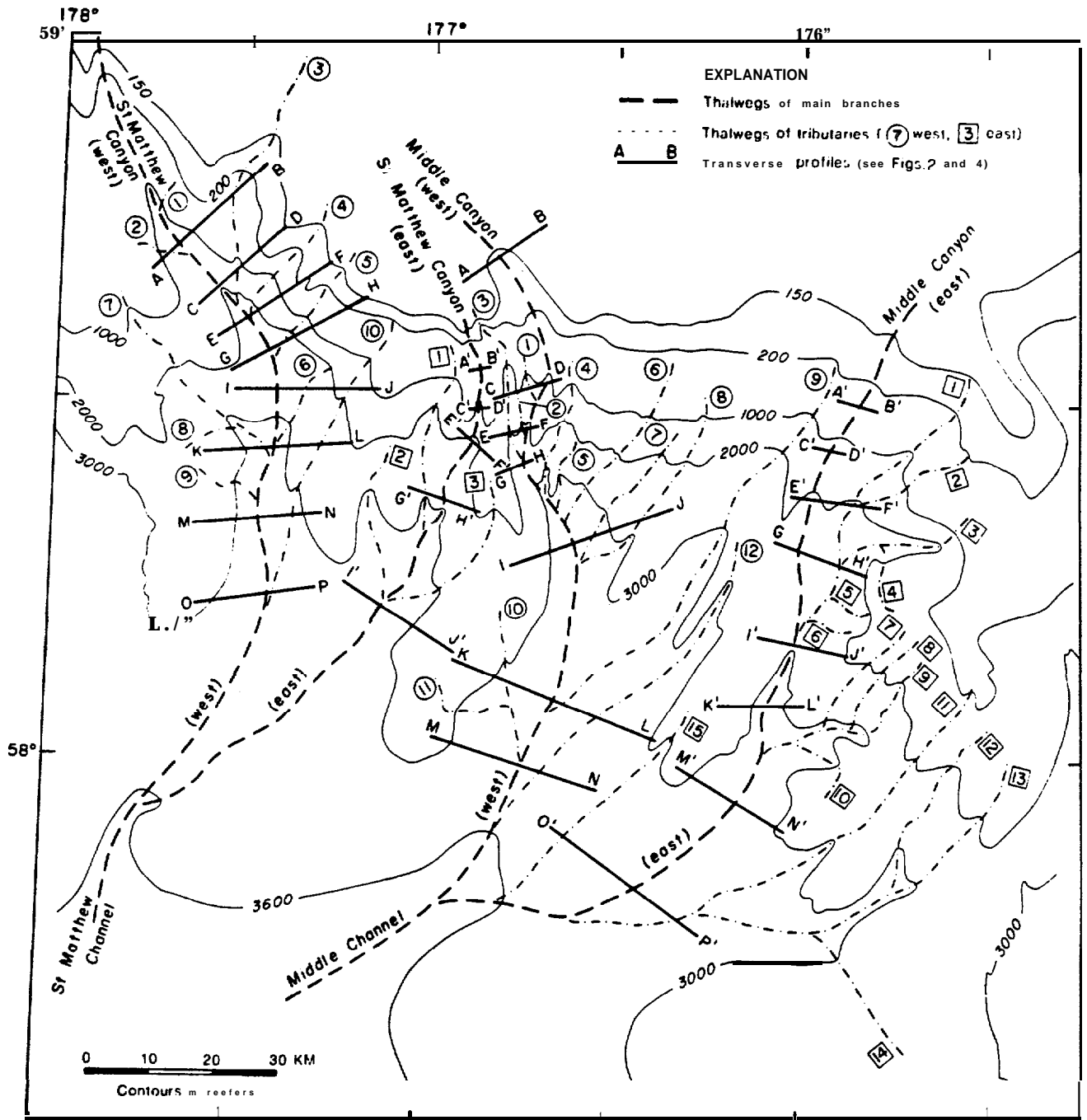


Figure E3. Map of St. Matthew and Middle Canyon systems, showing thalwegs of main branches and tributaries and locations of transverse profiles illustrated in Figures E2 and E4.

Table ~~West Branch, St. Matthew Canyon~~ wall gradients

<u>Section*</u>	<u>Length(km)</u>	<u>Relief (m)</u>	<u>Gradient</u>
A	5.1	650	7.3°
B	6.0	1050	10.0°
C	4.0	800	11.3°
D	8.2	1800	12.4°
E	5.0	1250	14.1°
F	8.3	2200	14.8°
G	7.6	400	3.0°
H	7.6	2200	16.1°
I	6.7	340	2.9°
J	9*5	1600	9.6°
K	7.0	1025	8.3°
L	12.3	1300	6.0°
M	8.0	800	5.7°
N	9.5	550	3*3°
O	9.0	450	2.9°
P	8.0	300	2.2°

Table E2b. East Branch, St. Matthew Canyon wall gradients

<u>Section*</u>	<u>Length(km)</u>	<u>Relief(m)</u>	<u>Gradient</u>
A'	1.5	100	3.80
B'	1.5	100	3.8°
C'	1	300	16.7°
D'	2	300	8.5°
E'	3	650	12.2°
F'	3	500	9.5°
G'	2	400	11.3°
H'	5.5	1000	10.3°
I'	6.5	125	1.1°
J'	12	1100	5.2°

\*Side of transverse profile from top of wall to thalweg of canyon.  
(see Fig. E3 for profile locations).

Table E3a. Tributaries of the **west** branch of St. Matthew Canyon system

<u>West branch Tributaries</u>	<u>Length(km)</u>	<u>Head(m)</u>	<u>Mouth (m)</u>	<u>Gradient</u>
1	6	200	<b>1100</b>	8.5°
2	8	800	<b>1500</b>	<b>5.0"</b>
3	42	140	<b>2300</b>	<b>2.9°</b>
4	22	<b>140</b>	<b>2500</b>	<b>6.1°</b>
5	20	140	<b>2700</b>	<b>7.3"</b>
6	16	2000	<b>3200</b>	<b>4.3"</b>
7	34	750	<b>3200</b>	<b>4.1°</b>
8	13	2200	<b>3300</b>	<b>4.8°</b>
9	14	2200	<b>3350</b>	<b>4*7"</b>
10	48	200	<b>3500</b>	<b>3.9°</b>
avg.	23.2			<b>5.2°</b>

<u>Fan Channel</u>	<u>Length(km)</u>	<u>Head(m)</u>	<u>Mouth(m)</u>	<u>Gradient</u>
8	3	3200	3300	<b>1.9°</b>
9	8	3200	3500	<b>2.1°</b>

Table E3b. Tributaries of the east branch of St. Matthew Canyon **system**

<u>East branch Tributaries*</u>	<u>Length(km)</u>	<u>Head(m)</u>	<u>Mouth ( m)</u>	<u>Gradient</u>
1	29	600	3050	4.8o
2	26.5	2200	3250	2.3°
3	30	1600	3250	3.2°
avg.	<b>28.5</b>			<b>3.4°</b>

\*See Figure E3 for locations of tributaries.

Table E4a. Wall gradients of the west branch of Middle Canyon

<u>Section*</u>	<u>Length(km)</u>	<u>Relief(m)</u>	<u>Gradient</u>
A	2	500	14.0"
<b>B</b>	2	500	14.0"
c	3	500	9.5"
D	1.2	450	20.6°
E	4	1100	<b>15.4°</b>
F	2	500	<b>14.0°</b>
G	6	850	8.1°
H	14	650	<b>2.7°</b>
I	8	1050	<b>7.5°</b>
J	16	450	<b>1.6°</b>
K	<b>13</b>	650	<b>2.90</b>
L	10	300	<b>1.7°</b>
M	14.5	725	<b>2.9°</b>
N	12	350	<b>1.7°</b>

Table E4b. Wall gradients of the east branch of Middle Canyon

A'	<b>3</b>	<b>125</b>	<b>2.4°</b>
B'	5	<b>125</b>	<b>2.0°</b>
c'	2.5	<b>125</b>	<b>2.9"</b>
D'	3.5	<b>125</b>	<b>2.0°</b>
E'	3.5	<b>150</b>	<b>2.50</b>
F'	3	<b>125</b>	<b>2.40</b>
G'	3	<b>450</b>	<b>8.5°</b>
H'	2	<b>725</b>	19*9"
I'	4.5	<b>450</b>	5*70
J'	7	<b>850</b>	<b>6.9°</b>
K'	5.5	<b>700</b>	<b>7.3°</b>
L'	6	<b>450</b>	4.3"
M'	10	<b>500</b>	2.90
N'	<b>7.5</b>	<b>300</b>	2.30
O''	<b>3*5</b>	<b>125</b>	<b>2.0°</b>
P'	<b>6.0</b>	<b>125</b>	<b>1.2°</b>

\* Side of transverse profile from top of wall to **thalweg** of canyon.  
 (See Fig. E3 for profile locations).

Table E5a. Tributaries of the west branch of Middle Canyon.

<u>Tributaries*</u>	<u>Length</u>	<u>(Length to 300 m)</u>	<u>H e a d ( Mouth)(m)</u>		<u>Gradient</u>
1	6		800	1700	8.5°
2	6		1100	2300	11.3*
3	26		140	2650	5.5°
4	22		600	3025	6.3*
5	12		2200	3100	4.3 (7.60)
6	33 (26)		200	3100	5.0 (6.2*)
7	26 (16)		1400	3200	4.0 (5.7°)
8	36 (26)		600	3200	4.1 (5.3°)
9	79 (32)		200	3425	2.3 (5.0°)
10	26 ( 9)		2200	34±0	2.8 (5.1°)
11	17 ( 8)		2400	3400	3.4 (4.3°)
12	58 ( 4)		2800	3575	0.8 (2.9 <sup>ε</sup> )
avg.	29				4.9°

<u>Fan Channels*</u>	<u>Length(km)</u>	<u>H e a d ( Mouth)(m)</u>		<u>Gradient</u>
5	6	3000	3100	1.0°
6	7	3000	3100	0.8°
7	10	3000	3200	1.1*
8	10	3000	3200	1.1°
9	47	3000	3425	0.5"
10	17	3000	34±0	1.54
11	9	3000	3400	2.5"
12	54	3000	3575	0.6*
avg.	15*1			1.2°

Table E5b. Tributaries of the east branch of Middle Canyon

<u>Tributaries*</u>	<u>Length (length km to 3000 m)</u>	<u>Head(m)</u>	<u>Mouth(m)</u>	<u>Gradient</u>
1	52	150	2900	3.2*
2	22	200	2100	4.9°
3	24	600	2700	5.0°
4	11	1400	2300	4.79
5	8	2000	2850	6.1°
6	7	2400	2900	4.19
7	23	1200	3050	4.6°
8	19	1200	3025	5.50
9	32 (28)	1400	3225	3.3° (3.7°)
10	12.5	2700	3200	2.3*
11	77 (37)	1000	3450	2.5° (3.4°)
12	31	1200	3200	3.7°
13	84 (30)	1200	3475	1.6° (3.8°)
14	23 (19)	2000	3225	3.1° (3.6°)
15	40 (17)	2800	3600	1.2° (1.4°)
ave.	31			3.7°

<u>Fan Channels</u>	<u>Length(h)</u>	<u>Head(m)</u>	<u>Mouth(m)</u>	<u>Gradient</u>
9	4	3200	3225	0.4°
11	40	3200	3450	0.4°
13	54	3200	3475	0.3°
14	4	3200	3225	0.4°
15	23	3200	3600	1.0°
avg.	25			0.5°

\* See Figure E3 for location of tributaries and fan channels. ;

The east branch of the Middle Canyon system is about the same size as the west branch and also has a complex **dendritic** "drainage" (Plate 1). The east branch begins at a water depth of **140 m** and winds across the slope in a **south-southeasterly** direction for 60 km where **it debouches** onto a deep-sea fan at a depth of 3200 m. The east branch of Middle Canyon has an average axial gradient of  $2.9^\circ$  and reaches a gradient of at **least**  $4.3^\circ$  in the steepest part of the canyon (Fig. E1; Table E1). At 3200 m the axial gradient becomes greatly reduced resulting in an **average gradient of  $0.4^\circ$  for the 60 km** of channel to a depth of 3600 m. The east branch merges with the west branch of Middle Canyon at a depth of about 3600 m.

Transverse profiles of the east branch of Middle Canyon are less V-shaped than those of the west branch, coming closer in profile to the east branch of the St. Matthew Canyon system (compare Figs. E2b and E4b). The walls of the east branch of Middle Canyon show maximum relief of 850 m and range in steepness from  $19.9^\circ$  (profile C-D, east wall) to  $1.2^\circ$  (profile I-J, southeast wall of fan channel). The walls have an average **slope** of  $6.5^\circ$  (Table E4b). The east branch of Middle Canyon has six tributaries that join the main **thalweg** at about 3000 m and nine that join the east branch deep-sea channel between 3200 and 3600 m (Fig. E3). These tributaries have an average length of about 30 km and an average gradient of  $3.7^\circ$  (Table E5b). The six canyon tributaries range in length from 7 to 35 km and in gradient from  $4.1^\circ$  to  $6.1^\circ$ . The nine tributaries, that join the east **branch** of Middle Canyon below 3200 m, range in length from 12.5 to 84 km and in gradient from  $1.2^\circ$  to  **$5.5^\circ$**  (Table E5b). The gradients of these tributary valleys across the upper part of the deep-sea fan vary from  $0.3^\circ$  to  $1.0^\circ$ .

#### GEOPHYSICAL PROFILES AND SEAFLOOR SAMPLES

Several seismic reflection profiles (sound source: 2 - 40 in<sup>3</sup> **airguns**) were shot across the newly-discovered canyon systems (**Carlson** and Karl, 1981, 1982). Rocks were dredged from the walls of the two canyons (Jones and others, 1981; **Marlow**, pers. **commun.**, 1982) and a total of 17 gravity cores (8.0 cm diameter) were collected from the two canyons and adjacent fans, six from the St. Matthew Canyon system and eleven from the Middle Canyon system (Karl and Carlson, 1982). **Locations** of these airgun profiles, dredges and gravity **cores** are shown in Figure #5.

Seismic-reflection profiles across both the St. Matthew and Middle Canyon systems show V-shaped gorges cut in layered sedimentary rocks. The reflectors that characterize the layered sedimentary sequences **are** sharply truncated at the canyon walls (Fig. #6). **Hummocky**, broken reflectors are present on some of the canyon walls and in some parts of the floor (Fig. 7).

A **diapir-like** feature has been found near the shelf-break adjacent to the southwest wall of St. Matthew Canyon (Fig. E8). A magnetometer record collected across this feature shows a 100 m gal **anomaly**, suggesting that the feature could be related to **some type** of igneous intrusive. The effect of this **diapir-like** mass on the overlying 200+ meters of sedimentary material is a slight amount of doming of the strata. This diapiric feature does not appear to have had a noticeable effect on the west branch of St. Matthew Canyon.

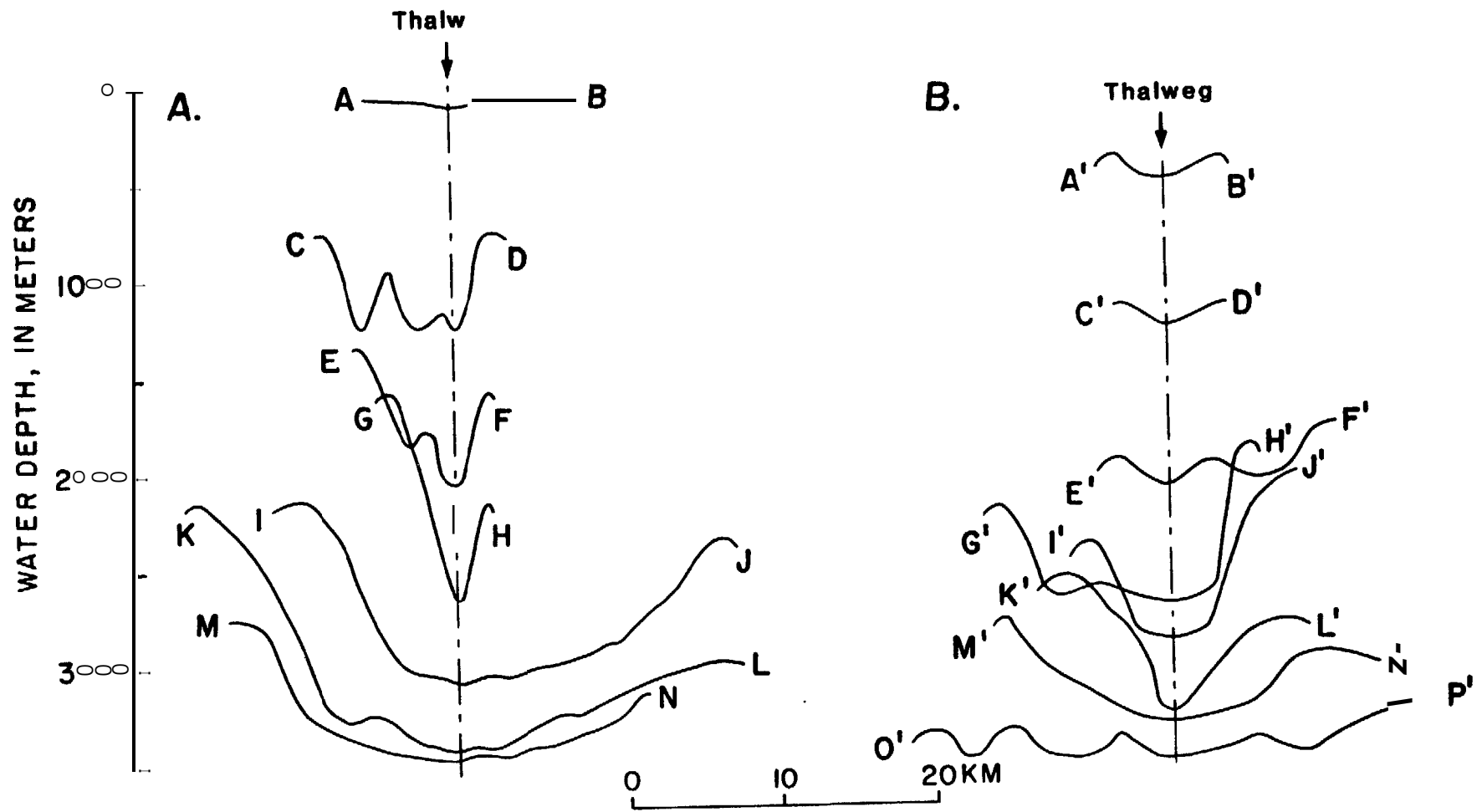


Figure E4. Transverse profiles of west (a) and east (b) branches of Middle Canyon (see Fig. E3 for transverse profiles).

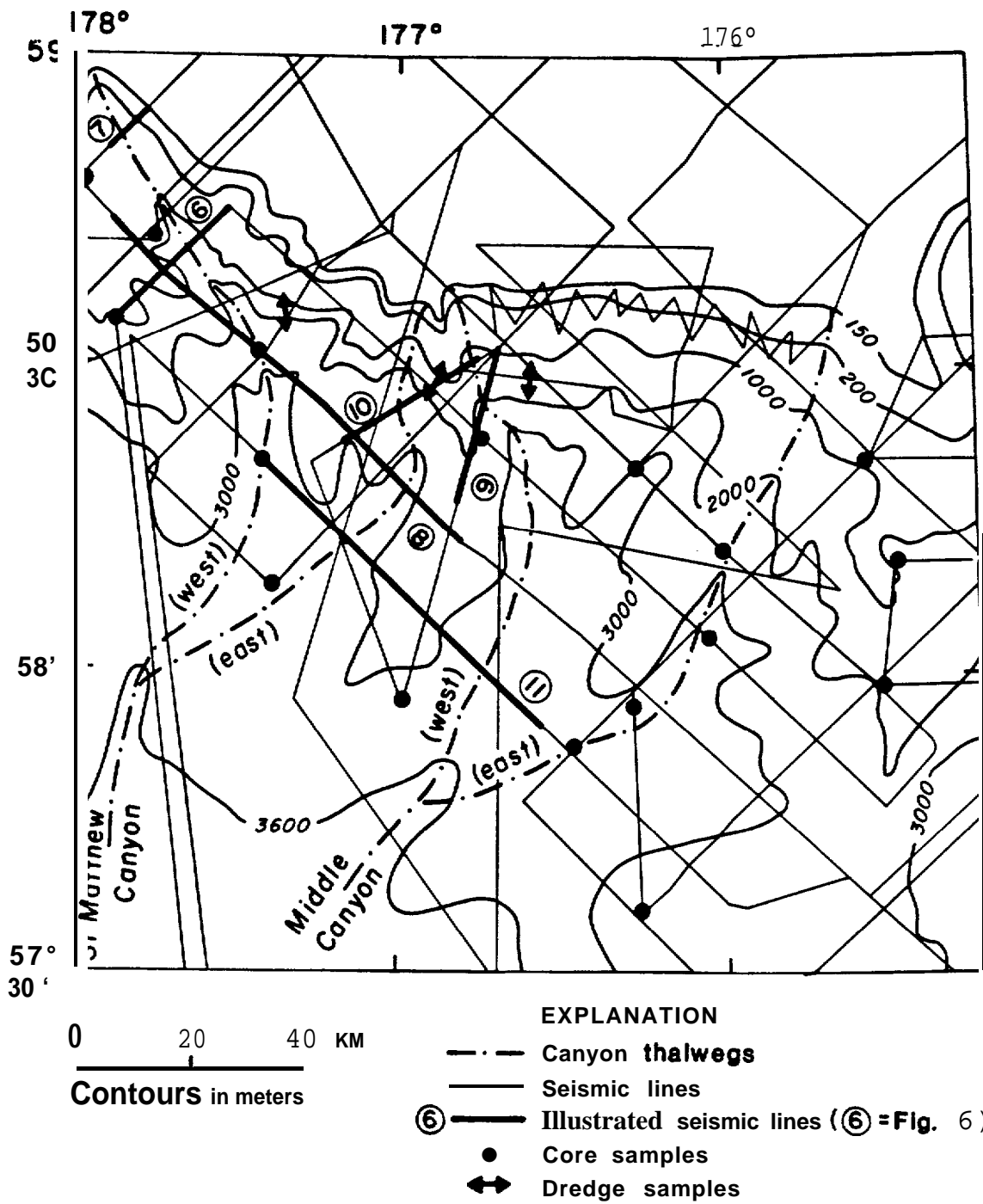


Figure E5. Map showing locations of core and dredge samples and seismic profiles, including illustrated line drawings.

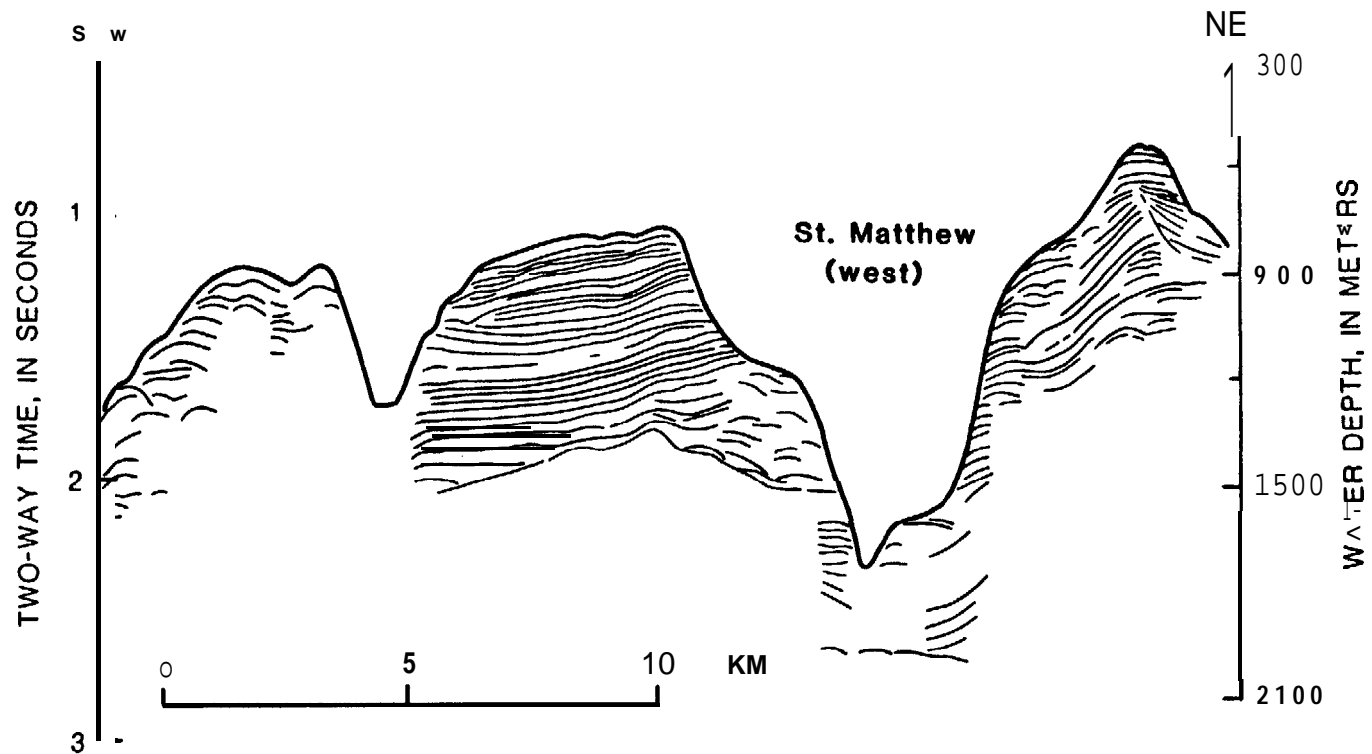


Figure E6. Interpretive line drawing of air-gun profile across west branch of St. Matthew Canyon (see Fig. ES for location); Vertical exaggeration (V.E.)  $\sim$ x7.

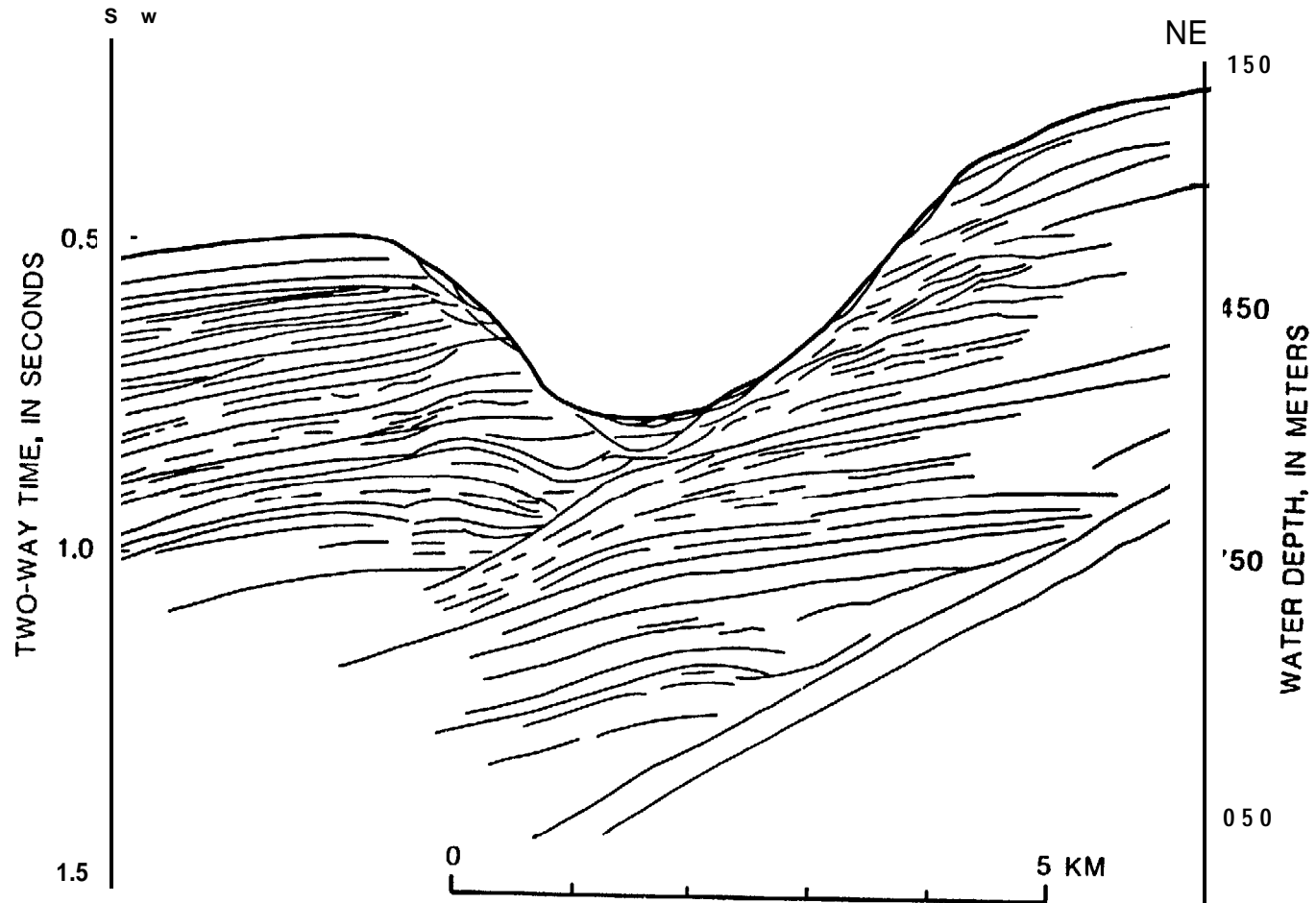


Figure E7. Interpretive line drawing of air-gun profile across west branch - of St. Matthew Canyon (see Fig. E5 for location) (V.E. 'x7).

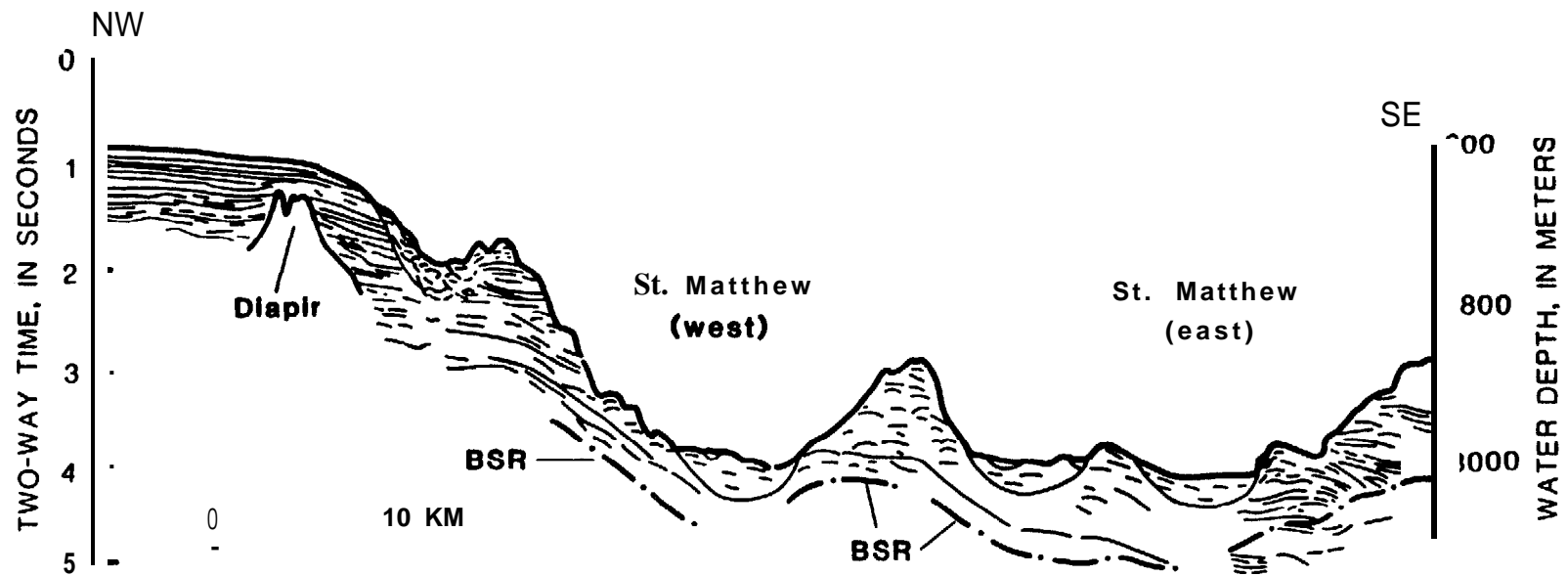


Figure E8. Interpretive line drawing of air-gun profile across west branch of St. Matthew Canyon (see Fig. E5 for location) (V.E. 'x7).

Several of the airgun profiles that were shot across the east and west branches of St. Matthew and the west branch of Middle Canyon (Fig. E9) show walls devoid of reflectors. In Middle Canyon, the opposite wall shows **well-**developed reflectors truncated by the canyon (Fig. #9). A dredge haul from the **reflectorless** wall of the east branch of St. Matthew Canyon (Fig. 10) yielded several pieces of basalt, one of which was dated by K-Ar methods to be at least as old as Eocene (Jones and others, 1981). A recent cruise of the R/V **S.P. LEE** (L-9-82] produced a dredge haul from the northeastern wall of the west branch of St. Matthew Canyon that yielded several igneous rocks ranging in type from basalt to **dacite** (M. Marlow, pers. **commun.**, 1982). Other **basalts** and some tuffs were dredged from other areas on the Beringian margin (Jones and others, 1981).

Burrowed, moderately indurated mudstones dredged from the wall of the west branch of Middle Canyon, that contains well-bedded reflectors, were dated as Eocene using **silicoflagellates** and **foraminifers** (Jones and others, 1981). Other sedimentary rocks, principally burrowed mudstones and a few sandstones, dredged from the **Beringian** margin have ranged in age from Jurassic to Quaternary (Jones and others, 1981).

Gravity *cores* collected on the walls of the two canyon systems contain sediment that is primarily clayey silt and ranges in age from Pliocene to Holocene (**Baldauf**, 1981). **This** sediment is in many places draped over the older Tertiary **mudstones**.

Air-gun profiles across the fan channels show broad (10-15 km wide), flat valleys at the present seafloor underlain by buried channels that contain as much as 400 m of sedimentary fill (Fig. E11). Some of the deep-sea fan channel walls contain flat-lying reflectors and in other places the walls are characterized by jumbled and broken reflectors and **hummocky** morphology. Gravity cores (3-5 m length) collected from the floor of St. Matthew and other Navarin margin canyons and channels contain occasional thin sand or silt layers interlayered with the diatom-rich, clayey silt that pervades the Navarin margin (**Baldauf**, 1981). Some of these coarse layers are graded and many contain benthic foraminifers that are typically thought to be diagnostic of much shallower water (**Quinterno**, 1981; **Carlson** and others, 1982). Some of the canyon cores also contain sections of pebbly, sandy, mud and disrupted, contorted sediment that is primarily Quaternary in age (**Baldauf**, 1981).

## DISCUSSION

### Similarities in the two canyon systems

St. Matthew and Middle Canyon systems, although smaller than the five large canyons of the **Beringian** margin, are comparable in size to most of the submarine canyons that cut into the continental margin of the east coast of the United States, and are considerably larger than the canyons off southern California (Table E6).

The large Beringian margin canyons are cut back further into the shelf than are the St. Matthew and Middle Canyons and as a result have considerably lower axial gradients (Table E6). The very steep gradient of the east branch

Table E6. Comparison of canyons of the Beringian continental margin with canyons of **the** east and west coasts of the U.S. (Data for east and west coast canyons from **Shepard** and Dill, 1966)

<u>East Coast Canyons</u>	<u>length (km)</u>	<u>gradient</u>
Corsair	<b>26</b>	<b>3*4"</b>
Lydon ia	30	<b>2.3"</b>
Gilbert	37	<b>3.4"</b>
Oceanographer	32	<b>3.6°</b>
Welker	50	<b>2.1°</b>
Hydrographer	50	<b>2.1°</b>
Hudson	92	<b>1.3°</b>
Wilmington	43	<b>2.7°</b>
Baltimore	52	<b>1.9°</b>
Washington	52	<b>2.1°</b>
Norfolk	<b>70</b>	<b>2.0°</b>
<u>West Coast Canyons</u>		
Astoria	115	<b>1.0°</b>
Ee 1	<b>50</b>	<b>2.9°</b>
Monterey	111	<b>1.5°</b>
Mugu	15	<b>2.8°</b>
Dume	5.6	<b>5*50</b>
Redondo	15	<b>2.2°</b>
Scripps	2.7	<b>5*50</b>
La Jolla	14	<b>2.3°</b>
Coronado	15	<b>3.3°</b>
<u>Beringian Margin Canyons</u>		
Navarinsky	<b>270</b>	<b>0.5°</b>
Pervenets	<b>160</b>	<b>1.3°</b>
St. Matthew	<b>70</b>	<b>2.5°</b>
Middle	40	<b>4.1°</b>
Zhemchug	125	0.8°
Pribilof	90	<b>1.2°</b>
Bering	875	<b>0.2°</b>

of St. Matthew Canyon,  $5.1^\circ$  (Table E1), is steeper than most of the submarine canyons reported by Shepard and Dill (1966) and even steeper than the world wide average gradient of continental slopes ( $4.3^\circ$ , Shepard, 1963). The east branch is cut into a slope that has an average gradient of about 60. The west branch of Middle Canyon (**thalweg** gradient  $4.1^\circ$ ) is also steeper than most of the world's submarine canyons. There are other similarities between St. Matthew and Middle Canyons in addition to their size and steepness. The west branch of each canyon makes an oblique traverse across the slope and the west branch of each is more V-shaped than the east branch. The two canyon systems apparently contribute to the build-up of one deep-sea fan; the fan channels appear to merge on the fan beyond the 3600 m isobath (Plate 1).

Both canyons are cut into Tertiary strata that ranges in age from Eocene to Pliocene. The principal rock type is a burrowed, moderately indurated mudstone. In many **places** throughout the Navarin province, this Tertiary mudstone is covered, probably **disconformably**, by several tens of meters of Pleistocene-Holocene unconsolidated sediment.

Sediment from the floor of both St. Matthew and Middle Canyon-fan-channel systems contains fine sand and silt layers interbedded with the normal **diatom-rich** mud. Many of these coarse layers are graded and many contain **benthic** foraminifers that are more typical of shallow water environments, suggesting emplacement by turbidity currents. The young ages of the sediment suggest that some turbidity current activity occurs from time to time even today. Several of the gravity cores also contain pebbly, sandy mud layers and some contain highly contorted, disrupted layers that indicate this material has slumped or slid to its present locality. The submarine sliding that is indicated by these coarse and contorted sediments very likely generates the turbidity currents. Both sliding and turbidity current activity can also be inferred from the seismic-reflection profiles we have obtained from these canyon-fan systems.

#### Differences between the two canyon systems

There are also several differences between the two canyons. Middle Canyon has the larger "drainage" area, has more tributaries, and has longer fan channels, whereas St. Matthew Canyon has the longest and shortest principal canyons.

**Stratigraphically**, the biggest difference between the canyons is the presence of an outcrop of Eocene basalt that forms part of the east wall of the east branch of **St. Matthew Canyon**. Basalt also has been dredged from the west branch of St. Matthew Canyon. In comparison, only sedimentary rocks have been dredged from the walls of Middle Canyon; however, additional dredging may show that the **reflectorless wall** of **Middle Canyon** (Figure E9) also contains basalt outcrops.

#### Genesis of the canyon systems

We subscribe to the hypothesis of Scholl and others (1976), that the large canyons of the Beringian margin were cut when lowered sea level exposed the Bering shelf to a depth of about 150 m and allowed large rivers such as

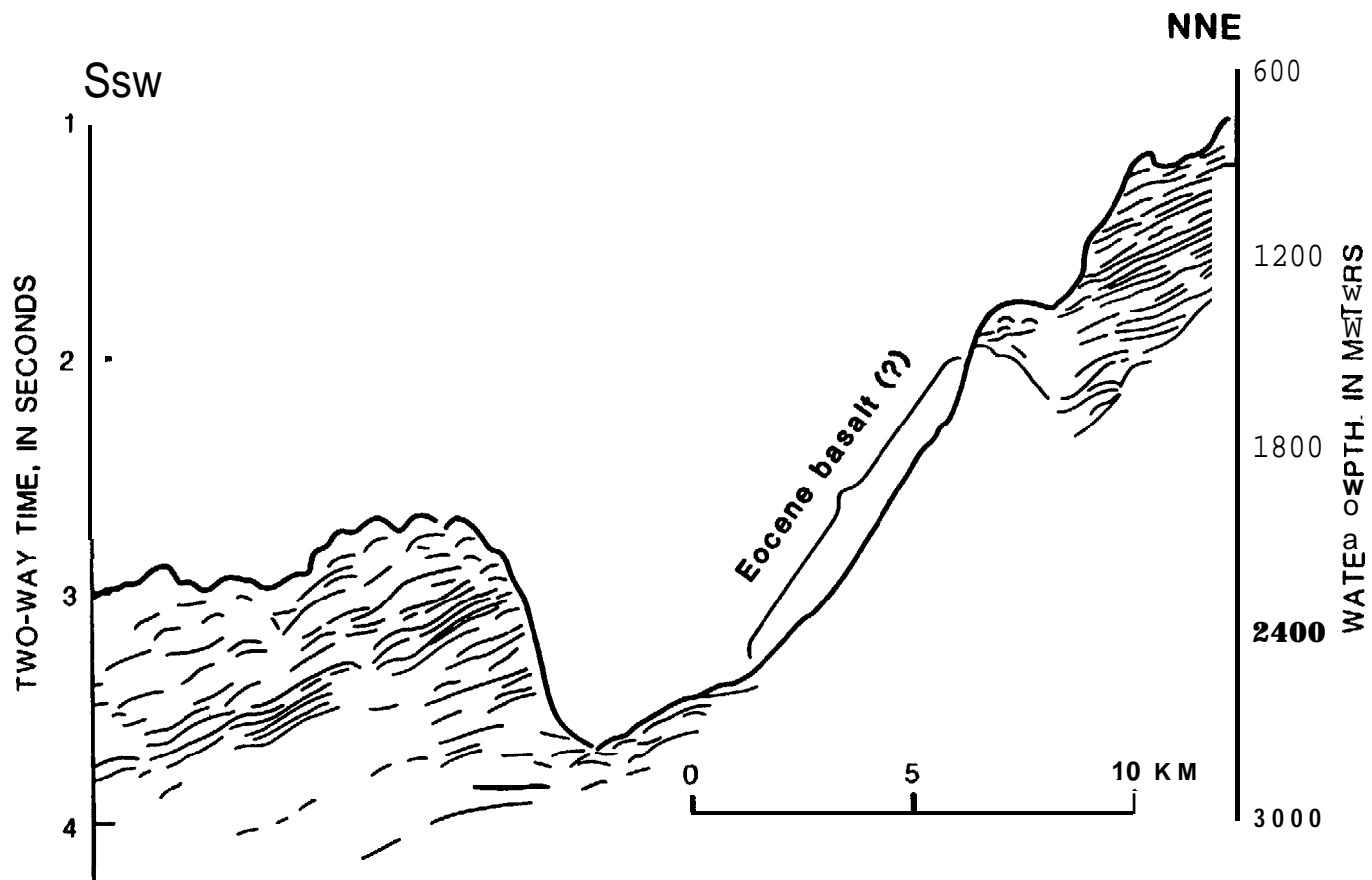


Figure E9. Interpretive line drawing of air-gun profile across west branch of St. Matthew Canyon (see Fig. E5 for location) (V.E. ~x7).

/ the Yukon and Anadyr to carry large amounts of sediment to the shelf edge. The most likely canyon-cutting agents were slumps and resulting turbidity currents supplemented by **bioturbation** of canyon walls and by erosional effects of canyon-focused waves and currents (Carlson and others, 1982).

We have deduced from seismic-reflection profiles and sediment-samples that similar processes appear to have been responsible for the carving of the St. Matthew and Middle Canyon systems. At question, however, is the reason for **the** much larger size of Navarinsky, Pervenets, and **Zhemchug** Canyons compared to **St.** Matthew and Middle Canyons. Perhaps the position of the canyons with respect to the major rivers (**Anadyr** and Yukon) that meandered across the flat Eering Shelf during Pleistocene and earlier low-stands of sea level was a key factor. If we look at a map of the Bering shelf (Plate 1 inset), we see that St. Matthew Island lies directly in line between the Yukon Delta and the heads of the St. Matthew and Middle Canyon systems. According to Patton and others (1976), St. Matthew Island is made up of some 500 m of subaerial volcanic rocks intruded by an early Tertiary age granodiorite. They suggest that the island is a southeastward extension of the **Cretaceous-Early** Tertiary volcanic arc that borders the Siberian Pacific margin. Perhaps this resistant island platform served as a deflector of the Yukon River as it meandered seaward across the broad shelf, thus inhibiting initiation of St. Matthew and Middle Canyons perhaps until the Pleistocene. **Also** the western edge of the large Navarin Basin, beneath the outer shelf and upper slope, is bordered by a northwestward trending basement high buried by 0.5 - 1.0 km of Cenozoic sediment (**Marlow** and others, 1976). This basement ridge would also result in restricted access of the **large** rivers to much of the area of the present continental slope until the basin was nearly full of sediment. Just as with any ridge system, the water gap is determined not only by low spots in the ridge but **also** by the presence of less-resistant or more faulted and fractured segments of the barrier. Compounding the problem, is the presence of basalt on the walls of at least St. Matthew Canyon and perhaps Middle Canyon. **If** this igneous rock is present as an elongate ridge parallel to the shelf-break, the cutting of these two-smaller canyons would indeed be retarded. However, igneous rocks also have been dredged from the **walls** of **Zhemchug** and Pervenets Canyons (Jones and others, 1981). Without further dredging we cannot assess the relative importance of the igneous rocks *as to* their influence on the rates of canyon cutting in any of the four canyons.

Our model of canyon development suggests that the large canyons began forming much earlier than did the St. Matthew and Middle Canyon systems. During low stands of sea level perhaps in the late Tertiary, the ancestral Yukon and Anadyr Rivers contributed to the development of the three large canyons. Geographically the Anadyr River seems most likely to have contributed to the formation of Navarinsky Canyon and the Yukon to **Zhemchug** Canyon. Pervenets Canyon could have been influenced by distributaries from either of the two major rivers. Proximity would suggest that distributaries of the Yukon **River** would be the most likely contributors to the St. Matthew and Middle Canyon systems.

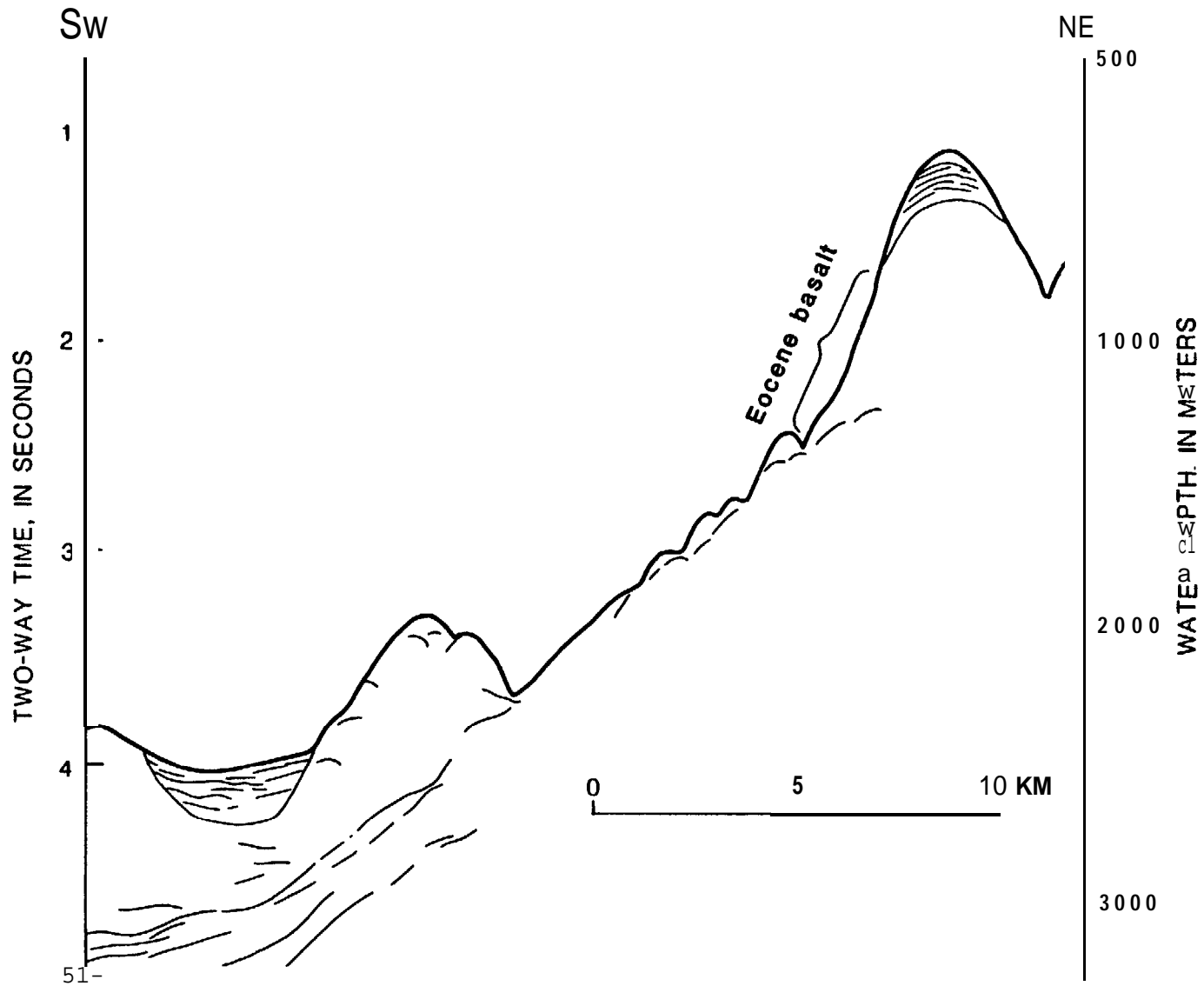


Figure E10. Interpretive line drawing of air-gun profile across west branch of St. Matthew Canyon (see Fig. ES for location) (V.E. 'x7).

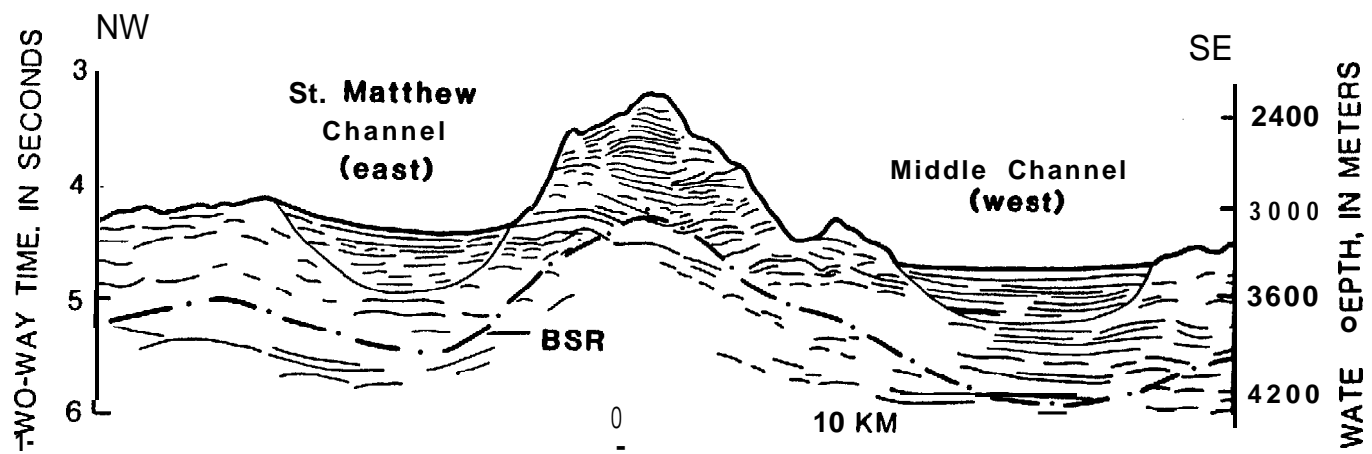


Figure En. Interpretive line drawing of air-gun profile across west branch of St. Matthew Canyon (see Fig. E5 for location) (V.E. -x7). (BSR = Bottom simulating reflector).

#### ACKNOWLEDGMENTS

We appreciate the assistance provided by the scientific personnel, the ship's captains and crew, *and* the marine logistics group. We thank Michael Marlow for a constructive review of the manuscript.

The cruises were supported jointly by the U.S. Geological Survey and by the Bureau of Land Management through interagency agreement with the National Oceanic and Atmospheric Administration, under which a multi-year environmental hazards study of the Alaskan continental shelf is managed by the OCSEAP office.

#### REFERENCES CITED

- Baldauf, J. G., 1981, Diatom analysis of late Quaternary sediments from Navarin Basin province, Bering Sea, Alaska, *in* Carlson, P. R. and Karl, H. A., eds., Seafloor geologic hazards, sedimentology, and bathymetry: Navarin Basin province, northern Bering Sea: U.S. Geological Survey Open-File Report 81-1217, p. 100-113.
- Carlson, P. R. and Karl, H. A., 1982, High-resolution seismic reflection profiles collected in 1981 in Navarin Basin province, Bering Sea: U.S. Geological Survey Open-File Report 82-786, 5 p., 1 map, scale 1:1,000,000.
- Carlson, P. R., Karl, H. A., Johnson, K. A., and Fischer, J. M., 1981, Submarine canyons flanking Navarin Basin, Bering Sea, *in*: U.S. Geological Survey Circular 844, p. 139-141.
- Carlson, P. R. and Karl, H. A., 1982, High-resolution seismic reflection profiles collected in 1981 in Navarin Basin province, Bering Sea: U.S. Geological Survey Open-File Report 82-786, 5 p., 1 map, scale 1:1,000,000.
- Carlson, P. R., Karl, H. A., and Quinterno, P., 1982, Sedimentologic processes in world's largest submarine canyons, Bering Sea, Alaska: Geological Society of America, Abstracts with Programs, v. 15, p. 459-460.
- Fischer, J. M., Carlson, P. R., and Karl, H. A., 1982, Bathymetric map of Navarin basin province, northern Bering Sea: U. S. Geological Survey Open-File Report 82-1038, 11 p., 1 map, scale 1:1,000,000.
- Jones, D. M., Kingston, M. J., Marlow, M. S., Cooper, A. K., Barron, J. A., Wingate, F. H., and Arnal, R. E., 1981, Age, mineralogy, physical properties, and geochemistry of dredge samples from the Bering Sea continental margin: U. S. Geological Survey Open-File Report 81-1297, 68 p.
- Karl, H. A. and Carlson, P. R., 1982, Location and description of sediment samples: Navarin Basin province, Bering Sea, 1980-81: U. S. Geological Survey Open-File Report 82-958, 5 p., 2 map sheets, scale 1:1,000,000.

- Kotenev, B. N., 1965, Submarine valleys in the zone of the continental slope in the Bering Sea: All-Union Research Inst. of Marine Fisheries and Oceanography. Transactions, v. 58, p. 35-44. (U. S. Navy Electronics Lab., San Diego, CA., NEL Translation 112).
- Marlow, M. S.** and Cooper, A. K., 1979, Multichannel seismic reflection profiles collected in 1977 in the southern Bering Sea shelf: U.S. Geological Survey Open-File Report 79-1147.
- Marlow, M. S. and Cooper, A. K., 1980, Multichannel seismic reflection profiles collected in 1976 in the southern Bering Sea shelf: U.S. Geological Survey Open-File Report 80-389.
- Marlow, M. S.**, Cooper, A. K., and **Childs, J. R.**, in press, Tectonic evolution of the Gulf of Anadyr and formation of **Anadyr** and Navarin **basins**: Bulletin of the American Association of Petroleum Geologists.
- Marlow, M. S., Scholl, D. W., Cooper, A. K., and Buffington, E. C., 1976, Structure and evolution of Bering Sea shelf south of St. Lawrence Island: Bulletin of the American Association of Petroleum Geologists, v. 60, no. 1, p. 161-183.
- Patton, W. W., **Lanphere, M. A.**, Miller, T. P., and Scott, R. A., 1976, Age and tectonic significance of volcanic rocks on St. Matthew Island, Bering Sea, Alaska: U. S. Geological Survey J. of Research, v. 4, p. 67-73.
- Quinterno, P. J., 1981, Preliminary report on benthic **foraminifers** from Navarin Basin province, Bering Sea, Alaska, in **Carlson, P. R.** and Karl, H. A. eds., Seafloor geologic hazards, **sedimentology**, and bathymetry: **Navarin** Basin province, northwestern Bering Sea: U. S. Geological Survey Open-File Report 81-1217, p. 114-129.
- Scholl, D. W. and **Marlow, M. S.**, 1970, Bering Sea region seismic reflection profiles, 1969: U. S. Geological Survey Open-File Report.
- Scholl, D. W., Buffington, E. C., and **Marlow, M. S.**, 1976, Aleutian-Bering Sea regional seismic reflection profiles: U. S. Geological Survey **Open-File** Report 76-748.
- Shepard, F. P.**, 1963, Submarine geology, 2nd ed.: Harper and Row, New York, 557 p.
- Shepard, F. P.** and Dill, R. F., 1966, Submarine Canyons and other sea valleys: Rand McNally and Co., Chicago, 381 p.

APPENDIX F:

GEOLOGIC HAZARDS IN **NAVARIN** BASIN PROVINCE,  
NORTH BERING SEA

by

Paul R. **Carlson**, Herman A. Karl,  
Jeffrey M. Fischer, and Brian D. Edwards

U.S. Geological Survey



OTC 4172

## Geologic Hazards in Navarin Basin Province, Northern Bering Sea

by Paul R. Carlson, Herman A. Karl, Jeffrey M. Fischer, and Brian D. Edwards, U.S. Geological Survey

This paper was presented at the 14th Annual OTC in Houston, Texas, May 3-6, 1982. The material is subject to correction by the author. Permission to copy is restricted to an abstract of not more than 300 words.

### ABSTRACT

Navarin Basin, scheduled for leasing in 1984 (OCS sale 83), may contain vast accumulations of oil and gas. Several geologic and oceanographic processes that may be active in and around Navarin Basin province could be hazardous to commercial development. These potential hazards include submarine slides; sea-floor instability resulting from disturbance of gas-charged sediment; sediment transport and erosion caused by storm waves, tsunamis, internal waves, or bottom currents; pack ice; and active faults and ground motion.

### INTRODUCTION

The quest for energy independence by the United States includes exploration of new segments of the outer continental shelf. The Navarin Basin lease sale (OCS sale 83) is scheduled for the spring of 1984. The study area, hereafter referred to as the "Navarin Basin province," is located on the outer continental shelf end upper slope in the northern Bering Sea (Fig. F1). The area is bounded on the northwest by the U.S.-U.S.S.R. convention line of 1867 and on the southwest by the base of the continental slope; it extends to within 100 km of St. Matthew Island to the northeast and of St. Paul Island to the southeast. This region potentially contains commercially exploitable accumulations of oil and gas, and it is likely to be the subject of intensive exploration. The purpose of this paper is to delineate, describe, and assess potential geologic hazards on the sea floor in the Navarin Basin province that must be considered in the design of offshore facilities.

### Data Collection

The principal sources of data for this study have been seismic-reflection profiles and sediment samples collected in 1980 and 1981 on the R/V *Discoverer* (Carlson and Karl, 1981). The seismic-reflection systems used included two 40-in<sup>3</sup> airguns, an 800-J minisparker, and a 3.5-kHz transducer as acoustic sources. Spacing between geophysical tracklines over this immense area averages about 15 km; sea-floor geological samples were taken at intersections of track lines and at selected geologically significant sites. Navigational control was LORAN C updated with satellite

positioning.

Shear-strength measurements were made on selected cores by means of a motorized Wykeham-Farrance\* miniature-vane shear device. Tests were made at 20-cm intervals on core segments that had been split longitudinally. Immediately following strength testing, water-content and bulk-density subsamples were obtained at the locations of the vane tests. Consolidation analyses were performed on selected cores.

Additional data collected in 1980 from the USCG *Polar Star* and the R/V *S.P. LEE* were incorporated into our data base as were seismic-reflection records collected over the past 15 years by the U.S. Geological Survey for resource evaluation (Marlow and others, 1981). Other sources of data include studies by scientists from the Universities of Washington and Alaska, and from Russia, and Japan (e.g. Knebel, 1972; Sharma, 1979; Lisitsyn, 1966; Takenouti and Ohtani, 1974).

### MORPHOLOGY OF NAVARIN BASIN PROVINCE

Three physiographic provinces comprise the Navarin study area. These are the flat, wide, continental shelf; the steep, rugged continental slope, and the continental rise that extends from the base of the slope to the 3600-m isobath. Three large submarine canyons deeply dissect the outer shelf and elope (Fig. F2). Coalescing fans at the mouths of these canyons form part of the wedge of sediment of the continental rise.

### Shelf

The Bering Sea continental shelf, one of the widest and flattest in the world, is about 700 km wide and has a gradient of 0.02° seaward of the Yukon River delta. By comparison, Shepard (1963) reported a world wide average continental-shelf gradient of 0.12°. The part of the Bering shelf that includes the Navarin Basin province lies between the 100-m and 150-m isobaths and ranges in width from about 120 km in the

● Use of trade names is for descriptive purposes only and does not constitute endorsement by the U.S. Geological Survey.

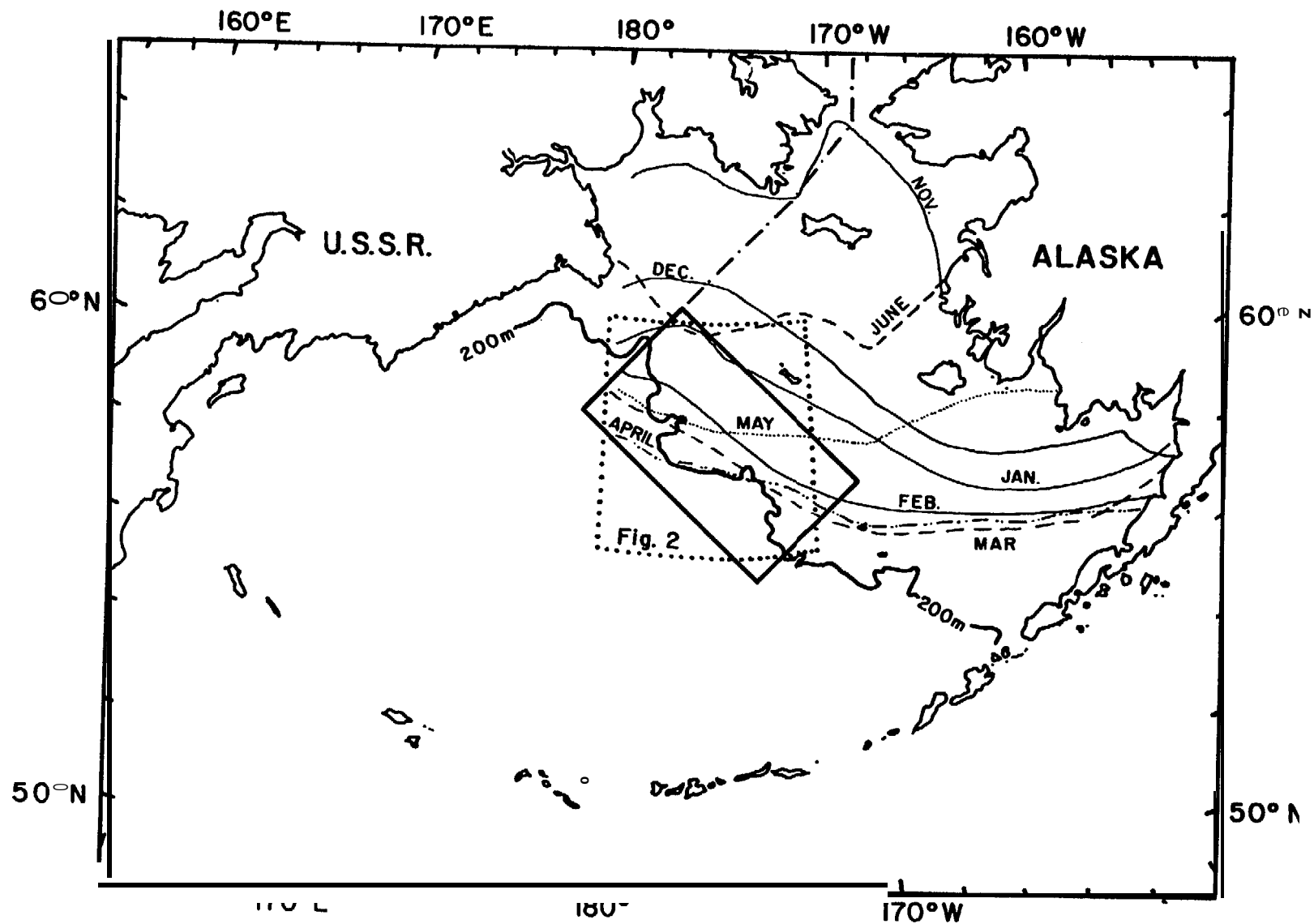


Fig. F1 — Location of Navarin Basin province (outlined) and lines of average monthly ice-front positions (after Webster, 1979); ice positions for the 15th of month

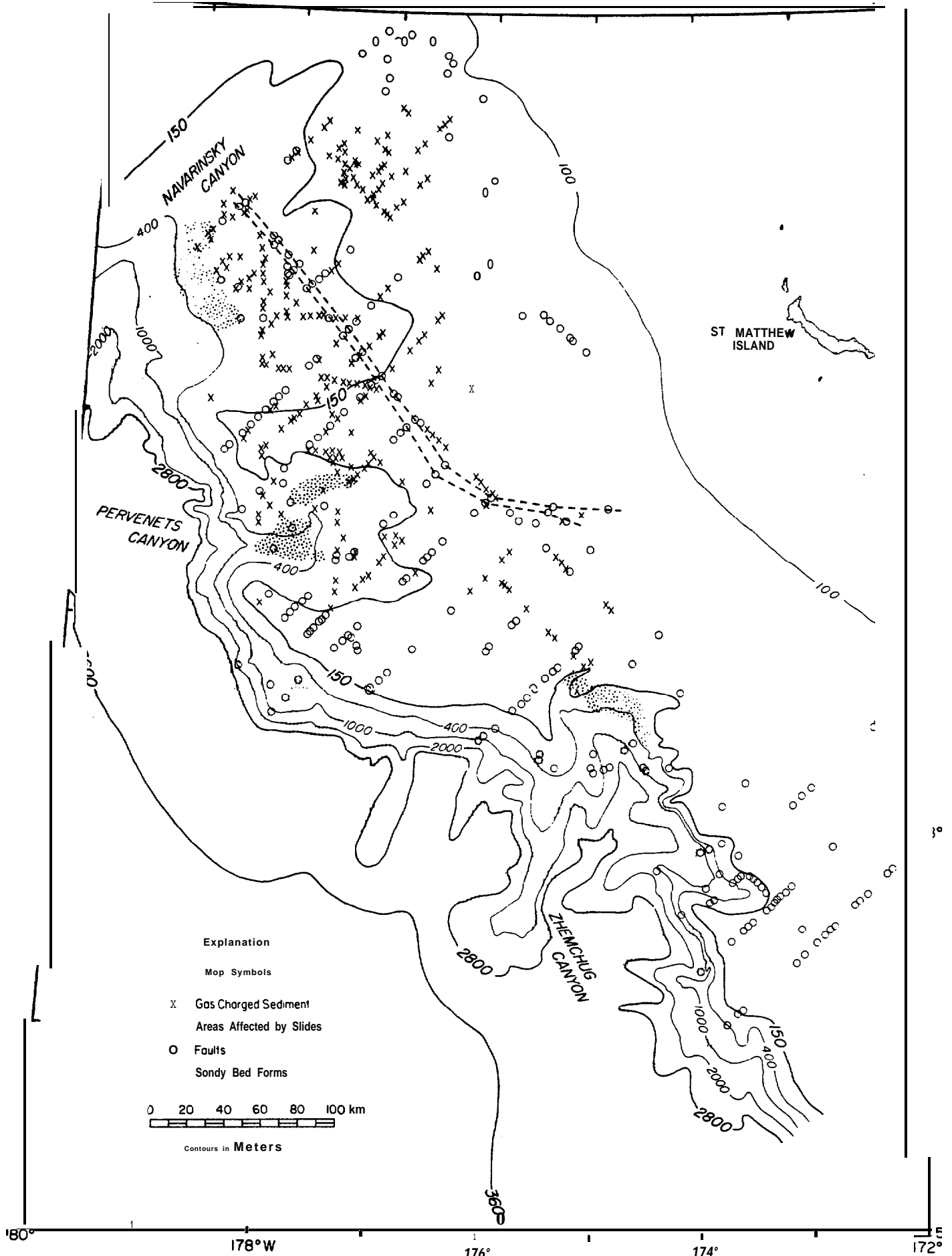


Fig. F2 — Preliminary map of sea-floor geologic hazards in Navarin Basin province

northern and southern parts of the study area to a maximum of about 235 km in the central part (Fig. F2). These boundaries define an area of about 100,000 km<sup>2</sup>. Although the outer continental shelf is cut by three massive submarine canyons, there are no apparent morphologic expressions of these canyons landward of the 125-m isobath.

### Slope

The continental slope that forms the southeastern boundary of the Navarin Basin province begins at the 150-m isobath and extends to a depth of 2800 m (Fig. F2). The width of the continental slope ranges from 47 km in the middle of the province to 19 km south of Zhemchug Canyon. The slope includes an area of about 47,000 km<sup>2</sup>. The gradients of the Navarin slope range from 3 to 8 with even steeper gradients locally. This compares with the world wide average gradient for continental slopes of about 4.30 (Shepard, 1963).

### Submarine Canyons

The three major submarine canyons that cut deeply into the Bering continental margin head in water depths less than 140 m (Fig. F2). Extensive deep-sea fans have developed at the mouths of the canyons in water depths of about 3000 m. Navarinsky is the longest canyon (340 km), Pervenets the shortest (125 km), and Zhemchug is intermediate in length (240 km). Both Navarinsky and Zhemchug Canyons are about 100 km wide at the shelf break, but the smaller Pervenets Canyon is only 30 km wide there. Local wall relief of the three canyons at the shelf break ranges from 700 m in Navarin and 800 m in Pervenets, to a spectacular 2600 m in Zhemchug. Each of the three canyons consists of two main branches or tributaries on the landward side of the shelf break. The two tributaries of Zhemchug Canyon trend 180° away from each other, forming a large trough-shaped basin. All three canyons are incised into Neogene and older, more lithified Paleogene rocks, principally mudstones, that are thought to make up much of Navarin Basin (Marlow and others, 1976). The shapes of the canyons, especially of Zhemchug, are apparently controlled by structures as old as Paleogene (Scholl and others, 1975). The major cutting of the canyons probably occurred when glacio-eustatically lowered sea levels exposed most of the Bering shelf.

### Rise

The continental rise begins at the base of the slope at a depth of about 2800 m and extends to the 3600-m isobath that marks the beginning of the abyssal plain (Fig. F2). The average width of the rise is about 75 km, ranging from 25 km northwest of Zhemchug Canyon to more than 100 km adjacent to the mouths of the three large canyons. The rise encompasses an area of 40,000 km<sup>2</sup>. The gradients across the rise range from 0.5" to 1.8". Deep-sea channels cross the rise in the area of the canyon mouths and apparently are connected to the submarine canyons. Gravity cores collected near the mouths of the canyons and on the adjacent rise contain sand lenses that suggest their deposition by turbidity currents.

### SEA-FLOOR GEOLOGIC HAZARDS

Potential geologic hazards in the Navarin Basin province include sea-floor instability marked by submarine slides, sediment transport and erosion, and

subsidence or blowouts resulting from the disturbance of gas-charged sediment; ice and faulting with attendant ground shaking (Fig. F2).

### SEAFLOOR INSTABILITY

Within the broad category of sea-floor instability, we have included discussions of three major types: submarine sliding, sediment transport and erosion, and gas-charged sediment. Liquefaction of saturated sands is another possible cause of sediment instability (Seed and Lee, 1966), but at this time we have inefficient data to assess the liquefaction potential of Navarin shelf sediment.

### Submarine Sediment Slides

Submarine elide is used as an all-inclusive term for a variety of slope movements. The preliminary nature of our study makes it impractical at this time to attempt to classify each of the areas according to type of movement and type of material. Many of the submarine elides have been found in association with the large submarine canyons that are cut into the continental margin (Fig. F2).

Because of the wide spacing between tracklines, we can not correlate slide masses from line to line. None of the slides begin in water shallower than 150 m, several head below 400 m, and one appears to originate at a depth of greater than 1200 m. Some of the zones affected by down-slope movement are 50 km in length and some appear to be 25 km wide. Composite slides may effect the upper 200-300 m of the sediment column (Fig. F3). Gravity cores (2-5m in length) were collected from a few of the slide masses. These cores recovered a variety of sediment types, from pebbly mud to sandy mud to very soft mud. Preliminary evaluation of the morphology and internal reflectors observed on seismic profiles that cross the outer continental shelf and slope suggest that the slides include slumps, debris-flow deposits, and mud-flow deposits according to the classification used by Nardin and others, (1979). The causes of these failures are unknown, but likely are related to seismic ground accelerations. The build-up of pore-water pressures with attendant decrease in shear strength that results from seismic shaking and the reduction of shear strength that accompanies build-up of bubble-phase gas can both contribute to sediment instability (Hampton and others, 1978). Considering the sedimentation rates in the area (1-25 cm/10<sup>3</sup>yr; Askren, 1972; Blunt and Kvenvolden, 1981), the coefficients of consolidation, and the overconsolidation ratios (Table F1) and using Gibson's equations (1958), it appears unlikely that the sediment is significantly underconsolidated. However, if the observed failures are Pleistocene in age and sedimentation rates were significantly higher at that time, underconsolidation may be a relatively more important factor. Instability due to the strength reduction caused by the cyclic loading that is associated with storm waves, internal waves, or tsunamis is minimal at the water depths (200 to 1200 m) in which the elide deposits are observed (see Seed and Rahman, 1978).

### Sediment Transport and Erosion

#### Large Bedforms

Large sediment waves have been found at the heads of Zhemchug, Pervenets, and Navarinsky Submarine

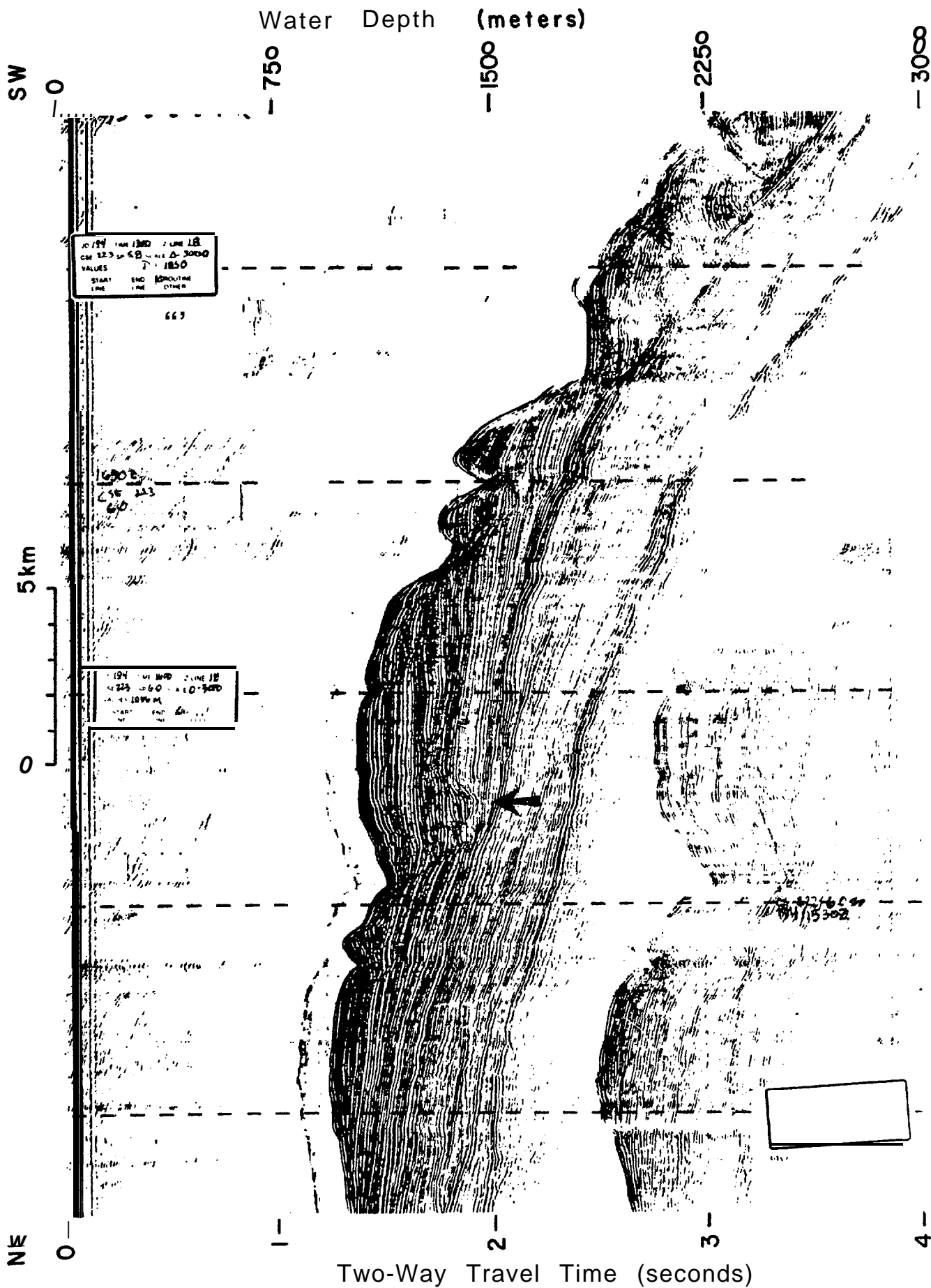


Fig. F3 — Air-gun profile showing slides in Navarinsky Canyon. Note buried channel (arrow) and associated cut-and-fill structures (V.E. ~x10).

Canyons (Fig. F2). The sediment waves in these areas are alike. Those at the head of Navarinsky Canyon have been studied in the greatest detail. These large bedforms occur on a substrate of silty, very fine sand within a 600 to 700 km<sup>2</sup> area between the 215- and 450-m isobaths. Crests of these bedforms trend approximately north-south; the waves have an average length of about 600 m, an average height of about 8 m, and a maximum height of 15 m (Fig. F4). Both symmetrical (the more common) and asymmetrical waves have been observed. The bedforms not only are expressed at the surface, but also are remarkably well defined in the subsurface. The stratigraphic unit containing the sediment waves developed over a flat-lying reflector, and it attains a maximum thickness of about 120 m in the sediment wave field. In a few places, the bedforms are covered by a thin layer of apparently younger sediment. One such locality occurs at the head of Parvenets Canyon, where the buried sediment waves are part of an intricate stratigraphic complex that lies below a unit of parallel-bedded reflectors (Fig. F5). The parallel-bedded unit is generally about 20 m thick, but it ranges in thickness from less than 5 m to about 110 m. If the sea-floor features are active, they, as well as the processes responsible for them, could represent hazards.

#### Surface Waves

Currents generated by surface waves probably are a more significant factor in the transport of silt and larger size particles on the open slope and shelf of Navarin Basin than, for example, tidal currents or the mean circulation. Bottom currents have not been measured in the study area, nor have there been good observations of surface waves. However, some surface-wave data have been compiled in areas adjacent to and including a part of the eastern boundary of the lease sale area (Brewer and others, 1977).

Storms, and consequently storm-generated waves, are strongest and most frequent during the fall and winter (Litsitsyn, 1966; Brewer and others, 1977). Waves as high as 15 m and with possible periods of 9 to 11 s have been observed east of the lease area (Brewer and others, 1977). Waves with these heights and periods do not generate bottom currents of a strength sufficient to erode sediments over a large part of the shelf. For example, assuming a threshold value of 10 cm/s for transporting fine sand (Komar and others, 1972), a 15-m-high wave generates currents strong enough to erode fine sand and smaller grains only in water shallower than about 135 m. A lower, but longer period wave, for example a wave 10 m high with 15-s period, produces near-bottom currents greater than 10 cm/s in water as deep as 208 m. Extreme waves, empirically estimated to be as large as 42.5 m high, occur on the average once every 100 years in the Navarin area (Brewer and others, 1977).

#### Gas-charged sediment

Gas-charged sediment can have a lower shear strength and bearing capacity than does equivalent gas-free sediment (Nelson and others, 1978; Whelan and others, 1976). An increase in the concentration of free or bubble-phase gas results in an increase of pore pressure and a concomitant decrease in shear strength until failure can occur. Such increases in bubble-phase gas can result from drilling into gas-charged sediment or disruption of the sediment by cyclic loading, and they may lead to the failure of pipelines

or platforms (U.S. Geological Survey, 1977).

The numerous areas of gas-charged sediment mapped in Navarin Basin (Fig. F2) are identifiable on the high-resolution seismic-reflection profiles by acoustic anomalies such as displaced reflectors and "wipe out" zones (Fig. F6). These anomalies are prevalent in the upper 50 to 100 m of sediment. Commonly these shallow anomalies coincide closely with well-developed "bright spots" that appear to occur deeper in the section on multi-channel or medium-resolution single-channel profiles.

Gravity cores collected throughout the basin province were analyzed for hydrocarbon (methane through butane) (Vogel and Kvenvolden, 1981). All of the cores sampled contained hydrocarbon gases, but none showed significant amounts of thermogenic hydrocarbons. Most of the hydrocarbon ratios can be attributed to microbial activity. Three cores, two from the shelf and one from the slope, contained concentrations of methane (5 to 9 times) and ethane (10 to 20 times) higher than background values (Vogel and others, 1981). These cores also contained ratios of ethane to ethene and of methane to ethane and propane that marginally suggest the presence of some thermogenic hydrocarbons. Possible explanations for the low concentration of hydrocarbons include the short length of the cores (i.e., <6 m; most of the cores collected on the shelf were <2 m long) and the exceedingly spotty areal concentrations of the hydrocarbons.

#### Geotechnical properties of Navarin Basin sediment

Cores from 68 stations were tested to define geotechnical variables useful in describing regional changes in Navarin Basin sediment properties. Shelf sediment (<150 m water depth) typically has a peak shear strength ( $S_v$ ) that ranges between 10 and 15 kPa at 1 m subbottom (1 psi = 6.9 kPa) (Fig. F7). An elongate zone of weaker sediment (shear strength <10 kPa) extends into the central part of the study area from the north and reflects the presence of a tongue of fine-grained, high-water-content sediment (Karl and others, 1961). A zone of stronger sediment (shear strength > 15 kPa) exists to the southeast, although the stations there are too sparse to allow definition. Shear strengths in the region of the shelf break (Fig. F7, lined area) are not shown because high sand content allows pore-water drainage during testing which in turn compromise measured  $S_v$  values, or because insufficient sample was recovered to warrant testing. Typically, peak shear strength decreases downslope, ranging from 11 kPa near the shelf break to 3 kPa on the abyssal floor. However, anomalously strong sediment was encountered at two stations, both at about 58°30'N, 178°30'W, in 3000 m of water. Here, the shear strengths are between 19 and 39 kPa.

Sediment at a 1-m-subbottom depth on the shelf has a water content that ranges from 40 to 1100 by dry weight (Fig. F8). An elongate zone having water contents greater than 100% is seen in the north-central part of the shelf. This zone coincides with the area of anomalously low peak undrained shear strength. The water content of shelf sediment is lowest toward the southeast, except for two stations that have water contents greater than 50%. Sediment from the shelf edge and uppermost slope typically has a low water content (<50%), a value which correlates with increased sand percentage. Water content increases downslope and reaches a maximum (>300%) to the southeast, in the

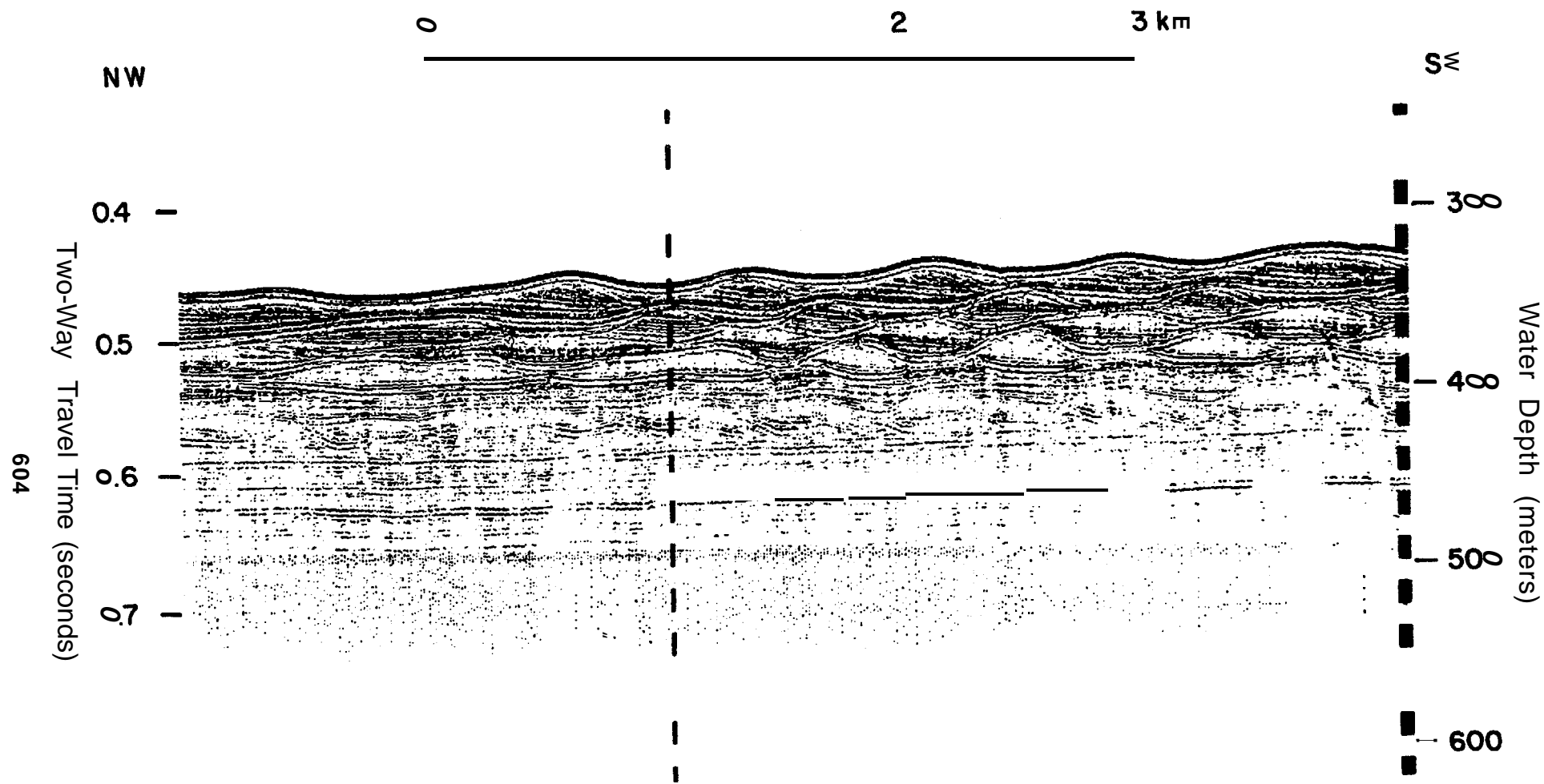
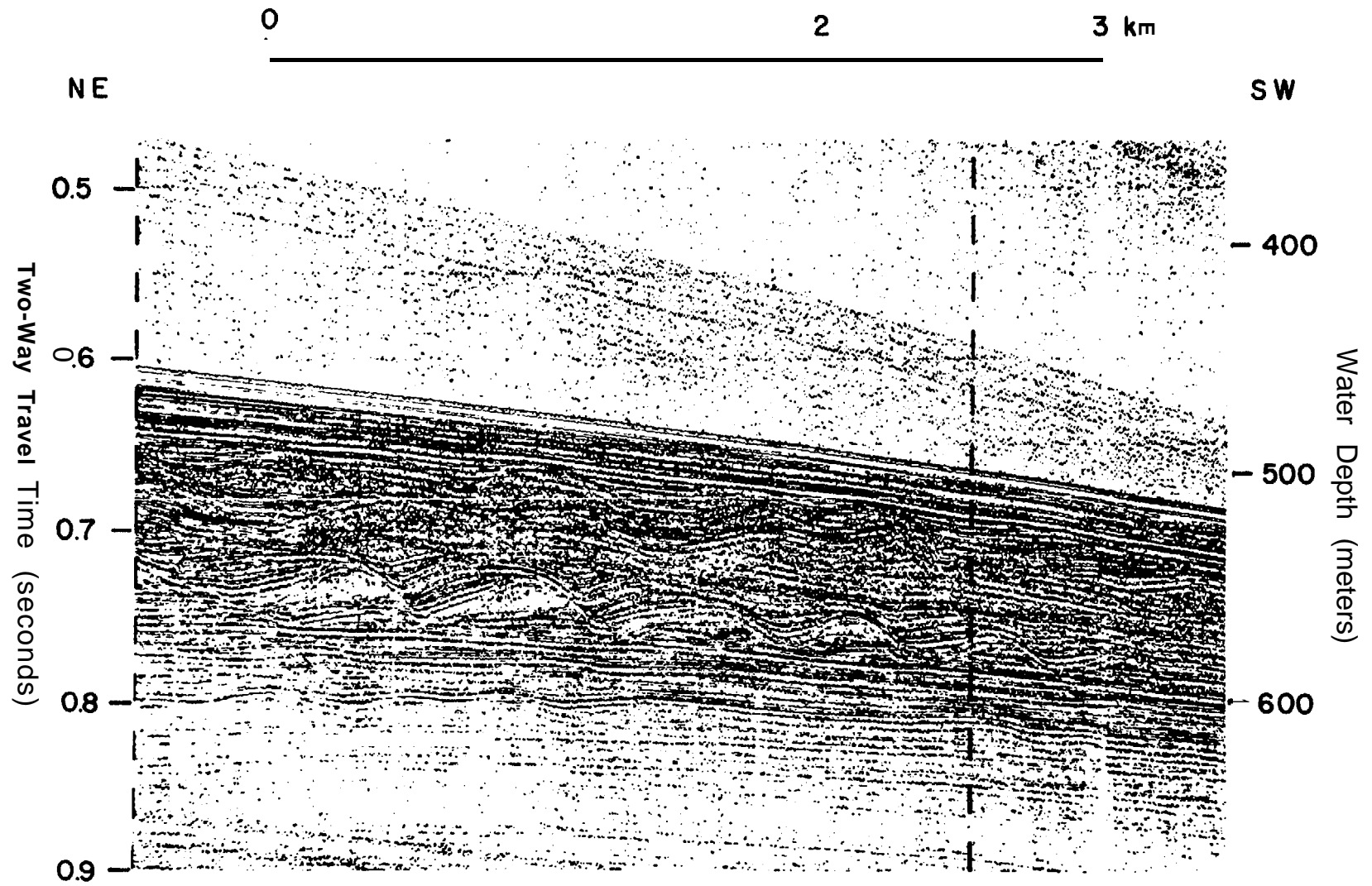


Fig. F4 — Minisparker profile showing sediment waves at head of Navarinsky Canyon (V.E.  $\sim$ x7.5).



605

Fig. F5 — Minisparker profile showing sediment waves covered by about 20 m of parallel-bedded sediment at head of Pervenets Canyon (V.E.  $\times 8.5$ ).

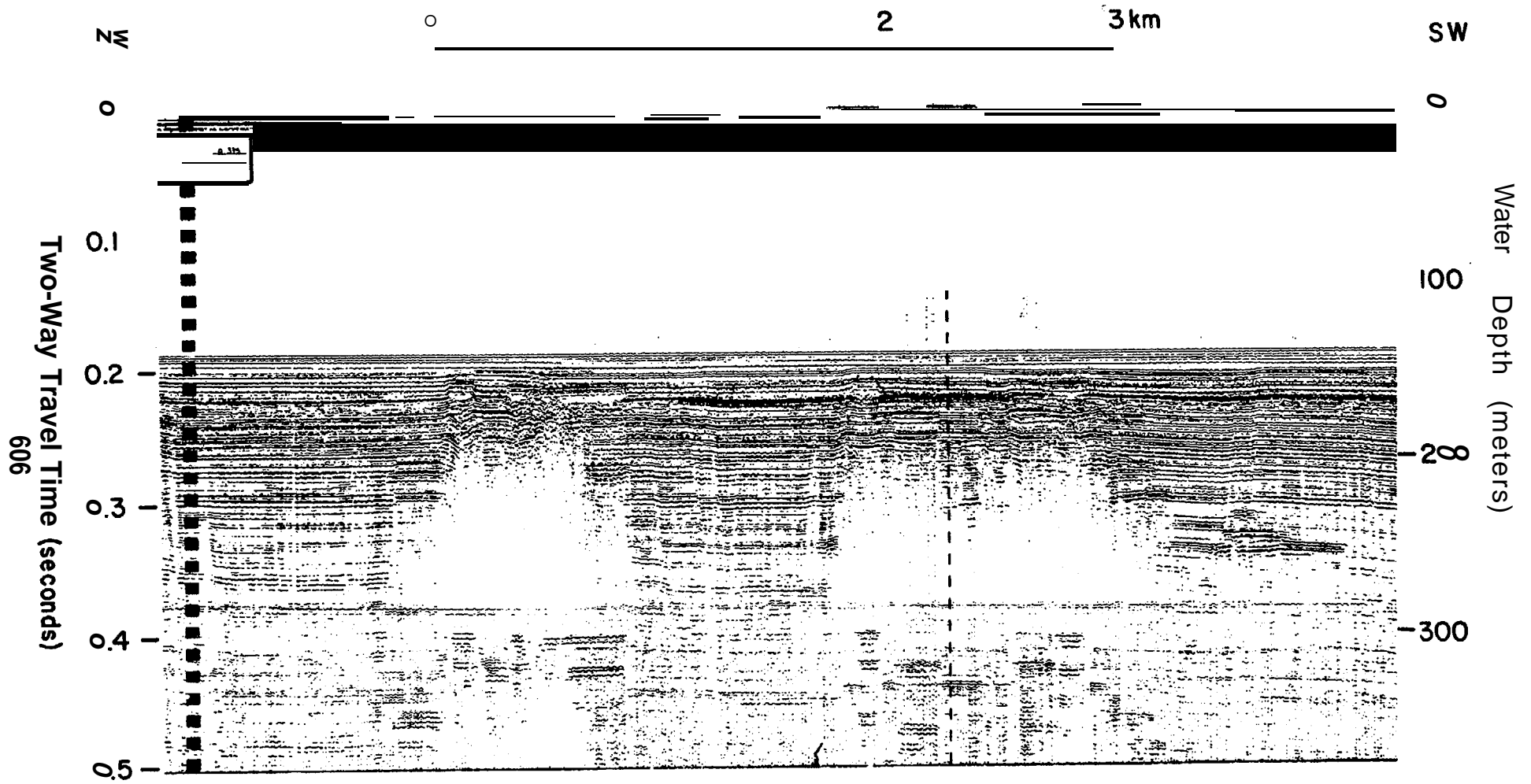


Fig. F6 — Minisparker profile from northern part of Navarin Basin province showing acoustic anomalies interpreted to be caused by gas-charged sediment (V.E.  $\sim x7.5$ ).

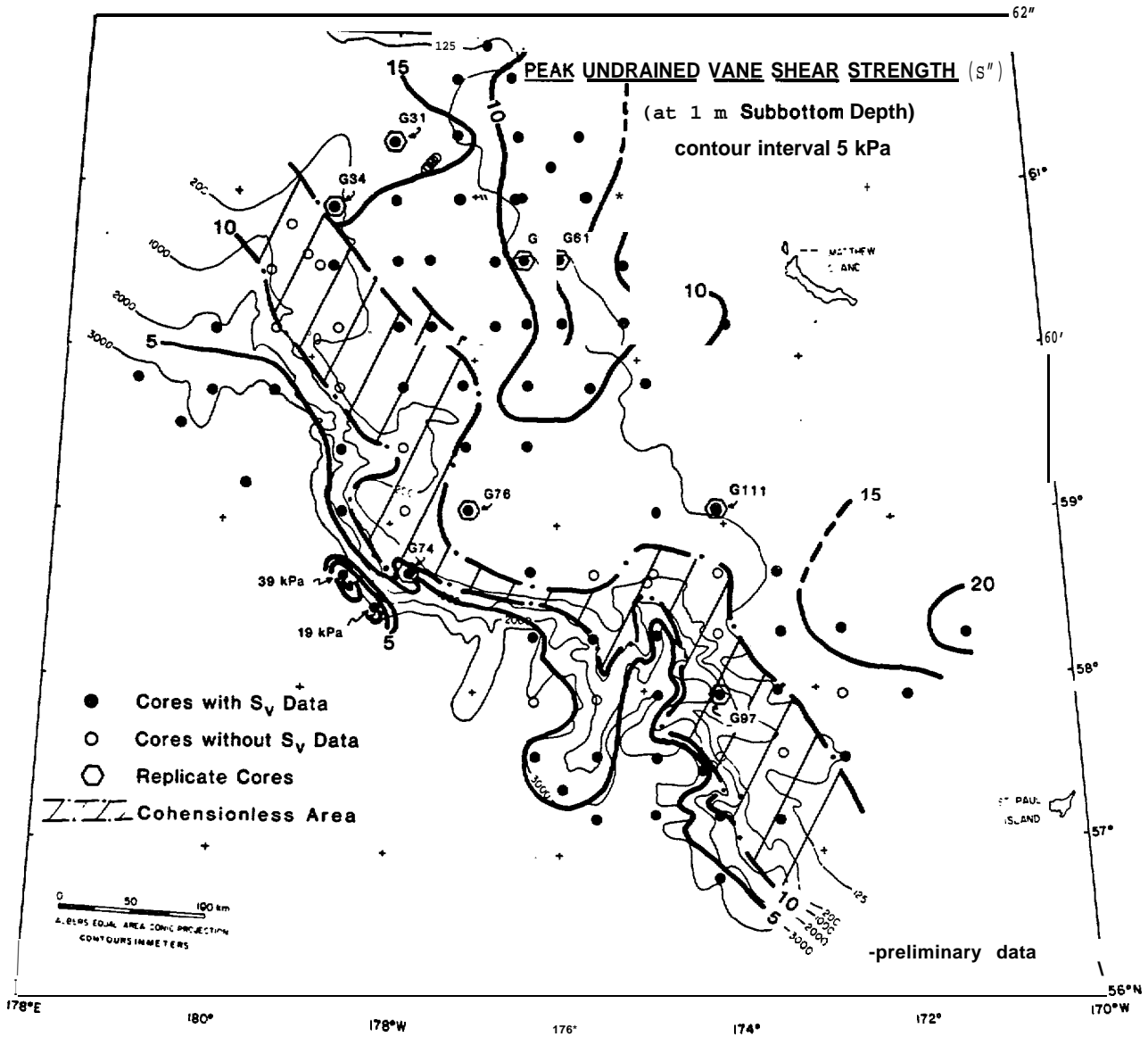


Fig. F7 — Area 1 distribution of peak undrained vane shear strength ( $S_v$ ) at 1-m subbottom depth

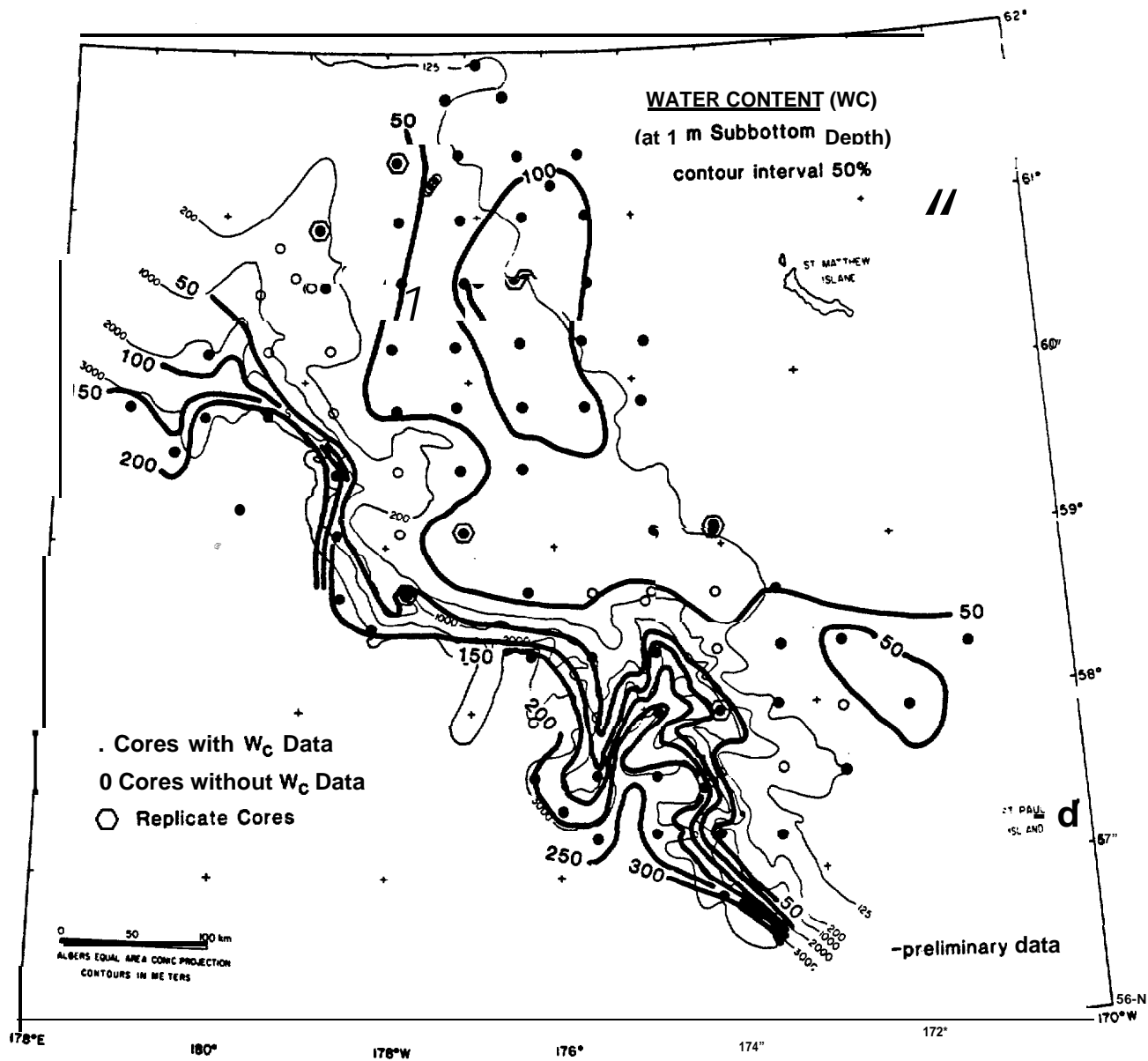


Fig. F 8 — Area 1 distribution of salt-corrected water content at a 1-m subbottom depth

## vicinity of Zhemchug Canyon.

Near-surface sediment from Navarin Basin is lightly to moderately overconsolidated (overconsolidation ratio, or OCR: 3 - 4) except on the shelf where OCR's as high as 22 are observed (Table F1). The cause of the observed overconsolidation is not known. Sediment on the shelf is subjected to a number of loads that might be capable of inducing this state of overconsolidation (e.g., erosion of overlying material, cyclic loading, ice, and subaerial exposure at low sea-level stands). At present, our data are insufficient to evaluate these mechanisms.

[ICE

We have estimated ice conditions in Navarin Basin province by synthesizing data reported by Lisitsyn (1966), McRoy and Goering (1974), and Brower and others (1977). The proposed lease area is ice free from June through October. Migratory pack ice begins to encroach upon the northern part of the lease area in November. The pack ice is fully developed by March or April, at which time the extreme southern limit of the ice edge extends over most of the lease area (Fig. F1). Ice concentrations begin to decrease in April, and the ice edge continues to retreat northward through May. First-year ice in the southern portion of the Bering Sea ranges in thickness from 30 to 71 cm, whereas ice farther north can attain a thickness of 1-2 m in unstressed floes (Lisitsyn, 1966). The southern limit and the concentration of the pack ice vary from year to year depending upon weather conditions--in some years migratory pack ice may not affect the lease area, but in other years concentration of ice may completely cover it. In addition to the hazards that pack ice creates for man-made structures and for ships, Ivanhoe (1981) points out the significant problem of severe superstructure icing that ships will undergo while operating in the Bering Sea during the winter.

## FAULTING AND SEISMICITY

The limited seismic-reflection coverage of the Navarin Basin province restricts interpretation of the length, orientation, and age of the faults. The distribution of the faults is shown in figure 2; however, because the spacing between the tracklines is as much as 30 km, correlation from line to line is uncertain. The only extensive correlation that we have attempted is to connect those points that represent the bounding faults on a graben that is oriented in a northwest-southeast direction (Fig. F2). This graben is about 5 km wide, and it has been mapped over a distance of nearly 240 km. The maximum apparent relief of this structure (Fig. F9) is about 50 m, the result of a series of offsets on each side of the down-thrown block. The throw of the individual faults varies from about 10 to 20 m. The graben is buried beneath 130 m of sediment over the depressed block and about 80 m of sediment over the adjacent flat-lying strata. The faults detected on lines oriented perpendicular to the long axis of Navarin basin greatly outnumber those on lines that parallel the basin; this pattern suggests that the faults have a northwest-southeast trend. This trend is parallel to the basin and to the shelf break. The majority of these faults occur on the continental slope and the outermost shelf.

Many of the faults shown on Figure F2 are mapped from high-resolution seismic-reflection records that have resolution of 1-3 meters; however, none of the

faults mapped to date show any offset of the Holocene sea floor. Although the ages of the faults are unknown, 14 C dates of sediment in the southern part of the area indicate the maximum accumulation rates of the upper 6 m of sediment to be about 25 cm/10<sup>3</sup> yr (Askren, 1972). Therefore, faults that reach to within 3 m of the seafloor may cut sediment as young as Holocene and are considered to be active.

According to Scholl and others (1975), Cooper and others (1976), Marlow and others (1976), subduction of the Kula plate beneath the Bering Sea margin apparently ceased in late Mesozoic or early Tertiary time, and subduction of the Pacific plate shifted to the Aleutian Trench. This transfer tectonically deactivated the Bering Sea margin. The absence of modern seismicity is readily seen on the maps of Alaska earthquake epicenters published by Meyers (1976). Only six earthquakes have been reported from the Navarin Basin province for the time period prior to 1974, and all were less than magnitude six. These data, however, may be somewhat misleading because of the wide spacing and limited number of seismograph stations in western Alaska.

## CONCLUSIONS

Several seafloor geologic processes of a potentially hazardous nature are identifiable in the Navarin Basin province (OCS lease-sale 83); they include sea-floor instability due to submarine slides, sediment transport and erosion, and subsidence or blowouts resulting from disturbance of gas-charged sediment; ice; and faulting with attendant ground shaking. These processes must be carefully delineated and well understood before drilling and other sea-floor operations pertinent to exploration and production, such as pipeline siting, can be accomplished with a good degree of safety.

Submarine slides are prevalent on the continental slope throughout the area, especially in association with the submarine canyons. Large bedforms are found at the heads of each of the three canyons. However, gas-charged sediment apparently is the primary concern as a possible geologic hazard on the continental shelf because it is particularly common in the northern two-thirds of the study area. The gas is primarily biogenic methane; however, a few cores contained higher hydrocarbon homologs, the ratios of which suggest possible thermogenic origin.

An inverse correlation exists between the peak undrained shear strength ( $S_u$ ) and the water content of Navarin Basin sediment. At a 1-m-subbottom depth, a tongue of relatively weak (<10 kPa), high water content (>100%), fine-grained sediment extends onto the central shelf from the north. To the southeast, near the head of Zhemchug Canyon, shear strengths are anomalously high (>15 kPa). Strength of the fine-grained, high-water-content sediment on the slope decreases with water depth from a typical value of 11 kPa near the shelf break to a low of 3 kPa at the base of the slope. Preliminary consolidation data indicate that the shelf sediment is lightly to heavily overconsolidated (OCR's range from 3 to 22 at a subbottom depth of 1 m). It is apparent that the central shelf is more heavily overconsolidated than are the adjacent areas.

Migratory pack ice will be a problem during most years in the Navarin Basin lease area. This ice can

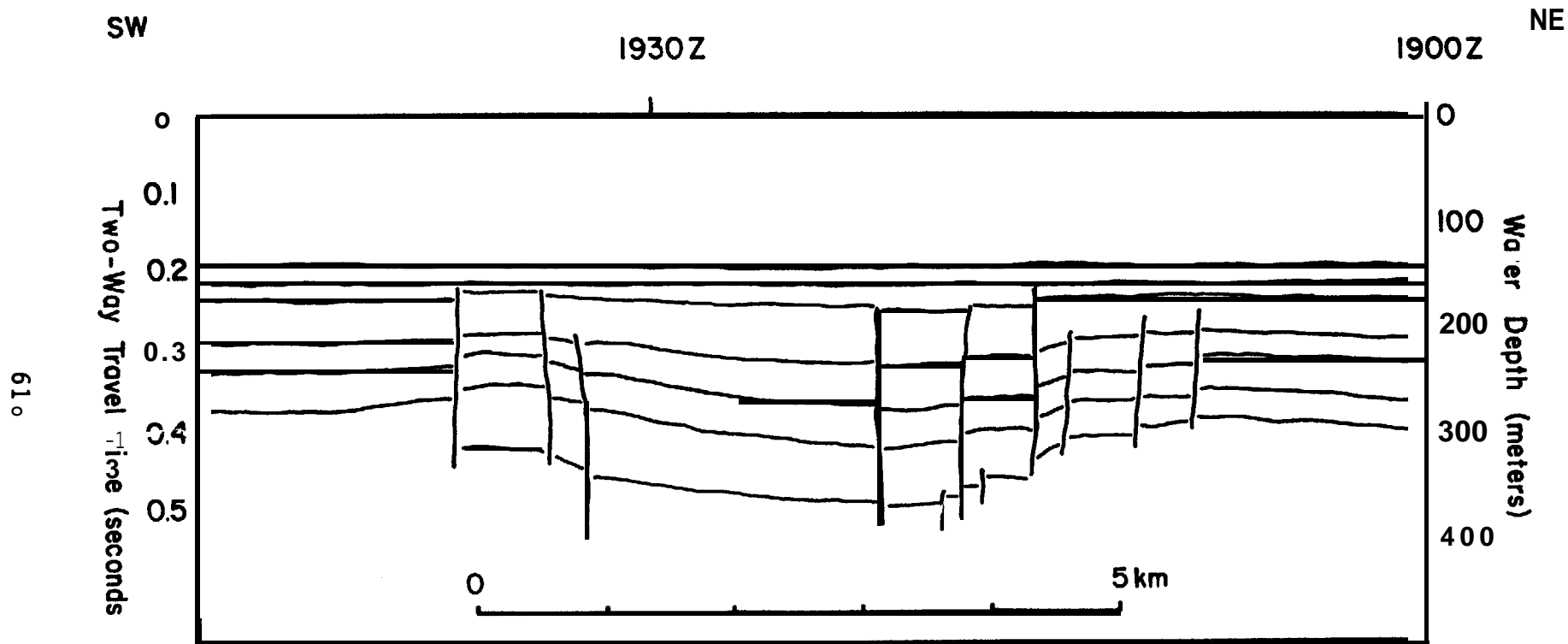


Fig. F9 — Interpretive line drawing of air-gun profile across graben in Navarin Basin province (see Fig. F2) (V.E. 'x8.5).

attain thicknesses of 1-2 m in the northern part of the area.

Earthquakes appear to be rare in the Navarin area however, some shallow faults may cut Holocene sediment and reach to within 3 m of the sea floor. These faults must be considered to be active and that activity should be accounted for in design plans for sea-floor structures.

#### ACKNOWLEDGMENTS

We acknowledge the assistance provided by the officers, crew, and scientific parties of the NOAA ship discoverer, the USCG Polar Star and the USGS R/V S.P. Lee. This paper has benefited from discussion with Homa J. Lee and from constructive reviews by Monty A. Hampton and William R. Normark. We thank La Vernne Hutchison for typing the manuscript.

This study was funded jointly by the U.S. Geological Survey and by the Bureau of Land Management through interagency agreement with the National Oceanic and Atmospheric Administration, as part of the Outer continental Shelf Environmental Assessment Program.

#### REFERENCES CITED

- Askren, D. R., 1972, Holocene stratigraphic framework, southern Bering Sea continental shelf: MS thesis, Univ. of Washington, 104 p.
- Blunt, D. J. and Kvenvolden, K. A., 1981, A preliminary report on amino acid diagenesis in fossil mollusks recovered from the Navarin Basin province, Bering Sea, in Carlson, P. R. and Karl, H. A., eds., Seafloor geologic hazards, sedimentology, and bathymetry: Navarin Basin province, northeastern Bering Sea: U.S. Geological Survey Open-File Report 81-1217, 149 p.
- Brewer, W. A., Jr., Bearby, H. W., Wise, J. L., Diaz, H. F., and Prechtel, A. S., 1977, Climatic atlas of the outer continental shelf waters and coastal regions of Alaska, vol. II, Bering Sea, NOAA OCSEAP Final Report-RU 347, 443 pp.
- Carlson, P. R. and Karl, H. A., 1981, High-resolution seismic reflection profiles: Navarin Basin province, Northern Bering Sea, 1980: U.S. Geological Survey Open-File Report 81-1221, 4 p., map, scale 1:1,000,000.
- Cooper, A. K., Scholl, D. W., and Marlow, M. S., 1976 Plate tectonic model for the evolution of the Bering Sea basin: Geological Society of America Bulletin, v. 87, p. 1119-1126.
- Gibson, R. E. 1958, The progress of consolidation in clay layer increasing in thickness with time: Geotechnique, v. 8, p. 171-182.
- Hampton, M. A., Bouma, A. H., Sangrey, D. A., Carlson P. R., Molnia, B. F., and Clukey, E. C., 1978, Quantitative study of slope instability in the Gulf of Alaska: Proceedings of the 1978 Offshore Technology Conference, p. 2307-2318.
- Ivanhoe, L. F., 1981, Bealce will increase operating costs in Alaska's Bering Sea waters: Oil and Gas Journal, October 26, 1981, p. 267-268.
- Karl, H. A., Carlson, P. R., Fischer, J., Johnson, X., and Lamb, B., 1981, Textural variations and composition of bottom sediment, in Carlson, P. R. and Karl, H. A., eds., seafloor geologic hazards, sedimentology, and bathymetry: Navarin Basin province, northwestern Bering Sea: U.S. Geological Survey Open-File Report 81-1217, 149 p.
- Nebel, H. J., 1972, Holocene sedimentary framework of the east-central Bering Sea continental shelf: Ph.D. thesis, Univ. Washington, Seattle, 186 p.
- Comar, P. A., Neudeck, R. H., and Kulm, L. D., 1972, Observation and significance of deep-water oscillatory ripple marks on the Oregon continental shelf, in Swift, D. S. P., Duane, D. B., and Pilkey, O. K., eds., Shelf sediment transport: process and pattern: Dowden, Hutchinson and Ross, Inc., Stroudsburg, Pa., p. 601-619.
- Lisitsyn, A. P., 1966, Recent sedimentation in the Bering Sea (in Russian): Inst. Okeanol. Akad. Nauk USSR, (translated by Israel Program for Scientific Translation, available from U. S. Dept. Commerce, Clearinghouse for Fed. Sci. and Tech. Info., 1969, 614 pp.).
- Marlow, M. S., Carlson, P. R., Cooper, A. X., Karl, H. A., McLean, H., McMullin, R., and Lynch, M. B., 1981, Resource report for proposed OCS sale number 83 Navarin Basin, Alaska: U. S. Geological Survey Open-File Report 81-252, 82 p.
- Marlow, M. S., Scholl, D. W., Cooper, A. K., and Buffington, E. C., 1976, structure and evolution of Bering Sea shelf south of St. Lawrence Island: American Association of Petroleum Geologists Bulletin, v. 60, p. 161-183.
- McRoy, C. P. and Goering, J. J., 1974, The influence of ice on the primary productivity of the Bering Sea, in Hood, D. W. and Kelley, E. J., eds., Oceanography of the Bering Sea with Emphasis on Renewable Resources: Univ. of Alaska, Fairbanks, Alaska, p. 403-419.
- Meyers, H., 1976, A historical summary of earthquake epicenters in and near Alaska: N.O.A.A. Tech. Memorandum EDS NGSDC-1, 80 p.
- Nardin, T. R., Hein, F. J., Gorsline, D. S., and Edwards, B. D., 1979, A review of mass movement processes, sediment and acoustic characteristics, and contrasts in slope and base-of-slope systems versus canyon-fan-basin floor systems, in Doyle, L. J. and Pilkey, O. H., eds., Geology of Continental Slopes: Society of Economic Paleontologists and Mineralogists, Special Publication No. 27, p. 61-73.
- Nelson, Hans, Kvenvolden, K. A. and Clukey, E. C., 1978, Thermogenic gases in near-surface sediments of Norton Sound, Alaska: Proceedings of the 1978 Offshore Technology Conference, p. 2623-2633
- Scholl, D. W., Buffington, E. C., and Marlow, M. S., 1975, Plate tectonics and the structural evolution of the Aleutian-Bering Sea region, in Forbes, R. B., ed., Contributions to the geology of the Bering Sea basin and adjacent regions: Geological Society of America Special Paper 151, p. 1-32.

Seed, H. B. and Lee, K. L., 1966, Liquefaction of saturated sands during cyclic loading: *American Soc. Civil Engineers Proc., Journal of Soil Mechanics and Foundation Division* v. 92, no. SM6, p. 105-134.

Seed, H. B. and Rahman, M. S., 1978, Wave-induced pore pressure in relation to ocean floor stability of cohesionless soils: *Marine Geotechnology*, v. 3, p. 123-150.

Sharma, G. D., 1979, The Alaska shelf, hydrographic, sedimentary, and geochemical environment: Springer-Verlag, New York, 498 p.

Shepard, F. P., 1963, Submarine geology: 2nd. ed. New York, Harper, 557 p.

Takenouti, A. Y. and Ohtani, K., 1974, Currents and water mesee in the Bering Sea: a review of Japanese work, in Hood, D. W. and Kelley, E. J., eds., *Oceanography of the Bering Sea*: Univ. Alaska, Inst. Marine Science, Occas. Publ. 2, p. 39-57.

U. S. Geological Survey, 1977, An investigation of Pennzoil's blow-out and loss of platform: U. S. Geological Survey Unpublished Administrative Report, 22 p.

Vogel, T. H. and Kvenvolden, K. A., 1981, Hydrocarbon gases in Navarin Basin province sediments, in Carlson, P. R. and Karl, H. A., eda., *Seafloor geologic hazards, sedimentology, and bathymetry: Navarin Basin province, northwestern Bering Sea*: U.S. Geological Survey Open-File Report S1-1217, 149 p.

Vogel, T. H., Kvenvolden, K. A., Carlson, P. R., and Karl, H. A., 1981, Geochemical prospecting for hydrocarbons in the Navarin Basin province: *American Association of Petroleum Geologists Bulletin*, v. 64, no. 4.

Webster, B. D., 1979, Ice edge probabilities for the eastern Bering Sea: N.O.A.A. Technical Memorandum NWS AR-26, 20 p.

Whelan, T., Coleman, J. H., Roberts, H. H., and Suhayda, J. N., 1976, The occurrence of methane in recent deltaic sediments and its effect on soil stability: *Bulletin of the International Association of Engineering Geology*, No. 14, p. 55-64.

TABLE F1. Summary consolidation data of near-surface\* sediment

Core	$\sigma_{vm}'$ (kPa)	$\sigma_v'$ (kPa)	( $cm^2/s\% \times 10^3$ )	OCR	Physiographic Province
G31	20	6.8	1.5 (120)	3	Shelf
G34	28	7.0	--	4	Canyon
G61	27	4.5	0.5 (120)	6	Shelf
G74	25	9.2	3.5 (165)	3	slope
G78	95(58)	4.3(58)	--	22	Shelf
G97	30	5.0	0.5 (190)	6	Canyon
Gill	60	6.5	1.0	9	Shelf

\* values at 100 cm subbottom depth except where shown in parentheses (e.g., (58) = 58 cm subbottom).

$\sigma_{vm}'$  = maximum peat pressure

$\sigma_v'$  = effective overburden stress

$c_v$  = coefficient of consolidation

OCR = overconsolidation ratio

APPENDIX G:

PUZZLING FEATURES IN THE HEAD OF **NAVARINSKY** CANYON,  
BERING SEA

by

Paul R. Carlson, Herman **A.** Karl, and Brian D. Edwards

U.S. Geological Survey

# Puzzling Features in the Head of Navarinsky Canyon, Bering sea

by

Paul R. Carlson, Herman A. Karl, and Brian D. Edwards  
U.S. Geological Survey  
Menlo Park, California 94025

## ABSTRACT

TWO types of morphologic features mapped in the head of Navarinsky Canyon are attributed to mass movement of the near-surface sediment. A series of pull-aparts(?) is located downslope of a field of large sand waves. These pull-aparts(?), possibly induced by liquefaction, affect the upper 5-10 m of sandy sediment in water depths of 350-600 m on a 1° slope. A hummocky elongate mound of muddy sand in water depths of 550-800 m that contains chaotic, disrupted internal reflectors to a subbottom depth of 30-40 m is believed to be the product of a shallow slide. We speculate that Holocene seismicity is the likely triggering mechanism.

## INTRODUCTION

Mass movement has been an important process in the evolution of the world's continental margins [1-3]. As coverage of frontier areas is increased, so is knowledge of the various forms of mass movement that are continually at work modifying the continental slopes.

The purpose of this report is to illustrate and discuss two puzzling types of mass-movement features discovered in the head of Navarinsky Canyon, one of the largest (4,900-km<sup>3</sup> volume) of the large canyons incised into the continental margin of the Bering Sea [4,5] (Fig. G1).

The study area is a part of the Navarin Basin province, a potential petroleum province that is scheduled for leasing in 1984. The Navarin Basin contains as much as 12 km of Tertiary and Cretaceous sedimentary strata [6], and thus has stimulated the interest of the petroleum industry. Understanding of the mass movement processes on the upper slope will be vital to the safe siting of sea-floor structures in water depths of >150 m.

### Data Collection

Seismic-reflection profiles and sediment samples (Fig. G1) discussed in this report were collected in 3 successive years of reconnaissance geohazards studies in the Navarin Basin area [7, 8]. Seismic systems included 20-80-in airguns, a 500-1000-J minisparker, a hull-mounted Uniboom\*, and 3.5 kHz, and 12 kHz sound sources. Seafloor-sediment samples were collected primarily

\*Any use of trade names in this publication is for descriptive purposes only and does not constitute endorsement by the U.S. Geological Survey.

with a gravity corer (8-cm-diameter barrel) ; supplementary samples were obtained with box corer and **vibra-corer** and a Van **Veen\*** grab sampler.

#### MORPHOLOGY OF CANYON HEAD

**Navarinsky** Canyon is the northernmost of the large canyons that dissect the Bering continental margin (Fig. G1). The U.S.-U.S.S.R. 1867 convention line nearly bisects this canyon, which heads in 150 m of **water**; the canyon extends 270 km across the slope at an average axial gradient of 0.50, where it debouches onto the continental rise at a depth of 3,200 m [9]. **Navarinsky** Canyon is cut into the extremely flat Bering shelf, which has a gradient of 0.040-0.10 [9]. The head of the canyon is a broad shallow amphitheater-shaped depression that covers an area of 16,600 km<sup>2</sup>. The study area is in the head of the canyon between the two main **thalwegs**, both of which have axial gradients of 0.2° to a depth of 400 m and steepen to ~1° between 400- and 1,000-m depth [9].

Within the head of **Navarinsky** Canyon, we mapped a field of large **bedforms** (1,000- km<sup>2</sup> area) that is bounded by the 200-400-m **isobaths** and has a seafloor gradient of 0.6° (Fig. G2). These **bedforms** have wavelengths of 600 m, heights of 5-15 m, and appear on seismic-reflection records as a stack of climbing dunes that extend to a subbottom depth of 75-100 m (Fig. G3b). Grab samples, box cores, and vibracores collected in the **bedform** field all recovered moderately well-sorted very fine to fine **sand**. We speculate that the sand in these large **bedforms** was transported to its present site near the shelf break during Pleistocene low stands of sea level. At that time, the shoreline was near the present 130-140-m isobath and large rivers meandered across the broad flat subaerial reaches of the **Bering** shelf [10]. Calculations that take into account the **bathymetry**, sea-floor gradient, present water depth, sediment type, and oceanographic **conditions** suggest that these large sand waves are possible products of internal waves [11].

#### TYPES OF MASS MOVEMENT

Seismic-reflection records from the head of **Navarinsky** Canyon show two kinds of seafloor irregularities that we interpret to be the result of mass movement. These mass-movement phenomena include: (1) depression or pull-apart-like features that adjoin and overlap the field of large **bedforms**, and (2) a mound or ridge-shaped mass of slide debris. Figures G2 and G3 show the areal relations of all three features -- **bedforms**, **pull-aparts**, and slide mass.

#### Pull-aparts?

High-resolution seismic-reflection profiles show some unusual breaks in the surface sediment downslope from the **bedform** field (Figs. G2, G3a, G3c). These features are irregularly spaced depressions or notches in the seafloor, 0.1 - 2.0 km apart; they average ~50 m wide, have a relief of 3-5 m, and appear to affect only the upper 5-10 m of sediment (Fig. G3c). Absence of side-scan-sonar coverage prevents determination of the true shape of these features; however, the notches are more abundant on lines perpendicular rather than parallel to the **isobaths**, and thus the notches appear to be

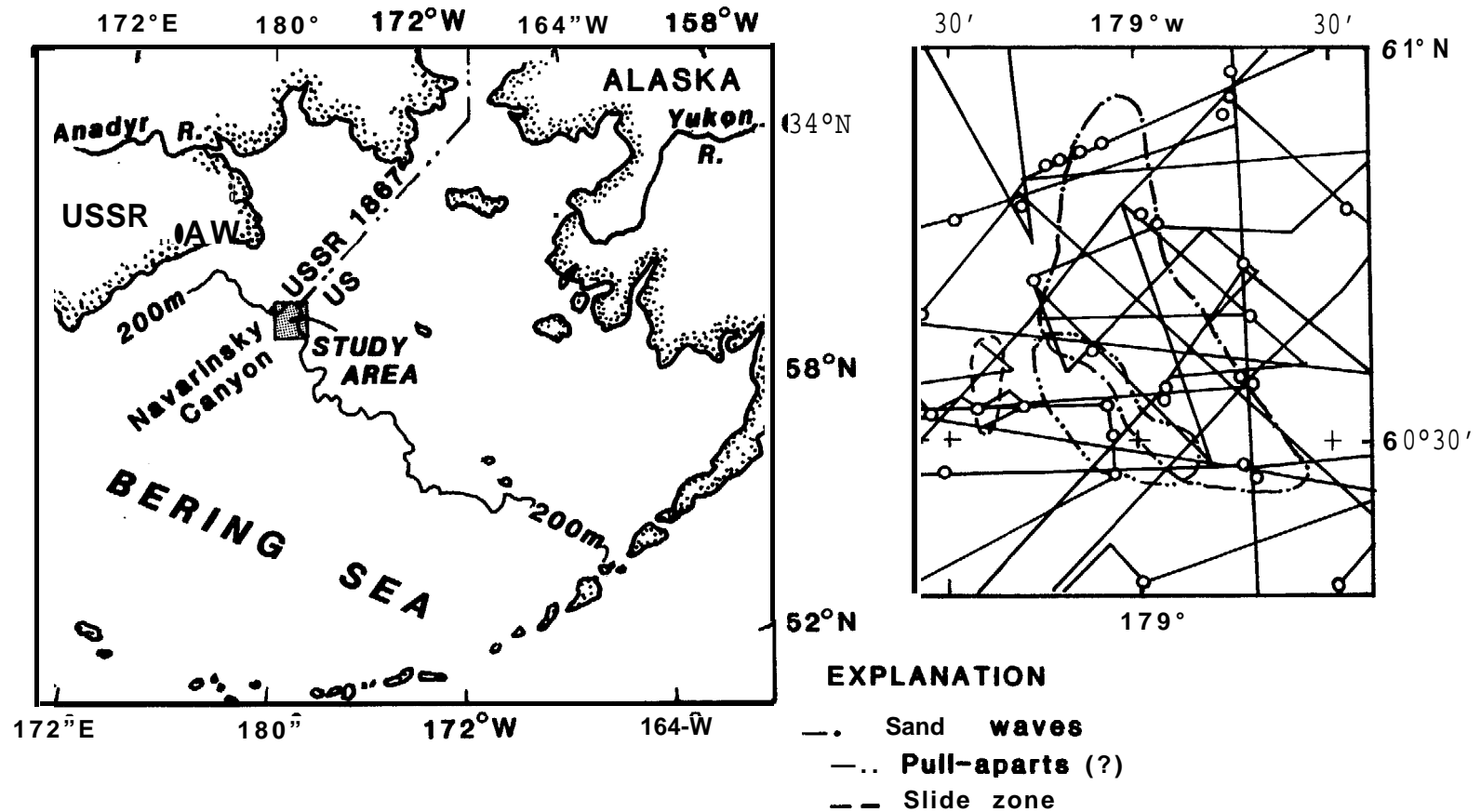


Figure G1. Sketch map of study area in northern Bering Sea, showing locations of high-resolution seismic-reflection lines, sample stations, and areas of seafloor features.

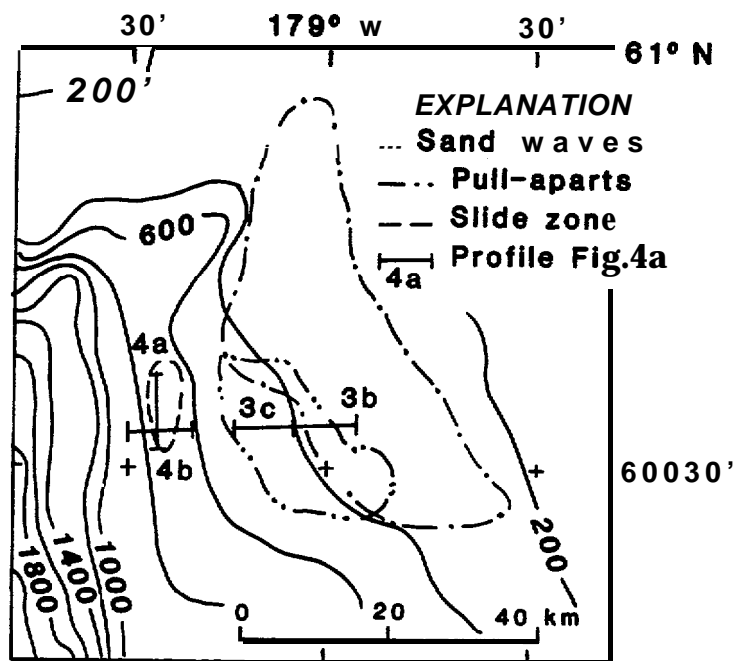


Figure G2. Seafloor morphologic features in head of Navarin sky Canyon, showing locations of illustrated profiles. Bathymetry after Fischer and others, 1982. Contour interval, 200 m.

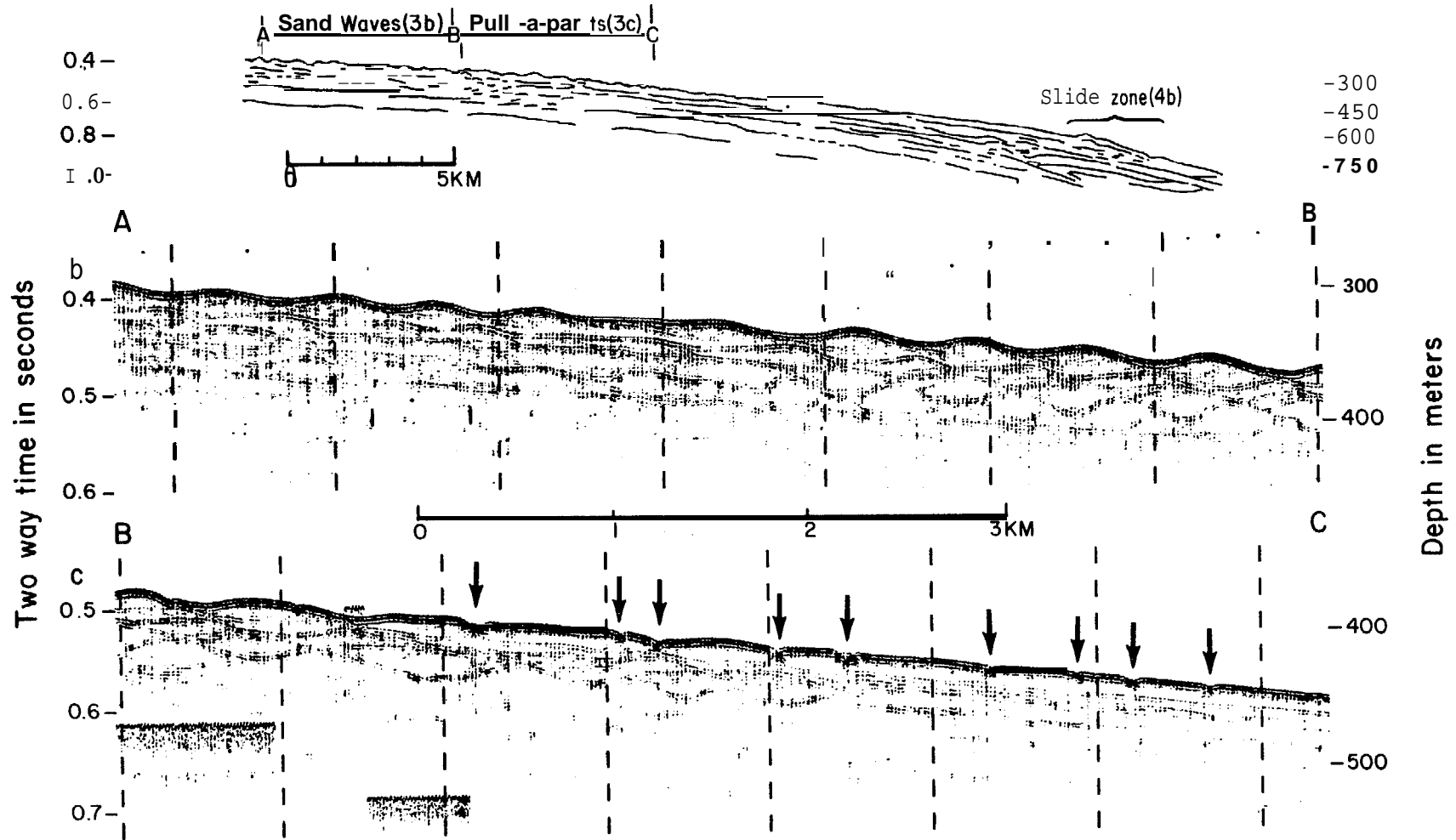


Figure G3. Seismic-reflection profiles in head of Navarinsky Canyon. (a) Line drawing of seismic-reflection profiles (20-40-in<sup>3</sup> airguns), showing relative positions of profiles in Figures G3b, G3c, and G4a. (b) Minisparker profile (1,000 J), showing sand waves. (c) Minisparker profile (1,000 J), showing pull-aparts (arrows). Vertical exaggeration (V.E.) 7.5x. See Figure G2 for locations.

oriented parallel to the **isobaths**. The notches, which are situated between the 350- and 600-m **isobaths** on a slope of  $1^\circ$ , have been mapped over an area of 300  $\text{km}^2$  (Fig. G2). The sediment in this part of the canyon is moderately well-sorted muddy to fine sand containing some pebbles and granules.

The zone of depressions, notches, or breaks in the surface sediment downslope from the field of large **bedforms** has the appearance and apparent orientation of **pull-aparts** or tensional breaks that may result from downslope flow. Another possibility is that these features are shallow craters, pockmarks, or sand boils formed by expulsion of "liquefied" sediment. The zone of **pull-aparts** or depressions overlaps the downslope side of the **bedform** field and thus has developed after the formation of the **bedforms** and may be continuing to develop at the present time.

### Slide Zone

An elongate mound-shaped mass of sediment of **hummocky** surface morphology that occupies an area of  $\sim 50 \text{ km}^2$  is situated 4-5 km downslope from the area of surface breaks (Figs. G2, G3a). The **hummocky** mound of muddy sand has the characteristics commonly associated with a submarine slide mass. This elongate mound is 3 by 14 km, and its long axis is oriented obliquely to the 550-800-m **isobaths**. The mound has a relief of 10-15 m', contains chaotic internal reflectors, affects the upper 30-40 m of **sediment**, and has formed where the slope gradient of the canyon changes from  $1.1^\circ$  to  $2.6^\circ$  (Fig. G4). Although some seismic-reflection profiles show jumbled and broken reflectors **within** the mound of sediment, all the profiles show well-developed relatively continuous reflectors beneath the mound, starting at a **subbottom** depth of 40 m (Fig. G4). Both **upslope** and **downslope** from the mound the internal reflectors are also continuous at all levels beneath the seafloor.

The **hummocky** mound of muddy sand that is apparently a product of a shallow slide (Figs. G3a, G4) may have been caused by liquefaction, as postulated for the formation of the **pull-aparts**, or else these features may have formed totally independently.

### TRIGGERING MECHANISM

To generate the types of mass movement that have occurred in the head of Navarinsky Canyon, both a supply of sediment and a mechanism to trigger the mass movement are necessary. The present rate of sediment accumulation on the outer **Navarin** shelf is relatively low ( $< 20 \text{ cm}/1,000 \text{ yrs}$  on the basis of <sup>14</sup>C ages; see ref. [12] ) because of the great distance ( $> 400 \text{ km}$ ) to the nearest river mouth. The rate of sediment accumulation must have been high during low stands of sea level, however, when large rivers, such as the ancestral **Anadyr** and Yukon, crossed the subaerially exposed shelf. When the rate of sediment accumulation is rapid, **high** pore-water pressures can develop and cause sediment instability [13, 14]. Although underconsolidation may be responsible for some of the sediment instability along parts of the Navarin margin, **underconsolidation** is unlikely in the head of **Navarinsky** Canyon because the sediment there is primarily noncohesive and pore-water drainage and **pressure equalization** are presumably rapid.

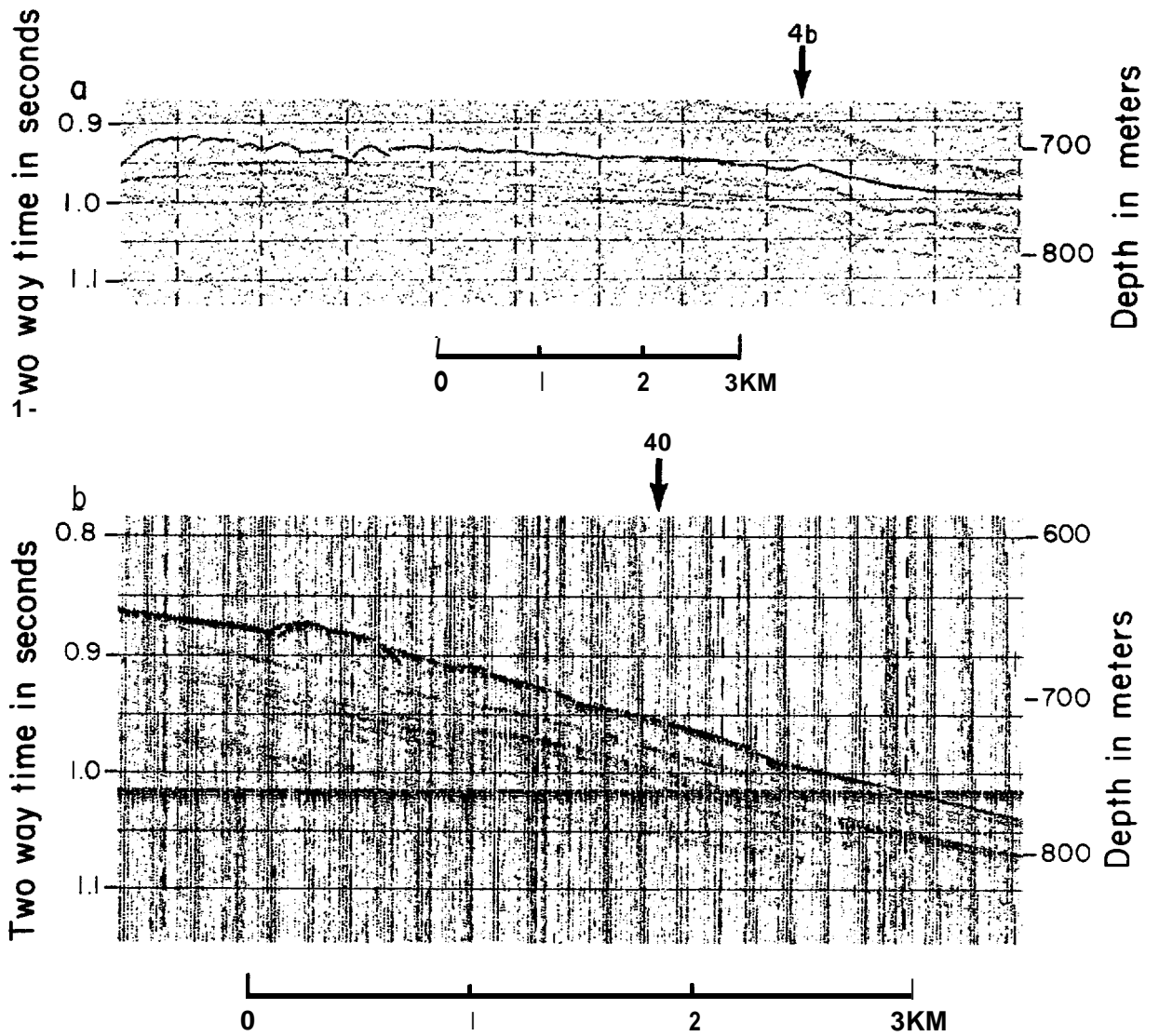


Figure G4. High-resolution profiles, showing slide zone in Navarinsk Canyon. (a) 3.5 kHz profile; V.E. '10X. (b) Uniboom profil (1200 J); V.E. '7.5x. See Figure G2 for locations.

The Bering Sea is a region of severe storms in which winds commonly exceed 100 km/h (62 **mi/h**) and, **at** times, exceed 165 km/h (103 **mi/h**); waves generated by storms **of** this magnitude may be as high as 15-20 m [15]. In the head of Navarinsky Canyon, the **cohesionless** sediment **in** the area of the **pull-aparts** and in the slide zone is presently in water depths of 350 m and probably was **at >200-m** depth during Pleistocene low stands of sea level. On the basis of wave-theory calculations according **to** the procedures of Seed and Rahman (1978), the **cohesionless** sediment in these areas would not appear to be vulnerable to cyclic loading from large storm waves. Thus, storm waves, either at present or during Pleistocene low stands **of** sea level, are an unlikely triggering mechanism for the observed failures.

Karl, and others [11] have shown that internal tides and higher frequency internal waves possibly formed the large **bedforms** in the head of Navarinsky Canyon. Whereas Karl and others [11] determined that energy from 4- and 12-h period internal waves **is** amplified in the sand-wave field and just downslope from this **field**, the **cohesionless** nature of the sediment and the small density contrasts across the **pycnocline** make internal waves an unlikely triggering mechanism for the **mass-movement** phenomena farther downslope.

Although the Aleutian Island arc is seismically **active** [17], the great distance (1,000 km) between the Aleutians and **Navarinsky** Canyon minimizes the effect of horizontal accelerations associated with ground shaking because accelerations drop off rapidly with distance from the epicenter [18]. Even a great (**M>8**) earthquake occurring along the Aleutian Island arc would likely cause low accelerations in the Navarinsky Canyon. Additional, Sereda (1980) located the epicenters for two small (**M<4**) earthquakes at Cape Navarin, U.S.S.R. Even these events, however, were **>200** km from the head of **Navarinsky** Canyon and thus would have had little effect on the canyon sediment. **Seismicity** in the northern Bering Sea has been minimal over the past 85 **years**. Only **eight** earthquakes have had epicenters within a radius of 200 km of the study area, all of which were of **M<5.8** [17]. On the basis of empirical evidence, for events of this magnitude to cause sediment flow or liquefaction on the Navarinsky slope the epicenter must be within '30 km [20]. Even **though** we find little evidence **in** the modern seismologic record to support earthquakes as a triggering mechanism, a few traces of shallow faults have been mapped in the head of **Navarinsky** Canyon [21]. Although none of **these** faults shows offset of the seafloor, all appear to cut sediment as young as Holocene and therefore are considered to be active.

We conclude that earthquakes are the most likely triggering mechanism. In spite of the **sparsity** of local seismic events in the historical record, we note that our data base covers less than **100 years**, and the features under discussion could have formed anytime in the past several thousand years. Thus, the odds of an **M> 6.0** event occurring in the proximity **of** Navarinsky Canyon and possibly causing **liquefaction** of the **cohesionless** sediment are greatly improved.

#### ACKNOWLEDGMENTS

We thank Monty Hampton, David Keefer, and Homa Lee for their constructive reviews of the manuscript. This study was supported by the U.S. Geological Survey and the U.S. **Bureau** of Land Management through interagency agreement with the U.S. National Oceanic and Atmospheric Administration.

## REFERENCES

- [1.] Moore, **D. G.**, 1977. Submarine slides. In **B. Voight**, (ed.), **Rockslides and Avalanches**, vol. 1, **Natural Phenomena**. Amsterdam, **Elsevier**: p. 563-604.
- [2.] **Nardin**, T. J., **Hein**, F. J., **Gorsline**, D. S., and **Edwards**, B. D., 1979. A review of mass movement processes, sediment and acoustic characteristics, and contrasts in slope and base-of-slope systems versus canyon-fan-basin floor systems. In **L. J. Doyle** and **O. H. Pilkey**, (eds.), **Geology of Continental Slopes**. Society of Economic Paleontologists and Mineralogists Special Publication 27, p. 61-73.
- [3.] **Cook**, H. E., **Field**, M. E., and **Gardner**, J. V., 1982. Characteristics of sediments on modern and ancient continental slopes. In **P. A. Scholle**, and **D. Spearing**, (eds.), **Sandstone Depositional Environments**: American Association of Petroleum Geologists Memoir 31 p. 329-364.
- [4.1] **Scholl**, D. W., **Buffington**, E. C., **Hopkins**, D. M., and **Alpha**, T. R., 1970. The structure and origin of the large submarine canyons of the Bering Sea. *Marine Geology*, v. 8, p. 187-210.
- [5.] **Carlson**, P. R., **Karl**, H. A., and **Quinterno**, Paula, 1982. **Sedimentologic** processes in **world's** largest submarine canyons, Bering Sea, Alaska. *Geological Society of America, Abstracts with Programs*, v. 14, no. 7, p. 459-460.
- [6.] **Marlow**, M. S., **Scholl**, D. W., **Cooper**, A. K., and **Buffington**, E. C., 1976. Structure and evolution of Bering Sea shelf south of **St. Lawrence** Island. *American Association of Petroleum Geologists Bulletin*, v. 60, p. 161-183.
- [7.] **Carlson**, P. R. and **Karl**, H. A., 1981. Seafloor geologic hazards, **sedimentology**, and **bathymetry**; **Navarin** Basin province, northern Bering Sea. U.S. Geological Survey Open-File Report 81-1217, 149 p.
- [8.] **Karl**, H. A. and **Carlson**, P. R., 1983. Seafloor Hazards and Related **Surficial** Geology, Navarin Basin Province, Northern Bering Sea. U.S. Geological Survey Open-File Report **83-** , in press.
- [9.] **Fischer**, J. M., **Carlson**, P. R., and **Karl**, H. A., 1982. Bathymetric map of Navarin continental margin, Bering Sea. U.S. Geological Survey Open-File Report 82-1038, 11 p., 1 map sheet **1:1,000,000**.
- [10.] **Karl**, H. A., **Carlson**, P. R., and **Lamb**, B., 1982. Sediment **waves** in the head of **Navarinsky**, **Pervenets**, and **Zhemchug** submarine canyons, northwestern Bering Sea. U.S. Geological Survey Circular (Accomplishments in Alaska) 844, p. 141-143.

- [11.] Karl, H. A., **Cacchione**, D. A., and Carlson, P. R., 1982. Large sand waves in canyon heads, Bering Sea: Products **of internal** waves or density currents?. **International** Association of Sedimentologists, 11th International Congress on **Sedimentology**, Hamilton, Ontario, Canada, p. 73.
- [12.] **Carlson**, P. R. and Karl, H. A., 1983. Rates of sediment accumulation in Navarin Basin province, Bering Sea. In: H. A. Karl and **P. R. Carlson, (eds.)**, Seafloor Hazards and Related **Surficial** Geology, Navarin Basin Province, Northern Bering Sea. U.S. Geological Survey Open-File Report **83-** in press.
- [13.] **Morgenstern, N., 1967.** Submarine slumping and the initiation of turbidity currents. In A. F. Richards, (cd.), Marine Geotechnique. **Urbana**, Ill., University of Illinois Press, p. 189-220.
- [14.] Hampton, M. A., **Bouma**, A. H., Carlson, P. R., **Molnia**, B. F., **Clukey**, E. C., and **Sangrey**, D. A., 1978. Quantitative study of slope instability in the Gulf of Alaska. 10th Offshore Technology Conference, Houston, Texas, Proceedings, v. 4, p. 2307-2318.
- [15.] **Brower, W. A., Jr . ,** Searby, H. W., Wise, J. L., Diaz, H. F., and Prechtel, A. S., 1977. Climatic atlas of the outer continental shelf **waters** and coastal regions of Alaska, v. II, Bering Sea. NOAA OCSEAP Final Report RU **347**, Arctic Environmental Information and Data Center, Anchorage, Alaska, Publication **B-77**, 443 p.
- [16.] Seed, H. B., and **Rahman**, M. S., 1978. Wave-induced pore pressure in relation to ocean floor stability of **cohesionless** soils. **Marine Geotechnology**, v. 3, p. 123-150.
- [17.] **Meyers, H., 1976.** A historical summary of earthquake epicenters in and near Alaska. National Oceanographic and Atmospheric Agency. Technical Memorandum EDS **NGSDC-1**, 80 p.
- [18.] **Joyner, W. B., and Boore, D. M., 1981.** Peak horizontal acceleration and velocity from strong-motion records including records from the 1979 Imperial Valley, California, earthquake. Bulletin Seismological Society of America, v. 71, p. 2011-2038.
- [19.] Sereda, L. I., 1980. Systems of deep-seated faults in the northeast U.S.S.R. **Geotectonics**, v. 14, p. 151-160.
- [20.] Keefer, D. K. 1983. Landslides caused by earthquakes. Bulletin Geological Society of America, in press.
- [21.] **Carlson**, P. R., Karl, H. A., Fischer, J. M. and Edwards, B. D., 1982. Geologic hazards in Navarin Basin province, northern Bering Sea. 14th Offshore **Techology** Conference, Houston, **Tex.**, Proceedings, v. 1, p. 73-87.

APPENDIX H:

LARGE SAND WAVES **IN** SUBMARINE CANYON HEADS, BERING SEA:

PRELIMINARY HYPOTHESIS OF THEIR DEPOSITIONAL HISTORY

by

Herman A. Karl and Paul R. **Carlson**

U.S. Geological Survey

## ABSTRACT

Sand waves occur in the heads **of** large submarine canyons in the northwestern Bering Sea. These sand waves **vary in height between ~5** to 15 m, and have wavelengths of 600 m. They are not only expressed on the seafloor, but are also well defined in the subsurface and resemble enormous climbing bed forms. we conjecture that the sand *waves originated* during lower stands of sea level in the Pleistocene. Although we cannot explain the mechanics of formation of the sand waves, internal-wave generated currents are among four types of current that could account for the sand waves.

## INTRODUCTION

We observed large bed forms in the heads of three enormous submarine canyons that incise the continental margin of the northern Bering Sea (Fig. Hi). Although similar in size and sediment composition to many of the large bed forms described by others, the depositional setting, internal stratification, and **stratigraphic** thickness of these bed forms combine to make these features unique among the bed forms heretofore reported in the literature [1,2,3,4,5]. The purpose of this paper is to describe these bed forms and to frame hypotheses about their depositional history and mode of formation.

### Regional Setting.

We investigated an **80,000-km<sup>2</sup>** area of the Bering Sea continental margin that lies about 100 km west of St. Matthew Island (Fig. HI). The **150-m** isobath delineates the northwest-trending **shelf** break that separates the broad, flat (average gradient of 0.02°) continental shelf from the rugged, steep (gradients range from 3° to 8°) continental slope. Three large canyons dissect the slope and outer shelf [6]. Navarinsky and **Zhemchug** Canyons are each about 100 km wide at the shelf break. Pervenets Canyon is about 30 km wide there. The canyons appear to be controlled by structures at least of Paleocene age [7], but we presume that the major canyon erosion occurred during lowered sea levels in the Pleistocene.

The closest point sources of sediment, the **Anadyr** River to the north in the U.S.S.R. and the Yukon River to the east in Alaska, are over 400 km from the study area. Surface sediments on the shelf and slope generally consist of silts and silty sands; however, there are zones of fine sand at the shelf break, on the upper slope, and in the heads of the submarine canyons [6].

Oceanographic data for this area of the Bering Sea is meager. The Bering Slope Current flows from southeast to northwest, paralleling the continental **slope** [8]. Circulation *on* the shelf is poorly understood. Investigation of the outer continental shelf of the southern Bering Sea indicates predominantly east-west tidal currents with little net flow [9]. Storms can generate waves large enough to affect sediment as deep as 200 m [6].

### Methods.

We collected seismic reflection profiles and sediment samples in the study area in the summers of 1980 and 1981 (Fig. Hi). Reconnaissance track

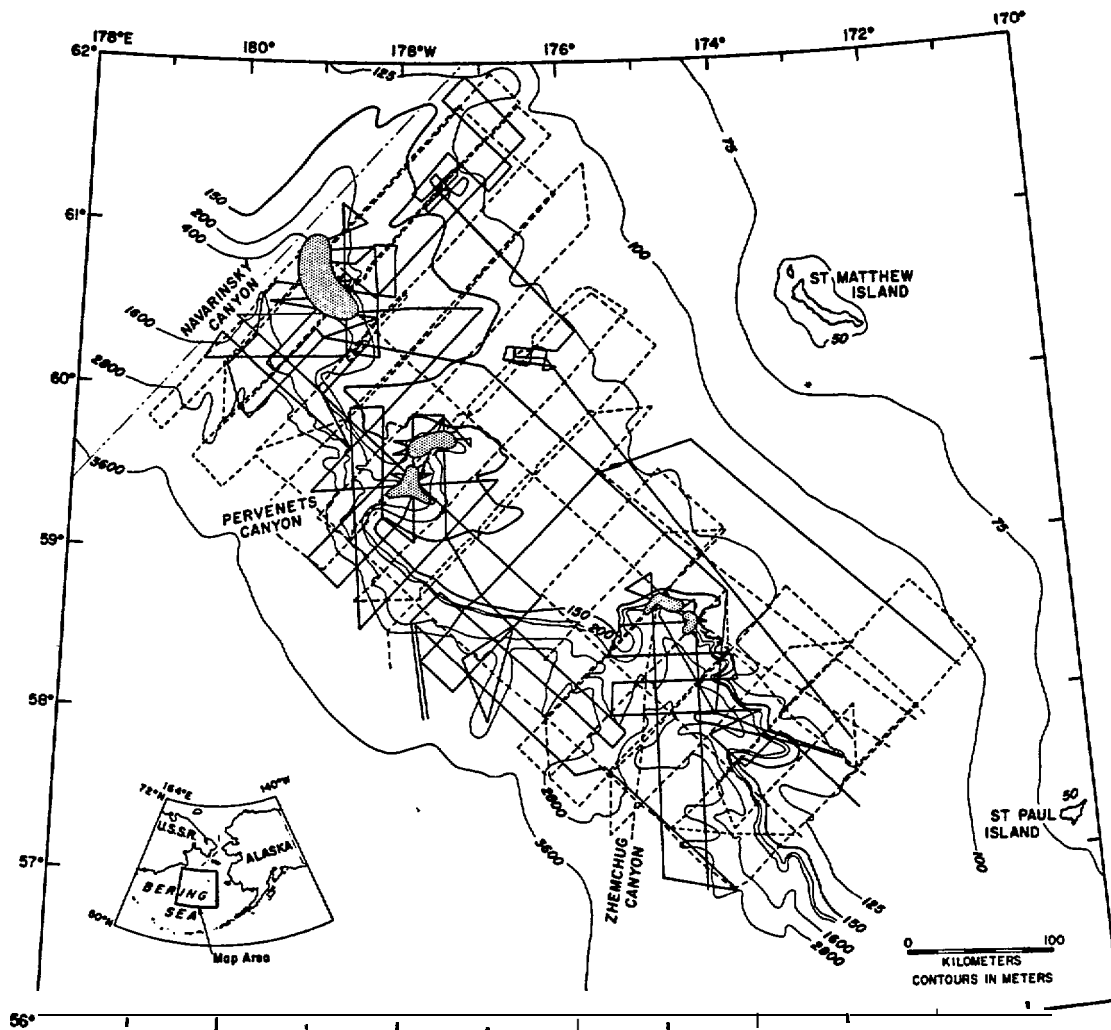


Figure H-1. **Map** of study area showing seismic survey **tracklines** and distribution of sand waves (stippled areas). Dashed lines are 1980 **tracklines** and solid lines are 1981 **tracklines**; 1981 data were collected during preparation of this manuscript; for clarity **tracklines** have **not** been shown within sand wave fields. The deeper sand wave area in Pervenets Canyon was defined almost entirely by buried bed forms.

lines were spaced 30 km apart in a rectilinear pattern; some areas were surveyed in greater detail. Sediment samples were taken at many alternate grid intersections and at sites chosen from seismic reflection profiles. Navigation was by Loran C updated by satellite.

#### OBSERVATIONS OF SAND WAVES

The surface sediment in the bed form area in the head of each of the submarine canyons (Fig. H1) is fine and very fine sand. Vibracores in the Navarinsky and Pervenets areas showed that sand comprised at least the upper 1.5 m of sediment. A box core collected in the Navarinsky area preserved the sediment at the water-sediment interface and revealed a thin (1-2 cm) layer of mud covering the sand.

A detailed survey of the sand waves in the head of **Navarinsky** Canyon disclosed that sand waves are confined within about a 1400 km<sup>2</sup> area between the 215- and 450-m isobaths. The area of the Pervenets sand wave fields is approximately 800 km<sup>2</sup> and that of the **Zhemchug** fields is about 400 km<sup>2</sup>. By measuring the apparent wavelengths of sand waves on three seismic lines that pass through the Navarinsky field at different azimuths and that nearly intersect in the southeastern corner of the sand wave field, we determined that the crests of the sand waves strike approximately north-south (**N5°E**), that the true wavelength is nominally 600 m, and that the heights vary from about 5 to 15 m. The sand waves are not only expressed on the seafloor, but also are remarkably well defined in the subsurface (Fig. H2). The stratigraphic unit containing the sand waves attains an aggregate thickness of 100-120 m and overlies flat, parallel reflectors. The cross-bedded unit thins to 10-15 m toward the northwestern boundary of the field, thins to about 70-90 m toward the southeastern margin, and appears to wedge out at the extreme southeastern corner of the field. The best developed sand waves occur in water depths of about 300-350 m. In shallower water the sand waves decrease progressively in amplitude, and in deeper water the bedforms often deteriorate into a "hummocky" morphology [10]. At least seven sets can be recognized in the thickest part of the section (Fig. H2). Individual cross-bedded pods within sets are as much as 20 m thick. The number of sets decreases as the unit thins. Both symmetric and asymmetric forms have been observed on the sea floor and in the subsurface. The steep faces of asymmetric waves and the internal stratification in this field have an apparent easterly dip.

#### DISCUSSION

The following discussion and conclusion pertain to the Navarinsky field sand waves, because we have investigated this field most thoroughly. We are *convinced* that the surface and buried Navarinsky field sand waves are **current-generated** bed forms; there is no evidence to justify the interpretation of these bed forms and cross-bedded sequences as foresets of prograding deltas or as slumps.

#### Mode of Formation.

Large sand waves and dunes on the continental shelf of about the same size as the Navarinsky sand waves have been attributed to **unidirectional** currents and to very strong tidal currents [1,11,12]. In **general, though,**

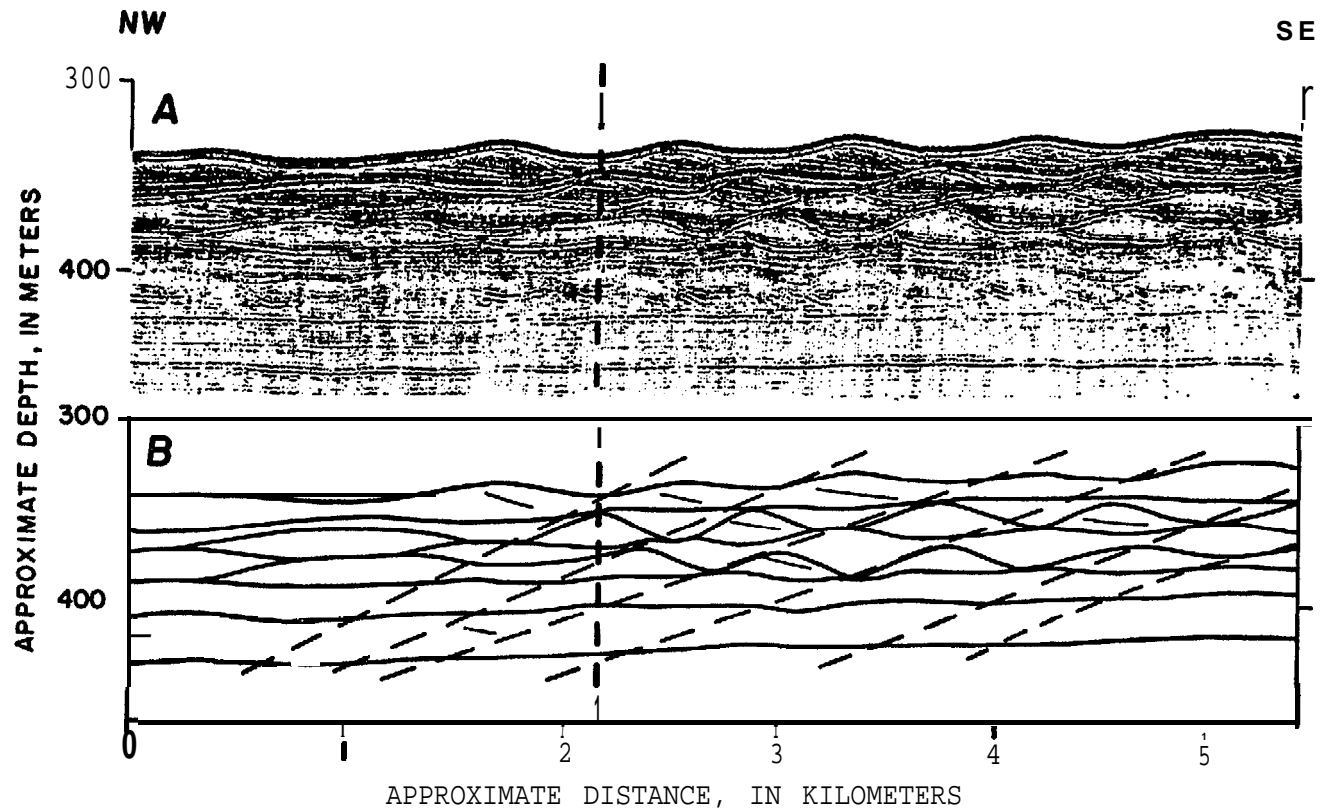


Figure H-2. Example of *Navarinsky Canyon* field sand waves; A, Mini-sparker record. B, Interpretive drawing; solid lines define sets of sand waves; dashed lines define angle of climb; heavy vertical dashed line is a recorder time mark.

these sand waves are more closely spaced and much more asymmetric than the Navarinsky field sand waves. Because of their sinusoidal form and low height-to-length ratio, the Navarinsky field sand waves are more closely analogous in form to those abyssal sediment waves that have been interpreted as antidunes formed by density currents -- that is to say, turbidity currents and strongly stratified flows [2,3]. However, the sand waves known to us that are most similar in shape and size to the Navarinsky field sand waves occur near the edge of the continental shelf off France in water depths of 150-160 m (La Chapelle bank); these sand waves range in height from about 8 to 12 m and are spaced about 850 m apart, and are thought to be caused by internal waves [4].

We do not know which (if any) of the four types of currents mentioned above - unidirectional, reversing unidirectional, density, and internal wave generated - is responsible for the Navarinsky field sand waves. Whichever mechanism or combination of mechanisms is responsible for the sand waves we observed, the mechanism must also explain four aspects of the sand wave fields: (1) distribution, (2) stratigraphic sequence, (3) lithology, and (4) size.

Given the uniformity of our seismic coverage of the study area, it is probably not by chance that we observed sand waves only in the heads of the submarine canyons; we think that the sand waves are causally associated with the submarine canyons. This suggests that there are processes that operate in submarine canyons that do not affect, at least as intensely, the nonincised outer shelf and upper slope. In order to deduce the mode of formation of the sand waves, it is necessary not only to identify these canyon-related processes, but also to determine whether the sand waves are active or relict features.

Using seismic reflection profiles, we have isopached the youngest stratigraphic unit in the study area [13]. The reflector defining the base of this unit is at least as old as  $30 \times 10^3$  yr [14]. We have been able to trace this reflector into the upper 10-20 m of the Navarinsky sand wave sequence; however, we cannot follow the reflector through the sand wave field (Carlson and Karl, unpublished data). The sets below this reflector are certainly relict and we speculate that those above are also older than Holocene.

Two lines of evidence support the interpretation that the uppermost set of sand waves is not active. First, no available oceanographic data indicate any strong or unusual currents that could generate the sand waves. Published oceanographic reports are based on summertime measurements, so we do not know the winter currents and circulation patterns; it is conceivable that conditions intensify sufficiently during the winter to activate the bed forms. However, we are not even sure that strong currents are required to generate the sand waves. Second, the thin layer of mud covering the sand waves and the absence of any evidence of small current ripples or other bedload grain movement suggest that the bed forms were not active at the time we observed them.

The thick stratigraphic sequence of bed forms in the Navarinsky Canyon field suggests that the processes responsible for the bed forms have operated over a long period of time and that a large amount of sand was delivered to the area during this period. The sequence of seven sets of cross-beds

resembles a greatly scaled-up sequence of climbing ripples (Fig. H2b). This analogy suggests continuously high rates of sedimentation during the formation of the 100-m-thick section. On the other hand, the seven sets appear to be stacked one on top of the other being separated by either non-depositional surfaces or strata draped over the sand wave surface (Fig. H2b); if this is **the** case, each set of sand waves was formed during a discrete period of activity that was followed by an interval of inactivity.

The sand waves on the surface, if inactive, remain unburied for at least **two** reasons. Only very small amounts of silt and clay are being deposited over the sand waves because the area is so great a distance from a significant sediment source; or currents in the area are sufficiently strong to inhibit deposition or to periodically remove the fine sediment that is currently being deposited; or both.

The fine and very fine sand in the canyon heads could result from the winnowing out of finer sediment by currents peculiar to the canyons. Clean sand and silty sand, however, composes the entire length of cores so long as 1.5 m, and it is not likely that this material was concentrated solely by winnowing. Major sources of sand lie hundreds of kilometers from the canyon heads. This sand could have been deposited at the canyon heads during lower stands of sea level in the Pleistocene, when **numerous** streams presumably flowed over the exposed shelf toward the topographically depressed canyon heads.

#### Conceptual **Model** of Depositional Environment.

**Most** workers estimate that the maximum eustatic lowering of sea level during the Pleistocene was 130 m [15]. A vast expanse of the Bering Sea continental shelf would have been exposed when the sea level was 130 m below the present mean sea level (Fig. H3) [16]. Pratt and **Dill** [17] have suggested sealevel stands as low as 240 m in the Bering Sea, but their interpretation is highly speculative. Hopkins [18] has synthesized the **sealevel** history of the Bering Sea during the last 250,000 years; one deduces that the **paleogeography** of the area is not reconstructed by simply lowering the sea level 130 m, because local tectonic and isostatic events complicate any reconstruction. Parts of the **Bering** Sea shelf may not have been tectonically stable during the Pleistocene (M. S. **Marlow**, U.S. Geological Survey, **pers. comm.**, 1981). **Moreover**, it is possible that the outer shelf could have rebounded **isostatically** after the removal of 130 m of water; in which case, the Pleistocene shoreline during the lowest stand of sea level would have been seaward of the present-day 130-m isobath. We cannot accurately determine the position of the Pleistocene shoreline, because the amount and rate of **isostatic** adjustment and the tectonic effects are unknown factors. Simply as a basis for discussion, then, let us take local sea level in our study area during the Pleistocene to have been 150 m below present sea level.

If local sea level in the Bering Sea was 150 m below the present mean sea level, much of the area of the canyon heads would have been large shallow **embayments** along the Pleistocene coastline (Fig. H3; note caption). **We use** the names of the three canyons to designate these embayments. Streams draining the lowlands adjacent to these canyons would have discharged large quantities of sediment into the three embayments. Owing to the low gradients of the

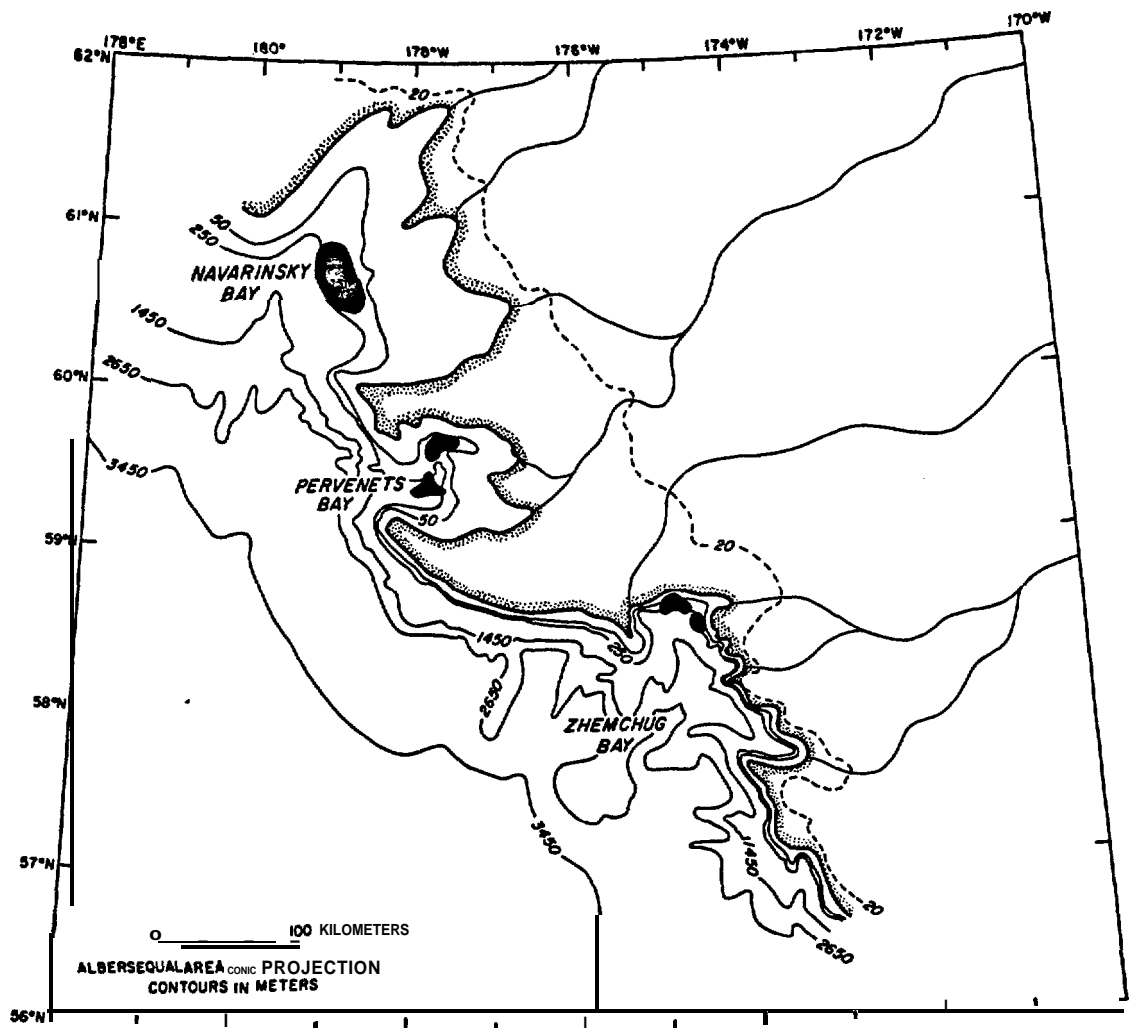


Figure H-3. Paleogeographic reconstruction of the depositional setting of the sand waves (stippled areas). Heavy solid line follows the present shelf edge and indicates the position of the Pleistocene shoreline assuming an arbitrary amount of tectonic and isostatic influence that caused local sea level to be 150 m below present sea level. Dashed line follows the present 130 m isobath. The area between these lines is that part of the shelf that would be submerged under 20 m of water assuming no local complications and only that sea level was lower ecstastically by 130 m. Presence of streams is speculative.

exposed shelf, the streams would not have been competent to carry coarse material, and most of the sediment entering the embayments would have been fine sand, silt and **clay**. Sand would have accumulated near shore and in shallow areas **of** the embayments and in the heads of the submarine canyons. Most of the silt and clay in suspension would have settled out farther from shore; waves and other strong currents would have winnowed out those silts and clays that had been deposited in shallow water. The fine-grained material could have been supplied in quantities sufficient to provide the concentrations necessary to produce a low-velocity density flow; the material settling out of this flow could form antidunes.

The canyons **would** have dominated the submarine physiography of the **embayments**. **Submarine** canyons influence coastal and shelf sediment dynamics in several important ways. Canyons that head close to shore trap sediment moving down current in the littoral drift [19]. Internal tides and other internal waves of higher frequency are **funnelled** along the axes of submarine canyons and are generated at the shelf break around canyon heads [20,21] . Thus, internal wave energy can be amplified in the canyons and can be concentrated on the adjacent shelf [22]. Southard and **Caccione** (1972) have shown in laboratory experiments that breaking internal waves can produce **bedforms**. Several studies present geologic evidence that suggests that currents and water circulation patterns modified by canyons do affect the movement of sediment on the **shelf** [5,24]. The **physiographic** configuration of the embayments and canyons also may amplify such water motions as the diurnal and **semidiurnal** tides [25]. Low-frequency reversing water motions generated by surface or internal tides could produce symmetric sand waves or breaking internal waves of higher frequency could generate the sand waves.

The topography of the embayments could have induced **vorticity** in an ancestral Bering Slope Current causing a secondary circulation system in each **embayment** [12,26]. The asymmetry of some of the sand waves and the apparent easterly dip of internal strata indicate a net migration toward the east which is toward shore and oblique to isobaths and opposite to the northwesterly flow the present-day Bering Slope Current. **Anticyclonic** eddies within Navarinsky Bay shed by an ancestral **Bering** Slope Current could account for this direction of migration.

#### CONCLUSIONS

We hypothesize that the sand waves in the heads of Navarinsky, Pervenets, and **Zhemchug** submarine canyons originated in shallow **embayments** during lower stands of sea level in the Pleistocene. Obviously, sufficient data are not available to prove this conclusions, and we do not intend, by focusing on this preliminary working **hypothesis**, to discount or refute alternative hypotheses, as for example that the sand waves developed only after the Holocene transgression.

The working hypothesis described herein is satisfying for several reasons: (1) It accounts for the fact that sand waves have only been observed in the heads of the canyons and not on the upper slope and outer shelf between canyons; (2) It helps explain the size of each sand wave field in that the **area** of each field correlates with the **physiography** of the embayments. For example, **Navarinsky Bay** had the largest expanse of shallow water (shoal area)

and the Navarinsky sand wave field, is the most extensive. (3) Fluctuating sea levels help explain the stratigraphy of the bed forms in the Navarinsky field if the sand waves are individual sets stacked one on the other; alternatively, the interpretation of this sequence as climbing bed forms is plausible if large amounts of sediment were supplied to the embayments during a continuous rise of sea level. The oceanic processes responsible for the sand waves became operative, and sediment was supplied to the sand wave sites, at times of lower sea level. This dynamic system was shut off or diminished in intensity during higher sea level stands. Small changes of sea level would rapidly affect large areas of the Bering Sea shelf.

#### ACKNOWLEDGMENTS

We thank J. B. Southard and D. M. Rubin for reviewing the manuscript. This investigation was supported by the U.S. Geological Survey and by the Bureau of Land Management through an interagency agreement with the National Oceanic and Atmospheric Administration, under which a **multiyear** program responding to the needs of petroleum development of the Alaskan continental shelf is managed by the Outer Continental Shelf Environmental Assessment Program Office.

#### REFERENCES

- [1] Swift, D.J.P. and Ludwick, J. C., 1976. **Substrate** response to hydrodynamic processes: grain-size frequency distributions and **bedforms**. D. J. Stanley and D.J.P. Swift, (eds.), **Marine sediment transport and environmental management: New York, John Wiley, p. 255-310.**
- [2] Damuth, J. E., 1980. Use of high-frequency (3.5 - 12 kHz) echograms in the study of near-bottom sedimentation processes in the deep-sea: a review. *Marine Geology*, v. 38, p. 51-75.
- [3] Normark, W. R., Hess, G. R., Stow, D.A.V., and Bowen, A. J., 1980. Sediment waves on the **Monterey** Fan levee: a preliminary physical interpretation. *Marine Geology*, v. 37, p. 1-18.
- [4] Stride, A. H. and Tucker, M. J., 1960. Internal waves and waves of sand. *Nature*, v. 188, p. 933.
- [5] Knebel, H. J. and Folger, D. W., 1976. Large sand waves on the Atlantic outer continental shelf around Wilmington Canyon, off eastern United States. *Marine Geology*, v. 22, p. **M7-M15.**
- [6] Carlson, P. R. and Karl, H. A., 1981. Geologic hazards in Navarin basin province, northwestern Bering Sea. U.S. **Geol.** Survey Open-File Report 81-1217, 149 p.
- [7] Scholl, D. W., **Buffington, E. C.**, and **Marlow, M. S.**, 1975. Plate tectonics and the structural evolution of the Aleutian-Bering Sea region. In: R. B. Forbes (cd.), *Contributions to the Geology of the Bering Sea Basin and Adjacent Regions*, **Geol. Soc. America Spec. Paper 151**, p. 1-32.
- [8] Kinder, T. H., Coachman, L. K., and Gait, J. A., 1975. The Bering Slope Current System. *Journal of Physical Oceanography*, v. 5, p. 231-244.
- [9] Schumacher, J. D. and others, 1979. Structural fronts over the continental shelf of the eastern Bering Sea. *Journal of Physical Oceanography*, v. 9, p. 79-87.

- [10] **Carlson, P. R., Karl, H. A., and Edwards, B. D.**, in review, Puzzling features in the head of Navarinsky Canyon, Bering Sea. *Gee-Marine Letters*, 12 **ms.p.**
- [11] **Bouma, A. H., Hampton, M. A., and Orlando, R. C.**, 1978. Sand waves and other **bedforms** in lower Cook Inlet, Alaska. *Marine Geotechnology*, V. 2, p. 291-308.
- [12] **Fleming, B. W.**, 1981. Factors controlling shelf sediment dispersal along the southeast African continental margin. In: C. A. Nittrouer (cd.), *Sedimentary dynamics of continental shelves, developments in sedimentology*, v. 32: Amsterdam, **Elsevier** Scientific Publishing Company, p. 259-277.
- [13] **Carlson, P. R., Fischer, J. M., Karl, H. A., and Larkin, C.**, 1983. **Isopach** map of Unit A, youngest sedimentary sequence in Navarin basin, Bering Sea. In: H. A. Karl and P. R. Carlson (**eds.**), *Geologic hazards in Navarin basin province, northwestern Bering Sea, Final report R.U. #588*. Alaska continental shelf, Principal Investigators reports. NOAA, OCSEAP, Boulder, CO.
- [14] **Carlson, P. R., and Karl, H. A.**, 1983. **Rates** of sediment accumulation in Navarin Basin province, Bering Sea. In: H. A. Karl and P. R. Carlson (**eds.**), *Geologic hazards in Navarin Basin province, northwestern Bering Sea, Final report R.U. #588*. Alaska continental shelf, Principal Investigators reports. NOAA, OCSEAP, Boulder, CO.
- [15] **Bloom, A. L.**, 1971. **Glacial-eustatic** and isostatic controls of sea level since the last glaciation. In: K. K. Turekian, (cd.), *Late Cenozoic glacial ages*, New Haven, Yale University Press, p. 355-379.
- [16] **Gardner, J. V., Dean, W. E., and Vallier, T. L.**, 1979. **Sedimentology** and geochemistry of surface sediments, outer continental shelf, southern Bering Sea. *Marine Geology*, v. 35, p. 299-329.
- [17] **Pratt, R. M. and Dill, R. F.**, 1974. Deep **eustatic** terrace levels: further speculations. *Geology*, **v. 2, p. 155-159.**
- [18] **Hopkins, D. M.**, 1973. **Sea level history** in Beringia during the past 250,000 years. *Quaternary Research*, v. 3, p. 520-540.
- [19] **Inman, D. L., Nordstrom, C. E., and Flick, R. E.**, 1976. Currents in submarine canyons: an air-sea-land interaction. *Annual Review Fluid Mechanics*, v. 8, p. 275-310.
- [20] **Apel, J. R., Byrne, H. M., Prone, J. R., and Charnell, R. L.**, 1975. Observations of oceanic internal and surface waves from the Earth Resources Technology satellite. *Journal of Geophysical Research*, V. 80, p. 865-881.
- [21] **Shepard, F. P., Marshall, N. F., McLaughlin, P. A., and Sullivan, G. G.**, 1979. Currents in submarine canyons and other sea valleys. *American Association Petroleum Geologists, Studies in Geology*, no. 8, p. 865-881.
- [22] **Karl, H. A., Cacchione, D. A., and Carlson, P. R.**, 1982. Large sand waves in canyon heads, Bering Sea: products of internal waves or density currents? (**abs.**). *International Association of Sedimentologists Abstracts of papers, 11th International Congress on Sedimentology*, p. 73.
- [23] **Shepard, F. P., Sullivan, G. G., and Wood, F. J.**, 1979. Perigean spring tides and unusual currents in La Jolla submarine canyons (**abs.**). *Geological Society of America Abstracts with Programs*, v. 11, no. 7, p. 515.

- [24] Karl, H. A., 1980. Influence of San Gabriel submarine canyon on **narrow-shelf** sediment dynamics, southern California. *Marine Geology*, v. 34, p. **61-78**.
- [25] **Southard**, J. B. and **Cacchione**, D. A., 1972. Experiments *on* bottom sediment movement by breaking internal waves. In: **D.J.P.** Swift, D. Duane, and O. **Pilkey**, (eds.), Shelf sediment transport: process and pattern: **Stroudsburg**, Pa., Dowden, **Hutchinson** and **Ross**, Inc., p. 83-97.
- [26] Janowitz, G. S. and Pietrafesa, L. J. , in press. Topographically induced **upwelling** in the regions of the Charleston Bump, The Carolina capes and the eastern Florida shelf. *Journal of Physical Oceanography*.

4.  
R